Enigmatic dinosaur precursors bridge the gap to the origin of Pterosauria

Martín D. Ezcurra[1,2*], Sterling J. Nesbitt[3], Mario Bronzati[4], Fabio M. Dalla Vecchia[5,6], Federico L. Agnolin[7,8], Roger B. J. Benson[9], Federico Brissón Egli[7], Sergio F. Cabreira[10], Serjoscha W. Evers[9,11], Adriel R. Gentil[7], Randall B. Irmis[12], Agustín G. Martinelli[1], Fernando E. Novas[7], Lúcio Roberto da Silva[13], Nathan D. Smith[14], Michelle R. Stocker[3], Alan H. Turner[15] & Max C. Langer[4]

[1]Sección Paleontología de Vertebrados CONICET−Museo Argentino de Ciencias Naturales "Bernardino Rivadavia", Avenida Ángel Gallardo 470, Buenos Aires, Argentina.
[2]School of Geography, Earth and Environmental Sciences, University of Birmingham, Edgbaston, Birmingham, U.K.
[3]Department of Geosciences, Virginia Tech, Blacksburg, Virginia, U.S.A.
[4]Departamento de Biologia, Universidade de São Paulo, Avenida Bandeirantes 3900, Ribeirão Preto, Brazil.
[5]Research Group of Mesozoic Faunas, Institut Català de Paleontologia Miquel Crusafont (ICP), Carrer de l'Escola Industrial 23, Sabadell, Catalonia, Spain.
[6]Museo Friulano di Storia Naturale, Via Sabbadini 22-34, Udine, Italy.
[7]Laboratorio de Anatomía Comparada y Evolución de los Vertebrados CONICET−Museo Argentino de Ciencias Naturales "Bernardino Rivadavia", Avenida Ángel Gallardo 470, Buenos Aires, Argentina.
[8]Fundación de Historia Natural 'Félix de Azara', Departamento de Ciencias Naturales y Antropología, Universidad Maimónides, Hidalgo 775, Buenos Aires, Argentina.
[9]Department of Earth Sciences, University of Oxford, South Parks Road, Oxford, U.K.
[10]Av. Antônio Bozzetto, 305, Faxinal do Soturno, Brazil.
[11]Department of Geosciences, University of Fribourg, Chemin du Musée 4, Fribourg, Switzerland.
[12]Natural History Museum of Utah and Department of Geology & Geophysics, University of Utah, Salt Lake City, Utah, U.S.A.
[13]Rua Venâncio Trindade 810, Cachoeira do Sul, Brazil.
[14]The Dinosaur Institute, Natural History Museum of Los Angeles County, Los Angeles, California, U.S.A.
[15]Department of Anatomical Sciences, Stony Brook University, Stony Brook, New York, U.S.A.
ORCID – M.D.E.: 0000-0002-6000-6450; S.J.N.: 0000-0002-7017-1652; M.B.: 0000-0003-1542-3199; F.M.D.V.: 0000-0003-3914-3896; F.L.A.: 0000-0001-5073-561X; R.B.J.B.: 0000-0001-8244-6177; F.B.E.: 0000-0001-8037-5467; S.F.C.: 0000-0003-4162-5296; S.W.E.: 0000-0002-2393-5621; A.G.M.: 0000-0003-4489-0888; F.E.N.: 0000-0002-6901-8677; L.R.D.S.: 0000-0003-0211-9147; N.D.S.: 0000-0001-5554-4994; M.R.S.: 0000-0002-6473-8691; A.H.T.: 0000-0002-4164-6727; M.C.L.: 0000-0003-1009-4605.

Pterosaurs −the flying reptiles− were the first vertebrates to evolve powered flight[1] and one of the main evolutionary radiations in Mesozoic terrestrial ecosystems (c. 252−66 Ma), but their origin has remained one of the most outstanding enigmas in

palaeontology since the 19th Century[2–4]. They have been hypothesised as close relatives of a wide variety of reptilian clades, including dinosaur relatives[2–8], and there is still a major morphological gap between those forms and the oldest, unambiguous pterosaurs from the Upper Triassic. Driven by recent discoveries of well-preserved cranial remains, µCT scans of fragile skull bones (jaws, braincases), and reliably associated postcrania, we demonstrate that lagerpetids, a group of cursorial, non-volant dinosaur precursors, are the sister group of pterosaurs, sharing numerous synapomorphies across the entire skeleton. This finding substantially shortens the temporal and morphological gap between the oldest pterosaurs and their closest relatives, simultaneously strengthening the evidence that pterosaurs belong to the avian-line of archosaurs. Neuroanatomical features related to the enhanced sensory capabilities of pterosaurs[9] are already present in lagerpetids, indicating that they evolved before flight. Our new evidence illuminates the first steps of the assembly of the unique pterosaur body plan, whose conquest of aerial space represents one of the most astonishing morphofunctional innovations in vertebrate evolution.

Pterosaurs are deeply rooted in popular culture, frequently portrayed in books and films[10], and include the largest flying animals ever known[11]. Their evolutionary history spans over 150 million years, ending at the close of the Mesozoic Era[10,11]. The oldest pterosaurs are from the Upper Triassic (219−201.3 Ma) of Europe and North America[12,13], and the clade diversified into multiple ecomorphologically disparate groups by the Middle-Late Jurassic[11,14]. The oldest recognized pterosaurs already have a highly specialized body plan linked to their ability to fly[12,15], which was conserved in all pterosaurs: shoulder girdle with strongly posteroventrally enlarged coracoid braced with

the sternum and laterally facing glenoid fossa; forelimb with pteroid bone and hypertrophied fourth digit supporting membranous wing; and pelvic girdle with prepubic bone and strongly developed preacetabular process[1]. This highly modified anatomy results in a large morphological gap between pterosaurs and all other known Mesozoic reptiles. To complicate matters, early pterosaur specimens are small, scarce, and generally represented by taphonomically compressed, almost bidimensional partial skeletons[12]. These preservational problems and the absence of fossils with transitional morphologies have made the origin of pterosaurs one of the most elusive questions in vertebrate evolution for more than 200 years.

Quantitative phylogenetic analyses have generally agreed that pterosaurs fall within the lineage of Archosauria (i.e. the least inclusive clade that contains birds and crocodylians) leading to dinosaurs (i.e. Pan-Aves = Avemetatarsalia)[2,3,5–8]. Yet, some studies have alternatively recovered pterosaurs as the sister group to all other pan-archosaurs[16], among tanystropheid archosauromorphs[17], among non-archosaurian archosauriforms[18], or sister to the probable stem-diapsid drepanosauromorphs[19]. New fossil discoveries of the past few years have greatly increased the understanding of the early evolution of Pan-Aves, and of the assembly of the dinosaur body plan[8,20,21]. Nevertheless, a clear morphological gap still remains between pterosaurs and other pan-avians. Here, using new and existing specimens of the enigmatic pan-avian clade Lagerpetidae[21], we report on a previously undocumented combination of features that reduces the morphological gap between pterosaurs and other reptiles, clarifying the phylogenetic placement of Pterosauria within Pan-Aves. We present anatomical information from across the entire skeleton demonstrating that lagerpetids are the closest evolutionary relatives of pterosaurs. This information derives from detailed first-

hand observation of lagerpetid specimens, enhanced by novel three-dimensional reconstructions from micro-computed tomographic (μCT) scans.

Lagerpetids are small to medium-sized (usually <1 meter long), gracile and cursorial reptiles from Middle-Upper Triassic rocks of South and North America and Madagascar[21,22]. Previous knowledge of lagerpetid anatomy was mostly limited to vertebrae, hindlimbs, and a few cranial bones. Our new data are based on improved observations across the entire skeleton of several lagerpetid taxa (*Lagerpeton*, *Ixalerpeton*, *Kongonaphon*, *Dromomeron* spp.; Fig. 1), which elucidate their relationship to pterosaurs (Fig. 2). A newly identified partial maxilla from the holotype of *Ixalerpeton* and the maxilla of *Kongonaphon*[22] have tooth crowns with convex and unserrated mesial and distal margins (Figs. 1a, 2c). The long anterior portion of the maxilla of the latter lagerpetid substantially contributes to the external naris, as in early pterosaurs[12,23] (Fig. 2c, d; Extended Data Fig. 1). The dentaries of both *Lagerpeton* and *Ixalerpeton* have an edentulous anterior end that tapers to a point (Figs. 1g, 2e), resembling the condition in the early pterosaurs *Seazzadactylus*, *Carniadactylus*, and *Raeticodactylus*[12,23,24] (Fig. 2f), and most silesaurids[20]. The anterior region of the lagerpetid dentary is ventrally curved (Fig. 1g), similar to those of the early pterosaurs *Austriadactylus* and *Peteinosaurus*[12,23,24]. The lower jaw of *Lagerpeton* preserves articulated dentaries and lack splenials (Extended Data Fig. 2); the latter bone is fused to the dentary or restricted to the mid-point of the medial surface of the mandible in pterosaurs[13]. *Lagerpeton* and *Ixalerpeton* have 26−27 dentary tooth positions, sharing the high tooth count (>20 teeth) of several early pterosaurs[13,23,24] (Figs. 1g, 2e, f; Extended Data Figs. 1, 2). The dentary tooth crowns of these lagerpetids have convex mesial and distal margins, and middle-distal crowns possess a large and tall central cusp flanked by mesiodistally aligned, small accessory cusps (Fig. 2g, Extended Data Fig. 2).

Multicusped tooth crowns are rare among archosauriforms, but also occur in several early pterosaurs (e.g. *Austriadraco*, *Seazzadactylus*, *Raeticodactylus*, *Carniadactylus*, *Eudimorphodon*[12,23,24]) (Fig. 2f, h). Both lagerpetids and pterosaurs lack interdental plates (Extended Data Fig. 2), contrasting with most other Triassic archosauriforms[6].

The main axis of the braincase floor of *Dromomeron gregorii* and *Ixalerpeton* is anteroventrally to posterodorsally oriented, with the basipterygoid processes positioned ventrally to the basal tubera (Fig. 1d; Extended Data Fig. 3a), as also occurs in pterosaurs and several other archosauromorphs[6,7]. The cranial endocasts of *D. gregorii* and *Ixalerpeton* show strongly developed and posterolaterally tapering cerebellar floccular lobes, which resemble the even more developed floccular lobes of pterosaurs[9,25] (Figs. 1e, 2a, b). The olfactory tract of *Ixalerpeton* is long and ends in broad olfactory bulbs (Fig. 1c), retaining the ancestral condition of Archosauromorpha[7], whereas these structures are strongly reduced in pterosaurs[9,25]. In the inner ear, the portion of the semicircular canals (SCCs) of the endosseous labyrinth of *D. gregorii*, *Ixalerpeton*, pterosaurs, and some early eusaurischian dinosaurs are taller than anteroposteriorly long, with an anterior semicircular canal (ASC) forming a considerably longer arc than the posterior semicircular canal (Figs. 2a, b; Supplementary Information).

The forelimbs of *Dromomeron romeri* and pterosaurs share a forearm longer than the humerus, including a proportionally elongated metacarpus (metacarpal III-humerus length ratio >0.35; Fig. 2i−m). The manual digits of *D. romeri* are longer than their respective metacarpal and at least one digit has a trenchant claw (Fig. 1k), as is the case in pterosaurs and some early dinosaurs (e.g. *Herrerasaurus* and *Tawa*[6]). By contrast, lagerpetids, like other archosauromorphs, lack the enlargement of both the deltopectoral crest of the humerus and the fourth manual digit that characterizes

pterosaur wings[1]. The pelvic girdles of *Lagerpeton* and *Ixalerpeton* have a long pubo-ischiadic contact that extends ventrally up to the level of the anterovental margin of the pubis, as is the case in several early pterosaurs (e.g. *Austriadraco*, *Peteinosaurus*, *Dimorphodon*[12,23]) (Fig. 1l–n; Extended Data Fig. 3b, c), but not in most other archosaurs[6,7].

The femora of lagerpetids and early pterosaurs (e.g. *Raeticodactylus*, *Peteinosaurus*, *Dimorphodon*) share a hook-shaped proximal head (Figs. 1o, 2n, o; Extended Data Fig. 3c, d). A co-ossified astragalus and calcaneum is present in both lagerpetids and pterosaurs (Fig. 2p–s), but also in heterodontosaurid ornithischians and early neotheropods[6,7]. The absence of both a posterior groove on the astragalus and a calcaneal tuber is shared by pterosaurs and lagerpetids (Fig. 2r, s), and independently arose in some silesaurids and early dinosaurs[6].

The new anatomical information available for lagerpetids was scored in an expanded version of the most comprehensive phylogenetic data matrix focused on Permo-Triassic pan-archosaurs[7]. Our data matrix comprises 157 species (or diagnostic specimens) scored across 822 characters, including all currently valid lagerpetid species, nine Triassic and four Jurassic pterosaurs, 13 early dinosauriforms, and most non-archosaurian archosauromorphs, including eight tanystropheids. Thus, our extensive dataset encompasses all previously hypothesised phylogenetic positions of Pterosauria based on quantitative phylogenetic analyses[2–8,16–18], except a sister group relationship to drepanosauromorphs[19].

Our phylogenetic analyses robustly support Lagerpetidae as the sister taxon to Pterosauria within Pan-Aves using both equally weighted maximum parsimony (Fig. 3; Extended Data Figs. 4, 5) and Bayesian inference with a relaxed Mkv morphological clock model incorporating taxon ages using a fossilized birth–death process (posterior

probability = 0.99 for the lagerpetid-pterosaur clade) (Extended Data Fig. 6). A minimum of 33 synapomorphies distributed across the skeleton provide strong support for the Lagerpetidae + Pterosauria clade (= Pterosauromorpha). Some of these synapomorphies are unique to pterosauromorphs among early archosaurs, including a subtriangular and dorsoventrally tall floccular fossa of braincase, height-anteroposterior length ratio of SCCs of inner ear >0.90, reduced to absent splenial, strongly ventrally extended pubo-ischiadic plate, and hook-shaped femoral head (complete list of synapomorphies in Supplementary Information). Bayesian inference indicates high rates of morphological change during deep pan-avian divergences, including on the branches leading to Pterosauromorpha and Lagerpetidae. These high rates contrast with the more typical 'background' rates found on the branch leading to Pterosauria and its internal branches (Fig. 3). By contrast, higher evolutionary rates occur on the pterosaur branch if we force the more traditional position of lagerpetids closer to dinosaurs (Extended Data Fig. 7). These results bolster the idea that lagerpetids bridge the morphological gap to the origin of Pterosauria and suggest that the acquisition of the highly specialized pterosaur body plan did not involve faster evolutionary rates.

Topologically constrained searches using parsimony show that the pterosaur-lagerpetid clade is robust regardless of recent instability in early pterosaur phylogenetic reconstructions[12,24,25] (Supplementary Information). Branch supports of Pterosaurosauromorpha are much higher than in other pan-archosaur clades (Extended Data Figs. 4, 5), and 23 additional steps are needed to force the more traditional position of lagerpetids as the sister taxon to Dinosauriformes. We also tested previous alternative hypotheses for pterosaur relationships, finding that 44 extra steps are required to place them as non-archosaurian archosauriforms and 64 steps to force their placement as sister taxon to Tanystropheidae (but the Pterosauria + Tanystropheidae clade is sister to

196 Lagerpetidae within Pan-Aves). These results agree with a poorly supported placement
197 of Pterosauria outside Archosauria[6,7]. The possible pterosaur relative[2,3], but highly
198 problematic taxon *Scleromochlus* (Upper Triassic of Scotland), was included in a
199 secondary phylogenetic analysis (see Methods), and was recovered as the sister taxon to
200 the Pterosauria + Lagerpetidae clade, within Pan-Aves (Extended Data Fig. 4).
201 Additional cladistic analyses included the geometric morphometric
202 configuration of the labyrinth of the inner ear as a continuous 3D character in an attempt
203 to avoid subjective discrete character-states on such a complex structure[26]
204 (Supplementary Information). The analyses suggest that the inner ear has a strong
205 phylogenetic signal that supports a pterosaur-lagerpetid affinity (Fig. 3; Extended Data
206 Figs. 8−10).
207 Our improved knowledge of lagerpetid anatomy illuminates the morphology of
208 the most immediate common ancestor before the evolution of the well-recognized
209 pterosaur body plan. Both lagerpetids and pterosaurs share a unique inner ear
210 morphology among archosaurs, characterized by taller than anteroposteriorly long SCCs
211 (ratio >0.9) (Fig. 3; Extended Data Fig. 9). This is also supported by principal
212 components analysis that identifies proportionally tall and highly rounded SCCs as a
213 trait combination uniquely shared by pterosaurs and lagerpetids (Extended Data Fig.
214 10c). Lagerpetids and pterosaurs exhibit a strong curvature of the ASC (arc-length
215 versus straight-line ratio >1.5) that results in an increased radius, which convergently
216 evolved in a few early saurischian dinosaurs and is present in birds. The semicircular
217 canals detect head movements (angular acceleration) and a larger radius increases the
218 sense of equilibrium in primates and birds, and therefore is inferred to be related to
219 arboreal, aerial, or other agile forms of terrestrial locomotion and rapid movements[27].
220 Lagerpetids and pterosaurs are the only archosauriforms with a greatly enlarged

floccular fossa, representing >40% the height of the endocranial cavity (Fig. 2a, b). A large flocculus might have been important for lagerpetid locomotion or predation, given the connection of this structure with coordination of eye, head, and neck movements[28]. In pterosaurs, floccular enlargement has been hypothesised to be important for information processing related to flight[9]. Although not as developed as in pterosaurs, the relatively large lagerpetid flocculus indicates that initial enlargement of that structure occurred along the Pterosauromorpha branch. Thus, the neuroanatomy of lagerpetids has intermediate features between those of pterosaurs and other Triassic archosauriforms and may have paved the way towards the origin of active flight in pterosaurs.

The evolution of other traits associated with the acquisition of flight remains difficult to trace at the base of Pterosauromorpha with the currently available fossil record. Lagerpetid girdles and limbs lack features correlated with the flying behaviour of pterosaurs, e.g. hypertrophied deltopectoral crest of the humerus and wing digit of the manus[1]. However, the strongly recurved manual claws, with an inner curvature >150º in *D. romeri* (Fig. 1k), suggests that the forelimbs had functions other than ground-dwelling locomotion, such as climbing or grasping/prey acquisition (the inner claw curvature of ground-dwelling birds and squamates ranges 21.5º−125.5º and in perchers-climbers-predators ranges 87º−170.3º)[29]. Non-archosaurian archosauriforms, early crocodylian-line archosaurs, and very likely aphanosaurians (the earliest pan-avians) were all quadrupedal[30]. Our observations suggest that functional forelimb versatility became widespread in ornithodirans (Fig. 3), allowing the evolution of disparate behaviours such as manual processing of food resources in dinosaurs and active flight in pterosaurs.

The recognition of lagerpetids as the sister taxon to pterosaurs provides a new framework to study the origin of Pterosauria, its specialized body plan, and flying capabilities. Previous phylogenetic hypotheses implied a long ghost lineage, minimally of 28 My, for Pterosauria[8]. Our results shorten this to about 18 My, because the oldest lagerpetids come from 237 My-old rocks, near the Ladinian-Carnian boundary[22] (Fig. 3). Along those millions of years, the enhancement of features already present in the common ancestor of lagerpetids and pterosaurs allowed the latter group to explore a new adaptive landscape and conquer aerial space, likely prompting their outstanding adaptive radiation.

Main References

1. Padian, K. The origins and aerodynamics of flight in extinct vertebrates. *Palaeontology* **28**, 413−433 (1985).
2. Padian, K. in *Third Symposium on Mesozoic Terrestrial Ecosystems: Short Papers* (eds Reif, W.-E. & Westphal, F.) 163-166 (Atempto, 1984).
3. Sereno, P. C. Basal archosaurs: phylogenetic relationships and functional implications. *Soc. Vertebr. Paleontol. Mem.* **2**, 1–53 (1991).
4. Benton, M. J. *Scleromochlus taylori* and the origin of dinosaurs and pterosaurs. *Phil. Trans. R. Soc. London B Biol. Sci.* **354**, 1423–1446 (1999).
5. Gauthier, J. A. Saurischian monophyly and the origin of birds. *Mem. Calif. Acad. Sci.* **8**, 1−55 (1986).
6. Nesbitt, S. J. The early evolution of archosaurs: relationships and the origin of major clades. *Bull. Am. Mus. Nat. Hist.* **352**, 1−292 (2011).
7. Ezcurra, M. D. The phylogenetic relationships of basal archosauromorphs, with an emphasis on the systematics of proterosuchian archosauriforms. *PeerJ* **4**, e1778

(2016).

8. Nesbitt, S. J. et al. The earliest bird-line archosaurs and the assembly of the dinosaur body plan. *Nature* **544**, 484−487 (2017).

9. Witmer, L. M., Chatterjee, S., Franzosa, J. & Rowe, T. Neuroanatomy of flying reptiles and implications for flight, posture and behaviour. *Nature* **425**, 950−953 (2003).

10. Wellnhofer, P. *The illustrated encyclopedia of pterosaurs* (Salamander Books Ltd., 1991).

11. Witton, M. P. *Pterosaurs: natural history, evolution, anatomy* (Princeton Univ. Press, 2013).

12. Dalla Vecchia, F. M. in *Anatomy, Phylogeny and Palaeobiology of Early Archosaurs and their Kin* (eds Nesbitt, S. J., Desojo, J. B. & Irmis, R. B.) 119–155 (Geol. Soc. Lond., 2013).

13. Britt, B. B. et al. *Caelestiventus hanseni* gen. et sp. nov. extends the desert-dwelling pterosaur record back 65 million years. *Nature Ecol. Evol.* **2**, 1386–1392 (2018).

14. Butler, R. J., Brusatte, S. L., Andres, B. & Benson, R. B. How do geological sampling biases affect studies of morphological evolution in deep time? A case study of pterosaur (Reptilia: Archosauria) disparity. *Evolution* **66**, 147−162 (2012).

15. Padian, K. Osteology and functional morphology of *Dimorphodon macronyx* (Buckland) (Pterosauria: Rhamphorhynchoidea) based on new material in the Yale Peabody Museum. *Postilla* **189**, 1–44 (1983).

16. Benton, M. J. Classification and phylogeny of the diapsid reptiles. *Zool. J. Linn. Soc.* **84**, 97−164 (1985).

17. Peters, D. A reexamination of four prolacertiforms with implications for pterosaur phylogenesis. *Riv. Ital. Paleontol. Strat.* **106**, 293−336 (2000).

18. Bennett, S. C. Reassessment of the Triassic archosauriform *Scleromochlus taylori*: neither runner nor biped, but hopper. *PeerJ* **8**, e8418 (2020).
19. Renesto, S. & Binelli, G. *Vallesaurus cenensis* Wild 1991, a drepanosaurid (Reptilia, Diapsida) from the Late Triassic of northern Italy. *Riv. Ital. Paleontol. Strat.* **112**, 77−94 (2006).
20. Langer, M. C., Nesbitt, S. J., Bittencourt, J. S. & Irmis, R. B. in *Anatomy, phylogeny and palaeobiology of early archosaurs and their kin* (eds Nesbitt, S. J., Desojo, J. B. & Irmis, R. B.) 157−186 (Geol. Soc. Lond. 2013).
21. Cabreira, S. F. et al. A unique Late Triassic dinosauromorph assemblage reveals dinosaur ancestral anatomy and diet. *Current Biology* **26**, 3090−3095 (2016).
22. Kammerer, C. F., Nesbitt, S. J., Flynn, J. J., Ranivoharimanana, L. & Wyss, A. R. A tiny ornithodiran archosaur from the Triassic of Madagascar and the role of miniaturization in dinosaur and pterosaur ancestry. *Proc. Nat. Ac. Sci.*, 10.1073/pnas.1916631117 (2020).
23. Dalla Vecchia, F. M. *Gli pterosauri triassici* (Publ. Mus. Friulano di St. Nat., 2014).
24. Dalla Vecchia, F. M. *Seazzadactylus venieri* gen. et sp. nov., a new pterosaur (Diapsida: Pterosauria) from the Upper Triassic (Norian) of northeastern Italy. *PeerJ* **7**, e7363 (2019).
25. Codorniú, L., Paulina-Carabajal, A., Pol, D., Unwin, D. & Rauhut, O. W. M. A Jurassic pterosaur from Patagonia and the origin of the pterodactyloid neurocranium. *PeerJ* **4**, e2311 (2016).
26. Goloboff, P. A. & Catalano, S. A. TNT version 1.5, including a full implementation of phylogenetic morphometrics. *Cladistics* **32**, 221−238 (2016).
27. Spoor F. & Zonneveld F. Comparative review of the human bony labyrinth. *Yearb. Phys. Anthropol*. **41**, 211−251 (1998).

28. Winship, I. R. & Wylie, D. R. Zonal organization of the vestibulocerebellum in pigeons (*Columba livia*): I. Climbing fiber input to the flocculus. *J. Comp. Neurol.* **456**, 127−139 (2003).
29. Birn-Jeffery, A. V., Miller, C. E., Naish, D., Rayfield, E. J. & Hone, D. W. Pedal claw curvature in birds, lizards and Mesozoic dinosaurs – complicated categories and compensating for mass-specific and phylogenetic control. *PLoS ONE* **7**, e50555 (2012).
30. Kubo, T. & Kubo, M. O. Associated evolution of bipedality and cursoriality among Triassic archosaurs: a phylogenetically controlled evaluation. *Paleobiol.* **38**, 474−485 (2012).

Fig. 1 | Newly discovered and selected bones characterizing the lagerpetid body plan. **a**, **b**, Partial right maxilla. **c**, Skull roof. **d**, Skull roof and braincase. **e**, Cranial endocast. **f**, Right scapula. **g**, Left dentary. **h**, Left humerus, **i**, partial ulna and radius, **j**, metacarpals I−IV and phalanx I-1, and **k**, ungual of manual digit IV. **l**, Right ilium. **m**, Right ischium. **n**, Left pubis, **o**, femur, and **p**, pes. **a**, **f**, **g**, **k**−**m**, Lateral, **b**, **c**, ventral, **d**, **e**, right lateral, **h**, **i**, **n**, **p**, medial, **j**, dorsal, and **o**, posteromedial views. **a**−**f**, **l**−**n**, *Ixalerpeton* (ULBRA-PVT059). **g**, **o**, **p**, *Lagerpeton* (**g**, PVL 4625; **o**, **p**, PVL 4619). **h**−**k**, *Dromomeron romeri* (GR 238). Arrows indicate anterior direction. Scale bars = 2 mm for a, b, e; 3 mm for c, d, f, g, k−n; 5 mm for h−j, o, p. Skeletal reconstruction by Scott Hartman in collaboration with authors based on *Lagerpeton*, *Ixalerpeton* and *D. romeri*. [two columns]

Fig. 2 | Key comparisons between pterosaur and lagerpetid cranial endocasts and bones. **a**, **b**, Cranial endocasts. **c**, Partial right maxilla. **d**, Left maxilla (reversed). **e**, Left

dentary. **f**, Right dentary. **g**, **h**, Dentary tooth crowns. **i**, **k**, Left humeri, and **j**, partial manus. **m**, Metacarpals I−III. **n**, **o**, Femora (**n**, left, reversed; **o**, right). **p**, **q**, **s**, Right distal portion of tibia, fibula and astragalocalcaneum. **r**, Right astragalocalcaneum. **a**, **b**, right lateral, **c**, **d**, **f**, lateral, **e**, **i**, **k**, medial, **g**, **h**, labial, **j**, dorsal, **m**, dorsal/ventral, **n**, **o**, **s**, anterolateral, **p**, **q**, anterior, and **r**, posterior views. **a**, Lagerpetid *Dromomeron gregorii* (TMM 31100-1334). **b**, Pterosaur *Allkaruen* (MPEF-PV 3613). **c**, Lagerpetid *Kongonaphon* (UA 10618). **d**, **k**, **m**, **o**, Pterosaur *Raeticodactylus* (BNM 14524). **e**, **g**, Lagerpetid *Ixalerpeton* (ULBRA-PVT059). **h**, **q**, Pterosaur *Austriadraco* (SNSB-BSPG 1994 I 51). **f**, Pterosaur *Seazzadactylus* (MFSN 21545). **i**, **j**, **n**, **r**, Lagerpetid *Dromomeron romeri* (**i**, **j**, GR 238; **n**, GR 218; **r**, GR 223). **p**, Lagerpetid *Lagerpeton* (PULR 06). **s**, Pterosaur *Peteinosaurus* (MCSNB 3496). Arrows indicate anterior direction. Scale bars = 3 mm for a, b, f, q; 2 mm for c, e, s; 5 mm for d, k−p, r; 0.3 mm for g, h; 1 cm for i, j. [two columns]

Fig. 3 | Time-calibrated strict reduced consensus tree (after a posteriori pruning of *Kongonaphon*) focused on Pterosauria and Lagerpetidae. Red dotted structures are ancestral optimizations of the labyrinth of the inner ear (blue lines are apomorphic displacements). Violet bars indicate node temporal calibration after Bayesian analysis. White-fill circles indicate node-based clades, half-circles stem-based clades, and the star an apomorphy-based clade. Labyrinths of the inner ear are in lateral view and belong to **1**, *Arizonasaurus*, **2**, *Dromomeron gregorii*, and **3**, *Allkaruen*. Further information in Supplementary Information. [two columns]

Methods

New phylogenetic definitions

Pan-Aves Gauthier and de Queiroz, 2001 [this work], converted clade name

Registration Number: 404.

Phylogenetic definition: the most inclusive clade containing *Vultur gryphus* Linnaeus, 1758 (Aves), but not *Crocodylus niloticus* Laurenti, 1768 (Crocodylia). This is a crown-based total-clade definition.

Reference phylogeny: phylogenetic hypothesis depicted in Fig. 3 and Extended Data Fig. 4 of this work. *Vultur gryphus* nests within Dinosauria and *Crocodylus niloticus* within Pseudosuchia.

Composition: based on the reference phylogeny, Pan-Aves includes Aphanosauria[8] and Ornithodira (see below).

Ornithodira Gauthier, 1986 [this work], converted clade name

Registration Number: 405.

Phylogenetic definition: the least inclusive clade containing *Compsognathus longipes* Wagner, 1859 (Dinosauria) and *Pterodactylus* (originally *Ornithocephalus*) *antiquus* (Sömmerring, 1812) (Pterosauria), but not *Alligator* (originally *Crocodilus*) *mississippiensis* (Daudin, 1802) (Crocodylia). This is a minimum-clade definition.

Reference phylogeny: phylogenetic hypothesis depicted in Fig. 3 and Extended Data Fig. 4 of this work. *Compsognathus longipes* nests within Dinosauria, *Pterodactylus antiquus* within Pterosauria, and *Alligator mississippiensis* within Pseudosuchia.

Composition: based based on the reference phylogeny, Ornithodira includes the main groups Lagerpetidae (see below), Pterosauria[31], and Dinosauromorpha (see below), and possibly *Scleromochlus taylori*.

Lagerpetidae Arcucci, 1986 [this work], converted clade name

Registration Number: 406.

Phylogenetic definition: the most inclusive clade containing *Lagerpeton chanarensis* Romer, 1971, but not *Eudimorphodon ranzii* Zambelli, 1973, *Silesaurus opolensis* Dzik, 2003, and *Vultur gryphus* Linnaeus, 1758. This is a maximum clade definition.

Reference phylogeny: phylogenetic hypothesis depicted in Fig. 3 and Extended Data Fig. 4 of this work.

Composition: based on the Reference phylogeny, Lagerpetidae includes *Lagerpeton chanarensis*, *Ixalerpeton polesinensis*, *Kongonaphon kely*, and *Dromomeron* spp.

Dinosauromorpha Benton, 1985 [this work], converted clade name

Registration Number: 407.

Phylogenetic definition: the most inclusive clade containing *Compsognathus longipes* Wagner, 1859 (Dinosauria), but not *Pterodactylus* (originally *Ornithocephalus*) *antiquus* (Sömmerring, 1812) (Pterosauria) or *Alligator* (originally *Crocodilus*) *mississippiensis* (Daudin, 1802) (Crocodylia). This is a maximum clade definition.

Reference phylogeny: phylogenetic hypothesis depicted in Fig. 3 and Extended Data Fig. 4 of this work. *Compsognathus longipes* nests within Dinosauria, *Pterodactylus antiquus* within Pterosauria, and *Alligator mississippiensis* within Pseudosuchia.

Composition: based on the Reference phylogeny, Dinosauromorpha includes the main groups Silesauridae[32,33] and Dinosauria[34], including Aves[35], plus some species level taxa such as *Lagosuchus talampayensis*.

Dinosauriformes Novas, 1992 [this work], converted clade name

Registration Number: 408.

Phylogenetic definition: the least inclusive clade containing *Compsognathus longipes* Wagner, 1859 (Dinosauria) and *Lagosuchus talampayensis* Romer, 1971. This is a minimum clade definition.

Reference phylogeny: phylogenetic hypothesis depicted in Fig. 3 and Extended Data Fig. 4 of this work. *Compsognathus longipes* nests within Dinosauria.

Composition: based on the Reference phylogeny, Dinosauriformes is composed of *Lagosuchus talampayensis*, Silesauridae[32,33], and Dinosauria[34], including Aves[35].

Micro-computed tomography scans and digital processing

The partial lower jaw of *Lagerpeton* (PVL 4625) was X-ray μCT scanned at YPF TECNOLOGÍA (Y-TEC, Berisso, Argentina) using a Bruker Skyscan, the bones of *Ixalerpeton* (ULBRA-PVT059) at Centro para Documentação da Biodiversidade, Universidade de São Paulo (Ribeirão Preto, Brazil) using a Nanotom Scan machine - GE Sensing & Inspection Technologies GmbH (Wunstorf Germany), and the braincase of *D. gregorii* (TMM 31100-1334) at University of Texas High-Resolution X-ray CT Facility (Austin, USA) using a custom built BIR scanner using a Feinfocus X-ray source and an Image Intensifier detector (further information about the scans is provided in the Supplementary Information). The images of *Lagerpeton* were processed using the software 3D Slicer version 4.7[36] and the images of *Ixalerpeton* and *Dromomeron* were processed using the software Amira (version 5.3.3, Visage Imaging, Berlin, Germany).

Morphogeometric sampling of the endosseous labyrinth of the inner ear. The course of each semicircular canal of the inner ear was quantitatively sampled in available taxa using sliding 3D semilandmarks (on left labyrinths or reflected right labyrinths). A midline skeleton of each canal was generated using the 'autoskeleton'

function of Avizo 9 (https://www.fei.com/software/amira-avizo/), which represents the mean endolymph flow path through a semicircular canal[37]. The landmarking of midline skeletons captures the relative lengths, orientations and morphology of the canals. Open semilandmark curves started at the intersection of the canal with its ampulla, ending at its intersection with the common crus. These start and end points represent six fixed, single-point landmarks. The posterior ampulla was estimated to be the ventralmost point on the trajectory of the posterior semicircular canal (PSC), and the intersection of the LSC with the common crus was estimated to be directly ventral to the intersection of the PSC with the common crus[38]. In addition, a closed loop of semilandmarks was placed around the inner surface of the anterior semicircular canal (ASC) to capture variation in relative canal thickness (e.g.[39]). This landmarking procedure involved placing arbitrary numbers of points in each semilandmark series. Thus, these series were resampled to equal numbers of points in each specimen using the digit.curves function of the package Geomorph version 3.2.1[40] written for R (version 3.6.0[41]): ASC midline skeleton (9 points), PSC midline skeleton (8 points), LSC midline skeleton (10 points), and ASC inner loop (13 points). Landmark configurations were transformed through a generalised Procrustes superimposition using the gpagen function of Geomorph in R. This procedure removes differences in orientation and position of specimens, and separates overall size information (centroid size) from shape information. Semilandmarks were allowed to slide along their curves during superimposition to minimise bending energy difference from the mean shape.

Principal components analysis. We conducted principal components analysis (PCA) of our geometric morphometric dataset using the plotTangentSpace() function of the R package geomorph version 3.2.1[40].

Phylogenetic analyses – maximum parsimony. The phylogenetic relationships of

pterosaurs and lagerpetids were analyzed using the data matrix of Ezcurra[7] as modified by subsequent authors (see[42] and references therein). We used this data matrix because it has the key taxa and characters that are required to test the phylogenetic position of those clades within the Permo-Triassic evolutionary radiation of Pan-Archosauria. Nevertheless, we increased the sampling of the matrix by adding taxa and characters that we considered informative to assess the phylogeny of early pan-avians. We added twelve pterosaurs, six lagerpetids, seven dinosaurs, and 127 characters (Supplementary Information). In addition, the formulation or wording was modified or additional states were added for 76 characters, and several scorings were changed with respect to previous versions of the matrix (Supplementary Information). Character 119 was excluded before the searches following Ezcurra et al.[43]. Because they represent nested sets of homologies, the following characters were considered additive: 1, 2, 7, 10, 17, 19−21, 28, 29, 36, 40, 42, 46, 50, 54, 66, 71, 74−76, 122, 127, 146, 153, 156, 157, 171, 176, 177, 187, 202, 221, 227, 263, 266, 278, 279, 283, 324, 327, 331, 337, 345, 351, 352, 354, 361, 365, 370, 377, 379, 386, 387, 398, 410, 414, 424, 430, 435, 446, 448, 454, 455, 458, 460, 463, 470, 472, 478, 482, 483, 485, 489, 490, 502, 504, 510, 516, 521, 529, 537, 546, 552, 556, 557, 567, 569, 571, 574, 581, 582, 588, 636, 648, 652, 662, 701, 731, 735, 737, 738, 743, 749, 766, 784, and 816. Several terminal taxa were also excluded because they were originally scored only with the purpose of conducting morphological disparity analyses and not to be included, yet, in phylogenetic analyses[44]. The final data matrix is composed of 822 active characters and 157 active taxa. A second analysis was conducted including *Scleromochlus taylori*, resulting in a total of 158 taxa. Interpretation of detailed anatomical features is extremely difficult for this species, due to the preservation of all its specimens as natural moulds of very small-sized bones in a coarse sandstone[4]. Thus, we decided to not include this taxon in the

492 first analysis, because this could introduce a subtantial amount of scoring errors.

493 The data matrix was analysed under equally weighted maximum-parsimony
494 using TNT 1.5[26]. The search strategies started using a combination of the tree-search
495 algorithms Wagner trees, tree bisection and reconnection (TBR) branch swapping,
496 sectorial searches, Ratchet and Tree Fusing, until 100 hits of the same minimum tree
497 length were achieved. The best trees obtained were subjected to a final round of TBR
498 branch swapping. Zero-length branches in any of the recovered most parsimonious trees
499 were collapsed. Branch support was quantified using Bremer support values and a
500 bootstrap resampling analysis, using 1,000 technical pseudo-replications and reporting
501 both absolute and GC (group present/ contradicted) frequencies. The minimum number
502 of additional steps necessary to generate alternative, suboptimal topologies was
503 calculated when constraining the position of pterosaurs and lagerpetids in different parts
504 of the tree or constraining the topology of pterosaur interrelationships found by previous
505 authors and rerunning the analyses.

506 An alternative analysis was conducted using the 3D morphogeometric
507 configuration of the endosseous labyrinth of the inner ear. The aligned (Procrustes)
508 coordinates were exported to TNT 1.5 and they were used as a single morphogeometric
509 continuous character[26] to test the presence of the phylogenetic signal recovered using
510 the discretized inner ear characters. The configurations were re-aligned in TNT applying
511 the minimum distances criterion[26] and using *Trilophosaurus buettneri* as the reference
512 taxon because it has been recovered as the earliest branching terminal taxon, among
513 those with 3D sampled endosseous labyrinths, in previous analyses of this data set[7,42,43].
514 The discrete characters of the inner ear (characters 729−743) were excluded during the
515 searches using the 3D morphogeometric character because of their non-independence.
516 The search strategy started using 10 technical replications of Wagner trees followed by

TBR branch-swapping algorithm (holding 10 trees per replication). The best trees obtained were subjected to a final round of TBR branch swapping. Zero-length branches and additive characters were treated as in the previous analyses.

Phylogenetic analyses – Bayesian inference. A Bayesian tip-dating analysis was conducted in MrBayes 3.2.6[45]. We used an Mkv substitution model and the same ordered characters as in the maximum parsimony analysis. *Petrolacosaurus kansensis* was used as the outgroup. We used an independent gamma rate relaxed clock model and uniform age priors modelled around the first appearance and last appearance dates for all tips of the tree. We implemented a node age calibration for Archosauria with a uniform prior of 249.2−257.3 Ma, in which the minimum is informed by the ages of the oldest archosaurian specimens[44], and the maximum by age estimates for the crocodile-lizard split[46]. We specified a fossilized-birth death process as the tree model using standard parameterizations and values. Fossils were specified to be tips. The deepest split within the tree was parameterized with a uniform (303.4−318.0 Ma) tree age prior, whereby the maximum is based on the age of the Joggins Formation, which documents the earliest crown-amniotes[47] and the minimum is based on the chronostratigraphic uncertainty of *Petrolacosaurus kansensis*, the outgroup and oldest taxon of our sample. We used Metropolis Coupling Markov chain Monte Carlo (MCMCMC) algorithms with two independent runs of four chains, using a heating coefficient of 0.05 and 3 swap attempts per generation. Topological convergence, indicated by average standard deviation of split frequencies decreasing below 0.01, was achieved after 23,496,000 generations. Potential Scale Reduction Factors (PSRF) of 1.0, visual inspection of trace plot with Tracer 1.7.1[48], and estimated sample sizes (ESS) for all parameters >200 further indicated convergence. An additional analysis was performed with the same settings, except that the topology was constrained to investigate topological effects on

evolutionary rates. The topology is constrained to follow the topology of one of the most parsimonious trees of the maximum parsimony analysis after constraining lagerpetids to be dinosauromorphs. This analysis was specified to run for 24,000,000 generations, and ESS values >200 indicated convergence. Additional phylogenetic analysis details are provided in the supplementary information.

Method References

31. Andres, B. & Padian, K. in *Phylonyms: A Companion to the PhyloCode* (eds de Queiroz, K., Cantino, P. D. & Gauthier, J. A.) 157 (CRC Press, 2020).
32. Langer, M. C., Ezcurra, M. D., Bittencourt, J. S. & Novas, F. E. The origin and early evolution of dinosaurs. *Biol. Rev.* **85**, 55−110 (2010).
33. Nesbitt, S. J. et al. Ecologically distinct dinosaurian sister group shows early diversification of Ornithodira. *Nature* **464**, 95−98 (2010).
34. Langer, M. C., Novas, F. E., Bittencourt, J., Ezcurra, M.D. & Gauthier, J. A. in *Phylonyms: A Companion to the PhyloCode* (eds de Queiroz, K., Cantino, P. D. & Gauthier, J. A.) 194 (CRC Press, 2020).
35. Clarke, J. A., Mindell, D. P., de Queiroz, K, Hanson, M., Norell, M. A. & Gauthier, J. A. in *Phylonyms: A Companion to the PhyloCode* (eds de Queiroz, K., Cantino, P. D. & Gauthier, J. A.) 113 (CRC Press, 2020).
36. Fedorov, A. et al. 3D Slicer as an image computing platform for the Quantitative Imaging Network. *Mag. Res. Imag.* **30**, 1323–1341 (2012).
37. David, R. et al. Motion from the past. A new method to infer vestibular capacities of extinct species. *C. R. Palevol* **9**, 397−410 (2010).
38. Evers, S. W. et al. Neurovascular anatomy of the protostegid turtle *Rhinochelys pulchriceps* and comparisons of membranous and endosseous labyrinth shape in an

extant turtle. *Zool. J. Linn. Soc.* **187**, 800−828 (2019).

39. Neenan, J. M. et al. Evolution of the sauropterygian labyrinth with increasingly pelagic lifestyles. *Current Biology* **27**, 3852−3858 (2017).
40. Adams, D., Collyer, M. & Kaliontzopoulou, A. *Geomorph: Software for geometric morphometric analyses. R package version 3.2.1* (https://cran.r-project.org/package=geomorph, 2020).
41. R Core Team. *R: A language and environment for statistical computing* (R Foundation for Statistical Computing, 2019).
42. Butler, R. J., Ezcurra, M. D., Liu, J., Sookias, R. B. & Sullivan, C. The anatomy and phylogenetic position of the erythrosuchid archosauriform *Guchengosuchus shiguaiensis* from the earliest Middle Triassic of China. *PeerJ* **7**, e6435 (2019).
43. Ezcurra, M. D. et al. Deep faunistic turnovers preceded the rise of dinosaurs in southwestern Pangaea. *Nature Ecol. Evol.* **1**, 1477−1483 (2017).
44. Ezcurra, M. D. & Butler, R. J. The rise of the ruling reptiles and ecosystem recovery from the Permo-Triassic mass extinction. *Proc. R. Soc. B Biol. Sci* **285**, 20180361 (2018).
45. Ronquist, F., van der Mark, P. & Huelsenbeck, J. P. in *The Phylogenetic Handbook: a Practical Approach to Phylogenetic Analysis and Hypothesis Testing* (eds Lemey, P., Salemi, M. & Vandamme, A.-M.) 210−266 (Camb. Univ. Press, 2009).
46. Ezcurra, M. D., Scheyer, T. M. & Butler, R. J. The origin and early evolution of Sauria: reassessing the Permian saurian fossil record and the timing of the crocodile-lizard divergence. *PLoS One* **9**, e89165 (2014).
47. Benton, M. J., et al. Constraints on the timescale of animal evolutionary history. *Palaeontol. Electron.* **18**, 1−116 (2015).

48. Rambaut, A., Drummond, A. J., Xie, D., Baele, G. & Suchard, M. A. Posterior summarisation in Bayesian phylogenetics using Tracer 1.7. *Syst. Biol.* **67**, 901−904 (2018).

Acknowledgements We thank C. Alsina and F. De Cianni (MACN) for repreparation, M. B. Epele and M. Cipollone for μCT scanning (Y-TEC, Berisso, Argentina), and F. Tricárico (MACN) for SEM microphotographs of PVL 4625; M. Colbert (UT Austin) for μCT scanning TMM 31100-1334; and D. Cavallari for μCT scanning ULBRA-PVT059. We also thank V. Radermacher and J. Choiniere for providing access to the μCT scan of a *Heterodontosaurus* specimen scaned at ESRF; and to ESI and SAHRA for permits for that work. UA allowed access to 3D data and first hand study of *Kongonaphon.* We thank A. Paulina-Carabajal for allowing access to the μCT scan of *Allkaruen*, S. Chapman, H. Furrer, Z. Gasparini, M. Moser, G. Muscio, P. Ortíz, A. Paganoni, J. Powell, O. Rauhut, E. Ruigómez, R. Stecher and A. Tintori for access to specimens, and J. Gauthier for discussion and suggestions about phylogenetic nomenclature. S. Hartman allowed using and modifying the lagerpetid skeletal reconstruction, and R. Nogueira digitally assembled and reconstructed the lagerpetid skull and created the life reconstruction. We appreciate the comments of the editor H. Gee, the reviewer S. Brusatte, and two anonymous reviewers that improved the overall quality of the manuscript. Study supported by the Sepkoski Grant of the Paleontological Society (to M.D.E.), Agencia Nacional de Promoción Científica y Técnica (PICT 2018-01186 to M.D.E.), The Coleman and Susan Burke Foundation (New York, to F.E.N.), Financiadora de Estudos e Projetos, Brazilian Federal Government (project CT- INFRA 01/2013), and São Paulo Research Foundation (FAPESP 2014/03825-3 to M.C.L. and 2018/18145-9 to M.B.).

Author Contributions M.D.E., S.J.N and M.C.L designed the project; M.D.E, S.J.N, M.B., F.L.A., A.G.M. and M.C.L. described the material; M.B., R.B.J.B., S.W.E. and A.R.G. processed and sampled CT data; M.D.E., S.J.N., M.B., F.L.A., F.M.D.V., S.W.E., N.D.S., and M.C.L. scored phylogenetic matrices; M.D.E. conducted the parsimony analyses; R.B.J.B. and S.W.E. conducted the Bayesian analyses; M.D.E., S.J.N., M.B. and M.C.L. wrote the bulk of the manuscript; M.D.E., S.J.N., M.B., F.M.D.V. and S.W.E. made figures; all authors collected data and contributed to the writing, discussion and conclusion.

Author Information Reprints and permissions information is available at www.nature.com/reprints. The authors declare no competing financial interests. Correspondence and requests for materials should be addressed to M.D.E. (martindezcurra@yahoo.com.ar).

Data availability

The data matrices for the phylogenetic analyses in NEXUS and/or TNT formats have been deposited in MorphoBank at http://morphobank.org/permalink/?P3773. 3D models of lagerpetid bones in STL format are available in MorphoSource at http://www.morphosource.org/Detail/ProjectDetail/Show/project_id/1095.

Supplementary Information is linked to the online version of the paper at http://www.nature.com/nature.

Extended Data Section

Extended Data Fig. 1 | Life reconstruction and 3D reconstruction of the skull of the lagerpetid *Ixalerpeton polesinensis* (ULBRA-PVT059, holotype) with additions of cranial bones of other lagerpetids. Images in **a**, **f**, **i**, right lateral, **b**, **g**, anterior, **c**, posterior, **d**, ventral, **e**, dorsal, and **h**, anterodorsolateral views. **f**−**h**, show transparent inferred bones to show the braincase and skull roof bones through them. Bones of *Ixalerpeton polesinensis* are indicated in yellow and those of *Kongonaphon kely* (UA 10618, holotype), *Dromomeron gregorii* (TMM 31100-1334, referred specimen), and *Lagerpeton chanarensis* (PVL 4625, referred specimen) in red, and inferred bones in light blue. Arrows indicate anterior direction. Complete scale bar = 5 mm. Life and skull reconstruction by Rodolfo Nogueira.

Extended Data Fig. 2 | Lagerpetid *Lagerpeton chanarensis* (PVL 4625, referred specimen), 3D reconstruction from µCT scan of articulated dentaries and close-ups of dentary tooth crowns. Images in **a**, left lateral, **b**, right dorsolateral, **c**, ventral, **d**, dorsal, **e**, anterodorsal, **f**, apicolingual, and **g**, **h**, lingual views. Smaller arrows indicate anterior direction and larger arrows point to accessory cusps. **a**−**e**, 3D models based on µCT scan data, **f**, Scanning Electron Microscope photograph, **g**, **h**, binocular microscope photographs. Scale bars = 5 mm for a−e; 0.5 mm for f, g.

Extended Data Fig. 3 | Additional images and comparisons between lagerpetids and pterosaurs. a, Partial skull roof and braincase of the lagerpetid *Dromomeron gregorii* (TMM 31100-1334) in left lateral view. **b**, Right hemipelvis of the lagerpetid *Lagerpeton chanarensis* (PVL 4619) in lateral view. **c**, Left hemipelvis and articulated proximal end of femur of the pterosaur *Dimorphodon macronyx* (NHMUK PV OR 41212, reversed) in lateral view. **d**, Right femur of the pterosaur *Dimorphodon macronyx* (YPM 9182) in anterolateral view. Arrows indicate anterior direction. Scale bars = 3 mm for a; 5 mm for b−d.

Extended Data Fig. 4 | Phylogenetic relationships of pterosaurs and lagerpetids among pan-archosaurs using discrete characters. Strict consensus of 280 most parsimonious trees (tree length = 5,002; consistency index = 0.21431; retention index = 0.65014). Absolute (left) and GC (right) bootstrap frequencies above each branch and Bremer support values below each branch. Position of *Scleromochlus* in the secondary analysis indicated with a dotted line.

Extended Data Fig. 5| Bremer support values in strict reduced consensus tree. Strict reduced consensus of the same most parsimonious trees of Extended Data Fig. 4 after pruning a posteriori *Spondylosoma*, *Dongusuchus* and PVSJ 883 to avoid reduction of Bremer support values because of missing data in these taxa. Bremer support values indicated on each branch.

Extended Data Fig. 6 | Majority rule tree recovered from the unconstrained Bayesian phylogenetic analysis. Branch colours indicate character state transition rates (= evolutionary rates), numbers at nodes indicate posterior probabilities, thin black horizontal line segments indicate 95% probability distribution of node ages, and dotted vertical bars indicate boundaries between geological periods. Thick black vertical bars indicate polytomies and, as a result, transition rates could not be calculated.

Extended Data Fig. 7 | Majority rule tree recovered from the constrained Bayesian phylogenetic analysis. The topology of this tree has been constrained a priori with one of the most parsimonious trees recovered after forcing the position of lagerpetids as the earliest branching dinosauromorphs in the maximum parsimony analysis. Branch colours indicate character state transition rates (= evolutionary rates), black horizontal line segments indicate 95% probability distribution of node ages, and dotted vertical bars indicate boundaries between geological periods. Posterior probabilities at nodes are not shown because the topology is fully constrained.

Extended Data Fig. 8 | Phylogenetic relationships of pterosaurs and lagerpetids among pan-archosaurs using discrete characters and the 3D morphogeometric configuration of the inner ear. Strict consensus tree generated from 256 most parsimonious trees (tree length = 4,927.67960; consistency index = 0.77624; retention index = 0.85756).

Extended Data Fig. 9 | Single most parsimonious tree (MPT) found when analysing only the 3D morphogeometric (MG) configuration of the inner ear and 3D examples of how distances and angles were measured in the 3D endosseous labyrinth models. a, Tree rooted with *Trilophosaurus buettneri*; **b**, 3D model of left endosseous labyrinth of *Plateosaurus* sp. (HMN R1937) in dorsolateral view; **c**, labyrinth with reference plane for sectioning indicated; **d**, landmark scheme for SSC length measurements; **e**, landmark scheme for ASC circumference and labyrinth height measurements; **f**, landmark scheme for labyrinth width measurements in ventral view on reference plane; **g**, landmark constellation explanation. asc, anterior semicircular canal; cc, common crus; enla, endosseous labyrinth; lsc, lateral semicircular canal; psc, posterior semicircular canal; ve, vestibule.

Extended Data Fig. 10 | Single MPT found when analysing only the 3D MG configuration of the inner ear and alternative rooting, and morphospace plot of archosauromorph labyrinths. a, Tree rooted with *Mesosuchus browni*; **b**, landmark constellation explanation; **c**, principal components analyses (n=22 species) with variation in PC1 plotted against PC2 (showing deformations along PC1–PC2), in which grey dots are non-pan-avian archosauromorphs, pink dots are non-pterosauromorph pan-avians, garnet dots are pterosaurs, and orange dots are lagerpetids. asc, anterior semicircular canal; cc, common crus; lsc, lateral semicircular canal; psc, posterior semicircular canal.

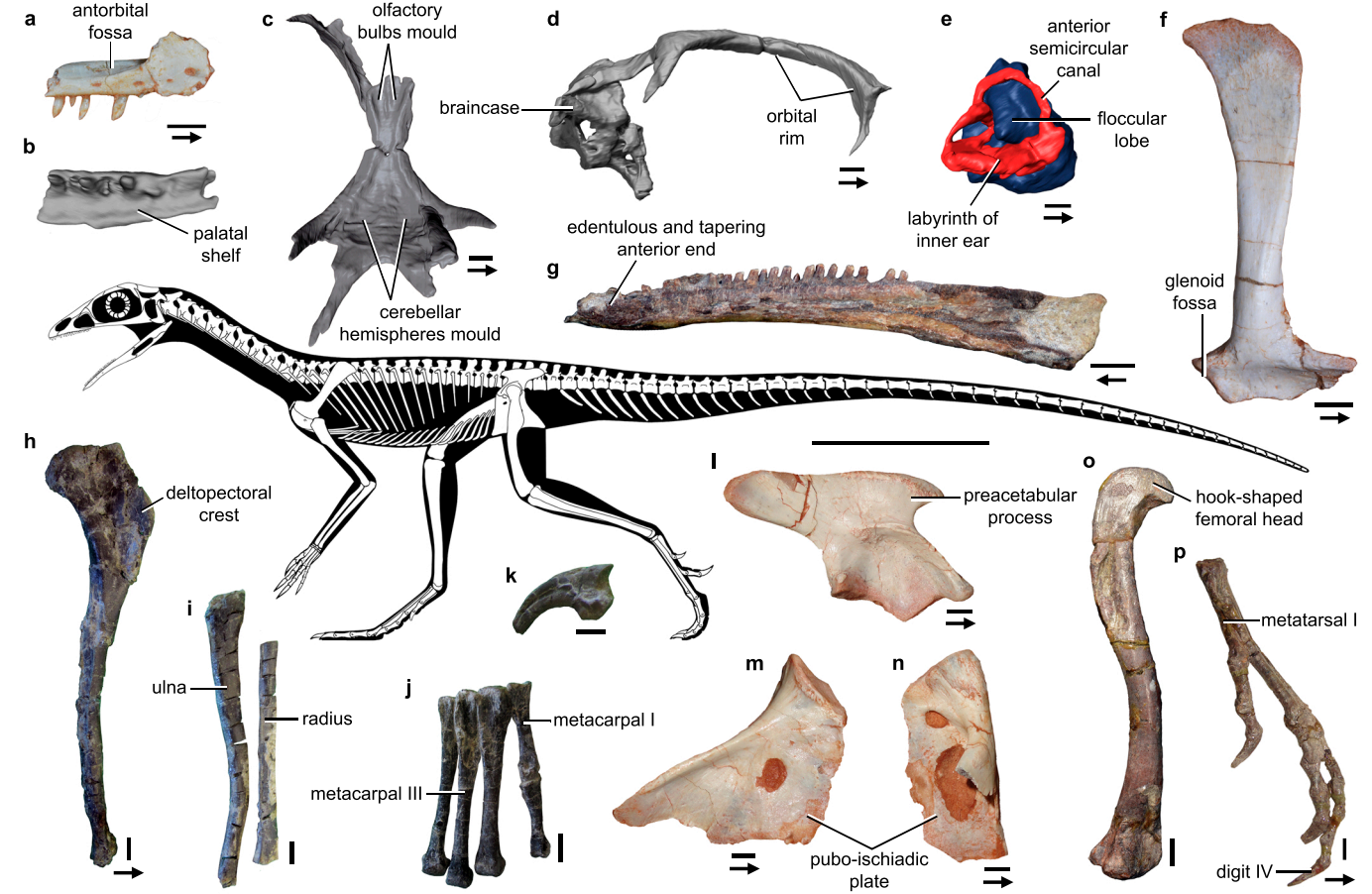
a
antorbital fossa
b
palatal shelf
c
olfactory bulbs mould
braincase
cerebellar hemispheres mould
d
orbital rim
e
anterior semicircular canal
floccular lobe
labyrinth of inner ear
f
glenoid fossa
g
edentulous and tapering anterior end
h
deltopectoral crest
i
ulna
radius
j
metacarpal I
metacarpal III
k
l
preacetabular process
m
n
pubo-ischiadic plate
o
hook-shaped femoral head
p
metatarsal I
digit IV

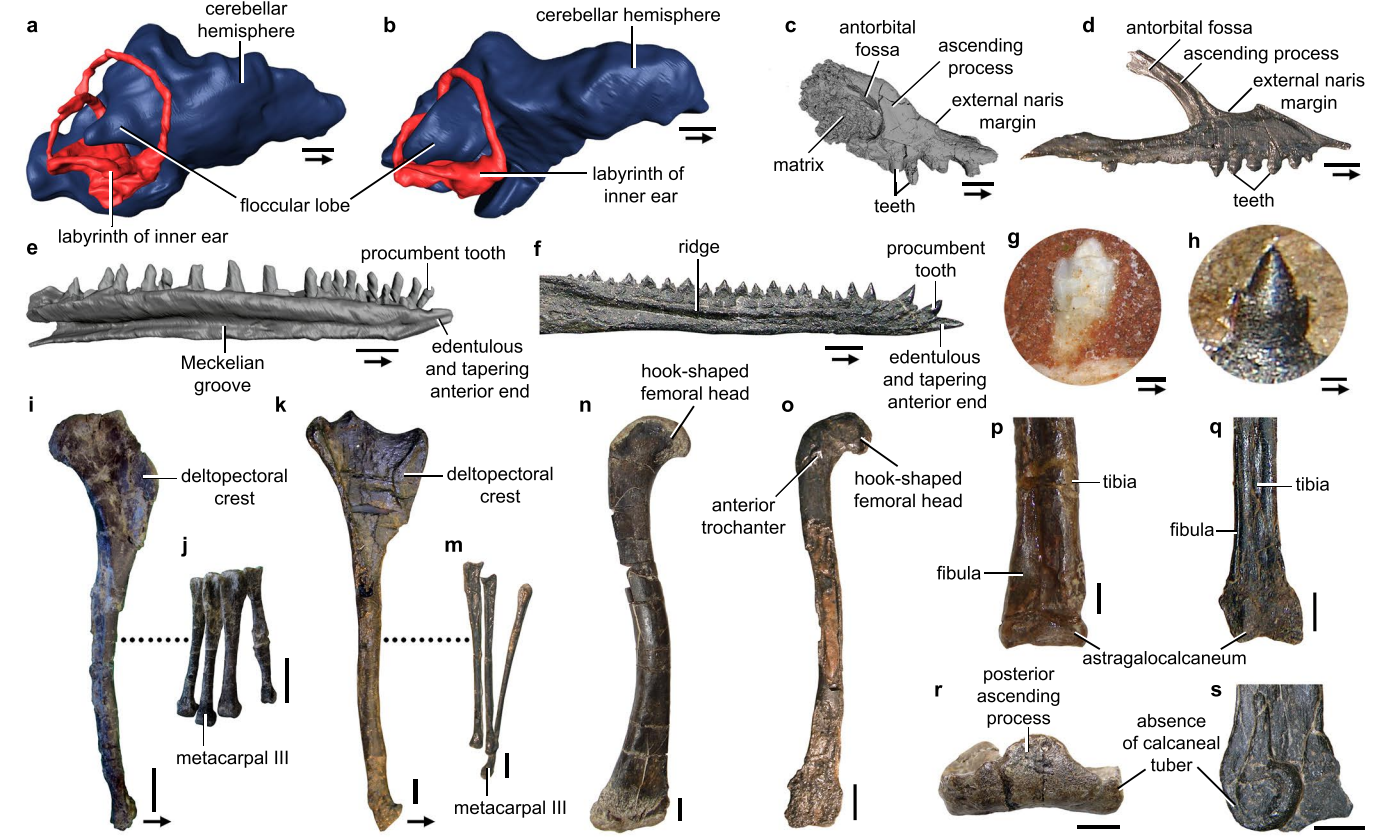
a
cerebellar hemisphere
floccular lobe
labyrinth of inner ear
b
cerebellar hemisphere
labyrinth of inner ear
c
antorbital fossa
ascending process
external naris margin
matrix
teeth
d
antorbital fossa
ascending process
external naris margin
teeth
e
procumbent tooth
Meckelian groove
edentulous and tapering anterior end
f
ridge
procumbent tooth
edentulous and tapering anterior end
g
h
i
deltopectoral crest
j
metacarpal III
k
deltopectoral crest
m
metacarpal III
n
hook-shaped femoral head
o
anterior trochanter
hook-shaped femoral head
p
tibia
fibula
q
tibia
fibula
astragalocalcaneum
r
posterior ascending process
s
absence of calcaneal tuber

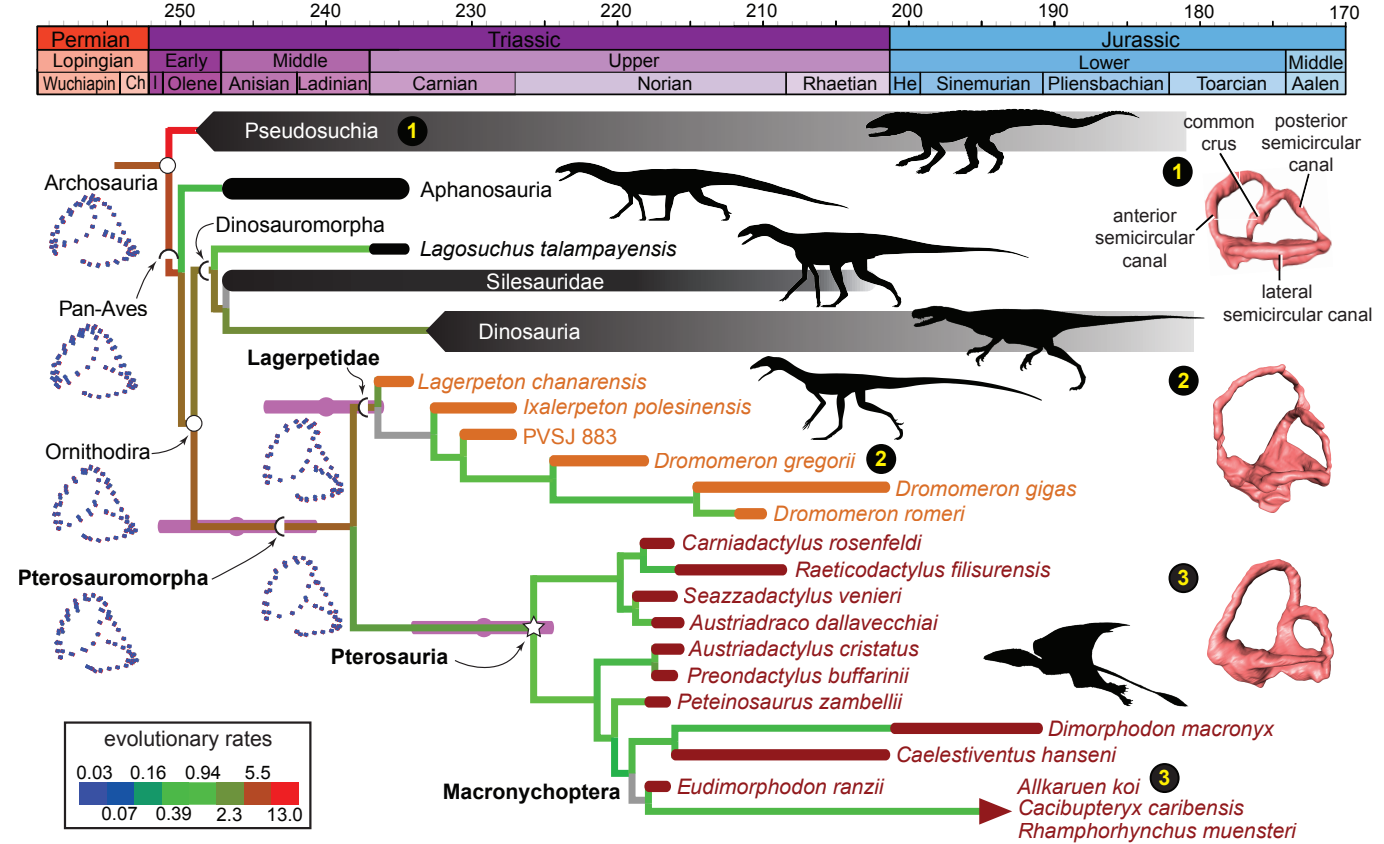
250
240
230
220
210
200
190
180
170
Permian
Triassic
Jurassic
Lopingian
Early
Middle
Upper
Lower
Middle
Wuchiapin
Ch
I
Olene
Anisian
Ladinian
Carnian
Norian
Rhaetian
He
Sinemurian
Pliensbachian
Toarcian
Aalen
Pseudosuchia
1
Archosauria
Aphanosauria
Dinosauromorpha
Lagosuchus talampayensis
Pan-Aves
Silesauridae
Dinosauria
Lagerpetidae
Lagerpeton chanarensis
Ixalerpeton polesinensis
PVSJ 883
Ornithodira
Dromomeron gregorii
2
Dromomeron gigas
Dromomeron romeri
Pterosauromorpha
Carniadactylus rosenfeldi
Raeticodactylus filisurensis
Seazzadactylus venieri
Austriadraco dallavecchiai
Austriadactylus cristatus
Preondactylus buffarinii
Pterosauria
Peteinosaurus zambellii
Dimorphodon macronyx
Caelestiventus hanseni
Macronychoptera
Eudimorphodon ranzii
3
Allkaruen koi
Cacibupteryx caribensis
Rhamphorhynchus muensteri
evolutionary rates
0.03
0.16
0.94
5.5
0.07
0.39
2.3
13.0
common crus
posterior semicircular canal
anterior semicircular canal
lateral semicircular canal
1
2
3

SUPPLEMENTARY INFORMATION

Enigmatic dinosaur precursors bridge the gap to the origin of Pterosauria

Martín D. Ezcurra, Sterling J. Nesbitt, Mario Bronzati, Fabio M. Dalla Vecchia, Federico L. Agnolin, Roger B. J. Benson, Federico Brissón Egli, Sérgio F. Cabreira, Serjoscha W. Evers, Adriel R. Gentil, Randall B. Irmis, Agustín G. Martinelli, Fernando E. Novas, Lúcio Roberto da Silva, Nathan D. Smith, Michelle R. Stocker, Alan H. Turner, Max C. Langer

Contents

1. Institutional abbreviations

AM, Albany Museum, Grahamstown, South Africa; AMNH, American Museum of Natural History, New York, New York, USA; BNM, Bündner Naturmuseum of Chur, Grisons, Switzerland; BP, Evolutionary Studies Institute (formerly Bernard Price Institute for Palaeontological Research), University of the Witwatersrand, Johannesburg, South Africa; BYU, Museum of Paleontology, Brigham Young University, Provo, Utah; CAPPA/UFSM, Centro de Apoio à Pesquisa Paleontológica da Quarta Colônia da Universidade Federal de Santa Maria, São João do Polêsine, Brazil; CM, Carnegie Museum of Natural History, Pittsburgh, Pennsylvania, USA; CRILAR-Pv, Centro Regional de Investigaciones y Transferencia Tecnológica de La Rioja, Paleontología de Vertebrados, Anillaco, La Rioja, Argentina; DMNH, Denver Museum of Natural History, Denver, Colorado, USA; GR, Ruth Hall Museum of Paleontology, Ghost Ranch, Abiquiu, New Mexico, USA; IGO, Museo Mario Sánchez Roig, Instituto de Geología y Paleontología, La Habana, Cuba; ISIR, Indian Statistical Institute, Reptiles, Kolkata, India; IVPP, Institute of Vertebrate Paleontology and Paleoanthropology, Beijing, China; HMN, Museum für Naturkunde der Humboldt Universität, Berlin, Germany; MCNAM, Museo de Ciencias Naturales y Antropológicas de Mendoza (J. C. Moyano), Mendoza, Argentina; MCSNB, Museo Civico di Scienze Naturali ‘E. Caffi’, Bergamo, Italy; MCP, Museu de Ciências e Tecnologia da Pontifícia Universidade Católica do Rio Grande do Sul, Porto Alegre, Brazil; MCZ, Museum of Comparative Zoology, Cambridge, Massachusetts, USA; MFSN, Museo Friulano di Storia Naturale, Udine, Italy; MGC SC, Museo Geologico della Carnia - Italian State Collections, Ampezzo, Italy; MNA, Museum of Northern Arizona, Flagstaff, Arizona, USA; MNHN, Muséum national d'Histoire naturelle, Paris, France; MPEF, Museo Paleontológico Egidio Feruglio, Trelew, Argentina; MPUM, Museo Paleontologico del

Dipartimento di Scienze della Terra, Università di Milano, Milano, Italy; NHMB (or QG in Raath, 1969, 1977), Natural History Museum of Zimbabwe, Bulawayo, Zimbabwe; NHMUK PV, The Natural History Museum, Palaeontology Vertebrates, London, UK; NHMW, Naturhistorisches Museum Wien, Vienna, Austria; NMMNH, New Mexico Museum of Natural History and Science, Albuquerque, New Mexico, USA; NMQR, National Museum, Bloemfontein, South Africa; NMT, National Museum of Tanzania, Dar es Salaam, Tanzania; PIMUZ, Paläontologisches Institut und Museum der Universität Zürich, Zurich, Switzerland; PIN, Paleontological Institute of the Russian Academy of Sciences, Moscow, Russia; PULR, Paleontología, Museo de Ciencias Naturales, Universidad Nacional de La Rioja, La Rioja, Argentina; PVL, Paleontología de Vertebrados, Instituto Miguel Lillo, San Salvador de Tucumán, Argentina; PVSJ, División de Paleontología de Vertebrados del Museo de Ciencias Naturales y Universidad Nacional de San Juan, San Juan, Argentina; SAM-PK, Iziko South African Museum, Cape Town, South Africa; SHYMS, Shropshire Museums, Ludlow, UK; SMNS, Staatliches Museum für Naturkunde Stuttgart, Stuttgart, Germany; SNSB-BSPG, Staatliche Naturwissenschaftliche Sammlungen Bayerns-Bayerische Staatssammlung für Paläontologie und Geologie, Munich, Germany; TMM, Texas Vertebrate Paleontology Collections, The University of Texas at Austin, Austin, Texas, USA; TTUP, Texas Tech University Paleontology Collections, Lubbock, Texas, USA; UA, University of Antananarivo, Antananarivo, Madagascar; UCMP, University of California Museum of Paleontology, Berkeley, California, USA; UFSM, Universidade Federal do Rio Grande do Sul, Porto Alegre, RS, Brazil; ULBRA, Museu de Ciências Naturais, Universidade Luterana do Brasil, Canoas, Brazil; USNM, National Museum of Natural History (formerly United States National Museum), Smithsonian Institution, Washington, D.C., USA; WTAMU, West Texas A&M University, Canyon, Texas,

USA; YPM, Yale Peabody Museum, New Haven, Connecticut, USA; ZAR, Muséum national d'Histoire naturelle (Zarzaitine collection), Paris, France; ZPAL, Institute of Paleobiology of the Polish Academy of Sciences, Warsaw, Poland.

2. Systematic Palaeontology

Archosauria Cope, 1869 [Gauthier and Padian, 2020]

Phylogenetic definition. The smallest crown clade containing *Alligator* (originally *Crocodilus*) *mississippiensis* (Daudin, 1802) (Crocodylia) and *Compsognathus longipes* Wagner, 1859 (Dinosauria).

Obs: this definition of Archosauria is taken from "Phylonyms: a companion to the PhyloCode" (de Queiroz et al., 2020).

Pan-Aves Gauthier and de Queiroz, 2001 [this work]

Phylogenetic definition. The most inclusive clade containing *Vultur gryphus* Linnaeus, 1758 (Aves), but not *Crocodylus niloticus* Laurenti, 1768 (Crocodylia).

Obs. 1: this newly proposed definition of Pan-Aves is modified after that originally prosposed by Gauthier and de Queiroz (2001).

Obs. 2: as defined here and based on the current phylogenetic orthodoxy (as implied and represented by the hypothesis of relationships depicted in Extended Data Fig. 4), Pan-Aves is equally inclusive as Ornithosuchia Huene, 1908 and Avemetatarsalia Benton, 1999, as originally defined on phylogenetic nomenclature grounds by Gauthier (1986) and Benton (1999), respectively.

Ornithodira Gauthier, 1986 [this work]

Phylogenetic definition. The least inclusive clade containing *Compsognathus longipes* Wagner, 1859 (Dinosauria) and *Pterodactylus* (originally *Ornithocephalus*) *antiquus* (Sömmerring, 1812) (Pterosauria), but not *Alligator* (originally *Crocodilus*) *mississippiensis* (Daudin, 1802) (Crocodylia).

Obs: this newly proposed definition of Ornithodira is modified after that originally prosposed by Sereno (1991), with the exclusion of *Scleromochlus* as a specifier and the selection of species-level specifiers, instead of 'Pterosauria' and 'Dinosauromorpha' (including birds), so that Ornithodira forms a node-stem triplet with Dinosauromorpha and Pterosauromorpha.

Pterosauromorpha Padian, 1997 [Andres and Padian, 2020]

Phylogenetic definition. The clade consisting of *Pterodactylus* (originally *Ornithocephalus*) *antiquus* (Sömmerring, 1812) (Pterosauria) and all organisms or species that share a more recent common ancestor with it than with *Alligator* (originally *Crocodilus*) *mississippiensis* (Daudin, 1802) (Crocodylia) and *Compsognathus longipes* Wagner, 1859 (Dinosauria).

Obs: this definition of Pterosauromorpha is taken from "Phylonyms: a companion to the PhyloCode" (de Queiroz et al., 2020)

Lagerpetidae Arcucci, 1986 [this work]

Phylogenetic definition: The most inclusive clade containing *Lagerpeton chanarensis* Romer, 1971a, but not *Eudimorphodon ranzii* Zambelli, 1973, *Silesaurus opolensis* Dzik, 2003, and *Vultur gryphus* Linnaeus, 1758.

Obs: this newly proposed definition of Lagerpetidae is modified after that originally proposed by Nesbitt et al. (2009a), with the exclusion (for conciseness) of *Alligator*

mississippiensis (Daudin, 1802), '*Marasuchus lilloensis*' Romer, 1972a, *Triceratops horridus* Marsh, 1889, and *Saltasaurus loricatus* Bonaparte and Powell, 1980 as external specifiers, and the use – for consistency with the definition of Aves in Phylonyms (Clarke et al., 2020) – of *Vultur gryphus* Linnaeus, 1758 instead of *Passer domesticus* Linnaeus, 1758 as an external specifer.

Lagerpeton chanarensis Romer, 1971a

Holotype. PULR 06, articulated right hindlimb (Romer, 1971a).

Referred specimens. PVL 4619, articulated sacrum, pelvis, and partial right and left hindlimbs; PVL 4625, articulated right prefrontal and frontal, articulated dentaries, articulated vertebral column including middle-posterior dorsal, sacral, and anterior caudal vertebrae, left scapula, left and right hemipelves, and left femur and tibia; MCZ 4121: partial right and left femora (modified from Sereno and Arcucci, 1994b). Here we added new data on cranial bones and scapula of PVL 4625 after mechanical repreparation of the specimen (see below).

Horizon and locality. PULR 06 comes from approximately 4 kilometres east of the Los Chañares locality, exposed on the northern flank of the north branch of the Chañares River. MCZ 4121 was collected from the Los Chañares locality (associated to the holotype of *Lewisuchus admixtus* and a *Massetognathus* specimen), while there is no precise information on provenance of PVL 4619 and 4625 (Sereno and Arcucci, 1994b). All these specimens were collected in the Talampaya National Park, La Rioja Province, Argentina, from the lower member of the Chañares Formation (*Massetognathus-Chanaresuchus* Assemblage Zone, early Carnian, c. 236−234 Ma, Late Triassic), Ischigualasto-Villa Unión Basin (Ezcurra et al., 2017).

Ixalerpeton polesinensis Cabreira et al., 2016

Holotype. ULBRA-PVT059, partially articulated skeleton including partial right maxilla, right prefrontal, both frontals, postfrontals and parietals, left laterosphenoid, braincase, both dentaries, 23 presacral, two sacral, and nine caudal vertebrae, right scapula, left humerus, pelvic girdle, femora, tibia, and fibula (modified from Cabreira et al., 2016). Here we newly referred the maxilla, prefrontal, and dentaries to ULBRA-PVT059 following a revaluation of the specimens preserved in the block of rock where it was found, which also includes the holotype of *Buriolestes schultzi* and an undescribed small dinosaur.

Horizon and locality. Buriol ravine (29°39′34.2″S; 53°25′47.4″W), São João do Polêsine, Rio Grande do Sul, Brazil (Cabreira et al., 2016; Müller et al., 2018); Alemoa Member of the Santa Maria Formation, lower part of the Candelária Sequence, Paraná Basin (Horn et al., 2014). The locality yielded taxa that allow its assignment to the *Hyperodapedon* Assemblage Zone, the rocks of which, from another site, were dated in c. 233 Ma, middle Carnian, Late Triassic (Langer et al., 2018).

Dromomeron romeri Irmis et al., 2007

Holotype. GR 218, complete left femur (Irmis et al., 2007).

Paratypes. GR 219, right femur; GR 220, left tibia; GR 221, partial left femur; GR 234, complete right femur; GR 222, complete left tibia; GR 223, complete astragalocalcaneum. GR 219 and 220 may belong to the same individual as the holotype (Irmis et al., 2007).

Referred specimens. GR 238, partial articulated skeleton; GR 239, isolated right tibia (cnemial crest crushed); NMMNH P-35379, complete astragalocalcaneum; AMNH FR 2721, distal portion of femur; AMNH FR 30648, distal portion of right tibia; AMNH

FR 30649, distal portion of a right tibia (Nesbitt et al., 2009a); MNA V7237, partial left astragalus (Marsh, 2018); GR 1036−1039, four femora (Griffin et al., 2019); DMNH EPV.54826, proximal half of left femur (Martz and Small, 2019); TTUP 12537X, proximal end of right tibia, WTAMU-V-8301, proximal end of right femur (Sarigül, 2016). Here we added new data on the partial skeleton GR 238 (see below).

Two specimens previously referred to *D. romeri* (DMNH EPV.63873, 29956; Martz and Small, 2019) are not considered here as part of the hypodigm because they lack autapomorphies or a unique combination of apomorphies diagnostic of the species. In addition, the morphology of the deltopectoral crest of DMNH EPV.29956 considerably differs from that of GR 238, suggesting it may correspond to a different taxon.

Horizons and localities. Holotype and paratypes come from Site 3, Hayden Quarry, Ghost Ranch, Rio Arriba County, New Mexico, USA (lower portion of the Petrified Forest Member of the Chinle Formation). The referred NMMNH specimen is from the nearby Snyder Quarry, located stratigraphically higher within the Petrified Forest Member. AMNH FR 30648 and 30649 are from the same general area as the other quarries, near Arroyo Seco, and are most likely from the Petrified Forest Member, although the exact provenance is unclear. MNA V7237 is from Ward Terrace, Badger Spring, Arizona (Owl Rock Member of the Chinle Formation). DMNH EPV.54826 is from Main Elk Creek, northern Colorado, USA ('red siltstone member' of the Eagle Basin Chinle Formation). The TTUP specimen is from the lower unit of the Cooper Canyon Formation of the Dockum Group, and the WTAMU specimen is from the Tecovas Formation of the Dockum Group. The hypodigm of *D. romeri* ranges from early Norian (stratigraphically lower beds have been dated in c. 225 Ma, Petrified Forest

Member) to early Rhaetian (stratigraphically lower beds have been dated in c. 208 Ma, Owl Rock Member) (Marsh, 2018).

Dromomeron gregorii Nesbitt et al., 2009a

Holotype. TMM 31100-1306, complete right femur (Nesbitt et al., 2009a).

Paratypes. TMM 31100-464, right femur; TMM 31100-1308, right femur; TMM 31100-1234, right femur; TMM 31100-764, right femur; TMM 31100-278, right tibia; TMM 31100-1314, left tibia (Nesbitt et al., 2009a).

Referred specimens. UCMP 25815, distal portion of a left femur (Nesbitt et al., 2009a); TMM 31100-1334, partial skull roof and braincase, and associated vertebrae (Stocker, 2013). Here we added new data on the latter specimen (see below); TTUP 11282, left femur, TTUP 18331, proximal end of left femur, TTUP 20046, distal end of left femur, WTAMU-V-8302, proximal end of right femur, WTAMU-V-8303, proximal end of right tibia (Sarigül, 2016).

Horizon and locality. TMM specimens are from the Otis Chalk Quarry 3 (TMM locality 31100), near Otis Chalk, Texas, USA; Colorado City Formation of the Dockum Group. The UCMP specimen is from the *Placerias* Quarry, near St. Johns, Arizona (UCMP locality A269), stratigraphically near the base of the Chinle Formation, possibly within the Mesa Redondo Member (Nesbitt et al., 2009a). The TTUP specimens are from the lower unit of the Cooper Canyon Formation of the Dockum Group and WTAMU specimens are from the Tecovas Formation of the Dockum Group (Sarigül, 2016). These specimens came from lower to middle Norian rocks, ranging c. 225−219 Ma (Marsh, 2018).

Dromomeron gigas Martínez et al., 2016

Holotype. PVSJ 898, proximal and distal portions of a left femur, lacking the mid-shaft and most of the medial condyle of the distal end (Martínez et al., 2016).

Horizon and locality. 'Quebrada del Puma' locality, Caucete Department, San Juan Province, Argentina; southern outcrops of the Quebrada del Barro Formation (late Norian-Rhaetian), Marayes-El Carrizal Basin (Martínez et al., 2016).

Dromomeron sp. indet.

Specimens. NMMNH P-3034, proximal end of left femur; NMMNH P-18092, distal end of right femur; NMMNH P-18091, distal end of left femur; NMMNH P-18079 and NMMNH P-18012, proximal ends of right and left tibiae, and may belong to the same individual; NMMNH P-18073, distal end of left tibia; NMMNH P-80469, proximal portion of left fibula; NMMNH P-80470, distal end of right fibula; NMMNH P-80471, proximal region of right metatarsal II; NMMNH P-80472, distal region of metatarsal II; NMMNH P-80473, distal region of metatarsal III or IV; NMMNH P-80474, distl portion of pedal element; NMMNH P-80475, pedal phalanx (Beyl et al., 2020).

Horizon and locality. NMMNH locality 149, New Mexico, USA; Los Esteros Member of the Santa Rosa Formation (Otischalkian, late Carnian-earliest Norian, early Late Triassic), base of the Dockum Group, Tucumcari Basin (Beyl et al., 2020).

Kongonaphon kely Kammerer et al., 2020

Holotype. UA 10618, right maxilla, distal portion of humerus, right femur lacking the distal tip, proximal portions of right and left tibia, proximal portion of fibula, possible two metatarsals, metatarsal II articulated to a pedal phalanx, an additional phalanx, a caudal vertebra, and indeterminate skeletal fragments (Kammerer et al., 2020).

Horizon and locality. Toliara, southwestern Madagascar; Basal Isalo II deposits or Makay Formation (close to the Ladinian-Carnian boundary, Middle-Late Triassic), Morondava Basin.

Lagerpetidae gen. et sp. indet.

Specimens. PVSJ 883, distal end of left femur; UFSM 11611, distal portion of left femur.

Horizons and localities. PVSJ 883 comes from the Valle Pintado locality, Ischigualasto Provincial Park, San Juan Province, Argentina; La Peña Member of the Ischigualasto Formation (*Scaphonyx-Exaeretodon-Herrerasaurus* biozone, middle third of the Carnian, stratigraphically close to a 231.4 ± 0.3 Ma level, late Carnian, Late Triassic), Ischigualasto-Villa Unión Basin (Martínez et al., 2013). UFSM 11611 comes from the Cerro da Alemoa site, Rio Grande do Sul, Brazil (Garcia et al., 2019); sediments of the site belong to the Alemoa Member of the Santa Maria Formation (base of the Candelária Sequence, Paraná Basin; Horn et al. 2014), within the *Hyperodapedon Assemblage* Zone, and were dated in 233.23 ± 0.73 Ma, middle Carnian, Late Triassic (Langer et al., 2018).

3. Rationale for the assignment of the new lagerpetid bones

The specimen PVL 4625 is referred to the Argentinian lagerpetid *Lagerpeton chanarensis* (see Sereno and Arcucci, 1994b) and was partially prepared and exposed only on the left side in its original plaster jacket. This specimen was requested on loan and mechanically reprepared in the facilities of the Laboratorio de Anatomía Comparada y Evolución de los Vertebrados of the Museo Argentino de Ciencias Naturales (Buenos Aires, Argentina) during 2018. This additional preparation not only

exposed the already visible and articulated middle-posterior dorsal, sacral, and anterior caudal vertebrae, left hemipelvis, and femur, but also the articulated right hemipelvis, various bones not articulated to these elements, and at least one associated and articulated proterochampsid.

The bones that are not articulated to the main part of the postcranium of PVL 4625 (articulated right prefrontal and frontal, articulated dentaries, and left scapula) differ from those of proterochampsids (e.g. *Chanaresuchus bonapartei*: PULR 07, PVL 4575, MCZ 4035, 4037; *Gualosuchus reigi*: PULR 05, PVL 4576; *Tropidosuchus romeri*: PVL 4601, 4604, 4606; *Proterochampsa barrionuevoi*: PVSJ 77, 606) in the following features: the prefrontal is poorly developed laterally and lacks ornamentation on its dorsal surface (contrasting with those of all proterochampsids); the frontal is more strongly bowed dorsoventrally (although similar to that of *Tropidosuchus*, but not to those of other proterochampsids) and lacks external ornamentation (contrasting with those of all proterochampsids); the dentaries possess an edentulous and tapering anterior end, subthecodont tooth implantation, tricuspid tooth crowns, and lack interdental plates (contrasting with those of all proterochampsids); and the scapular blade is proportionally longer and more posteriorly expanded at its distal end (contrasting with those of all proterochampsids), with the proximal part of the bone lacking the strongly laterally developed acromion process present in most proterochampsids (with the exception of *Tropidosuchus*). As a result, we consider that these bones do not belong to the associated proterochampsid and their morphology also differs from that of other archosauriforms of the Chañares Formation (e.g. *Lewisuchus admixtus*, *Lagosuchus talampayensis*, *Gracilisuchus stipanicicorum*). By contrast, the morphology of the prefrontal, frontal, and scapula closely resembles that of *Ixalerpeton*, and the size of the prefrontal, frontal, dentaries, and scapula match that expected for an individual of the

size of the articulated parts of PVL 4625. Therefore, we consider that there is strong evidence to assign these bones to the *Lagerpeton* specimen PVL 4625.

As for the articulated dentaries, their unusual morphology among archosauromorphs led us at first to consider the possibility that they could belong to a new taxon, rather than to *Lagerpeton*. Yet, at approximately the same time, we were reevaluating the pair of dentaries now associated to the holotype of *Ixalerpeton polesinensis* (ULBRA-PVT059), which are extremely similar to those associated with PVL 4625 in their edentulous and tapering anterior end, a slightly downturned anterior portion, tricuspid tooth crowns, and no interdental plates. In fact, these shared character states were also key for determining that the pair of dentaries found together with the *Ixalerpeton* holotype also belonged to ULBRA-PVT059. This is because disarticulated remains of a small dinosaur were also found in the same block and the dentaries could (based on relative size and lack of articulation) also potentially belong to that specimen. However, dentaries with a combination of an edentulous, tapering, and slightly downturned anterior end are unknown in any early dinosaur, which also lack tricuspid tooth crowns. Furthermore, the dentaries now associated with ULBRA-PVT059 and the previously identified skeletal parts of that specimen match the relative sizes of the bones of PVL 4625. In sum, we consider that the presence of dentaries with the same, very unusual morphology associated to specimens of both *Lagerpeton* and *Ixalerpeton* is strong evidence that they belong to these lagerpetid specimens.

The partial maxilla associated to *Ixalerpeton* resembles the dentaries of this taxon and *Lagerpeton* in the presence of tooth crowns with convex mesial and distal margins, subthecodont tooth implantation, and no interdental plates. In addition, the 3D model generated from the μCT scan data shows the presence of an extensive and broad palatal shelf on the medial surface of the maxilla (Fig. 1b), closely resembling the

condition present in the Malagasy lagerpetid *Kongonaphon* (Kammerer et al., 2020), whereas a similar condition is absent in other non-crocodylomorph archosauromorphs and may represent an apomorphy of Lagerpetidae. The Brazilian partial maxilla matches the relative sizes of the dentaries and other bones of the *Ixalerpeton* holotype, as it would be expected for a single individual. In conclusion, we consider that this maxilla can be assigned to the holotype of *Ixalerpeton* (ULBRA-PVT059).

An isolated right prefrontal is preserved next to the braincase of the holotype of *Ixalerpeton*. It is mostly covered with matrix, but was prepared digitally using the μCT scan data. This prefrontal (1) closely resembles the morphology of that associated to the referred specimen of *Lagerpeton* PVL 4625, (2) perfectly articulates (digitally) with the frontal of the holotype of *Ixalerpeton*, and (3) matches the relative size of the other bones of that specimen, as it would be expected for a single individual. Accordingly, this prefrontal is also assigned here to the holotype of *Ixalerpeton* (ULBRA-PVT059).

The partial skull of the referred specimen of *Dromomeron gregorii* TMM 31100-1334 was originally collected by the Work Progress Administration (USA) during excavation of Otis Chalk Quarry 3 (TMM 31100) from 1939−1941 (Stocker, 2013). The specimen was found unprepared in the same drawer with the initially unprepared holotype femur of *Dromomeron gregorii* (Nesbitt et al., 2009a). It is possible that the femur may have been found with the skull, but that data is now lost. Alongside and partially connected with the skull, twelve vertebrae were also collected and their size match that of the skull. These vertebrae are nearly identical to those found with associated skeletons of *Dromomeron romeri* (see above) from the Hayden Quarry.

The skull preserves the orbital and temporal regions of the skull roof and a nearly complete and well-preserved braincase. This specimen possesses a similar morphology in the areas that overlap with the holotype of *Ixalerpeton*. In addition, the

cranial endocast of both specimens show the same, unique combination of character states, including the presence of a dorsoventrally large and tapering cerebellar floccular lobe and an endosseous labyrinth of the inner ear with an anterior semicircular canal considerably larger than the posterior canal. These similarities reinforce the association of the skull roof and braincase of *Ixalerpeton* to the other skeletal parts of ULBRA-PVT059 with clear lagerpetid apomorphies to which they were found closely associated (Cabreira et al., 2016), composing a single holotypic individual.

4. Additional Micro-computed tomography scanning details

The µCT scans were conducted with the following settings and resulted in the following datasets:

- The scan of the partial lower jaw of *Lagerpeton* (PVL 4625) was set at 80 kV and 100 µA, and 2,162 images were generated (voxel size = 0.01894 mm).
- The scans of the bones of *Ixalerpeton* (ULBRA-PVT059) were set at 100 kV and 120 µA. The scan of the braincase + prefrontal resulted in 705 images (voxel size = 0.0516858 mm), the skull roof in 546 images (voxel size = 0.0582229 mm), the right maxilla in 1,000 images (voxel size = 0.0606113 mm), the left dentary in 1,000 images (voxel size = 0. 0341517 mm), and the right dentary in 1,000 images (voxel size = 0.0268455 mm).
- The scan of the braincase of *D. gregorii* (TMM 31100-1334) was set at 210 kV and 120 µA, and 581 images were generated (voxel size = X axis 0.02832 mm, Y axis 0.02832 mm, Z axis 0.06136 mm).

5. Results of the phylogenetic analyses

The analysis of the modified version of the data matrix of Ezcurra (2016) (as modified by subsequent authors; see Methods) found 280 most parsimonious trees (MPTs) with a length of 5,002 steps and consistency index (CI) of 0.21431 and retention index (RI) of 0.65014. The general topology of the strict consensus tree (Extended Data Fig. 4) is completely congruent with that recovered by other recent analyses of this dataset (Butler et al., 2019; Ezcurra et al., 2019) and will not be further discussed here. Regarding the newly added taxa, we recovered ornithischians (*Heterodontosaurus* and *Lesothosaurus*) as the sister taxon to Saurischia (Sauropodomorpha + Theropoda). The middle-late Carnian *Buriolestes*, *Saturnalia* and *Eoraptor* compose Sauropodomorpha, whereas *Herrerasaurus* (late Carnian) and *Tawa* (middle Norian) are found as sucessive sister taxa to Neotheropoda (*Megapnosaurus* + *Coelophysis*). The Bremer support values are 2 for Pan-Aves and its most diverse branches (Ornithodira, Pterosauromorpha, Pterosauria, Dinosauromorpha/Dinosauriformes, Dracohors, Dinosauria, Saurischia, and Theropoda). Silesauridae and Ornithischia have particularly high Bremer values of 4. The absolute bootstrap frequencies are higher than 50%, and equal to or higher than 80% for Pan-Aves, Ornithodira, Pterosauromorpha, Lagerpetidae, Pterosauria, Dinosauromorpha/Dinosauriformes, Dracohors, Dinosauria, Ornithischia, Saurischia, Sauropodomorpha, and Neotheropoda. In particular, the absolute bootstrap frequencies are very high (≥ 80%) for Pterosauromorpha, Pterosauria, Ornithischia, Saurischia, and Neotheropoda, and the difference between absolute and GC bootstrap frequencies is lower than 10% for all these latter branches. A small difference between absolute and GC frequencies indicates a small amount of contradictory phylogenetic signal for the given branch (Goloboff et al., 2003). In this regard, none of the character states optimized as ornithodiran synapomorphies are recovered as pterosaur apomorphic reversals. This indicates the absence of a considerable amount of underlying

372 phylogentic signal in support for the historic placement of pterosaurs as the sister taxon
373 to a Dinosauromorpha including lagerpetids.

374 The relatively low Bremer support values for most of the pan-avian branches are
375 probably the result of a few taxa that become unstable in suboptimal topologies. We
376 used the iterPCR protocol (Pol and Escapa, 2009) to detect these unstable taxa in a
377 sample of suboptimal trees. *Dongusuchus*, *Spondylosoma*, and PVSJ 883 were
378 recovered as unstable taxa within Pan-Aves and the Bremer supports were recalculated
379 after their a posteriori pruning. The recalculated Bremer supports increase to 3 for Pan-
380 Aves, Aphanosauria, Ornithodira, Dinosauromorpha/Dinosauriformes, and Theropoda,
381 and to 4 for Pterosauromorpha, Lagerpetidae, Dracohors, Silesauridae, Dinosauria,
382 Saurischia, and Sauropodomorpha (Extended Data Fig. 5). In particular, the Bremer
383 support of Pterosauria increases to 5.

384 As discussed in the main text, the sister taxon relationship between pterosaurs
385 and lagerpetids is the most interesting result of our new analysis. The phylogenetic
386 relationships within Lagerpetidae are poorly resolved in the strict consensus tree as a
387 result of the alternative positions that *Kongonaphon* acquires among the MPTs. This
388 agrees with a recent analysis that included this species (Kammerer et al., 2020) and
389 when this taxon is excluded a posteriori from the strict consensus tree, the
390 interrelationships among lagerpetids are fully resolved and consistent with previous
391 analyses (Müller et al., 2018). By contrast, the interrelationships among pterosaurs
392 differ from those found by recent analyses, but it is true that the most recent analyses
393 have also recovered different topologies among early pterosaurs, which is probably the
394 result of different taxon and character samplings (e.g. Dalla Vecchia, 2009a, b; Wang et
395 al., 2009; Andres et al., 2010, 2014; Lü et al., 2012; Codorniú et al., 2016; Britt et al.,
396 2018; Dalla Vecchia, 2019; see Dalla Vecchia, 2013). Our analysis found a clade

composed of (*Carniadactylus* + *Raeticodactylus*) plus (*Austriadraco* + *Seazzadactylus*) as sister to all other pterosaurs. By contrast, this position was occupied by a *Preondactylus* + *Austriadactylus* clade in the analyses of Dalla Vecchia (2009a, b, 2019), by Anurognathidae in the work of Wang et al. (2009), by *Preondactylus* (with *Austriadactylus* occupying a more deeply nested position) in the analyses of Andres et al. (2010) and Lü et al. (2012), and by a large clade composed of most of the currently known Triassic taxa in the study of Andres et al. (2014) [e.g. *Eudimorphodon*, *Carniadactylus*, *Raeticodactylus*, *Peteinosaurus*, *Austriadactylus*, *Preondactylus*; i.e. Eopterosauria; the least inclusive clade containing *Preondactylus buffarinii* Wild, 1984 and *Eudimorphodon ranzii* Zambelli, 1973 (sensu Andres et al., 2014)]. Eopterosauria is recovered here as a polyphyletic group.

The identity of the earliest branching pterosaurs has important implications in the possible optimization of character states for Pterosauromorpha and Pterosauria. As a result, we have tested if the Lagerpetidae + Pterosauria clade is still recovered in our analyses if we force the topologies recovered for Pterosauria by other authors (setting pterosaur taxa absent in those analyses as floating taxa). All these analyses recovered the lagerpetid-pterosaur clade, with the following results: the constraint following Dalla Vecchia (2009a) resulted in 280 MPTs, six steps longer than our unconstrained analysis; the constraint following Wang et al. (2009) found 280 MPTs, eleven steps longer; the constraint following Andres et al. (2010) found 420 MPTs, nine steps longer; the constraint following Lü et al. (2012) recovered 280 MPTs, eleven steps longer; the constraint with a monophyletic Eopterosauria following Andres et al. (2014) found 560 MPTs, 15 steps longer; and the constraint following Dalla Vecchia (2019) resulted in 280 MPTs, three steps longer. As a result, the close relationship between lagerpetids

421 and pterosaurs is stable in our data set regardless of which hypothesis of early pterosaur
422 interrelationships is considered.
423 It should be noted that when constraining the position of lagerpetids within
424 Dinosauromorpha (sister taxon to Dinosauriformes), the analysis recovered 280 MPTs
425 of 5,025 steps, with minor topological changes in the pterosaur interrelationships with
426 respect to the unconstrained analysis. *Austriadactylus* + *Preondactylus* are positioned as
427 the sister clade to all other Pterosauria, with *Carniadactylus* + *Raeticodactylus* and
428 *Seazzadactylus* + *Austriadraco* forming a clade sister to the remaining pterosaurs. This
429 latter topology matches that recently recovered by Dalla Vecchia (2019), where
430 lagerpetids were not included as outgroup, showing how the position of lagerpetids as
431 the sister taxon to Pterosauria affects the interrelationships at the base of the latter clade.
432 Among more deeply nested pterosaurs, our analysis recovered Preondactylia
433 (sensu Andres et al., 2014) and *Peteinosaurus* as the successive sister taxa to
434 Macronychoptera (sensu Unwin, 2003). Dimorphodontidae (*Dimorphodon* +
435 *Caelestiventus*) is the sister taxon to Lonchognatha (sensu Unwin, 2003). *Allkaruen* and
436 *Cacibupteryx* have been recovered closer to *Rhamphorhynchus* than to *Eudimorphodon*
437 and non-lonchognathan pterosaurs, in agreement with a recent analysis that included
438 these taxa (Codorniú et al., 2016). However, here we recovered *Allkaruen* closer to
439 *Rhamphorhynchus* than the latter to *Cacibupteryx*, contrasting with the result of
440 Codorniú et al. (2016). This difference of results is probably because of the poor sample
441 of lonchognathan taxa in our analysis. The interrelationships of Pterosauria are
442 relatively poorly supported in our analysis, with minimal Bremer support values for all
443 its branches with the exception of the *Seazzadactylus* + *Austriadraco* clade and
444 Dimorphodontidae, which have Bremer support values of 2. The absolute bootstrap
445 frequencies are below 50% for all the branches with the exception of the *Austriadraco* +

Seazzadactylus clade, Preondactylia, Dimorphodontidae, and the *Cacibupteryx* + (*Rhamphorhynchus* + *Allakaruen*) clade. The a posteriori pruning of the three unstable taxa mentioned above resulted in an increase of Bremer support value only for Dimorphodontidae, from 2 to 3.

The list of synapomorphies of Pan-Aves and its internal clades is as follows:

Pan-Aves

All trees:

Char. 67: 0 --> 1. Maxilla, palatal process distinctly dorsally to the ventral margin of the medial surface of the maxilla or base of the interdental plates if they are present.

Char. 386: 1 --> 2. Scapula-coracoid, glenoid fossa orientation posteroventral.

Char. 387: 0 --> 1. Scapula, total length of the scapula versus minimum anteroposterior width of the scapular blade ratio = 7.92−11.31.

Char. 458: 1 --> 0. Ilium, maximum height of the acetabulum versus length of the femur ratio ≤0.17.

Char. 460: 1 --> 2. Ilium, preacetabular process longer than two thirds of its height and not extending beyond the level of the anterior margin of the pubic peduncle.

Char. 462: 0 --> 2. Ilium, lateral crest dorsal to the supraacetabular crest/rim confluent with the anterior extent of the preacetabular process.

Char. 466: 1 --> 0. Ilium, dorsal margin of the iliac blade convex.

Char. 502: 0 --> 1. Femur, anterior trochanter (= lesser or minor trochanter) (= iliofemoralis cranialis muscle insertion) present and forms a steep margin with the shaft but is completely connected to it.

Char. 602: 0 --> 1. Scapula, posterior edge of the blade just dorsal to the glenoid region with a distinct, longitudinal sharp ridge.

Char. 603: 0 --> 1. Ilium, ventral portion of ischial peduncle in lateral view with distinct notch (=dorsal expansion) between the posterior and anterior ends.

Char. 604: 0 --> 1. Femur, distal end, medial condyle in posterior view with well defined proximodistally oriented scar extending from the posterior portion of the condyle well proximally.

Char. 737: 0 --> 1. Inner ear, labyrinth general proportions, maximum height of the labyrinth versus maximum anteroposterior depth of the labyrinth ratio = 0.78−0.85.

Char. 741: 0 --> 1. Inner ear, orientation of common crus posterodorsal, deviating from the vertical plane in an angle higher than 10º.

Aphanosauria

All trees:

Char. 343: 0 --> 1. Cervical vertebrae, anterior and middle postaxial cervical neural spines with an anterior overhang, anteriorly curved anterior margin of the neural spine.

Teleocrater* + *Dongusuchus* + *Yarasuchus

All trees:

Char. 512: 1 --> 2. Femur, distal articular surface, both condyles do not project distally (distal articular surface concave or almost flat).

Some trees:

Char. 356: 0 --> 1. Dorsal vertebrae, diapophysis and parapophysis in anterior dorsals expanded on stalks.

Char. 419: 1 --> 0**.** Humerus, proximal end in anterior view approximately symmetric.

Ornithodira

All trees:

Char. 342: 0 --> 1. Cervical vertebrae, shape of postaxial anterior cervical neural spines long and low, with height lower than length.

Char. 384: 1 --> 0. Scapula-coracoid, both bones fused with each other in mature individuals present, without a complete line of suture.

Char. 399: 0 --> 1. Coracoid, subglenoid lip more extended posteriorly than the supraglenoid lip on the scapula.

Char. 427: 1 --> 2. Humerus, ectepicondylar region, supinator process, groove or foramen absent.

Char. 457: 0 --> 1. Pelvic girdle, acetabular antitrochanter present.

Char. 464: 1 --> 0. Ilium, main axis of the postacetabular process in lateral or medial view posterodorsally oriented.

Char. 490: 2 --> 3. Femur, minimum transverse width versus minimum transverse width of the humerus ratio = 1.46−1.80.

Char. 499: 1 --> 0. Femur, trochanteric fossa (sensu Novas, 1996) on the ventral/posterior surface of the proximal end present.

Char. 508: 0 --> 1. Femur, bone wall thickness at or near midshaft thin, thickness/diameter <0.3.

Char. 736: 0 --> 1. Inner ear, relative position of the common crus, positioned posterior to the midpoint of the anteroposterior axis of the labyrinth.

Char. 801: 1 --> 0. Femur, medial articular facet of the proximal portion in posterior view rounded.

Pterosauromorpha

All trees:

Char. 1: 12 --> 0. Skull and lower jaws, interdental plates absent.

Char. 36: 2 --> 1. Premaxilla, postnarial process (= maxillary process) short, ends well anterior to the posterior margin of the external naris.

Char. 59: 0 --> 1. Maxilla, anterior margin of the base of the ascending process concave.

Char. 126: 1 --> 0. Postorbital-squamosal, upper temporal bar positioned distinctly ventral to the level of the dorsal border of the orbit, broadly exposing the supratemporal fenestra in lateral view.

Char. 227: 0 --> 1. Basioccipital-parasphenoid/parabasisphenoid, basal tubera partially connected.

Char. 231: 0 --> 1. Basioccipital, occipital neck absent or extremely short.

Char. 278: 0 --> 1. Dentary, teeth absent in the anterior end of the bone.

Char. 303: 0 --> 2. Teeth, distal edge of the maxillary tooth crowns in labial view convex in at least some anterior tooth crowns.

Char. 304: 2 --> 0. Teeth, serrations on the maxillary/dentary crowns absent or present in just two or a few centrally placed maxillary crowns.

Char. 448: 1 --> 0. Metacarpus, transverse width of the distal end of metacarpal I versus the total length of the bone ratio ≤ 0.33.

Char. 466: 0 --> 2. Ilium, dorsal margin of the iliac blade concave.

Char. 470: 1 --> 0. Pubis-ischium, contact present and extended ventrally up to or beyond the distal end of the pubi shaft or tubercle.

Char. 472: 2 --> 1. Pubis, total length (along anterior margin or pubic shaft or tubercle) versus total length of the femur ratio = 0.32−0.45.

Char. 476: 1 --> 3. Pubis, laterally thickened anterior edge with a proximodistally concave anterior surface.

Char. 492: 0 --> 1. Femur, femoral head distinctly inturned with respect to the shaft.

Char. 539: 0 --> 1. Astragalus, posterior groove absent.

Char. 545: 1 --> 0. Calcaneum, calcaneal tuber (= expansion of the lateral margin of the bone) absent or incipient.

Char. 606: 0 --> 1. Proximal tarsals, fusion between astragalus and calcaneum present.

Char. 694: 0 --> 1. Prootic, inferior and superior anterior processes separation between each other in lateral view closely approach or join together to form most or the entire anterior border of the trigeminal foramen (CN V).

Char. 701: 0 --> 2. Premaxilla, postnarial process (= maxillary process) contact with nasal absent.

Char. 706: 0 --> 1. Maxilla, anteroposterior width of ascending process in lateral or medial view very thin, resulting in an external naris separated from the antorbital fenestra by a strap-like bar of bone.

Char. 725: 0 --> 1. Periotic bones, dorsoventral height of the base of the floccular fossa equal to or more than 40% of the height of the cranial endocast at the level of anteroposterior mid-length of the fossa.

Char. 726: 0 --> 1. Periotic bones, shape of the lateral end of the floccular fossa tapering laterally, resulting in a subtriangular floccullar cast in anterolateral view.

Char. 737: 1 --> 2. Inner ear, labyrinth general proportions, maximum height of the labyrinth versus maximum anteroposterior depth of the labyrinth ratio > 0.90.

Char. 738: 0 --> 12. Inner ear, curvature of the anterior semicircular canal (ASC) = 1.53−2.00.

Char. 739: 0 --> 1. Inner ear, curvature of the posterior semicircular canal (PSC), PSC-arc-length versus PSC-straight-line ratio ≥ 1.20.

Char. 743: 1 --> 2. Inner ear, curvature of the lateral semicircular canal (LSC), LSC-arc-length versus LSC-straight-line ratio = 1.31−1.37.

Char. 753: 0 --> 1. Splenial, reduced to the posterior region of the hemimandible or bone absent.

Char. 763: 0 --> 1. Teeth, first dentary tooth long axis with respect to the longitudinal axis of the bone, inclined anteriorly (i.e. procumbent).

Char. 774: 0 --> 1. Humerus, shape in lateral view (dorsolateral view in pterosaurs), sigmoid.

Char. 782: 0 --> 1. Metacarpus, metacarpal III-humerus ratio ≥ 0.35.

Char. 800: 0 --> 1. Femur, profile of femoral head in medial or lateral view when it is distinctly inturned, hook-shaped.

Char. 823: 0 --> 1. Metatarsus, metatarsal V shorter than 50% of metatarsal III.

Lagerpetidae

All trees:

Char. 305: 1 --> 0. Teeth, tooth shape at crown base of the marginal dentition circular.

Char. 497: 0 --> 1. Femur, posterior tuber on the femoral head present and largest of the proximal tubera.

Char. 498: 0 --> 1. Femur, anterior tuber (= anterolateral tuber of Nesbitt, 2011) on the femoral head absent.

Char. 501: 0 --> 2. Femur, transition between femoral head and shaft with concave emargination.

Some trees:

Char. 75: 2 --> 4. Maxilla, number of tooth positions (if the maxillary tooth count is not available the character can be scored using the dentary tooth count) 23−35 (26−40 dentary tooth positions).

Char. 299: 1 --> 0. Teeth, geometry of tooth implantation subthecodont (= protothecodont).

Char. 358: 1 --> 0. Dorsal vertebrae, transverse processes in middle and posterior dorsals short.

Char. 361: 0 --> 1. Dorsal vertebrae, dorsally opened pit lateral to the base of the neural spine shallow.

Char. 368: 0 --> 1. Dorsal ribs, proximal end of middle dorsal ribs holocephalous.

Char. 514: 0 --> 1. Femur, surface between the lateral condyle and crista tibiofibularis on the distal surface with deep groove.

Char. 523: 0 --> 1. Tibia, posterior side of the distal portion with dorsoventrally oriented groove or gap.

Char. 531: 0 --> 1. Fibula, distal end in lateral view rounded or flat (symmetrical).

Char. 646: 0 --> 1. Dentary, anterior extent of the Meckelian groove present through the dentary symphysis.

Char. 700: 0 --> 1. Orbital and temporal regions, dorsal margin outline in lateral view strongly convex dorsally.

Char. 754: 0 --> 1. Teeth, nature of tooth attachment, ankylosis.

Char. 794: 0 --> 1. Ilium, position of dorsal margin concavity posteriorly displaced.

Dromomeron romeri* + *Dromomeron gigas

All trees:

Char. 803: 1 --> 0. Femur, development of attachment of muscle caudofemoralis on the posterior surface of the bone not distinct or developed as a rugose scar.

Some trees:

Char. 672: 0 --> 1. Femur, angle between the lateral condyle and the crista tibiofibularis in distal view right or acute angle as a result of the lateral expansion of the crista tibiofibularis.

Char. 806: 0 --> 1. Femur, sharp ridge on the anteromedial edge of the distal end present.

Char. 807: 0 --> 1. Femur, lateral tuberosity on the anterolateral edge of the distal end present.

Pterosauria

All trees:

Char. 54: 2 --> 0. Maxilla, antorbital fossa on the lateral surface of the bone absent or not exposed in lateral view (antorbital fossa present in *Raeticodactylus*).

Char. 247: 0 --> 3. Basisphenoid/parabasisphenoid, basipterygoid processes extremely long and rod-like, being longer than the body of the basisphenoid.

Char. 262: 1 --> 0. Lower jaw, external mandibular fenestra absent (present in *Austriadraco*).

Char. 300: 0 --> 1. Teeth, maxillary and/or dentary tooth crowns markedly heterodont (gross change in morphology).

Char. 370: 0 --> 1. Sacral vertebrae, number, three.

Char. 386: 2 --> 0. Scapula-coracoid, glenoid fossa orientation mainly lateral, being more laterally facing than posteriorly and without a posteriorly prominent supraglenoid lip in lateral view.

644 Char. 390: 1 --> 0. Scapula, anterior margin of the scapular blade in lateral view
645 straight or convex along entire length.
646 Char. 414: 1 --> 2. Forelimb-hindlimb, length ratio = 1.5−3.0.
647 Char. 428: 1 --> 0. Humerus, capitellum (radial condyle) and trochlea (ulnar
648 condyle) developed as strongly convex structures distinct from the ectepicondyle and
649 entepicondyle.
650 Char. 435: 1 --> 3. Radius, total length versus total length of the humerus ratio =
651 1.12−1.28.
652 Char. 445: 1 --> 0. Manus, longest metacarpal + digit longer than humeral length.
653 Char. 450: 1 --> 0. Metacarpus, metacarpal IV longer than metacarpal III.
654 Char. 460: 2 --> 3. Ilium, preacetabular process present and extending beyond the
655 level of the anterior margin of the pubic peduncle.
656 Char. 467: 0 --> 1. Ilium, angle between anterior margin of the pubic peduncle and
657 longitudinal axis across pubic and ischiadic peduncles equal or higher than 45º.
658 Char. 477: 1 --> 0. Pubis, anterior apron absent, symphysis extended along the
659 ventral margin of the pelvic girdle and visible in lateral view.
660 Char. 489: 1 --> 0. Femur, total length versus total length of the humerus <1.02.
661 Char. 516: 2 --> 3. Tibia, total length versus total length of the femur ≥1.35.
662 Char. 569: 2 --> 3. Metatarsus, length of metatarsal I versus metatarsal III ratio
663 >0.90.
664 Char. 571: 1 --> 2. Metatarsus, length of the metatarsal II versus length of the
665 metatarsal IV ratio = 1.06−1.15.
666 Char. 578: 0 --> 1. Metatarsus, metatarsal V outer process on the proximal lateral
667 margin present, prominent pointed process.

Char. 587: 0 --> 1. Pedal digits, ventral tubercle in unguals well developed and extended ventral to the articular portion of the ungual.

Char. 681: 1 --> 2. Cervical and dorsal vertebrae, shape of posterior articular surface of the centrum convex (= procoelous).

Char. 765: 0 --> 1. Cervical vertebrae, postaxial cervical vertebrae with an anteroposteriorly elongated and large lateral pneumatic foramen around the mid-length of the centrum (this condition cannot be assessed for the entire postaxial cervical series of Triassic and Early Jurassic pterosaurs because of lack of preservation, but it occurs in the last cervical vertebra of *Carniadactylus* and at least some cervical vertebrae of *Raeticodactylus*, *Austriadraco* and *Dimorphodon*; pneumatic foramina are extensively present in the postaxial cervical vertebrae of chronostratigraphically younger pterosaurs).

Char. 771: 0 --> 1. Haemal arches, haemal spines developed as filiform processes below and parallel to adjacent centra present posterior to the third caudal vertebra.

Char. 775: 0 --> 1. Humerus, size of deltopectoral crest, hypertrophied anteriorly and with a proximal apex close to the level of the humeral head.

Char. 783: 0 --> 1. Metacarpus, metacarpal IV-humerus ratio more than 0.35.

Char. 784: 1 --> 2. Metacarpus, metacarpal IV shaft width at mid-length two times or more broader than that of metacarpals I−III.

Char. 785: 0 --> 1. Metacarpus, posteroventrally or posteriorly projecting crest on the middle of the proximoposterior surface of the shaft of metacarpal IV (crista metacarpi of Wild, 1979) present.

Char. 795: 0 --> 1. Pubis-ischium, ventral margin of pubo-ischiatic plate (if it extends ventrally up to or beyond the distal end of the pubic shaft or tubercle) convex or with ventrally pointing projection.

Char. 799: 0 --> 1. Prepubis, as a separate ossification, present.

(Austriadraco + Seazzadactylus) + (Raeticodactylus + Carniadactylus)

All trees:

Char. 271: 0 --> 1. Dentary, dorsal margin of the anterior portion compared to the dorsal margin of the posterior portion dorsally expanded, resulting in a convex anterior margin and a straight or concave posterior portion (unknown in *Austriadraco*).

Char. 744: 0 --> 1. Mandible, shape of the dorsal margin anterior to the glenoid fossa in lateral or medial view with a dorsal projection (coronoid process or surangular dorsal process in pterosaurs) approximately at mid-length between the last tooth position and glenoid fossa.

Austriadraco + Seazzadactylus

All trees:

Char. 284: 0 --> 2. Surangular-articular, retroarticular process ventrally expanded, resulting in a concave ventral margin of the hemimandible at the level of the glenoid fossa.

Char. 748: 0 --> 1. Dentary, low dorsal projection placed immediately posterior to the last tooth position, present.

Raeticodactylus + Carniadactylus

All trees:

Char. 10: 0 --> 1. External naris, nonterminal position in the rostrum, being considerably posteriorly displaced a distance equivalent to the length of the external

naris from the anteriormost point of the premaxilla-maxilla suture, but posterior rim of the naris anterior to or at the level of the anterior border of the antorbital fenestra.

Char. 36: 1 --> 0. Premaxilla, postnarial process (= maxillary process) absent or incipient.

Char. 92: 2 --> 3. Jugal, anterior process shape in lateral view with a strongly developed ascending subprocess that excludes the lacrimal from the posterior border of the antorbital fenestra (also in *Eudimorphodon*).

Preondactylia + Macronychoptera

All trees:

Char. 696: 0 --> 1. Skull openings, relative size of external naris longer anteroposteriorly than the antorbital fenestra.

Preondactylia

All trees:

Char. 304: 0 --> 2. Teeth, serrations on the maxillary/dentary crowns, present and distinct on both margins of most crowns.

Char. 705: 0 --> 1. Maxilla, shape of anterior process (= premaxillary process) in lateral or medial view continuously tapering, ending in a pointed end, and as low and long as the posterior process.

Char. 760: 0 --> 1. Teeth, maxillary teeth much enlarged below the dorsal process, present (also in *Eudimorphodon*).

***Peteinosaurus* + Macronychoptera**

All trees:

Char. 381: 0 --> 1. Caudal vertebrae, prezygapophysis of middle or posterior caudal vertebrae elongated more than a quarter of the adjacent centrum.

Char. 773: 0 --> 1. Coracoid, relative dorsoventral length 2/3 or more length of scapula.

Char. 790: 0 --> 1. Manus, manual unguals twice the size, or more, of pedal unguals.

Macronychoptera

All trees:

Char. 435: 3 --> 4. Radius, total length versus total length of the humerus ratio ≥ 1.33.

Char. 744: 0 --> 1. Mandible, surangular with a coronoid process or dorsal process.

Char. 772: 1 --> 2. Coracoid, coracoidal shaft with a strut-like posteroventral shaft, slender and cylindrical at midshaft.

Dimorphodontidae

All trees:

Char. 698: 0 --> 1. Skull openings, relative size of orbit equal or shorter anteroposteriorly than antorbital fenestra.

Char. 705: 0 --> 2. Maxilla, shape of anterior process in lateral or medial view trapezoidal, with an extensive diagonal suture with the premaxilla, and approximately as low as the posterior process.

Char. 708: 0 --> 1. Maxilla, dorsoventrally elongated foramen on the lateral surface of the base of the ascending process present (also present in *Preondactylus* and *Seazzadactylus*).

Char. 747: 0 --> 1. Dentary, ventral mandibular bony crest present.

Char. 750: 0 --> 1. Dentary, diastema (over 5 times longer than the distance between adjacent non-symphysial teeth) between the first two dentary teeth and those following distally present.

Char. 756: 0 --> 1. Teeth, bifid apex of at least some marginal tooth crowns present.

Char. 762: 0 --> 1. Teeth, post-symphysial mandibular tooth crown size compared to maxillary tooth crown size, much smaller.

Lonchognatha

All trees:

Char. 21: 1 --> 0. Rostrum, dorsoventral height at the level of the anterior tip of the maxilla versus dorsoventral height at the level of the anterior border of the orbit ≤0.33.

Char. 92: 2 --> 3. Jugal, anterior process shape in lateral view with a strongly developed ascending subprocess that excludes the lacrimal from the posterior border of the antorbital fenestra.

Char. 430: 1 --> 0. Ulna, olecranon process absent or low.

Char. 492: 1 --> 0. Femur, femoral head not distinctly inturned with respect to the shaft.

Char. 777: 0 --> 1. Pteroid, pteroid-humerus ratio = 0.30−0.60.

***Cacibupteryx* + (*Rhamphorhynchus* + *Allkaruen*)**

Some trees:

Char. 22: 1 --> 0. Rostrum, proportions at the level of the anterior border of the orbit transversely broader than dorsoventrally tall or subequal.

Char. 63: 1 --> 0. Maxilla, shape of the posterior portion of the bone (ventral to the antorbital fenestra if it is present) tapers posteriorly.

Char. 697: 1 --> 0. Skull openings, shape of antorbital fenestra, length more than twice the height.

Char. 706: 1 --> 0. Maxilla, anteroposterior width of ascending process in lateral or medial view broad, its base occupies most of the anterior half of the bone.

Rhamphorhynchus* + *Allkaruen

Some trees:

Char. 115: 1 --> 0. Frontal, dorsal surface flat or slightly depressed.

Char. 724: 0 --> 1. Basisphenoid/parabasisphenoid, divergence between basipterygoid processes in the transverse plane narrow (angle < 35°).

Dinosauromorpha / Dinosauriformes

All trees:

Char. 63: 1 --> 0. Maxilla, shape of the posterior portion of the bone (ventral to the antorbital fenestra if it is present) tapers posteriorly.

Char. 352: 0 --> 1. Dorsal vertebrae, length of the centrum versus height of the centrum in posterior dorsal vertebrae = 1.48−1.86.

Char. 402: 0 --> 1. Coracoid, postglenoid process separated from the glenoid fossa by a notch present.

Char. 470: 1 --> 2. Pubis-ischium, contact present and reduced to a thin proximal contact.

Char. 473: 0 --> 1. Pubis, anterior and posterior portions of the acetabular margin recessed.

Char. 474: 1 --> 0. Pubis, tuberosity for the attachment of the ambiens muscle in mature individuals prominent.

Char. 483: 0 --> 1. Ischium, proximal articular surfaces with the ilium and pubis continuous but separated by a fossa.

Char. 503: 0 --> 1. Femur, trochanteric shelf present in mature individuals.

Char. 513: 1 --> 0. Femur, anterior extensor groove absent, anterior margin of the bone straight or convex in distal view.

Char. 519: 1 --> 0. Tibia, lateral posterior condyle of the proximal end offset anteriorly from the medial posterior condyle.

Char. 521: 0 --> 1. Tibia, posterolateral process (= lateral malleolus) on the distal end present, distinctly medial or extends laterally approximately at the same level as the anterolateral corner.

Char. 524: 0 --> 1. Tibia, lateral side of the distal portion with proximodistally oriented groove.

Char. 537: 0 --> 1. Astragalus, ascending process (= anterior ascending process) present, occupying most of the anteroposterior depth of the astragalus.

Dracohors

All trees:

Char. 210: 0 --> 1. Supraoccipital, posterior surface with a prominent median, vertical peg.

Char. 336: 0 --> 1. Cervical vertebrae, epipophysis in postaxial cervicals present in at least the third to fifth cervical vertebrae.

Char. 472: 2 --> 3. Pubis, total length versus total length of the femur ratio ≥ 0.60.

Char. 482: 1 --> 2. Ischium, total length versus anteroposterior length of the acetabulum ratio = 2.72−3.53.

Char. 484: 0 --> 1. Ischium, longitudinal groove on the dorsal surface of shaft present.

Char. 485: 0 --> 1. Ischium, medial contact with antimere extensive but the dorsal margins are separated.

Char. 500: 0 --> 1. Femur, dorsolateral trochanter on the anterolateral surface of the proximal end present.

Char. 526: 0 --> 1. Fibula, anterior edge of the proximal portion tapers to a point and arched anteromedially.

Char. 547: 0 --> 1. Calcaneum, proportions of calcaneal tuber at the midshaft about the same or broader than tall.

Char. 575: 0 --> 1. Metatarsus, distal articulation surface of the metatarsal IV broad as deep or deeper than broad (asymmetrical).

Char. 802: 0 --> 1. Femur, greater trochanter shape in posterior view angled.

Silesauridae

All trees:

Char. 38: 0 --> 1. Premaxilla, sharp dorsal flange at the base of the postnarial process delimiting the posteroventral border of the external naris present.

Char. 457: 1 --> 0. Pelvic girdle, acetabular antitrochanter absent.

Char. 737: 1 --> 0. Inner ear, labyrinth general proportions, maximum height of the labyrinth versus maximum anteroposterior depth of the labyrinth ratio < 0.70.

Char. 754: 0 --> 1. Teeth, nature of tooth attachment ankylosis.

Char. 801: 0 --> 1. Femur, medial articular facet of the proximal portion in posterior view straight.

Asilisaurus* + *Silesaurus

All trees:

Char. 52: 0 --> 1. Maxilla, anterior maxillary foramen present.

Char. 278: 0 --> 1. Dentary, alveolar margin absent in the anterior portion.

Char. 305: 1 --> 0. Teeth, tooth shape at crown base of the marginal dentition circular.

Char. 308: 0 --> 1. Teeth, multiple maxillary and dentary tooth crowns distinctly mesiodistally expanded above the root present.

Char. 494: 1 --> 0. Femur, proximal articular surface (= posterolateral portion of the head sensu Nesbitt 2011) limited to the proximal surface of the bone.

Char. 495: 0 --> 1. Femur, proximal surface transverse groove present.

Char. 647: 0 --> 1. Dentary, anterior extremity tapers to a sharp point.

Char. 671: 0 --> 1. Femur, medial articular facet of the proximal portion straight.

Char. 674: 0 --> 1. Femur, distal condyles of the femur divided posteriorly between 1/3 and 1/4 the length of the shaft.

Char. 798: 1 --> 0. Pubis, medial articulation of the pair complete, reaches the distal edge of the pubis.

Dinosauria

All trees:

Char. 455: 0 --> 1. Pelvic girdle, acetabulum perforated, slightly concave, straight or slightly conve.

Char. 464: 0 --> 1. Ilium, main axis of the postacetabular process in lateral or medial view mainly posteriorly oriented.

Char. 476: 1 --> 2. Pubis, form of the shaft (= pubic tubercle, = pectineal tuberosity) rod-like and straight.

Char. 483: 1 --> 2. Ischium, proximal articular surfaces with the ilium and pubis separated by a non-articulating concave surface.

Char. 492: 0 --> 1. Femur, femoral head distinctly offset from the shaft.

Char. 505: 0 --> 1. Femur, shape of the process for the attachment of the caudofemoralis musculature, sharp flange.

Char. 506: 0 --> 1. Femur, process for the attachment of the caudofemoralis musculature in medial or lateral view asymmetrical, with the distal margin forming a steeper angle to the shaft.

Char. 517: 1 --> 2. Tibia, distinctly anteriorly projected process beyond the articular portion for the femur on the proximal end (= cnemial crest) present and curved anterolaterally.

Char. 522: 0 --> 1. Tibia, posterior surface of the distal end with distinct proximodistally oriented ridge.

Char. 537: 1 --> 2. Astragalus, ascending process (= anterior ascending process) present, restricted to the anterior half of the astragalar depth.

Char. 539: 0 --> 1. Astragalus, posterior groove absent.

Char. 545: 1 --> 0. Calcaneum, calcaneal tuber (= expansion of the lateral margin of the bone) absent or incipient.

Char. 564: 1 --> 0. Pes, foot length (articulated fourth metatarsal and digit) versus tibia-fibula length ratio >1.

Char. 823: 0 --> 1. Metatarsus, length of metatarsals III and V metatarsal V shorter than 50% of metatarsal III.

Ornithischia

All trees:

Char. 1: 12 --> 0. Skull and lower jaws, interdental plates absent.

Char. 55: 0 --> 3. Maxilla, anteroposterior length of the antorbital fossa anterior to the antorbital fenestra versus length of the antorbital fenestra ratio > 2.00.

Char. 67: 1 --> 0. Maxilla, position of the palatal process adjacent to the ventral margin of the medial surface of the maxilla or base of the interdental plates if they are present.

Char. 142: 0 --> 1. Squamosal, posterior process shape ventrally curved.

Char. 145: 0 --> 1. Squamosal, ventral process anteroventrally directed at 45º or less.

Char. 151: 0 --> 1. Quadratojugal, subtriangular.

Char. 174: 0 --> 1. Palpebral/s present.

Char. 228: 1 --> 2. Basioccipital, position of the posterior margin of the occipital condyle posterior to craniomandibular joint.

Char. 261: 0 --> 2. Lower jaw, distinct dorsal process behind the alveolar margin present, formed by a dorsally well-developed posterodorsal ramus of the dentary and sometimes a dorsally well-developed coronoid bone.

Char. 277: 0 --> 1. Posterior-most dentary teeth on the posterior half of lower jaw.

Char. 287: 0 --> 1. Surangular, dorsal margin in lateral view strongly convex.

Char. 298: 1 --> 0. Teeth, posterior extent of mandibular and maxillary tooth rows subequal.

Char. 306: 0 --> 1. Teeth, multiple maxillary or dentary tooth crowns with longitudinal labial or lingual striations or grooves present.

Char. 307: 0 --> 1. Teeth, multiple maxillary and dentary tooth crowns with extensive wear facets present.

Char. 315: 1 --> 0. Cervical and dorsal vertebrae, anterior centrodiapophyseal lamina or paradiapophyseal lamina in posterior cervicals and anterior dorsals absent.

Char. 316: 1 --> 0. Cervical and dorsal vertebrae, posterior centrodiapophyseal lamina in posterior cervicals and anterior dorsals absent.

Char. 317: 1 --> 0. Cervical and dorsal vertebrae, prezygodiapophyseal lamina in posterior cervicals and anterior dorsals absent.

Char. 327: 12 --> 0. Cervical vertebrae, ventral surface of the centrum in anterior cervicals transversely convex.

Char. 333: 1 --> 0. Cervical vertebrae, position of diapophysis or dorsal margin of synapophysis in anterior postaxial cervicals at or near dorsoventral level of pedicles.

Char. 356: 0 --> 1. Dorsal vertebrae, diapophysis and parapophysis in anterior dorsals expanded on stalks.

Char. 370: 0 --> 2. Sacral vertebrae, four or more.

Char. 460: 2 --> 3. Ilium, preacetabular process present and extending beyond the level of the anterior margin of the pubic peduncle.

Char. 462: 2 --> 0. Ilium, lateral crest dorsal to the supraacetabular crest/rim absent.

Char. 473: 1 --> 0. Pubis, anterior and posterior portions of the acetabular margin continuous.

Char. 474: 0 --> 1. Pubis, tuberosity for the attachment of the ambiens muscle in mature individuals incipient or absent.

Char. 482: 2 --> 3. Ischium, total length versus anteroposterior length of the acetabulum ratio = 4.25−4.48.

Char. 502: 1 --> 3. Femur, anterior trochanter (= lesser or minor trochanter) (= iliofemoralis cranialis muscle insertion) present and approaches the proximal articulation of the bone.

Char. 503: 1 --> 0. Femur, trochanteric shelf absent.

Char. 521: 1 --> 2. Tibia, posterolateral process (= lateral malleolus) on the distal end present and extends well lateral to the anterolateral corner.

Char. 566: 1 --> 0. Metatarsus, metatarsals overlapping proximally absent.

Char. 653: 0 --> 1. Teeth, serrations present and enlarged and coarser (lower density) = denticles.

Char. 663: 0 --> 1. Sacral vertebrae, centra coossified at the ventral edge.

Char. 695: 0 --> 1. Axis, neural spine posterior margin acute, posterodorsally oriented apex extending posteriorly beyond the postzygapophysis through a distance equal or longer than the length of the postzygapophysis.

Char. 696: 0 --> 1. Skull openings, external naris longer anteroposteriorly than the antorbital fenestra.

Char. 710: 0 --> 1. Maxilla, buccal emargination dorsolateral to the alveolar margin present.

Char. 714: 0 --> 1. Jugal, long axis of the body oblique to the alveolar margin of the maxilla when both bones are articulated.

Char. 715: 0 --> 1. Jugal, ventral margin across anterior and posterior processes in lateral or medial view forming angle of less than 180°.

Char. 718: 0 --> 1. Postorbital, anterior process shorter than the posterior process.

Char. 720: 0 --> 2. Quadrate, orientation in lateral or medial view inclined posteriorly (>110°).

Char. 746: 0 --> 1. Predentary bone present.

Char. 752: 0 --> 1. Dentary, mandibular buccal emargination present, lateral dentary surface with a posterior shelf bordering an emargination that encompasses half of the dentary length.

Char. 796: 0 --> 1. Pubis, prepubic process present.

Saurischia

All trees:

Char. 86: 0 --> 1. Lacrimal, exposure on the skull roof in dorsal view present.

Char. 396: 0 --> 1. Scapula, acromion process sharply raised in an angle close to 90º from the anterior margin of the scapular blade.

Char. 422: 0 --> 1. Humerus, shape of the deltopectoral crest in lateral view subrectangular or trapezoidal.

Char. 487: 0 --> 1. Ischium, cross section of the distal portion semicircular or subtriangular.

Char. 712: 0 --> 1. Lacrimal, shape of ventral process in lateral view folds and extends over the posterodorsal part of the antorbital fenestra.

Char. 721: 1 --> 0. Opisthotic, base of paraoccipital process in occipital view directed laterally or dorsolaterally.

Char. 769: 0 --> 1. Sacral vertebrae, transverse processes and ribs development anteroposteriorly long, roofing the space between ribs.

Char. 770: 0 --> 1. Sacral vertebrae, first primordial sacral rib articular surface in lateral view C-shaped.

Char. 784: 1 --> 0. Metacarpus, metacarpal IV shaft width at mid-length distinctly narrower than that of metacarpals I-III.

Char. 788: 0 --> 1. Manus, phalanx I-1 is the longest non-ungual phalanx of the manus.

Char. 789: 0 --> 1. Manus, digit V no phalanges.

Char. 819: 0 --> 1. Distal tarsal 4, posterior prong pointed.

Char. 820: 0 --> 1. Distal tarsal 4, medial process distinct in the anteroposterior middle of the element.

Sauropodomorpha

All trees:

Char. 37: 0 --> 1. Premaxilla, postnarial process thin.

Char. 55: 0 --> 1. Maxilla, anteroposterior length of the antorbital fossa anterior to the antorbital fenestra versus length of the antorbital fenestra ratio = 0.28−0.66.

Char. 125: 0 --> 1. Postorbital-jugal, postorbital bar composed mostly of the postorbital.

Char. 129: 1 --> 0. Postorbital, supratemporal fossa extending onto the ascending process absent.

Char. 144: 0 --> 1. Squamosal, ventral process shape anteroposteriorly narrow and strap-like.

Char. 188: 1 --> 0. Palatine-pterygoid, teeth on the palatine and/or ventral surface of the anterior ramus of the pterygoid present.

Char. 204: 0 --> 1. Ectopterygoid, articulation with pterygoid complex overlap between ectopterygoid and pterygoid.

Char. 495: 0 --> 1. Femur, proximal surface transverse groove present.

Char. 709: 0 --> 1. Maxilla, ventral margin of the antorbital fossa elevated relative to the ventral surface (sharp longitudinal ridge present) (= alveolar ridge).

Char. 739: 0 --> 1. Inner ear, curvature of the posterior semicircular canal (PSC), PSC-arc-length versus PSC-straight-line ratio ≥ 1.20.

Char. 768: 0 --> 1. Dorsal vertebrae, lamina partially subdividing the centrodiapophyseal postzygapophyseal fossa present.

Saturnalia* + *Eoraptor

All trees:

Char. 308: 0 --> 1. Teeth, multiple maxillary and dentary tooth crowns distinctly mesiodistally expanded above the root present.

Char. 370: 0 --> 1. Sacral vertebrae, three.

Char. 424: 1 --> 2. Humerus, length of the deltopectoral crest versus total length of the bone in mature individuals ratio = 0.52−0.55.

Char. 564: 0 --> 1. Pes, foot length (articulated fourth metatarsal and digit) versus tibia-fibula length ratio < 1.

Theropoda

All trees:

Char. 21: 1 --> 2. Rostrum, dorsoventral height at the level of the anterior tip of the maxilla versus dorsoventral height at the level of the anterior border of the orbit ratio = 0.59−0.80.

Char. 381: 0 --> 1. Caudal vertebrae, prezygapophysis of posterior caudals elongated more than a quarter of the adjacent centrum.

Char. 447: 0 --> 1. Metacarpus, proximal ends abut one another without overlapping.

Char. 451: 0 --> 1. Manual digits, unguals length distinctly longer than the last phalanx of the same digit.

Char. 455: 1 --> 2. Pelvic girdle, acetabulum perforated, markedly concave.

Char. 458: 0 --> 1. Ilium, maximum height of the acetabulum versus length of the femur ratio = 0.21−0.47.

Char. 466: 0 --> 2. Ilium, dorsal margin of the iliac blade concave.

Char. 481: 0 --> 1. Pubis, transverse width of the distal portion significantly narrower than the proximal width.

Char. 602: 1 --> 0. Scapula, posterior edge of the blade just dorsal to the glenoid region smoothly transversely convex.

Char. 685: 0 --> 1. Caudal vertebrae, length of the anterior caudal vertebrae (caudal vertebrae 1−10) relative to posterior caudal vertebrae (25+), posterior caudal vertebrae much longer.

Char. 698: 0 --> 1. Skull openings, relative size of orbit equal or shorter anteroposteriorly than antorbital fenestra.

Char. 786: 0 --> 1. Manus, length of digit III accounts for more than 0.4 of the total length of humerus plus radius.

***Tawa* + Neotheropoda**

All trees:

Char. 26: 0 --> 1. Premaxilla, alveolar margin does not reach the contact with the maxilla and forms a diastema (= subnarial gap) present.

Char. 34: 0 --> 1. Premaxilla, prenarial process length greater than the anteroposterior length of the main body of the premaxilla.

Char. 153: 2 --> 3. Quadratojugal, anterior process distinctly present, in which the lower temporal bar is complete and participates in the posteroventral border of the infratemporal fenestra, and process finishes close to the base of the posterior process of the jugal.

Char. 286: 2 --> 1. Surangular, lateral shelf present, low ridge near dorsal margin.

Char. 332: 1 --> 2. Cervical vertebrae, diapophysis and parapophysis of anterior to middle cervical postaxial vertebrae situated on different processes and nearly touching.

Char. 383: 0 --> 1. Gastralia present, well separated.

Char. 436: 1 --> 0. Radius, shorter length in comparisons with that of the ulna.

Char. 506: 1 --> 0. Femur, process for the attachment of the caudofemoralis musculature in medial or lateral view symmetrical, with the proximal and distal margins forming similar low-angle slopes to the shaft.

Char. 521: 1 --> 2. Tibia, posterolateral process (= lateral malleolus) on the distal end present and extends well lateral to the anterolateral corner.

Char. 644: 0 --> 1 Parasphenoid/parabasisphenoid, between basal tubera and basipterygoid processes significantly elongated, at least 1.5 times longer than wide.

Char. 802: 1 --> 0. Femur, greater trochanter shape in posterior view rounded.

Char. 818: 0 --> 1. Calcaneum, transversely compressed and subrectangular, without or with incipient medial process.

Neotheropoda

All trees:

Char. 36: 2 --> 1. Premaxilla, postnarial process (= maxillary process) short, ends well anterior to the posterior margin of the external naris.

Char. 37: 0 --> 1. Premaxilla, postnarial process thin.

Char. 54: 2 --> 3. Maxilla, antorbital fossa present on the horizontal process (= posterior process) of the maxilla ventral to the antorbital fenestra, reaching the posteroventral corner of the maxillary contribution to the border of the opening.

Char. 144: 0 --> 1. Squamosal, ventral process anteroposteriorly narrow and strap-like.

Char. 218: 0 --> 1. Opisthotic, ventral ramus covered by the lateralmost edge of the exoccipital in posterior view.

Char. 277: 0 --> 1. Posterior-most dentary teeth on the posterior half of lower jaw.

Char. 327: 2 --> 1. Cervical vertebrae, ventral surface of the centrum in anterior cervicals with a low median longitudinal keel.

Char. 331: 0 --> 1. Cervical vertebrae, length of the fourth and fifth cervical centra versus the height of their anterior articular surface ratio = 2.92−4.12.

Char. 370: 0 --> 2. Sacral vertebrae, four or more.

Char. 396: 1 --> 0. Scapula, acromion process gently raised from the anterior margin of the scapular blade.

Char. 444: 1 --> 0. Carpals, distal carpal five absent.

Char. 460: 2 --> 3. Ilium, preacetabular process present and extending beyond the level of the anterior margin of the pubic peduncle.

Char. 461: 1 --> 2. Ilium, preacetabular process with squared outline.

Char. 463: 1 --> 3. Ilium, length of the postacetabular process versus anteroposterior length of the acetabulum ratio = 1.49−1.90.

Char. 466: 2 --> 1. Ilium, dorsal margin of the iliac blade mostly straight.

Char. 502: 1 --> 2. Femur, anterior trochanter (= lesser or minor trochanter) (= iliofemoralis cranialis muscle insertion) present and separated from the shaft by a marked cleft.

Char. 513: 0 --> 1. Femur, anterior extensor groove present, anterior margin of the bone concave in distal view.

Char. 606: 0 --> 1. Proximal tarsals, fusion between astragalus and calcaneum present.

Char. 709: 0 --> 1. Maxilla, ventral margin of the antorbital fossa elevated relative to the ventral surface (sharp longitudinal ridge present) (= alveolar ridge).

Char. 712: 1 --> 0. Lacrimal, shape of ventral process in lateral view does not fold over the posterodorsal part of the antorbital fenestra.

Char. 779: 0 --> 1. Carpus, medialmost distal carpal (distal carpal 1 or its fusion to other element) distinctly larger than other distal carpals.

Char. 781: 0 --> 1. Metacarpus, metacarpal II equal to or longer than metacarpal III.

Char. 792: 0 --> 1. Ilium, pubic peduncle anteroposterior width at mid-length versus its total length ratio ≥ 0.5.

Char. 798: 1 --> 0. Pubis, medial articulation of the pair complete, reaches the distal edge of the pubis.

Char. 811: 0 --> 1. Tibia, distal surface outline (excluding the posterolateral process if present) mediolaterally expanded.

Char. 819: 1 --> 0. Distal tarsal 4, posterior prong blunt.

Char. 821: 1 --> 0. Metatarsus, proximal portion of metatarsal IV narrow.

Inclusion of* Scleromochlus taylori *in the phylogenetic analysis

The phylogenetic analysis with the inclusion of *Scleromochlus taylori* found 280 most parsimonious trees (MPTs) with a length of 5,010 steps, a consistency index (CI) of 0.21397, and a retention index (RI) of 0.64992. The result of this analysis is completely congruent with that of the first analysis, and *Scleromochlus* is recovered as the sister taxon to all other Pterosauromorpha (i.e. the Lagerpetidae + Pterosauria clade) in all the MPTs (Extended Data Fig. 4). The inclusion of *Scleromochlus* does not substantially modify the absolute bootstrap frequencies of the pan-avian branches, with the exception of a slight decrease in Pan-Aves (from 58% to 49%), a slight increase in Dinosauromorpha/Dinosauriformes (from 60% to 65%), and another decrease in the Pterosauria + Lagerpetidae clade (from 81% to 76%). The boostrap frequencies of Pterosauromorpha with the inclusion of *Scleromochlus* are below 50%. The Bremer support values of Pan-Aves and less inclusive branches are not modified with the inclusion of this taxon. The placement of *Scleromochlus* within Pterosauromorpha agrees with some previous results (e.g. Padian, 1984; Sereno, 1991a; Andres et al., 2010; Ezcurra et al., 2010; Benton and Walker, 2010), but differs from its position as the sister taxon to all other Pan-Aves (Benton, 1999, 2004) or closer to dinosauriforms than to pterosaurs or aphanosaurs (Bennett, 1996; one of the analyses of Nesbitt et al., 2017). Under topological constrains, three additional steps are necessary to force the position of *Scleromochlus* outside of Ornithodira (sister taxon to all other pan-avians), four extra steps to place it as a Dinosauromorpha, sister taxon to Dinosauriformes (but there is no synapomorphy supporting this placement), five steps to force it as the sister taxon to Pterosauria, and six steps to force its position within Lagerpetidae.

The following list of pan-avian synapomorphies supports the placement of *Scleromochlus* as a Pterosauromorpha (we indicate here only characters that can be scored in *Scleromochlus*):

Pan-Aves

All trees:

Char. 387: 0 --> 1. Scapula, total length of the scapula versus minimum anteroposterior width of the scapular blade ratio = 7.92−11.31.

Pterosauromorpha

All trees:

Char. 2: 0 --> 1. Skull, total length versus length of the presacral vertebral column ratio = 0.44−0.72.

Char. 472: 2 --> 01. Pubis, total length (along anterior margin or pubic shaft or tubercle) versus total length of the femur ratio ≤ 0.45.

Char. 492: 0 --> 1. Femur, femoral head distinctly inturned with respect to the shaft.

Char. 823: 0 --> 1. Metatarsus, metatarsal V shorter than 50% of metatarsal III.

The following list includes synapomorphies of the Pterosauria + Lagerpetidae clade that are absent in *Scleromochlus*, excluding this species from that clade.

Pterosauria + Lagerpetidae

All trees:

Char. 231: 0 --> 1. Basioccipital, occipital neck absent or extremely short.

Char. 267: 0 --> 2. Dentary, shape of the anterior region of the tooth bearing portion ventrally curved or deflected.

Char. 470: 1 --> 0. Pubis-ischium, present and extended ventrally up to or beyond the distal end of the pubic shaft or spine.

Char. 706: 0 --> 1. Maxilla, anteroposterior width of ascending process in lateral or medial view very thin, resulting in an external naris separated from the antorbital fenestra by a strap-like bar of bone.

Char. 774: 0 --> 1. Humerus, shape in lateral view sigmoid.

Char. 782: 0 --> 1. Metacarpus, metacarpal III-humerus ratio ≥ 0.35.

Char. 800: 0 --> 1. Femur, profile of femoral head in medial or lateral view when it is distinctly offset, hook-shaped.

Results using the 3D morphogeometric character of the inner ear labyrinth

This analysis found 256 most parsimonious trees (MPTs) with a length of 4,927.67960 steps (morphogeometric character with 4.67960 steps under weight = 1), a consistency index (CI) of 0.77624, and a retention index (RI) of 0.85756. The topology of the strict consensus tree (Extended Data Fig. 8) is completely congruent with that recovered in the previous analyses, and some of the previous polytomies are resolved. Distinct apomorphic landmark displacements of the morphogeometric character are optimized along Pan-Aves. The main apomorphic change for Pterosauromorpha found by the analysis is an increase of the diameter of the ASC with respect to the condition reconstructed for the common ancestor of Ornithodira. Lagerpetids show an increase of the diameter of the PSC with respect to the condition at the base of Pterosauromorpha. These changes agree with those found in the analyses using the set of 15 discrete characters of the endosseous labyrinth of the inner ear.

In addition, we analysed the 3D morphogeometric character alone for its 22 sampled operational units (*Triopticus primus* was excluded before the analysis following the original analysis). We set the tree search strategy in 50 replications of Wagner trees followed by TBR branch-swapping algorithm (holding 10 trees per

replication) because computational times were expected to be lower due to the lower number of taxa in the data set. The best tree(s) obtained were subjected to a final round of TBR branch swapping. This analysis found optimal trees 26 times of the 50 replications and one MPT of 4.10604 steps, with a consistency index (CI) of 0.33001. This analysis based solely in the 3D morphology of the labyrinth of the inner ear recovered a paraphyletic arrangement of pan-avians, with the exception of *Teleocrater rhadinus* that was found as the sister taxon to the pseudosuchian *Arizonasaurus babbitti* (Extended Data Fig. 9). Deeper branches of the tree include an arrangement of both non-archosaurian pan-archosaurs and pseudosuchians. The presence of pan-avians close to one another indicates a phylogenetic signal, at least for pan-avians, rather consistent with that of the topology of the MPTs found with the complete data set of discretized characters. The position of pan-avians as the earlier branches of the tree, rather than non-archosaurian pan-archosaurs and pseudosuchians, is very likely a result of rooting the tree with the allokotosaur *Trilophosaurus buettneri*. This species possesses a morphology of the labyrinth of the inner ear (e.g. lengthening of the ASC arc length) strongly convergent with that of pan-avians, mainly lagerpetids, pterosaurs and early dinosaurs, and this results in the optimization of such 3D configuration as ancestral for the tree. In particular, the lagerpetids *Ixalerpeton polesinensis* and *Dromomeron gregorii* are recovered as the earliest branching species of the tree (with exception of *Trilophosaurus buettneri* that has been used as the root). These lagerpetids are successive sister taxa to *Saturnalia tupiniquim*, *Megapnosaurus rhodesiensis*, Pterosauria (recovered as monophyletic), and other more deeply nested species. Thus, the paraphyletic arrangement of lagerpetids, pterosaurs, and eusaurischians (saurischians excluding *Herrerasaurus ischigualastensis*) indicates the presence of a

phylogenetic signal that supports the lagerpetid-pterosaur affinities and its convergence with early dinosaurs.

We also analysed the latter dataset rooting the trees and re-aligning the configurations with the early rhynchosaur *Mesosuchus browni*, which has a labyrinth morphology more similar to that of other non-archosaurian archosauromorphs (e.g. *Prolacerta broomi*, *Proterosuchus fergusi*, *Euparkeria capensis*, *Chanaresuchus bonapartei*). We used the same search strategy as before. This analysis found optimal trees 6 times of the 50 replications and one MPT of 3.92408 steps, with a consistency index (CI) of 0.34592 (Extended Data Fig. 10). Two main clades are recovered in this tree, one including pan-avians plus *Arizonasaurus babbitti* and the other composed of non-archosaurian archosauromorphs and pseudosuchians. As a result, the optimization of the morphogeometric character is reversed with respect to the previous analysis. Proportionally lower labyrinths, with shorter arc lengths, are optimized as ancestral for both clades and proportionally higher labyrinths, with a longer ASC arch length, is acquired in pan-avians. A stronger asymmetry between the ASC and PSC occurs in the clade that includes pterosaurs, lagerpetids, the early eusaurischians *Saturnalia tupiniquim* and *Megapnosaurus rhodesiensis*, and the allokotosaur *Trilophosaurus buettneri*.

In conclusion, the phylogenetic signal of the 3D morphogeometric configuration of the labyrinth of the inner ear supports the lagerpetid-pterosaur affinities recovered with the complete data set, as well as convergences with some early dinosaurs and the herbivorous, quadupredal stem-archosaur *Trilophosaurus buettneri*.

6. Additional information of the methods and results of the Bayesian analysis

Additional methods

We used the Mkv model of Lewis (2001) as the substitution model. It specifies equal state frequencies and a correction for ascertainment bias of morphological matrices, which systematically omit constant characters during matrix construction. This corrects for the ascertainment bias in morphological matrices by conditioning on only variable characters being observed (excluding any constant characters scored automatically in the matrix). If such a correction is not applied, evolution rates are overestimated (Lewis, 2001). Rate variation across characters was drawn from a gamma distribution.

We specified a relaxed clock model, in which each branch has an independent rate drawn from a gamma distribution (Lepage et al., 2007). The variance of the gamma distribution was drawn from an exp(10) distribution. Uncertainty in the base substitution rate of the tree was accommodated by assigning a normal prior probability distribution to the substitution rate with a mean of 0.001 and variance of 0.1. Using a standard deviation larger than the mean establishes a relatively wide distribution for the prior, allowing the analysis to sample from highly-variable clock rates.

Uniform age priors were assigned to all of the tips of the tree, in which maximum and minimum values for the probability distribution correspond the last and first appearance datums of fossil taxa, respectively. In addition, we used a single node calibration for Archosauria, where the prior age probability was assigned a uniform distribution (249.2−257.3 Ma). The minimum age (249.2 Ma) is based on the late Olenakian maximum ages for several pseudosuchian taxa (Butler et al., 2011), which represent the oldest archosaur occurrences known to date. The maximum age (257.3 Ma) is based on the minimum age for the crocodile-lizard split, given by the geochronological age of the Kupferschiefer, which contains the oldest unambiguous non-archosaurian member of Pan-Archosauria, as determined by Ezcurra et al. (2014).

1303 The deepest split within the tree was parameterized with a uniform tree age prior
1304 (303.4−318.0 Ma) (see Methods).
1305 The fossilized birth-death (FBD) process was used for the tree model (Stadler,
1306 2010; Heath et al., 2014). The speciation rate (λ), extinction rate (μ), and fossilization
1307 rate (φ) of the FBD model are parameterized in MrBayes as the net diversification prior
1308 d = λ–μ, turnover prior e = μ/λ, and fossil sampling probability prior s = φ/(μ+φ), so that
1309 turnover and fossil sampling probability range from 0 to 1 (Zhang, 2016). For the
1310 parameters of these priors, we used default values [d = exp(10); e = beta(1,1); s =
1311 beta(1,1)] as implemented in MrBayes. For the sampling strategy, fossils were defined
1312 as tips without the possibility of being ancestors of other lineages within the tree.
1313 To estimate the posterior distribution, we used Metropolis Coupling Markov
1314 chain Monte Carlo (MCMCMC) algorithms (Ronquist et al., 2009). We used two
1315 independent runs of four Markov chains (three heated chains, one cold chain), with a
1316 heating coefficient of 0.05 and 3 swaps of states between chains being attempted every
1317 generation of the run. We used a stop-rule so that the analysis terminates when the
1318 specified average deviation of split frequencies of 0.01 is reached. For all MCMC runs
1319 across the analyses, samples from the posteriors were recorded every 500th generation
1320 with 25% of the trees discarded as burn-in.
1321 Our stop-rule value of 0.01 average standard deviation of split frequencies was
1322 reached after 23,496,000 generations, indicating that sampled trees were very similar
1323 between runs. The Potential Scale Reduction Factors (PSRF), which should approach
1324 1.0, indicating similar between- and within-run variances of posterior samples (Gelman
1325 and Rubin, 1992; Ronquist et al., 2009), was 1 for the posterior distributions of all
1326 parameters, indicating good non-topology parameter convergence. Visual inspection of
1327 the trace plot of the number of generations versus the log probability of the data

indicated convergence on stationary posteriors as well. Finally, effective sample sizes (ESS) for all parameters were >200, which is an arbitrary cut-off taken to indicate convergence (Rambaut et al., 2018).

Results

The majority rule tree computed from the Bayesian analysis (Extended Data Fig. 6) is broadly congruent with that of the strict consensus tree of the parsimony analysis (Extended Data Fig. 4). The main differences are: the position of *Aenigmastropheus parringtoni* as the sister taxon to all other lepidosauromorphs [posterior probability (pp) = 0.73]; choristoderans as the sister taxon to Squamata/Rhynchocephalia within Lepidosauromorpha (pp = 0.96); *Antarctanax shackletoni* as the sister taxon to *Tasmaniosaurus triassicus* (pp = 0.67) in a polytomy with proterosuchids and crownward archosauriforms; *Fugusuchus hejiapanensis* as the sister taxon to *Sarmatosuchus otschevi* (pp = 0.72); *Cuyosuchus huenei* as an erythrosuchid, sister taxon to *Guchengosuchus shiguaiensis* (pp = 0.61); *Halazhaisuchus qiaoensis*, *Dorosuchus neoetus* and *Asperoris mnyama* as more closely related to one another than to other taxa (pp = 0.65); and *Nundasuchus songeaensis* as the sister taxon to all other Phytosauria (pp = 0.74). However, the posterior probabilities of all these relationships that differ from the parsimony analysis results, with exception of those within Lepidosauromorpha, are below 0.75. In addition, contrasting with the parsimony results, the majority rule tree of the Bayesian inference analysis shows a polytomy among allokotosaurs, rhynchosaurs, and crownward archosauromorhs, and a large polytomy at the base of Pseudosuchia, being composed of Phytosauria, Aetosauria, Ornithosuchidae, Erpetosuchidae, and the Gracilisuchidae + Loricata clade.

Lagerpetids are also recovered in the Bayesian analysis as the sister taxon to Pterosauria, within a taxonomically broad Pterosauromorpha (pp = 0.99) (Extended Data Fig. 6). The supports of Lagerpetidae and Pterosauria are also very high, both with posterior probabilities of 1.00. As a result, the lagerpetid-pterosaur clade found in the parsimony analysis is also strongly supported by our Bayesian analysis using a time-calibrated FBD model.

The estimation of the divergence dates calculated the origin of Pan-Archosauria with a mean in 273.1 Ma [95% highest posterior density (HPD) = 279.1−268.6 Ma, early-middle Permian]. The age estimation for the origin of Archosauriformes has a mean of 263.8 Ma (95% HPD = 267.4−260.1 Ma, middle Permian), Archosauria of 256.4 Ma (95% HPD = 258.5−255.0 Ma, early-middle late Permian), Pan-Aves of 254.6 Ma (95% HPD = 257.2−251.7 Ma, late Permian−earliest Triassic), Pseudosuchia of 255.7 Ma (95% HPD = 257.8−253.9 Ma, late Permian), and Dinosauria of 242.0 Ma (95% HPD = 246.6−237.4 Ma, Middle Triassic). All these age estimations of node origins are consistent with those previously inferred from the fossil record (e.g. Sereno, 1991a; Nesbitt, 2011; Ezcurra et al., 2014; Ezcurra, 2016). Regarding the lagerpetid-pterosaur clade, the age estimation for the origin of Pterosauromorpha has a mean of 246.1 Ma (95% HPD = 251.5−240.6 Ma, Induan−early Ladinian), Lagerpetidae of 240.0 Ma (95% HPD = 244.3−236.0 Ma, latest Anisian−earliest Carnian), and Pterosauria of 229.1 Ma (95% HPD = 234.1−224.4 Ma, late Carnian−early Norian). As a result, the mean ghost lineage of Pterosauria is estimated in 17.0 Myr in the Bayesian analysis; a value slightly lower to that calculated in the time-calibrated parsimony tree. This supports the ‘Big Bang’ model versus the ‘iceberg model’ (Unwin, 2006) for early pterosaur evolution as hypothesized by Dalla Vecchia (2013: 143−144) based on the pterosaur fossil record and taphonomic evidence.

Evolutionary rates have been calculated for the majority rule tree during the tree searches in the Bayesian analysis. The highest evolutionary rates are concentrated around the Permo-Triassic boundary and there is a trend to lower average rates towards the end of the Triassic and Jurassic. This result agrees with that recovered by Ezcurra and Butler (2018) for Permian to early Carnian pan-archosaurs using a maximum likelihood optimization on most parsimonious trees. In particular, the earliest branch of Pan-Aves and Pseudosuchia, respectively, possess some of the highest evolutionary rates for the entire tree (Pseudosuchia: 10.183; Pan-Aves: 5.41; Extended Data Fig. 6). Within Pan-Aves, the evolutionary rates of the early branches of Pterosauromorpha (4.168) and Lagerpetidae (3.461) are the highest among the non-terminal branches. By contrast, the evolutionary rates of Pterosauria (2.008) are considerably lower, indicating that the acquisition of apomorphies that characterizes the pterosaur body plan occurred under lower evolutionary rates to other branches of the ornithodiran tree (e.g. Dinosauromorpha: 3.188; Dinosauria: 2.427; Saurischia: 2.562).

In the second Bayesian inference analysis, with the fully constrained topology placing lagerpetids as the sister group of Dinosauriformes, the highest evolutionary rates are also temporally concentrated around the Permo-Triassic boundary, occurring in the topology at earliest branches of Archosauria, Pan-Aves, and Pseudosuchia. The evolutionary rates of Pterosauria are higher in this topologically constrained analysis (2.200) than in the unconstrained analysis. The length of the branch leading to Pterosauria is considerably longer in the constrained analysis (branch length between mean age values in the unconstrained analysis = 17 Myr; branch length between mean age values in the constrained analysis = 23.1 Myr). If the number of transformations in the branch is the same in both analyses, the evolutionary rates would decrease if the branch becomes longer. As a result, the position of lagerpetids as the sister taxon to

pterosaurs have a direct impact on the evolutionary rates related to the acquisition of the pterosaur body plan. The presence of lower rates in the unconstrained tree shows that the number of character state transitions between pterosaurs and other pan-avians is reduced in our phylogenetic hypothesis. This reduces the morphological gap between pterosaurs and other pan-avians and the number of transformations per Myr necessary for establishment of the ancestral pterosaur morphology.

7. Principal components analysis

This analysis identified shared aspects of simialrity between pterosaur and lagerpetid labyrinths, which shared positive values of PC2 combined with negative values of PC1. PC1 explains 39.3% of total shape variance and separates taxa with proportionally tall labryrinths (negative PC1 scores; pan-avians plus the stem-archoaur *Trilophosaurus*) from taxa with proportionally low, broad labyrinths (positive PC1 scores). PC2 explains 13% of total shape variance and separates taxa with more triangular semicircular canals (negative values) from taxa with more rounded canals (positive values).

8. Taxonomic nomenclature implications of our results

The placement of Lagerpetidae as the sister taxon to Pterosauria has important implications for the taxonomy of early pan-avian clades. The stem-based phylogenetic definition of Pterosauromorpha (Andres and Padian, 2020) implies that lagerpetids (and also *Scleromochlus*, see Section 5 above and Extended Data Fig. 4) are members of this clade, whereas the original node-based definition of Dinosauromorpha (Sereno, 1991) results in the inclusion of Pterosauromorpha within this group. On the contrary, the definition of Dinosauromorpha proposed here (see Methods) avoids that problem, creating a node-stem triplet (Sereno, 1999) with Ornithodira and Pterosauromorpha.

This agrees with the use of the term by almost all subsequent authors (e.g. Benton, 2004) and also, in fact, with the original intention of Sereno (1991) as expressed in the paragraph that follows its original definition, where he stated that Dinosauromorpha is supposed to include "ornithodirans more closely related to the dinosaur-avian clade than to pterosaurs". Dinosauromorpha and Dinosauriformes (see Methods) are equally inclusive according to the phylogenetic hypothesis employed here (Extended Data Fig. 4), but their differentiation might be useful in the future to accommodate taxa on the Dinosauromorpha stem that fall outside the minimal clade composed of *Lagosuchus talampayensis* and dinosaurs.

9. Modifications to previous versions of the phylogenetic data matrix

Terminals added to the data matrix of Butler et al. (2019)

Operational taxonomic unit	Age	Completeness (proportion of scored characters)	Sources of scoring
Allkaruen koi	Toarcian-earliest Bathonian	14.9%	MPEF-PV 3609, 3613, 3615, 3616; Codorniú et al. (2016)
Austriadactylus cristatus	middle-late Norian (late Alaunian-earliest Sevatian)	25.5%	SMNS 56342 (holotype); MGC SC 332466; Dalla Vecchia et al. (2002); Dalla Vecchia (2009b, 2014)
Austriadraco dallavecchiai	middle-late Norian (late Alaunian-earliest Sevatian)	21.1%	SNSB-BSPG 1994 I 51; Wellnhofer (2003)
Buriolestes schultzi	late Carnian	81.2%	ULBRA-PVT280; CAPPA/UFSM 0035; Cabreira et al. (2016); Müller et al. (2018)
Cacibupteryx caribensis	middle-late Oxfordian	17.5%	cast of IGO-V 208; Gasparini et al. (2004)
Caelestiventus hanseni	late Norian-Rhaetian	18.2%	BYU 20707; Britt et al. (2018)
Carniadactylus rosenfeldi	middle Norian (late Alaunian)	36.5%	MFSN 1797 (holotype); MPUM 6009; Dalla Vecchia (2009a, 2014, 2018)
Coelophysis bauri	Rhaetian	91.8%	several specimens (see Colbert, 1989); Rinehart et al. (2009)
Dromomeron gigas	late Norian-Rhaetian	3.8%	PVSJ 898; Martínez et al. (2016)
Dromomeron gregorii	early-middle Norian	16.4%	TMM 31100-278, 464, 764, 1306, 1308, 1314, 1234, 1334; Nesbitt et al. (2009a)
Dromomeron romeri	late Norian-early Rhaetian	18.2%	GR 218−223, 234, 238; AMNH FR 2721; Irmis et al. (2007); Nesbitt et

			al. (2009a)
Eoraptor lunensis	late Carnian	79.0%	PVSJ 512; Sereno et al. (2013)
Eudimorphodon ranzii	middle Norian (latest Alaunian)	37.7%	MCSNB 2888; Wild (1979); Dalla Vecchia (2014)
Ixalerpeton polesinensis	late Carnian	41.8%	ULBRA-PVT058, 059; Cabreira et al. (2016)
Kongonaphon kely	late Ladinian-early Carnian	8.6%	UA 10618; Kammerer et al. (2020)
Lesothosaurus diagnosticus	Hettangian-Sinemurian	86.9%	NHMUK PV RU B17, R8501, R11002, R11004, R11956, RU B23, NMQR 3076; Thulborn (1972); Sereno (1991b); Butler (2005); Porro et al. (2015); Baron et al. (2016)
Megapnosaurus rhodesiensis	Hettangian-Sinemurian	88.9%	casts of NHMB 11470; cast of small QG specimen; Raath (1969, 1977); Bristowe and Raath (2004); Bristowe et al. (2004)
Peteinosaurus zambellii	middle Norian (latest Alaunian)	25.9%	MCSNB 2886 (holotype), 3359, 3496; Wild (1979); Dalla Vecchia (2003, 2014)
Preondactylus buffarinii	middle-late Norian (latest Alaunian-earliest Sevatian)	27.1%	MFSN 1770 (holotype), 25161; Wild (1984); Dalla Vecchia (1998, 2014)
PVSJ 883	late Carnian	1.1%	PVSJ 883; Martínez et al. (2013)
Raeticodactylus filisurensis	late Norian (Sevatian 1)	27.5%	BNM 14524; Stecher (2008); Dalla Vecchia (2014)
Rhamphorhynchus muensteri	late Kimmeridgian-early Tithonian	76.0%	SNSB-BSPG 1929 I 69, 1938 I 503; and those listed in Wellnhofer (1975a, b)
Saturnalia tupiniquim	late Carnian	60.7%	MCP 3844−3846-PV; Langer et al. (1999, 2007); Langer (2003); Bronzati et al. (2017, 2019)
Seazzadactylus venieri	middle-late Norian (late Alaunian-earliest Sevatian)	28.3%	MFSN 21545; Dalla Vecchia (2019)
Tawa hallae	late Norian	72.6%	GR 155, 241−243, 1033; Nesbitt et al. (2009b); Burch (2014); Bradley et al. (2020)

List of terminals scored for the 3D morphogeometric character

The endosseous labyrinth of the inner ear of the following 16 taxa was 3D morphogeometrically sampled and this configuration included in the phylogenetic analysis as a continuous character: *Mesosuchus browni*, *Trilophosaurus buettneri*, *Prolacerta broomi*, *Proterosuchus fergusi*, *Triopticus primus* (deactivated), *Herrerasaurus ischigualastensis*, *Parringtonia gracilis*, *Teleocrater rhadinus*, *Asilisaurus kongwe*, *Heterodontosaurus tucki*, *Euparkeria capensis*, *Lewisuchus*

admixtus, *Megapnosaurus rhodesiensis*, *Chanaresuchus bonapartei*, *Gracilisuchus stipanicicorum*, *Arizonasaurus babbitti*, *Parasuchus hislopi*, *Wannia scurriensis*, *Saturnalia tupiniquim*, *Dromomeron gregorii*, *Ixalerpeton polesinensis*, *Allkaruen koi*, and *Rhamphorhynchus muensteri*.

Characters modified from the data matrix of Butler et al. (2019)

10. External naris, anteroposterior position in the rostrum: (0) terminal, close to the anteriormost point of the premaxilla-maxilla suture; (1) nonterminal, considerably posteriorly displaced a distance equivalent to the length of the external naris from the anteriormost point of the premaxilla-maxilla suture, but posterior rim of the naris anterior to or at the level of the anterior border of the antorbital fenestra; (2) nonterminal, considerably posteriorly displaced a distance equivalent to the length of the external naris from the anteriormost point of the premaxilla-maxilla suture, and posterior rim of the naris posterior to the anterior border of the antorbital fenestra. The formulations of the character states were slightly modified here.
11. External naris, facing: (0) laterally; (1) dorsally; (2) anteriorly. The wording of the character was slightly modified.
12. External naris, shape: (0) sub-circular; (1) non-sub-circular. The wording of the second state was modified here, but without implying changes in scorings.
14. Antorbital fenestra, anterior margin in lateral view: (0) gently rounded; (1) nearly pointed, with the dorsal and ventral margins of the fenestra diverging at a low angle. This wording of this character was slightly modified here, but without affecting scorings.
17. Orbit, laterally thickened orbital rim along the jugal, postorbital, frontal, prefrontal and lacrimal: (0) absent or incipient; (1) present, restricted to the ascending process

of the jugal and sometimes also onto the ventral process of the postorbital; (2) present, well-developed along the jugal, postorbital, frontal, prefrontal and lacrimal. The formulation of this character was modified here, without affecting scorings.

20. Rostrum, rostrum length (anterior tip of the skull to anterior margin of the orbit) versus total length of the skull: (0) 0.29-0.40; (1) 0.43-0.64; (2) 0.70-0.76. The wording of this character was slightly modified, without affecting scorings.

21. Rostrum, dorsoventral height at the level of the anterior tip of the maxilla versus dorsoventral height at the level of the anterior border of the orbit: (0) <=0.33; (1) 0.40-0.52; (2) 0.59-0.80. The lower boundary of the second character state was expanded here.

22, 23 and 27. Changed ‘snout’ by ‘rostrum’ in character formulation.

34. Premaxilla, prenarial process (= nasal process) length: (0) less than the anteroposterior length of the main body of the premaxilla; (1) greater than the anteroposterior length of the main body of the premaxilla. The wording of this character was slightly modified, without affecting scorings.

35. Premaxilla, base of the prenarial process (= nasal process): (0) anteroposteriorly shallow; (1) anteroposteriorly deep. The wording of this character was slightly modified, without affecting scorings.

36. Premaxilla, postnarial process (= maxillary process): (0) absent or incipient; (1) short, ends well anterior to the posterior margin of the external naris; (2) well-developed, forms the vast majority of the ventral border of the external naris. The formulation of the first and third character states were modified here.

53. Maxilla, shape of the neurovascular foramina on the lateral surface of the anterior and horizontal processes: (0) laterally or lateroventrally facing; (1) lateroventrally

facing and extending ventrally as deep, well-defined grooves. The wording of the definition of this character was slightly modified here.

54. Maxilla, antorbital fossa on the lateral surface of the bone: (0) absent or not exposed in lateral view; (1) present on the ascending process of the maxilla, but not along the horizontal process (= posterior process) of the maxilla; (2) present on the horizontal process (= posterior process) of the maxilla ventral to the antorbital fenestra, but not reaching the posteroventral corner of the maxillary contribution to the border of the opening; (3) present on the horizontal process (= posterior process) of the maxilla ventral to the antorbital fenestra, reaching the posteroventral corner of the maxillary contribution to the border of the opening. ORDERED. The formulations of the third and fourth character states were modified here.

55. Maxilla, anteroposterior length of the antorbital fossa anterior to the antorbital fenestra versus length of the antorbital fenestra: (0) 0.09-0.23; (1) 0.28-0.66; (2) 0.83-0.94; (3) >2.00. The upper range of the second state was expanded here.

58. Maxilla, ascending process shape: (0) simply tapers to point dorsally; (1) the dorsal apex of the maxilla is a separate, distinct process differentiated from the rest of the maxilla by strongly concave or sharply flexed margins; (2) the dorsal apex of the maxilla is a distinct process with a sub-vertical anterior margin at its base. The formulations of the second and third character states were modified to ensure their independence with character 706.

59. Maxilla, anterior margin of the base of the ascending process: (0) convex or straight; (1) concave. The wording of the formulation of the character was slightly modified.

67. Maxilla, position of the palatal process: (0) adjacent to the ventral margin of the medial surface of the maxilla or base of the interdental plates if they are present; (1) distinctly dorsally to the ventral margin of the medial surface of the maxilla or base

of the interdental plates if they are present. Here, the character states were slightly reworded.

75. Maxilla, number of tooth positions (if the maxillary tooth count is not available the character can be scored using the dentary tooth count): (0) 4-7 (<7 dentary tooth positions); (1) 8-9 (8-10 dentary tooth position); (2) 10-14 (10-17 dentary tooth positions); (3) 15-22 (13-25 dentary tooth positions); (4) 23-35 (26-40 dentary tooth positions); (5) >36 (>41 dentary tooth positions).

It was found a significant correlation between the number of tooth positions in the maxilla and those in the dentary for 39 of the pan-archosaur species sampled in this analysis (cor = 0.9494992, p-value = 2.2e-16). As a result, the number of tooth positions in the dentary was not included as an independent character, but as a complementary state of the original character that sampled the number maxillary teeth. A biplot of the number of maxillary versus dentary teeth was used to determine the ranges of lower jaw tooth positions that matched those in the maxilla. The intention is to use the number of dentary tooth positions for the terminals in which that number is unknown for the maxilla. Observation: the dentary tooth count should not be used to score this character for terminals in which the premaxilla and maxilla are subequal in length (e.g. phytosaurs) or the maxillary and dentary teeth have very differend sizes (e.g. several pterosaurs).

Terminal	#mx	#dt	Reference
Aetosaurus ferratus	9	8	Schoch, 2007: 18
Arizonasaurus babbitti	12	13	Nesbitt, 2005: 25, 29
Asilisaurus kongwe	12	10	Nesbitt et al., 2020
Azendohsaurus madagaskarensis	14	17	Flynn et al., 2010: 682
Batrachotomus kupferzellensis	11	12	Gower, 1999: 15
Boreopricea funerea	33	35	Tatarinov, 1978: 510
Chanaresuchus bonapartei	18	18	Romer, 1971b: 13
Cteniogenys sp.	30	30	Evans, 1990
Dinocephalosaurus orientalis	15	21	Rieppel et al., 2008
Eoraptor lunensis	17	20	Sereno et al., 2013: 119

Erpetosuchus granti	4	11	Benton and Walker, 2002: 32
Erythrosuchus africanus	11	13	Gower, 2003: 13
Eudimorphodon ranzii	25	26	Wild, 1979: fig. 1
Garjainia prima	14	13	Ezcurra et al., 2019
Herrerasaurus ischigualastensis	18	16	Sereno and Novas, 1994
Heterodontosaurus tucki	13	13	AM 4765
Lesothosaurus diagnosticus	15	17	Porro et al., 2015
Lewisuchus admixtus	20	22	PULR 01
Litorosuchus somnii	12	21	Li et al., 2016: 5, 6
Macrocnemus bassanii	34	40	PIMUZ T4822, T2472
Macrocnemus fuyuanensis	36	42	Jiang et al., 2011: 1233
Megapnosaurus rhodesiensis	20	25	Raath, 1977
Ornithosuchus woodwardi	9	10	Walker, 1964: 78
Planocephalosaurus robinsonae	17	14	Fraser, 1982: 719
Preondactylus buffarinii	19	25	Dalla Vecchia, 1998
Prestosuchus chiniquensis	13	14	Mastrantonio et al., 2019
Prolacerta broomi	26	27	Gow, 1975
Rhamphorhynchus muensteri	7	7	Wellnhofer, 1975a
Riojasuchus tenuisceps	8	9	Baczko and Desojo, 2016: 22
Seazzadactylus venieri	14	21	Dalla Vecchia, 2019
Shansisuchus shansisuchus	13	16	Young, 1964; Wang et al., 2013
Silesaurus opolensis	11	12	Dzik, 2003
Simoedosaurus lemoinei	41	49	Russell-Sigogneau and Russel, 1978
Spinosuchus combined	11	11	Spielmann et al., 2008: 105, 107
Stagonolepis robertsoni	12	10	Walker, 1961: 132
Tanystropheus longobardicus	15	19	Nosotti, 2007: 21, 27
Tarjadia ruthae	6	13	CRILAR-Pv 495
Ticinosuchus ferox	15	18	PIMUZ T2817
Xilousuchus sapingensis	15	13	Nesbitt et al., 2011: 272, 275
Youngosuchus sinensis	11	13	IVPP V3239

77. Changed ‘snout’ by ‘rostrum’ in character formulation.

81. Nasal, descending process, which results from the articulation of the postnarial process (= maxillary process) of the premaxilla on the anterodorsal surface of the nasal and has an extensive contact with the ascending process of the maxilla: (0) anteroposteriorly narrow; (1) anteroposteriorly very broad, being considerably broader than the ascending process of the maxilla. The formulation of this character was slightly modified here.

92. Jugal, anterior process shape in lateral view: (0) continuously tapering or subrectangular, being lower than the portion of the maxilla underneath it; (1) subrectangular or slightly dorsoventrally expanded, being higher than the portion of the maxilla underneath it; (2) with an ascending subprocess excluding the lacrimal from the posteroventral border of the antorbital fenestra; (3) with a strongly developed ascending subprocess that excludes the lacrimal from the posterior border of the antorbital fenestra. The third character state was slightly reworded and a fourth character state was added.

101. Jugal posterior process with a distinct lateroventral orientation with respect to the sagittal axis of the rostrum: (0) absent; (1) present. Changed ‘snout’ by ‘rostrum’ in character formulation.

112. Frontal, frontals fused to one another in skeletally mature individuals: (0) absent; (1) present. The formulation of this character was slightly modified here.

120. Frontal, ventral surface: hour-glass-shaped median longitudinal canal for the passage of the olfactory duct and olfactory bulb moulds on the anterior end of the bone (0); median longitudinal canal for the passage of the olfactory duct only slightly constricted, no olfactory bulb moulds and distinct semilunate posteromedially-to-anterolaterally oriented ridge on the orbital roof, extending onto the prefrontal (1); olfactory tract and bulbs strongly reduced (2). A third character state was added here.

126. Postorbital-squamosal, upper temporal bar: (0) positioned distinctly ventral to the level of the dorsal border of the orbit, broadly exposing the supratemporal fenestra in lateral view; (1) positioned approximately aligned to the dorsal border of the orbit and the supratemporal fenestra is almost not exposed in lateral view. The character states were reworded here.

159. Parietal, median contact between both parietals in skeletally mature individuals: (0) suture present; (1) fused with loss of suture. The formulation of this character was slightly modified here.

175. Neomorphic bone (= septomaxilla of phytosaurs), separate ossification anterior to nasals and surrounded by the premaxilla on the dorsal surface of the rostrum: (0) absent; (1) present. Changed ‘snout’ by ‘rostrum’ in character formulation.

188. Palatine-pterygoid, teeth on the palatine and/or ventral surface of the anterior ramus of the pterygoid: (0) present; (1) absent. The formulation of the character was slightly modified here.

247. Basisphenoid/parabasisphenoid, basipterygoid processes: (0) moderately short, finger-like and with short articulating facets; (1) long, with hemispherical articulating facets; (2) very short and subcylindrical; (3) extremely long and rod-like, being longer than the body of the basisphenoid. A fourth character state was added here.

266. Dentary, minimum height of the bone (excluding the downturning anterodorsal margin) versus length of the alveolar margin (including edentulous anterior end if present): (0) 0.05-0.14; (1) 0.16-0.19; (2) 0.22-0.29; (3) 0.32-0.36. The formulation of the character was slightly modified here. This character is considered inapplicable if at least the anterior half of the dentary tapers continuously towards its tip (e.g. rhynchosaurids).

267. Dentary, shape of the anterior region of the tooth bearing portion: (0) mostly straight; (1) distinctly dorsally curved during all or most of its extension; (2) ventrally curved or deflected. The formulation of this character was slightly modified here.

271. Dentary, dorsal margin of the anterior portion compared to the dorsal margin of the posterior portion: (0) horizontal (in the same plane); (1) dorsally expanded, resulting

in a convex anterior margin and a straight or concave posterior portion. The wording of the second state was modified here.

278. Dentary, tooth row: (0) teeth present along entire length of the dentary; (1) teeth absent in the anterior end; (2) dentary edentulous. The states of this character have been reworded, but without modification of their definition.

284. Surangular-articular, retroarticular process: (0) subrectangular, approximately straight dorsal and ventral margins; (1) upturned, resulting in a concave dorsal margin immediately posterior to the glenoid fossa; (2) ventrally expanded, resulting in a concave ventral margin of the hemimandible at the level of the glenoid fossa. A third character state was added here because of the condition in some early pterosaurs and the other states were reworded.

299. Teeth, geometry of tooth implantation: (0) subthecodont (= protothecodont); (1) thecodont; (2) pleurodont; (3) acrodont. The “thecodont” [former state (4)] and “ankylothecodont” [former state (1)] were merged into “thecodont” (state 1) to follow the nomenclature of Bertin et al. (2018). The nature of tooth attachment (sensu Bertin et al., 2018) is sampled in character 752.

304. Teeth, serrations on the marginal crowns: (0) absent or present in just a two or a few centrally placed maxillary crowns; (1) distinctly present on the distal margin and usually apically restricted, low or absent on the mesial margin of most crowns; (2) present and distinct on both margins of most crowns. The formulation of the character was slightly modified here.

324. Cervical vertebrae, number of vertebrae in the neck: (0) less than eight; (1) eight or nine; (2) ten or more. The formulation of the third character state was modified here.

343. Cervical vertebrae, anterior and middle postaxial cervical neural spines with an anterior overhang: (0) absent, straight anterior margin of the neural spine; (1)

present, anteriorly curved anterior margin of the neural spine. Character states slightly reworded from their original formulations.

351. Dorsal vertebrae, length of the centrum versus height of the centrum in anterior dorsal vertebrae: (0) 0.45-1.10; (1) 1.18-2.00; (2) 2.19-2.74; (3) >3.00. ORDERED. A fourth state was added here.

352. Dorsal vertebrae, length of the centrum versus height of the centrum in posterior dorsal vertebrae: (0) 0.66-1.39; (1) 1.48-1.86; (2) 1.95-2.10; (3) 2.39-2.46. ORDERED. The upper boundary of the third state was expanded here.

367. Dorsal ribs, angle between proximal end and shaft in anterior and middle dorsal ribs in anterior or posterior view: (0) low, gentle bowing; (1) sharp flexure close to an angle of 90°. The character states were inverted and their wording modified here. However, these changes did not imply a rescoring of the terminals.

385. The formulation of this character did not change, but it was added that the character is inapplicable in taxa with a hook-shaped anterior margin of the coracoid (i.e. phytosaurs).

414. Forelimb-hindlimb, length ratio: (0) <0.55; (1) >0.55–<1.5; (2) 1.5–3.0; (3) >3.0 (modified from Codorniú et al., 2016: 88). The first and second character states were swept and third and fourth character states were added here.

422. Humerus, shape of the deltopectoral crest in lateral view: (0) rounded or subtriangular; (1) subrectangular or trapezoidal, broad, and short (campylognathoid-like in pterosaurs); (2) trapezoidal, narrow, and long (*Dimorphodon*-like in pterosaurs); (3) mid-proximally constricted with an expanded and rounded apex (*Rhamphorhynchus*-like in pterosaurs). Third and fourth character states were added here because of the condition present in some pterosaurs. Character state (2) can be also described as ‘lobular and proximally curved’.

1650 432. Ulna, olecranon process as a separate ossification in skeletally mature individuals:
1651 (0) absent; (1) present. The formulation of this character was slightly modified here.
1652 435. Radius, total length versus total length of the humerus: (0) 0.62-0.66; (1) 0.69-
1653 0.92; (2) 0.95-0.97; (3) 1.12-1.28; (4) ≥1.33. ORDERED. The upper range of the
1654 fourth character state and a fifth character-sate were modified and added here,
1655 respectively.
1656 446. Metacarpus, length of the longest metacarpal versus length of the longest
1657 metatarsal: (0) <0.45; (1) 0.54-0.59; (2) 0.69-1.35. The lower range of the first
1658 character state and the lower and upper ranges of the third character state were
1659 modified here.
1660 448. Metacarpus, transverse width of the distal end of metacarpal I versus the total
1661 length of the bone: (0) ≤0.33; (1) 0.36-0.45; (2) 0.48-0.53; (3) 0.58-0.64; (4) 0.73-
1662 0.75; (5) >1.00. The lower range of the first character state was modified here in
1663 order to sample the condition in *Dromomeron romeri* and pterosaurs.
1664 455. Pelvic girdle, acetabulum: (0) completely closed; (1) perforated, slightly concave,
1665 straight or slightly convex; (2) perforated, markedly concave (Bakker and Galton,
1666 1974; Cabreira et al., 2016: 148) ORDERED. The formulation of the second state
1667 was changed here and it was added the third state.
1668 458. Ilium, maximum height of the acetabulum versus length of the femur: (0) ≤0.17;
1669 (1) 0.21-0.47; (2) 0.54-0.57. The range of the first state was modified here.
1670 461. Ilium, outline of preacetabular process in lateral or medial view: (0) semicircular;
1671 (1) subtriangular or finger-like; (2) squared (Galton, 1976; modified from Cabreira et
1672 al., 2016: 143). A third character state was added here.

463. Ilium, length of the postacetabular process versus anteroposterior length of the acetabulum: (0) 0.31-0.63; (1) 0.79-1.24; (2) 1.31-1.37; (3) 1.49-1.90. ORDERED. The upper limit of the fourth state was expanded here.

470. Pubis-ischium, contact: (0) present and extended ventrally up to or beyond the distal end of the pubic shaft or spine; (1) present and extended ventrally but not reaching the level of the distal end of the pubic shaft or spine; (2) present and reduced to a thin proximal contact; (3) absent (modified from Nesbitt, 2011) ORDERED. This character is inapplicable in taxa with a thyroid fenestra.

472. Pubis, total length (along anterior margin or pubic shaft or tubercle) versus total length of the femur: (0) ≤0.29; (1) 0.32−0.45; (2) 0.48−0.57; (3) ≥0.60. ORDERED. The formulation of this character was modified (pubis versus femur length, instead of pubis versus acetabulum length) and, as a result, all the ratios were recalculated. The character was turned into four discrete states and the scorings of most terminals were modified.

476. Pubis, shape: (0) plate-like, with approximately constant transverse width anteroposteriorly; (1) laterally thickened anterior edge or distinct shaft (= pubic tubercle, = pectineal tuberosity) that curves posteriorly in lateral view; (2) laterally thickened anterior edge or distinct shaft (= pubic tubercle, = pectineal tuberosity) that is straight in lateral view; (3) laterally thickened anterior edge or distinct shaft (= pubic tubercle, = pectineal tuberosity) with a proximodistally concave anterior surface. A fourth character state was added here and the wording of this character was modified.

482. Ischium, total length versus anteroposterior length of the acetabulum: (0) 1.04-1.24; (1) 1.55-2.50; (2) 2.72-3.53; (3) 4.25-4.48. The lower range of the fourth character state was extended here.

489. Femur, total length versus total length of the humerus: (0) <1.02; (1) 1.09-1.56; (2) 1.62-1.74; (3) 1.86-1.96; (4) >2.05. The lower range of the first character state was modified and a fifth character state was added here.

492. Femur, femoral head: (0) not distinctly inturned with respect to the shaft; (1) distinctly inturned with respect to the shaft. The wording of the character states was reworded here.

502. Femur, anterior trochanter (= lesser or minor trochanter) (= iliofemoralis cranialis muscle insertion): (0) absent; (1) present and forms a steep margin with the shaft but is completely connected to it; (2) present and separated from the shaft by a marked cleft; (3) present and approaches the proximal articulation of the bone (Bakker and Galton, 1974; Cabreira et al., 2016: 182) ORDERED. The second character state was reworded and the third and fourth character states were added here.

516. Tibia, total length versus total length of the femur: (0) 0.46-0.55; (1) 0.60-0.65; (2) 0.70-1.30; (3) ≥1.35. The upper boundary of the third state and the boundaries of the fourth state were expanded here.

521. Tibia, distal portion, posterolateral process (= lateral malleolus): (0) absent; (1) present, distinctly medial or extends laterally approximately at the same level as the anterolateral corner; (2) present and extends well lateral to the anterolateral corner (Novas, 1992; modified from Cabreira et al., 2016: 205) ORDERED. The second character state was reworded and the third character state was added here.

569. Metatarsus, length of metatarsal I versus metatarsal III: (0) 0.17-0.21; (1) 0.27-0.42; (2) 0.46-0.79; (3) >0.90. ORDERED. The upper range of the fourth character state was slightly increased.

574. Metatarsus, length of metatarsal IV versus length of metatarsal III: (0) 0.80-1.00; (1) 1.04-1.08; (2) 1.11-1.28; (3) 1.31-1.34. The lower boundary of the first state was expanded here.

581. Pedal digits, length of digit III versus length of digit IV (excluding metatarsals): (0) 0.64-0.77; (1) 0.81-0.83; (2) 0.87-1.44. The formulation of this character was slightly reworded.

583. Pedal digits, ratio of lengths of pedal digits V and I (excluding metatarsals): (0) 0.30-0.85; (1) 1.13-3.60. ORDERED. The upper range of the second character state was increased, and the formulation was also slightly reworded.

627. Jugal, orientation of the ascending process in lateral view when articulated with the maxilla: (0) mainly dorsal to posterodorsal in an angle higher than 45º; (1) strongly posterodorsally oriented in an angle equal to or lower than 45º. The formulation of this character was slightly modified here, without affecting scorings.

636. Quadratojugal, orientation of the main axis of the dorsal process with respect to the coronal plane of the skull: (0) approximately vertical (ca. 90°) or slightly anterodorsally to posteroventrally oriented in an angle higher than 60º; (1) moderately anterodorsally to posteroventrally slanted in an angle between 60° and 40º; (2) strongly anterodorsally to posteroventrally slanted in an angle lower than 40º (Upchurch et al., 2007; Cabreira et al., 2016: 33; modified from Ezcurra et al., 2017: 636). ORDERED. This character is inapplicable in taxa that lack a distinct anterior process of the quadratojugal or a quadratojugal bone.

656. Cervical vertebrae, epipophyses: (0) absent in posterior cervical vertebrae (6–9); (1) present in at least one of the posterior cervical vertebrae (6–9). The second state was slightly reworded.

663. Sacral vertebrae, centra in skeletally mature individuals: (0) separate; (1) coossified at the ventral edge. The formulation of this character was slightly reworded here.

671. Femur, medial margin of the femoral head in proximal view: (0) rounded; (1) straight. The formulation of this character was modified here, without affecting scorings.

672. Femur, angle between the lateral condyle and the crista tibiofibularis in distal view: (0) obtuse or approximately right angled, crista tibiofibularis not laterally expanded; (1) right or acute angle as a result of the lateral expansion of the crista tibiofibularis. Character states were reworded here.

680. Teeth, generalized morphology of maxillary and dentary tooth crowns: (0) single, pointed crown; (1) flattened platform with pointed cusps; (2) mesiodistally arranged cusps, tri- to quinticuspid tooth crowns (modified from Dalla Vecchia, 2009a: 33; Britt et al., 2018: 43). The formulation of the third character state was expanded here.

681. Cervical and dorsal vertebrae, shape of posterior articular surface of the centrum: (0) planar; (1) concave; (2) convex. The wording of the character was slightly modified here.

689. Pedal digits, penultimate phalanges (last phalanx before ungual if ungual present): (0) shorter or sub-equal than the more proximal phalanges; (1) distinctly longer than the more proximal phalanges. Minor modification to the wording of the character.

Characters added to the data matrix of Butler et al. (2019)

Introductory remarks to characters of the endosseous labyrinth of the inner ear. After detailed and careful comparisons of diapsid inner ear labyrinths, we discretized a total of 15 independent characters sampling their shape variation (e.g. height-width ratio of

labyrinth, curvature of semicircular canals, canal slenderness; characters 728−742, see below). We have found that measurements of 3D structures of the labyrinth can include substantial error when they are approximated from 2D screenshots, because even subtle deviations in orientation of the 3D object can have large downstream effects, especially for angle measurements. We also found difficult to take measurements from complete 3D models because key structures can be obstructed by others. As a result, we think that the assessment of most of these characters should ideally be based on angles and length measurements derived from 3D landmark coordinate data using 3D Euclidean distance algebra in R (R Core Team, 2019). In order to allow that, landmarks were placed on 3D models of endosseous labyrinths in Avizo lite 9.2 (https://www.fei.com/software/amira-avizo/).

To capture the arc length of the semicircular canals (SSCs), landmarks were densely placed along the inner perimeter of the SSCs (Extended Data Fig. 9B). SSC arc lengths were calculated as the sum of the Euclidean distances between these landmarks, and SSC straight lengths were calculated as the Euclidean distance between the first and last arc landmark. The circumference of the anterior semicircular canal (ASC) was calculated as the sum of the Euclidean distances between landmarks placed densely around the ASC, near its connection with the anterior ampulla (Extended Data Fig. 9E). Only the ASC was sampled for its circumference because our observations indicate that SSC diameters are subequal among the tree SSCs. For the placement of the remaining landmarks, the 3D models of the endosseous labyrinth were horizontally sectioned through the course of the lateral semicircular canal (LSC) to produce a reference plane (Extended Data Fig. 9C). This plane allows coherent placement of landmarks and subsequent distance measurements. The height of the common crus (CC) was defined by two landmarks on top of the CC and ventrally underneath it on the reference plane

(Extended Data Fig. 9E). The mediolateral width of the labyrinth was defined by two landmarks placed on the reference plane, at the lateral-most margin of the lateral semicircular canal (LSC) and at the medial margin of the labyrinth (Extended Data Fig. 9F). The vestibular width was also defined by the medial labyrinth landmark, and a landmark placed at the lateral margin of the vestibule on the reference plane (Extended Data Fig. 9F). A landmark on the dorsal-most point of the vestibular surface and another vertically underneath it on the reference plane quantified the vestibular expansion (Extended Data Fig. 9E). The resulting morphometric measurements were used to quantify variation in labyrinth shape among specimens, and formed the basis for some of the labyrinth characters of this phylogenetic analysis.

Characters added:

696. Skull openings, relative size of external naris: (0) as long as or shorter anteroposteriorly than the antorbital fenestra; (1) longer anteroposteriorly than the antorbital fenestra (Unwin, 2003: 8; modified from Britt et al., 2018: 20). This character is inapplicable in taxa that lack an antorbital fenestra [character 13(0)].

697. Skull openings, shape of antorbital fenestra: (0) length more than twice the height; (1) length twice the height or less (Unwin, 2003: 10; Britt et al., 2018: 22). This character is inapplicable in taxa that lack an antorbital fenestra [character 13(0)].

698. Skull openings, relative size of orbit: (0) longer anteroposteriorly than antorbital fenestra; (1) equal or shorter anteroposteriorly than antorbital fenestra (Unwin, 2003: 14; Cabreira et al., 2016: 45; Britt et al., 2018: 26). This character is inapplicable in taxa that lack an antorbital fenestra [character 13(0)].

699. Rostrum, dorsal margin outline of rostrum in lateral view: (0) strongly convex; (1) approximately straight, slightly sigmoid or concave (Unwin, 2003: 1; reworded from Britt et al., 2018: 4).

700. Orbital and temporal regions, dorsal margin outline in lateral view: (0) rather straight; (1) strongly convex dorsally (New character).

701. Premaxilla, postnarial process (= maxillary process) contact with nasal: (0) broad contact; (1) point contact; (2) no contact (Yates, 2003; Cabreira et al., 2016: 4) ORDERED. This character is inapplicable in taxa that lack a postnarial process of the premaxilla [character 36(0)].

702. Premaxilla, prenarial process (= posterodorsal process) contact with frontal: (0) absent; (1) present (reworded from Codorniú et al., 2016: 12). This character is inapplicable in taxa that lack the prenarial process of the premaxilla.

703. Premaxilla, palatal process widely visible in lateral view ventral to the postnarial process: (0) absent or incipiently visible; (1) present (Rauhut, 2003; reworded from Cabreira et al., 2016: 8). This character is considered independent to character 29 because, for example, *Tawa hallae* has a downturned premaxilla but possesses an incipiently visible premaxillary palatal process in lateral view. This character is inapplicable if a premaxillary palatal process is absent [character 41(0)].

704. Maxilla, neurovascular foramina on the lateral surface: (0) absent; (1) present (New character).

705. Maxilla, shape of anterior process (= premaxillary process) in lateral or medial view: (0) sub-triangular, shorter and considerably dorsoventrally higher than the posterior process; (1) continuously tapering, ending in a pointed end, and as low and long as the posterior process; (2) trapezoidal, with an extensive diagonal suture with

the premaxilla, and approximately as low as the posterior process (modified and reworded from Britt et al., 2018: 11).

706. Maxilla, anteroposterior width of ascending process in lateral or medial view: (0) broad, its base occupies most of the anterior half of the bone; (1) very thin, resulting in an external naris separated from the antorbital fenestra by a strap-like bar of bone (Unwin, 2003: 5; modified from Britt et al., 2018: 7).

707. Maxilla, shape of the ascending process of the maxilla in lateral or medial view: (0) straight; (1) posteriorly arched (Unwin, 2003: 5; modified from Britt et al., 2018: 7). This character is inapplicable in taxa that lack an antorbital fenestra. See modification of character 58 to ensure its independence.

708. Maxilla, dorsoventrally elongated foramen on the lateral surface of the base of the ascending process: (0) absent; (1) present (Britt et al., 2018: 10).

709. Maxilla, ventral margin of the antorbital fossa: (0) smooth (continuous to the more ventral area); (1) elevated relative to the ventral surface (sharp longitudinal ridge present) (= alveolar ridge) (Rowe, 1989; Nesbitt, 2011; Cabreira et al., 2016: 12). This character is inapplicable in taxa that lack an antorbital fenestra or an antorbital fossa ventral to the antorbital fenestra.

710. Maxilla, buccal emargination dorsolateral to the alveolar margin: (0) absent; (1) present (reworded form Butler, 2005).

711. Nasal, posterolateral process: (0) does not envelop part of the anterior process of the lacrimal; (1) has a V-shaped notch that receives part of the anterior process of the lacrimal (Yates, 2003; reworded from Cabreira et al., 2016: 16). This character is inapplicable in taxa that lack a nasal-lacrimal contact.

712. Lacrimal, shape of ventral process in lateral view: (0) does not fold over the posterodorsal part of the antorbital fenestra; (1) folds and extends over the

posterodorsal part of the antorbital fenestra (Sereno, 1999; Cabreira et al., 2016: 19). This character is inapplicable in taxa that lack an antorbital fenestra or a lacrimal bone.

713. Lacrimal, height: (0) distinctly less than the height of the orbit and usually fails to reach the ventral margin of the orbit; (1) approximately as high as the orbit and contacts the jugal at the level of the ventral margin of the orbit (Rauhut, 2003; Cabreira et al., 2016: 20). This character is inapplicable in taxa that lack a lacrimal bone.

714. Jugal, long axis of the body when articulated with the maxilla: (0) nearly horizontal to the alveolar margin of the maxilla; (1) oblique to the alveolar margin of the maxilla (Nesbitt, 2011; Cabreira et al., 2016: 26).

715. Jugal, ventral margin across anterior and posterior processes in lateral or medial view: (0) straight or forming an angle of more than 180°; (1) forming angle of less than 180° (Cabreira et al., 2016: 27). This character is inapplicable in taxa that lack a posterior process of the jugal.

716. Jugal, forked posterior process: (0) ventral tine longer than the dorsal one; (1) dorsal tine longer than or subequal to the ventral one (Tykoski and Rowe, 2004; Cabreira et al., 2016: 30). This character is inapplicable in taxa that lack a posterior process of the jugal or a forked posterior process of the jugal.

717. Frontal, transverse development posterior to the contribution to the orbital margin: (0) narrower than, or subequal to, the transverse width of the bone on the orbital margin; (1) broader than the transverse width of the bone on the orbital margin (modified from Pritchard et al., 2015: 15).

718. Postorbital, anterior process: (0) equal to or longer than the posterior process; (1) shorter than the posterior process (Ezcurra, 2006; Cabreira et al., 2016: 25).

719. Quadratojugal, dorsal process: (0) longer than the anterior process; (1) equal to or shorter than the anterior process (Langer and Benton, 2006; Cabreira et al., 2016: 32). This character is inapplicable in taxa that lack a distinct anterior process of the quadratojugal or a quadratojugal bone.

720. Quadrate, orientation in lateral or medial view: (0) inclined anteriorly (<90º with respect to the transverse plane of the skull); (1) vertical or subvertical (90-110°); (2) inclined posteriorly (>110°) (Unwin, 2003: 49; Britt et al., 2018: 18).

721. Opisthotic, base of paraoccipital process in occipital view: (0) directed laterally or dorsolaterally; (1) directed ventrolaterally (Rauhut, 2003; Cabreira et al., 2016: 38).

722. Perilymphatic foramen: (0) with an incompletely ossified border; (1) border entirely ossified such that the ventral ramus of the opisthotic forms a perilymphatic loop incorporating a loop closure suture with itself (Nesbitt, 2011: 129).

723. Parasphenoid/parabasisphenoid, outline of posterior margin in ventral view: (0) approximately straight or slightly concave; (1) deeply concave, with bone at median line anterior to basal tubera (reworded from Cabreira et al., 2016: 37).

724. Basisphenoid/parabasisphenoid, divergence between basipterygoid processes in the transverse plane: (0) widely diverging (angle between processes ≥35°); (1) narrow (angle < 35°) (Codorniú et al., 2016: 36).

725. Periotic bones, dorsoventral height of the base of the floccular fossa: (0) lower than 40% of the height of the cranial endocast at the level of anteroposterior mid-length of the fossa; (1) equal to or more than 40% of the height of the cranial endocast at the level of anteroposterior mid-length of the fossa (New character).

726. Periotic bones, shape of the lateral end of the floccular fossa: (0) rounded, resulting in a finger-like floccular cast in anterolateral view; (1) tapering laterally, resulting in a subtriangular floccular cast in anterolateral view (New character).

727. Prootic, pendant process in the crista prootica: (0) absent; (1) present (Sampson and Witmer, 2007).

728. Endocast, dorsal surface of midbrain and base of forebrain: (0) mostly flat or anteroposteriorly convex; (1) midbrain with a dorsal eminence and an anteroposteriorly concave surface between hindbrain and forebrain (New character).

729. Inner ear, geometry of the anterior semicircular canal (ASC): (0) ASC is relatively straight, with a course that remains within a vertical plane for its full length; (1) ASC bowed posterolaterally so its course deviates from a vertical plane (New character).

730. Inner ear, geometry of the posterior semicircular canal (PSC): (0) PSC is relatively straight, with a course that remains within a vertical plane for its full length; (1) PSC bowed anterolaterally so its course deviates from a vertical plane (New character).

731. Inner ear, ratio between maximum height of anterior semicircular canal and posterior semicircular canal: (0) <1.05; (1) 1.09–1.14; (2) 1.22–1.35; (3) 1.46–1.60; (4) 1.75–1.89 (New character). ORDERED.

See 'Ratios calculated for the scoring and/or discretization of characters' for the ratios calculated for each terminal scored here and that were used for the discretization of the character.

732. Inner ear, dorsal intersection between anterior semicircular canal (ASC) and posterior semicircular canal (PSC): (0) ASC and PSC meet in an angle of c. 180°, forming a dorsally convex or essentially flat intersection at the common crus; (1) ASC and PSC meet in an angle lower than c. 90º, forming a dorsal embayment; (2) ASC and PSC meet in an angle of c. 90º, forming a posterior embayment (New character). This character is inapplicable when the ASC intersects the common crus well dorsal to the PSC.

733. Inner ear, thickness of common crus: (0) common crus has roughly the same cross-sectional area as the semicircular canals; (1) common crus is very thick, with a much larger cross-sectional area than semicircular canals (New character).

734. Inner ear, angle between portions of the anterior semicircular canal and posterior semicircular canal that are adjacent to the common crus in the coronal plane: (0) angle is approximately 90°, generally less broad labyrinths; (1) angle significantly exceeds 90°, generally low, broad labyrinths (New character).

The angle between the ASC and PSC is defined herein as the inner angle between the two vertical planes that best describe the courses of these canals. This angle can be assessed in dorsal view, but the vertical planes need to be orthogonal to a horizontal plane laid through the LSC. Ideally, we suggest the following procedure to measure the angle: 1. cut the labyrinth model horizontally, 2. turn the labyrinth model on its head, so that the horizontal cut plane is perfectly parallel to your screen, 3. render the model transparent, 4. draw straight lines through the course of the ASC and PSC onto the horizontal plane, and 5. measure the angle on the horizontal plane.

735. Inner ear, posterior part of the lateral semicircular canal (LSC): (0) the posterior section of the LSC is not or only vaguely discernible, because the lateral semicircular duct shares a single osseous cavity, i.e. is confluent with the vestibular cavity and the cavity for the ventral section of the posterior semicircular canal (PSC); (1) near separated LSC and PSC, most aspects of the canals are visible, including the position of the posterior ampulla, but the ventral surface of the LSC is still confluent with the vestibular cavity; (2) LSC (and PSC) are completely separated from the vestibular cavity, and are separated from one another expert for a short intersection segment (New character). ORDERED.

736. Inner ear, relative position of the common crus: (0) the common crus is positioned centrally on the anteroposterior axis between the anterior semicircular canal and posterior semicircular canal; (1) the common crus is positioned posterior to the midpoint of the anteroposterior axis of the labyrinth (New character).

The relative position of the common crus can be measured assuming a horizontal plane through the LSC, and then taking the distance of the ventral base of the common crus on that plane to the intersection of the ASC and the PSC with that plane, respectively. When both distances are equidistant, character state 0 is scored; when the ASC distance is (much) larger, character state 1 applies.

737. Inner ear, labyrinth general proportions, maximum height of the labyrinth versus maximum anteroposterior depth of the labyrinth: (0) <0.70; (1) 0.78–0.85; (2) >0.90 (New character). ORDERED.

The height of an osseous labyrinth is hard to measure, but we think that the common crus is the best candidate for constraining the height of a labyrinth. Our comparative observations indicate that the height of the common crus varies independently from shape aspects of the ASC, which, in many taxa, extends dorsally above the common crus and is therefore often the tallest (= furthest dorsally reaching) structure of osseous labyrinths. The height of the common crus is here defined as a straight-line measurement of a sub-vertical line that extends from the intersection of the PSC and ASC through the center of the cylindrical common crus with a horizontal plane laid through the LSC. Note that this straight line does not need to intersect the horizontal plane at an orthogonal angle because the common crus can meet the horizontal plane at an oblique angle. The ratio is calculated dividing the common crus length by the anteroposterior length of the labyrinth. This length is here defined as the straight-line

distance between the ASC and PSC intersections with the horizontal plane (Extended Data Fig. 9C).

See ‘Ratios calculated for the scoring and/or discretization of characters’ for the ratios calculated for each terminal scored here and that were used for the discretization of the character.

738. Inner ear, curvature of the anterior semicircular canal (ASC), ASC-arc-length versus ASC-straight-line ratio: (0) <1.40; (1) 1.53–1.64; (2) 1.85–2.00; (3) >2.00 (New character). ORDERED.

Our comparative observations indicate that the ASC is very differently curved across taxa. There is a spectrum between taxa in which the ASC is basically straight for most of its course (with relatively strong curvature concentrated at either end of the canal) and taxa in which the ASC is continuously curved to form a near-circular arc. Mathematically, several ways to quantify the curvature of an object exist. Here, we chose to define curvature as the ratio between the outer (=dorsal) arc-length of the ASC (extending from the common crus to the ASC’s intersection with a horizontal plane laid through the LSC) and the straight-line measurement between those points. This measurement was chosen because it is easier to measure than alternatives that include the radius of the arc.

See ‘Ratios calculated for the scoring and/or discretization of characters’ for the ratios calculated for each terminal scored here and that were used for the discretization of the character.

739. Inner ear, curvature of the posterior semicircular canal (PSC), PSC-arc-length versus PSC-straight-line ratio: (0) ≤1.16; (1) ≥1.20 (New character).

Our comparative observations indicate that the PSC is also differently curved across taxa. There is a spectrum between taxa in which the PSC is basically straight for most of its course (with relatively strong curvature concentrated at either end of the canal) and taxa in which the PSC is continuously curved to form a near-circular arc. The curvature is here defined as the ratio between the outer (=dorsal) arc-length of the PSC (extending from the common crus to the PSC's intersection with a horizontal plane laid through the LSC) and the straight-line measurement between those points. This measurement was chosen because it is easier to measure than alternatives that include the radius of the arc. Our observations indicate that the PSC and ASC curvatures are not correlated (character 737 for *Postosuchus*, see above).

See 'Ratios calculated for the scoring and/or discretization of characters' for the ratios calculated for each terminal scored here and that were used for the discretization of the character.

740. Inner ear, spatial relation between anterior and lateral ampullae: (0) anterior and lateral ampullae are close to one another; (1) very clear anteroposterior separation of anterior and lateral ampullae (New character).

741. Inner ear, orientation of common crus: (0) vertical; (1) posterodorsal, deviating from the vertical plane in an angle higher than 10º (New character).

When assessing this character the LSC should be oriented parallel to the horizontal plane.

742. Inner ear, straightness of common crus: (0) straight; (1) bowed, anteriorly convex (New character).

743. Inner ear, curvature of the lateral semicircular canal (LSC), LSC-arc-length versus LSC-straight-line ratio: (0) ≤1.05; (1) 1.09−1.21; (2) 1.31–1.37; (3) >1.45 (New character). ORDERED.

See 'Ratios calculated for the scoring and/or discretization of characters' for the ratios calculated for each terminal scored here and that were used for the discretization of the character.

744. Mandible, shape of the dorsal margin anterior to the glenoid fossa in lateral or medial view: (0) continuously convex, without distinct apices or depressions; (1) with a dorsal projection (coronoid process or surangular dorsal process in pterosaurs) approximately at mid-length between the last tooth position and glenoid fossa (modified from Dalla Vecchia, 2009a: 25 and Britt et al., 2018: 29).

745. Mandible, articular glenoid location: (0) at level with the dorsal margin of the posterior portion of the dentary; (1) ventral to the level of the dorsal margin of the posterior portion of the dentary (Gauthier, 1986; Cabreira et al., 2016: 57).

746. Predentary bone: (0) absent; (1) present (Sereno, 1986; Cabreira et al., 2016: 48).

747. Dentary, ventral mandibular bony crest: (0) absent; (1) present (Andres et al., 2014: 132; Britt et al., 2018: 34).

748. Dentary, low dorsal projection placed immediately posterior to the last tooth position: (0) absent; (1) present, formed only by the dentary and not by the coronoid (modified from Dalla Vecchia, 2009a: 25 and Britt et al., 2018: 29).

749. Dentary, separation between teeth: (0) distance between teeth less than mesiodistal diameter of the teeth; (1) distance between first two teeth more than mesiodistal diameter of the teeth; (2) distance between three or more teeth more than

mesiodistal diameter of the teeth (modified from Codorniú et al., 2016: 61). ORDERED.

750. Dentary, diastema (over 5 times longer than the distance between adjacent non-symphysial teeth) between the first two dentary teeth and those following distally: (0) absent; (1) present (slightly reworded from Britt et al., 2018: 52).

751. Dentary, arched ridge bounded dorsally and ventrally by narrow grooves along the lateral side of the mandibular ramus: (0) absent; (1) present (Britt et al., 2018: 36).

752. Dentary, mandibular buccal emargination: (0) absent, lateral dentary surface smooth; (1) present, lateral dentary surface with a posterior shelf bordering an emargination that encompasses half of the dentary length (Langer and Benton, 2006; Cabreira et al., 2016: 54).

753. Splenial, development: (0) anteriorly developed covering more than three-quarters of the length of the dentary; (1) reduced to the level of the posterior half of the dentary or bone absent (New character).

754. Teeth, nature of tooth attachment: (0) gomphosis; (1) ankylosis (based on nomenclature of Bertin et al., 2018).

755. Teeth, labial or lingual overlap of adjacent maxillary and dentary crowns: (0) absent; (1) present (Sereno, 1986; Cabreira et al., 2016: 66). This character is inapplicable in taxa with a maxillary tooth plate and a dentary cutting blade. If the overlap occurs in only one region of the maxilla or dentary, this is scored as (1).

756. Teeth, bifid apex of at least some marginal tooth crowns: (0) absent; (1) present (Britt et al., 2018: 41). This character is inapplicable in taxa with a maxillary tooth plate and a dentary cutting blade.

757. Teeth, serrations in the mesial margin of the premaxillary crowns: (0) present; (1) absent (Rowe, 1989; Cabreira et al., 2016: 246). This character is not applicable if

2091 the marginal teeth lack serrations [character 304(0)] or the premaxilla is edentulous
2092 [character 42(5)].
2093 758. Teeth, some with moderately developed lingual ledge of maxillary and dentary
2094 crown (= cingulum): (0) absent; (1) present, crown asymmetric in mesial or distal
2095 view (Sereno, 1986; Cabreira et al., 2016: 67). This character is inapplicable in taxa
2096 with a maxillary tooth plate and a dentary cutting blade.
2097 759. Teeth, shape of serrations in maxillary tooth crowns in labial or lingual view: (0)
2098 square or chisel-like; (1) triangular (New character). This character is inapplicable in
2099 taxa without serrated maxillary crowns.
2100 760. Teeth, maxillary teeth much enlarged below the dorsal process: (0) absent; (1)
2101 present (Dalla Vecchia, 2009a: 30; Britt et al., 2018: 47). This character is
2102 inapplicable in taxa with a maxillary tooth plate and is independent of the presence
2103 of a maxillary caniniform region [character 301(1)], in which there is a gradual
2104 increase in height of the tooth crowns rather than a few crowns distinctly higher
2105 tooth crowns.
2106 761. Teeth, mesial dentary crowns size: (0) crowns remain relatively same size
2107 throughout anterior portion of dentition; (1) crowns distinctly decrease in height
2108 anteriorly; (2) hypertrophied crown or crowns among the first three dentary teeth
2109 (Kammerer et al., 2011; modified from Cabreira et al., 2016: 72).
2110 762. Teeth, post-symphysial mandibular tooth crown size compared to maxillary tooth
2111 crown size: (0) comparable at least to part of maxillary crowns; (1) much smaller
2112 (Britt et al., 2018: 48).
2113 763. Teeth, first dentary tooth long axis with respect to the longitudinal axis of the
2114 bone: (0) vertical; (1) inclined anteriorly (i.e. procumbent) (Kammerer et al., 2011;

modified from Cabreira et al., 2016: 73). This character is inapplicable in taxa with groove-and-blade occlusion (i.e. rhynchosaurids).

764. Cervical vertebrae, development of parapophysis in the axis: (0) well developed on a distinct peduncle; (1) reduced to a low, mound-like structure or absent (Tykoski and Rowe, 2004; modified from Cabreira et al., 2016: 77).

765. Cervical vertebrae, postaxial cervical vertebrae with an anteroposteriorly elongated and large lateral pneumatic foramen around the mid-length of the centrum: (0) absent; (1) present (Codorniú et al., 2016: 72).

766. Cervical vertebrae, neural arch (from base of neural canal to top of postzygapophysis) in postaxial cervical vertebrae: (0) higher than posterior articular facet of the centrum; (1) lower than posterior articular facet of the centrum; (2) depressed down onto, or even confluent with, the centrum (Galton and Upchurch, 2004; character states merged from Cabreira et al., 2016: 87, and Codorniú et al., 2016: 75) ORDERED.

767. Cervical vertebrae, neural spine of the fourth to sixth cervical vertebrae in lateral view: (0) vertical or posterodorsally canted, with the top of the neural spine aligned with the parasagittal plane; (1) at least one vertebra with a distinctly anterodorsally canted neural spine, with the top of the neural spine anterodorsally oriented and parallel anterior and posterior margins of the neural spine (inspired from Nesbitt et al., 2015).

768. Dorsal vertebrae, lamina partially subdividing the centrodiapophyseal postzygapophyseal fossa: (0) absent; (1) present (Yates, 2004; Cabreira et al., 2016: 94). This character is inapplicable in taxa that lack a posterior centrodiapophyseal and/or postzygodiapophyseal laminae.

769. Sacral vertebrae, transverse processes and ribs development: (0) anteroposteriorly short not roofing the space between ribs; (1) anteroposteriorly long, roofing the space between ribs (Langer and Benton, 2006; Cabreira et al., 2016: 104).

770. Sacral vertebrae, first primordial sacral rib articular surface in lateral view: (0) circular; (1) C-shaped (Langer and Benton, 2006; Cabreira et al., 2016: 103).

771. Haemal arches, haemal spines developed as filiform processes below and parallel to adjacent centra posterior to the first three to seven caudal vertebrae: (0) absent; (1) present (reworded from Britt et al., 2018: 60).

772. Coracoid, shape of the coracoidal shaft (when the bone is posteriorly or dorsoventrally expanded, depending of orientation, to form an L-shaped shoulder girdle in lateral or medial view): (0) flat bone continuously tapering posteriorly and ventrally; (1) with an elongated and broad posteroventral shaft, flattened at midshaft; (2) with a strut-like posteroventral shaft, slender and cylindrical at midshaft (Sereno, 1991a; modified and reworded from Britt et al., 2018: 63). This character is inapplicable if the coracoid is not posteriorly expanded to form an L-shaped shoulder girdle.

773. Coracoid, relative dorsoventral length: (0) less than 2/3 length of scapula; (1) 2/3 or more length of scapula (Unwin, 2003: 33; Britt et al., 2018: 64).

774. Humerus, shape in lateral view (dorsolateral view in pterosaurs): (0) straight; (1) sigmoid (Rauhut, 2003; Cabreira et al., 2016: 120).

775. Humerus, size of deltopectoral crest: (0) scarcely or moderately anteriorly developed; (1) hypertrophied anteriorly and with a proximal apex close to the level of the humeral head (reworded from Britt et al., 2018: 67).

776. Pteroid bone: absent (0); present (1) (Sereno, 1991a).

777. Pteroid, pteroid-humerus ratio: (0) <0.30 (0); (1) 0.30−0.60 (Codorniú et al., 2016: 98).

778. Carpus, proximal carpals: (0) ulnare and radiale as different, separate ossifications; (1) single proximal carpal ossification (= proximal syncarpal) (New character).

779. Carpus, medialmost distal carpal (distal carpal 1 or its fusion to other element) size: (0) subequal to other distal carpals; (1) distinctly larger than other distal carpals (Gauthier, 1986; Cabreira et al., 2016: 125). This character is inapplicable if a distal carpal 1 is absent or not ossified.

780. Metacarpus, metacarpal I distal condyles: (0) approximately aligned or slightly offset; (1) lateral condyle strongly distally extended relative to medial condyle (Bakker and Galton, 1974; Cabreira et al., 2016: 132).

781. Metacarpus, length of metacarpals II and III: (0) metacarpal II shorter than metacarpal III; (1) metacarpal II equal to or longer than metacarpal III (Gauthier, 1986; Cabreira et al., 2016: 136).

782. Metacarpus, metacarpal III-humerus ratio: (0) <0.35; (1) ≥0.35 (New character).

783. Metacarpus, metacarpal IV-humerus ratio: (0) less than 0.35; (1) more than 0.35 (Unwin, 2003: 29; modified from Britt et al., 2018: 75).

784. Metacarpus, metacarpal IV shaft width at mid-length: (0) distinctly narrower than that of metacarpals I-III; (1) approximately the same width as that of metacarpals I-III; (2) two times or more broader than that of metacarpals I-III (Sereno et al., 1993; modified from Cabreira et al., 2016: 140). ORDERED.

785. Metacarpus, posteroventrally or posteriorly projecting crest on the middle of the proximoposterior surface of the shaft of metacarpal IV (crista metacarpi of Wild, 1979): (0) absent; (1) present (Britt et al., 2018: 74).

786. Manus, length of digit III: (0) accounts for less than 0.4 of the total length of humerus plus radius; (1) accounts for more than 0.4 of the total length of humerus plus radius (Gauthier, 1986; modified from Cabreira et al., 2016: 126).

787. Manus, phalanx I-1 twisting of the transverse axis: (0) absent; (1) present (Sereno, 1999; Cabreira et al., 2016: 133).

788. Manus, phalanx I-1: (0) not the longest non-ungual phalanx of the manus; (1) longest non-ungual phalanx of the manus (Gauthier, 1986; Cabreira et al., 2016: 134).

789. Manus, digit V: (0) one or more phalanges; (1) no phalanges (Bakker and Galton, 1974; Cabreira et al., 2016: 141). This character is inapplicable in taxa lacking a metacarpal V.

790. Manus, manual unguals versus pedal unguals size: (0) similar; (1) manual unguals twice the size, or more, of pedal unguals (Unwin, 2003: 3; Codorniú et al., 2016: 102; Britt et al., 2018: 77).

791. Ilium, iliac blade dorsoventral height relative to acetabular height: (0) shorter than two times; (1) two times higher or more (Makovicky and Sues, 1998; Cabreira et al., 2016: 249).

792. Ilium, pubic peduncle anteroposterior width at mid-length versus its total length: (0) less than 0.5; (1) 0.5 or more (Galton, 1976; Cabreira et al., 2016: 247).

793. Ilium, pubic peduncle distal articulation: (0) not expanded anteroposteriorly; (1) expanded anteroposteriorly (Smith et al., 2007; Cabreira et al., 2016: 151).

794. Ilium, position of dorsal margin concavity: (0) above the acetabulum; (1) posteriorly displaced (Cabreira et al., 2016: 155). This character is inapplicable in taxa that lack a concavity on the dorsal margin of the iliac blade.

795. Pubis-ischium, ventral margin of pubo-ischiatic plate (if it extends ventrally up to or beyond the distal end of the pubic shaft or tubercle): (0) straight or concave; (1) convex or with a ventrally pointing projection (partly and modified from Codorniú et al., 2016: 112). This character is inapplicable if character 470 is scored as (1), (2) or (3).

796. Pubis, prepubic process: absent (0); present (1) (Sereno, 1986).

797. Pubis, pubic shaft in anterior or posterior view: (0) straight; (1) laterally curved (New character).

798. Pubis, medial articulation of the pair: (0) complete, reaches the distal edge of the pubis; (1) forms a medial hiatus on the distal portion (bevel) (Tykoski, 2005; Cabreira et al., 2016: 161). This character is inapplicable in taxa that lack an anterior apron in the pubis.

799. Prepubis, as a separate ossification: (0); absent; (1) present (modified from Codorniú et al., 2016: 113).

800. Femur, profile of femoral head in medial or lateral view when it is distinctly inturned: (0) rounded; (1) hook-shaped (Sereno and Arcucci, 1994b; Cabreira et al., 2016: 180). This character is not applicable in taxa lacking a femoral head distinctly offset from shaft.

801. Femur, medial articular facet of the proximal portion in posterior view: (0) rounded; (1) straight (Nesbitt, 2011; Cabreira et al., 2016: 183).

802. Femur, greater trochanter shape in posterior view: (0) rounded; (1) angled (Sereno, 1999; Cabreira et al., 2016: 187).

803. Femur, development of attachment of muscle caudofemoralis on the posterior surface of the bone: (0) not distinct or developed as a rugose scar; (1) distinct, crest-like (Butler et al., 2008: 201; reworded from Baron et al., 2017: 377).

804. Femur, anterior surface of the distal portion: (0) smooth; (1) distinct scar orientated mediolaterally (Nesbitt et al., 2009b; Cabreira et al., 2016: 194).

805. Femur, anteromedial corner of the distal end: (0) rounded; (1) squared off near 90° or acute (Nesbitt et al., 2009b; Cabreira et al., 2016: 196).

806. Femur, sharp ridge on the anteromedial edge of the distal end: (0) absent; (1) present (Martínez et al., 2016: character 291; Müller et al., 2018: 257).

807. Femur, lateral tuberosity on the anterolateral edge of the distal end: (0) absent; (1) present (Martínez et al., 2016: character 292; Müller et al., 2018: 258).

808. Femur, crista tibiofibularis size/shape: (0) subequal to or smaller than the lateral condyle; (1) larger than the lateral condyle and globular (Sereno and Arcucci, 1994b; modified from Cabreira et al., 2016: 195).

809. Femur, wide concavity on the posterolateral surface of the crista tibiofibularis: (0) absent; (1) present (Martínez et al., 2016: character 293; Müller et al., 2018: 259).

810. Tibia, separation of the proximal posterior hemicondyles: (0) separated by a shallow notch; (1) separated by a deep groove (Rauhut, 2003; Cabreira et al., 2016: 203).

811. Tibia, distal surface outline (excluding the posterolateral process if present): (0) anteroposteriorly longer, rounded or subquadrangular (approximately as wide as long); (1) mediolaterally expanded (Rauhut, 2003; modified from Cabreira et al., 2016: 207).

812. Tibia, deep slot in the anteromedial corner of the distal surface: (0) absent; (1) present (it receives the anteromedial process of the astragalus) (New character; based on Nesbitt et al., 2009a).

813. Fibula, distal development: (0) subequal in length to the tibia; (1) less than 80 percent the length of the tibia (Codorniú et al., 2016: 119; cf. Britt et al., 2018: 89).

814. Astragalus, dorsally expanded process adjacent to the posterior margin: (0) absent or poorly developed; (1) expanded into a distinctly raised posterior ascending process (Sereno and Arcucci, 1994b; Cabreira et al., 2016: 212).

815. Astragalus, posterolateral portion of the tibial articular surface: (0) continuous to the medial articular surface; (1) markedly rimmed and elliptical fossa (separated by a ridge or step from the medial surface) (Langer and Benton, 2006; reworded from Cabreira et al., 2016: 215). This character is inapplicable in taxa with a fused tibia and astragalus.

816. Astragalus, proximal articular facet for fibula: (0) equal more than 0.3 of the transverse width of the bone; (1) less than 0.3 of the transverse width of the bone; (2) vertical (no horizontal platform) (Langer and Benton, 2006; Cabreira et al., 2016: 216) ORDERED. This character is inapplicable in taxa with a fused tibia and astragalus

817. Astragalus, base of anterior ascending process: (0) separated from the anterior surface of the astragalar body by an oblique slope; (1) separated from the anterior surface of the astragalar body by a platform (Langer, 2004; modified from Cabreira et al., 2016: 222). This character is inapplicable in taxa lacking an anterior ascending process in the astragalus.

818. Calcaneum, shape: (0) proximodistally compressed and subtriangular, with short medial process; (1) transversely compressed and subrectangular, without or with incipient medial process (Langer and Benton, 2006; Cabreira et al., 2016: 228).

819. Distal tarsal 4, posterior prong: (0) blunt; (1) pointed (Langer and Benton, 2006; Cabreira et al., 2016: 230).

820. Distal tarsal 4, medial process: (0) absent; (1) distinct on the anteroposterior middle of the element; (2) distinct on the anteromedial corner of the element (Nesbitt, 2011; modified from Cabreira et al., 2016: 231).

821. Metatarsus, proximal portion of metatarsal IV: (0) narrow; (1) expanded, overlapping the anterior surface of metatarsal V (Sereno, 1999; Cabreira et al., 2016: 237).

822. Metatarsus, shape of metatarsal IV in anterior/dorsal or posterior/ventral view: 0, straight; (1) laterally curved at the distal end (Novas, 1996; Cabreira et al., 2016: 238).

823. Metatarsus, length of metatarsals III and V: (0) metatarsal V equal to or longer than 50% of metatarsal III; (1) metatarsal V shorter than 50% of metatarsal III (Carrano et al., 2002; Cabreira et al., 2016: 239).

Scorings modified from previous data matrices (from Butler et al. 2019, unless stated otherwise)

Character 54: changes in the formulation of character states forced the following changes:
Changed from (2) to (2/3) in *Garjainia madiba* combined, *Shansisuchus shansisuchus*, *Chalishevia cothurnata*, *Rhadinosuchus gracilis*.
Changed from (2) to (3) in *Diandongosuchus fuyuanensis*.

Character 141: the swapping of the first two character states resulted in a swap of the scorings of the terminals that were scored as (0) or (1).

Character 299: the modification of state (1) from “ankylothecodont” to “thecodont” resulted in a changed of all terminals scored as (4) to (1).

Character 636: changes in the formulation of the character and addition of a third character state forced the following changes:
Changed from (0) to (1) in *Garjainia prima*, *Youngosuchus sinensis*, *Euparkeria capensis*, *Osmoslkina* complete, *Tropidosuchus romeri*, *Cerritosaurus binsfeldi*, *Proterochampsa barrionuevoi*, *Proterochampsa nodosa*, *Diandongosuchus fuyuanensis*, *Gracilisuchus stipanicicorum*, *Qianosuchus mixtus* and *Decuriasuchus quartacolonia*.
Changed from (0) to (1/2) in *Venaticosuchus rusconii*.

Changed from (0) to (?) in *Rhadinosuchus gracilis*.
Changed from (0) to (-) in *Dimorphodon macronyx*.
Changed from (1) to (2) in *Proterosuchus fergusi*, '*Chasmatosaurus*' *yuani*, *Tarjadia ruthae*, *Erpetosuchus granti*, *Erpetosuchus* sp, *Ornithosuchus woodwardi*, *Riojasuchus tenuisceps* and *Parringtonia gracilis*.
Changed from (0&1) to (1) in *Gualosuchus reigi*.
Changed from (?) to (0) in *Batrachotomus kupferzellensis*.
Changed from (?) to (1) in *Garjainia madiba*, *Erythrosuchus africanus*, *Pseudochampsa ischigualastensis*, *Turfanosuchus dabanensis*, *Yonghesuchus sangbiensis* and *Silesaurus opolensis*.

Character 470: the addition of a state (0) to sample the condition present in lagerpetids and pterosaurs forced to rescore multiple taxa as follows:
Changed from (0) to (-) in *Planocephalosaurus robinsonae*, *Gephyrosaurus bridensis*, *Amotosaurus rotfeldensis*, *Macrocnemus bassanii*, *Macrocnemus fuyuanensis* and *Tanystropheus longobardicus*.
Changed form (0) to (1) in *Pamelaria dolichotrachela*, *Azendohsaurus madagaskarensis*, *Shringasaurus indicus*, *Garjainia prima*, *Erythrosuchus africanus*, *Shansisuchus shansisuchus*, *Vancleavea campi*, *Euparkeria capensis*, *Teleocrater rhadinus*, *Tropidosuchus romeri*, *Chanaresuchus bonapartei*, *Archeopelta arborensis*, *Tarjadia ruthae*, *Doswellia kaltenbachi*, *Parasuchus hislopi*, *Smilosuchus spp*., *Ornithosuchus woodwardi*, *Riojasuchus tenuisceps*, *Gracilisuchus stipanicicorum*, *Aetosauroides scagliai*, *Aetosaurus ferratus*, *Stagonolepis robertsoni* and *Scleromochlus taylori*.
Changed from (0) to (0/1) in *Spinosuchus caseanus* and *Mesosuchus browni*, *Cuyosuchus huenei*, *Garjainia madiba*, *Proterochampsa barrionuevoi*
Changed from (?) to (1) in *Yarasuchus deccanensis*.
Changed from (1) to (2) in *Stagonosuchus nyassicus*, *Qianosuchus mixtus*, *Lotosaurus adentus*, *Batrachotomus kupferzellensis*, *Prestosuchus chiniquensis*, *Marasuchus lilloensis*, *Lutungutali sitwensis*, *Asilisaurus kong*we, *Silesaurus opolensis*, *Heterodontosaurus tucki*, *Herrerasaurus ischigualastensis*.
Changed from (2) to (3) in *Arizonasaurus babbitti*.
Changed from (1/2) to (2/3) in *Lewisuchus admixtus*.

Character 472: the modification of the formulation of the character and addition of a state resulted in the following rescorings:
Changed from (0) to (1) in *Acerosodontosaurus piveteaui*, *Youngina capensis*, *Macrocnemus fuyuanensis*, *Tanystropheus longobardicus*, *Pamelaria dolichotrachela*, *Trilophosaurus buettneri*, *Teraterpeton hrynewichorum*, *Noteosuchus colletti*, *Mesosuchus browni*, *Isalorhynchus genovefae*, *Hyperodapedon gordoni*, *Hyperodapedon huxleyi*, *Prolacerta broomi*, *Tropidosuchus romeri*, *Chanaresuchus bonapartei*, *Parasuchus hislopi* and *Lagerpeton chanarensis*.
Changed from (0) to (2) in *Garjainia prima*, *Erythrosuchus africanus*, *Euparkeria capensis* and *Diandongosuchus fuyuanensis*.

Changed from (0) to (3) in *Gracilisuchus stipanicicorum*, *Aetosauroides scagliai*, *Mandasuchus tanyauchen* and *Prestosuchus chiniquensis*.
Changed from (0) to (1/2) in *Smilosuchus* spp.
Changed from (0) to (?) in *Petrolacosaurus kansensis*, *Planocephalosaurus robinsonae*, *Fuyuanosaurus acutirostris*, *Howesia browni*, *Cuyosuchus huenei*, *Litorosuchus somnii*, *Tarjadia ruthae*, *Doswellia kaltenbachi*, *Aetosaurus ferratus* and *Stagonolepis robertsoni*
Changed from (1) to (2) in *Yarasuchus deccanensis*, *Qianosuchus mixtus* and *Lagosuchus talampayensis*.
Changed from (1) to (3) in *Riojasuchus tenuisceps* and *Turfanosuchus dabanensis*.
Changed from (1) to (?) in *Prestosuchus nyassicus*.
Changed from (2) to (3) in *Ornithosuchus woodwardi*, *Asilisaurus kongwe*, *Silesaurus opolensis*, *Heterodontosaurus tucki*, *Lesothosaurus diagnosticus*, *Eoraptor lunensis*, *Saturnalia tupiniquim*, *Coelophysis bauri* and *Megapnosaurus rhodesiensis*.
Changed from (2) to (?) in *Tawa hallae*.
Changed from (1/2) to (3) in *Lewisuchus admixtus*.
Changed from (1&2) to (3) in *Herrerasaurus ischigualastensis*.
Changed from (?) to (0) in *Pectodens zhenyuensis*, *Langobardisaurus pandolfii*, *Tanytrachelos ahynis* and *Rhynchosaurus articeps*
Changed from (?) to (1) in *Protorosaurus speneri*, *Pseudochampsa ischigualastensis* and *Nundasuchus songeaensis*.
Changed from (?) to (2) in *Azendohsaurus madagaskarensis* and '*Chasmatosaurus*' *yuani*.
Changed from (?) to (3) in *Ticinosuchus ferox* and *Decuriasuchus quartacolonia*.
Changed from (?) to (-) in *Jesairosaurus lehmani*.

Aetosauroides scagliai (modified from the new information from Brust et al., 2018)
Character 16, 263, 286: changed from (?) to (2).
Character 20: changed from (?) to (1/2).
Character 21, 71, 92, 97, 176, 182, 207, 283, 289, 290, 292, 301, 623, 627, 651, 690: changed from (?) to (1).
Character 28: changed from (2/3/4) to (4).
Character 30, 32, 35, 47, 84, 93, 94, 95, 175, 183, 260, 264, 265, 268, 271, 276, 281, 282, 284, 285, 287, 288, 291, 300, 302, 307, 308, 608, 622, 624, 625, 650: changed from (?) to (0).
Character 48: changed from (?) to (-).
Character 50: changed from (0/1) to (1).
Character 63: changed from (1) to (0&1).
Character 75: changed from (?) to (2) because of the presence of 11 tooth position in the dentary (PVL 2059).
Character 76: changed from (1/2) to (1).
Character 88, 275: changed from (1/2) to (2).
Character 113: changed from (0/1) to (0).

Aetosaurus ferratus
Character 41: changed from (0) to (?).
Character 48: changed from (?) to (-).
Character 75: changed from (0) to (1).
Character 440: changed from (1) to (-).

Asilisaurus kongwe (modified from the new information from Nesbitt et al., 2020)
Character 1: changed from (0) to (2).
Characters 4, 5, 7, 9, 10, 11, 18, 24, 25, 26, 29, 30, 31, 32, 33, 35, 37, 40, 43, 53, 61, 62, 68, 69, 70, 72, 73, 74, 78, 79, 80, 83, 86, 93, 94, 95, 98, 107, 108, 109, 112, 115, 116, 118, 120, 121, 130, 136, 139, 142, 143, 144, 145, 147, 148, 149, 151, 152, 179, 180, 206, 261, 267, 268, 269, 271, 281, 331, 343, 367, 368, 373, 376, 384, 387, 394, 416, 431, 432, 434, 437, 438, 446, 449, 458, 478, 479, 481, 486, 488, 513, 514, 530, 531, 561, 562, 568, 570, 572, 574, 578, 579, 580, 583, 584, 585, 607, 608, 609, 611, 612, 613, 622, 625, 629, 636, 637, 648, 665, 678, 689, 690, 691: changed from (?) to (0).
Characters 6, 44, 51, 56, 374, 614–621, 649: changed from (?) to (-).
Character 17: changed from (?) to (0/1).
Characters 22, 27, 38, 41, 52, 57, 67, 71, 97, 114, 117, 135, 141, 150, 203, 207, 286, 347, 352, 375, 414, 415, 430, 433, 435, 436, 461, 484, 528, 529, 564, 566, 571, 576, 577, 582, 651, 659: changed from (?) to (1).
Characters 28, 63, 75, 88, 472, 516, 567, 569, 581: changed from (?) to (2).
Characters 36, 66, 489: changed from (?) to (1/2).
Character 42: changed from (?) to (5).
Character 54, 153: changed from (?) to (2/3).
Character 336, 393, 396, 403, 420, 422, 424, 512: changed from (0) to (1).
Character 371: changed from (1) to (0).
Character 385: changed from (0) to (?).
Character 427: changed from (2) to (1).
Character 460: changed from (1/2/3) to (1).
Character 465: changed from (0) to (3).
Character 490: changed from (?) to (3/4).

Asperoris mnyama
Character 75: changed from (?) to (2/3/4/5) because of the presence of at least 10 tooth position in the preserved portions of the maxilla (Nesbitt et al., 2013).

Azendohsaurus madagaskarensis
Character 643: changed from (0) to (1).
Character 669: changed from (-) to (0).

Bentonyx sidensis
Character 266: changed from (?) to (-).

Boreopricea funerea

Character 75: changed from (4) to (3/4) because Benton and Allen (1997) estimated a total of 20–25 maxillary teeth.
Character 246: changed from (1) to (?).
Character 299: changed from (0/2/4) to (?).
Character 327: changed from (0) to (?) because the anteriormost preserved cervical vertebra only preserves the posteriormost region of the centrum and the subsequent vertebra may belong to a fourth or fifth cervical vertebra (Benton and Allen, 1997); thus not belonging unambiguously to an anterior cervical vertebra.
Character 413: changed from (1) to (?). Tatarinov (1978) reported the presence of ossified, paired sternal plates in this species. However, no evidence of the described sternal plate is currently preserved and since this condition is very unusual among early archosauromorphs, it was decided here to recscore it as unknown.

Brasinorhynchus mariantensis
Character 266: changed from (?) to (-).

Chanaresuchus bonapartei
Character 523: changed from (0) to (1).
Character 524: changed from (1) to (0).

Chasmatosuchus magnus
Character 343: changed from (0) to (1).

Chasmatosuchus rossicus
Character 343: changed from (0) to (1).

Ctenosauriscus koeneni
Character 343: changed from (1) to (0).

Cuyosuchus huenei
Character 343: changed from (0) to (?).

Decuriasuchus quartacolonia
Character 25: changed from (0) to (1) because the posterior margin of the premaxillary body is concave in lateral view and when articulated with the maxilla both elements form an opening along its suture ventral to the external naris (França et al., 2013).
Character 571: changed from (?) to (1).

Diandongosuchus fuyuanensis
Character 8 and 113: changed from (0) to (1).
Character 17: changed from (0) to (1) because the jugal possesses a distinctly elevated lateral orbital rim.
Character 56: changed from (0) to (-).
Character 145: changed from (1) to (0).

Character 356: changed from (?) to (0) based on the scoring of Stocker et al. (2017: character 199).
Character 385: changed from (0) to (-).

Dimorphodon macronyx (modified from new observations from the authors)
Character 54: changed from (2) to (0) based on NHMUK PV OR 41212 and R1034.
Character 69: changed from (0) to (1) (see Padian, 1983; Britt et al., 2018).
Character 81: changed from (0) to (-) because the maxillary process (= postnarial process of other archosauromorphs) of the premaxilla does not reach the nasal.
Character 176: changed from (1) to (0).
Character 177: changed from (?) to (-).
Character 262: changed from (?) to (0) based on Bennett (2015) (see also Britt et al., 2018).
Characters 263 and 650: changed from (?) to (-) because of the absence of an external mandibular fenestra.
Characters 267 and 681: changed from (1) to (2).
Character 278: changed from (0) to (1) because of the presence of an edentulous anterior end of the dentary (NHMUK PV OR 41212; Britt et al., 2018: fig. 4c).
Character 283: changed from (?) to (1).
Characters 1, 284: changed from (?) to (0).
Character 299: changed from (0/2/4) to (1).
Character 422: changed from (0) to (2) because of the addition of a character state.
Characters 430, 436, 439: changed from (?) to (1) based on NHMUK PV R1034.
Characters 432, 434, 437, 438: changed from (?) to (0) based on NHMUK PV R1034.
Character 435: changed from (?) to (4) based on measurements of NHMUK PV R1034.
Characters 440: changed from (?) to (-) based on NHMUK PV R1034.
Character 448: changed from (-) to (0) based on NHMUK PV R1034 and the modification in the inapplicability of this character for pterosaurs.
Character 475: changed from (1) to (0) because the pubic shaft has a distinct anterior component in lateral view in NHMUK PV OR 41212.
Character 476: changed from (2) to (3) because the pubis has a proximodistally concave anterior surface in NHMUK PV OR 41212.
Character 499: changed from (?) to (0) because the area immediately lateral to the posterior tuber is ventrally depressed and not dorsally raised at the same level as the medial portion of the femoral head in NHMUK PV OR 41212 and YPM 9182, resembling the condition in most dinosauromorphs (see Nesbitt, 2011).
Character 513: changed from (?) to (1). There is a broad extensor groove on the anterior surface of the distal end of the left femur of NHMUK PV R1034.
Characters 564 and 566: changed from (?) to (1) based on NHMUK PV OR 41212.
Character 576: changed from (1) to (0) based on NHMUK PV OR 41212.
Character 581: changed from (?) to (2) based on NHMUK PV OR 41212.
Character 584: changed from (0) to (1) based on NHMUK PV OR 41212.
Character 602: changed from (?) to (1). A distinct longitudinal ridge is present on the posterior edge of the scapula in NHMUK PV R1034.

Doswellia kaltenbachi
Character 75: changed from (4/5) to (4) because the dentary possesses 33 tooth positions (Weems, 1980).

Dynamosuchus collisensis (modifications from Müller et al., 2020)
Character 299: changed from (4) to (1) because this character was modified here.
Character 414: changed from (0) to (1) because the first and second character states of this character were swept here.
Character 470: changed from (0) to (1/2) because this character was modified here.
Character 636: changed from (0) to (0/1).

Eohyosaurus wolvaardti (modified from the new information provided by Sobral and Müller, 2019)
Character 228, 296: changed from (?) to (1).
Characters 235, 240, 241, 248: changed from (?) to (0).
Character 247: changed from (?) to (0/1).

Garjainia madiba
Character 75: changed from (?) to (2/3) because of the presence of 14 tooth positions in the dentary.

Gracilisuchus stipanicicorum (based on new observations of PVL 4597)
Character 321: changed from (3) to (1) following Baczko et al. (2020).
Character 376, 455, 603, 665, 683: changed from (?) to (0).
Character 495: changed from (0) to (1).
Character 372, 499 and 525: changed from (?) to (1).

Gualosuchus reigi
Character 523: changed from (0) to (1).
Character 524: changed from (1) to (0).

Herrerasaurus ischigualastensis
Character 455: changed from (1) to (2) because of the addition of a third state in this character.

Heterodontosaurus tucki
Character 455: changed from (1) to (2) because of the addition of a third state in this character.
Character 502: changed from (1) to (3) because of the addition of states sampling different morphologies of the anterior trochanter.
Character 521: changed from (1) to (2) because of the addition of a third state sampling a different morphology of the posterolateral process of the distal end of tibia.

Isalorhynchus genovefae
Characters 97, 190, 194 and 395: changed from (0) to (1).
Characters 39 and 193: changed from (0) to (?).
Character 266: changed from (3) to (-).
Character 279: changed from (2) to (1).

Jaxtasuchus salomoni
Character 523: changed from (0) to (1).
Character 524: changed from (1) to (0).

Jesairosaurus lehani
Character 123: changed from (1) to (0) because in ZAR 06 the postorbital-parietal contact excluded the postfrontal from the border of the supratemporal fenestra and the postorbital bones of ZAR 07 (which apparently has a contribution of the postfrontals to the supratemporal fenestrae) are slightly out of place to assess the condition confidently (see Jalil, 1997: 510).
Character 139: changed from (1) to (-) because there jugal contacts the squamosal and, as a result, there is no free transition between the anterior and ventral processes of the squamosal.
Characters 166, 343 and 358: changed from (0) to (?).
Character 389: changed from (?) to (0).
Character 687: changed from (1) to (0).

Lagerpeton chanarensis (modified from new information based on PVL 4625)
Characters 1, 5, 107, 109, 110, 111, 112, 115, 120, 121, 174, 260, 261, 266, 268, 270, 271, 278, 279, 280, 299, 300, 304, 305, 308, 312, 320, 353, 355, 358, 360, 362, 363, 378, 383, 389, 394, 472, 486, 588, 601, 602, 609, 648, 665, 682, 683: changed from (?) to (0).
Characters 6, 365, 589–598, 649, 653: changed from (?) to (-).
Character 75: changed from (?) to (4).
Characters 114, 116, 262, 269, 278, 306, 307, 310, 354, 361, 364, 368, 387, 390, 391, 395, 646, 659: changed from (?) to (1).
Character 267, 377, 462, 680: changed from (?) to (2).
Character 393: changed from (?) to (0/1).
Character 476: changed from (1) to (3).
Character 496, 499: changed from (1) to (0).
Character 501: changed from (0) to (2).
Character 523: changed from (0) to (1).

Langeronyx brodiei
Character 266: changed from (3) to (-).

Lewisuchus admixtus (modified from the new information in CRILAR-Pv 552, PULR V-111 and PULR V-113, and the currently lost posterior region of the lower jaw figured and described by Romer, 1972b)
Characters 24, 91, 139, 149, 282, 284, 287, 290, 369, 370, 373, 380, 456, 458, 464, 466, 486, 513, 652, 664, 690: changed from (?) to (0).
Character 36, 472: changed from (?) to (1/2).
Character 249, 336, 337: changed from (0) to (1).
Character 262, 286, 295, 372, 375, 460, 461, 601, 645, 659: changed from (?) to (1).
Character 270: changed from (1) to (0).
Character 283, 462: changed from (1/2) to (2).
Character 304: changed from (2) to (0&1&2).
Character 321: changed form (0) to (3).
Character 322, 323: changed from (-) to (0).
Character 374: changed from (?) to (-).
Character 476: changed from (1/2) to (1).
Character 482: changed from (?) to (2).
Character 485: changed from (0/1) to (1).

Litorosuchus somnii
Character 17: changed from (?) to (1) because the jugal possesses a distinctly elevated lateral orbital rim.
Character 301: changed from (0) to (1).
Character 430: changed from (1) to (0) because the development of the olecranon process of the ulna in the holotype does not differ from that of the *Euparkeria capensis* specimen SAM-PK-6047.

Lotosaurus adentus
Character 343: changed from (1) to (0).

Mandasuchus tanyauchen
Characters 480 and 487: changed from (0) to (1) based on Butler et al. (2018: 113).
Character 530: changed from (?) to (0) based on Butler et al. (2018: 116).
Character 552: changed from (1) to (2) based on Butler et al. (2018: 117).

Lagosuchus talampayensis
Character 23: changed from (?) to (0) based on PVL 3870.
Character 60: changed from (0) to (?) based on PVL 3870.
Character 135, 213, 214, 215, 249, 358: changed from (?) to (1) based on PVL 3872.
Character 138, 143, 144, 145, 147, 148, 149, 641: changed from (?) to (0) based on PVL 3872.
Character 216: changed from (?) to (0) based on PVL 3870 and PVL 3872.
Character 221, 330: changed from (1) to (?) based on PVL 3870 and PVL 3872.
Character 231: changed from (0) to (0&1) because of the presence of state (0) in PVL 3872 and state (1) in PVL 3870.

Character 245: changed from (0) to (1) because of the presence of an anterior tympanic recess in PVL 3872.
Character 247: changed from (0/1) to (0) based on PVL 3872.
Character 299: changed from (4) to (0/1) based on PVL 3870.
Character 316 and 317: changed from (0) to (1) based on the tenth presacral vertebra of PVL 3872.
Character 325, 329: changed from (0) to (?) based on PVL 3870 and PVL 3872.
Character 373: changed from (0) to (?) based on PVL 3870 and PVL 3871.
Character 374: changed from (-) to (?) based on PVL 3870 and PVL 3871.
Character 387: changed from (?) to (0) based on PVL 3871 because although the distal margin of the scapula is broken, this ratio should have been considerably lower than 6.0.
Character 396, 397, 398, 403, 422: changed from (0) to (?) based on PVL 3871.
Character 466: changed from (2) to (0) based on PVL 3870.
Character 529: changed from (0) to (1) based on PVL 3871.
Character 530: changed from (?) to (0) based on PVL 3871.
Character 532: changed from (2) to (?).
Character 639: changed from (0) to (1) based on PVL 3872.
Character 681: changed from (?) to (1) based on PVL 3870.
Character 775: changed from (0) to (-) based on PVL 3870.

Mesosuchus browni (modified based on the new information published by Sobral and Müller, 2019)
Characters 224, 242, 243, 249 and 257: changed from (?) to (0).
Characters 296 and 297: changed from (?) to (1).

Nicrosaurus kapffi
Character 10: changed from (1) to (2).
Character 96: changed from (1) to (0).
Characters 140, 167 and 641: changed from (0) to (1).
Character 260: changed from (0) to (2).
Character 359: changed from (1) to (?).

Nundasuchus songeaensis
Character 75: changed from (?) to (2/3/4/5) because of the presence of at least 14 tooth position in the preserved portion of dentary (Nesbitt et al., 2014).
Character 359: changed from (1) to (0) based on Stefanic and Nesbitt (2019).

Ornithosuchus woodwardi
Character 149: changed from (1) to (0).
Character 321: changed from (3) to (1) following Baczko et al. (2020).

Otter Sandstone archosaur
Character 75: changed from (?) to (2/3/4/5) because of the presence of at least 12 tooth positions in the preserved portion of dentary (Benton, 2011).

Pagosvenator candelariensis (modifications from Müller et al., 2020)
Character 16: changed from (2) to (?) because of the subequal preserved length and height of the orbits in the taphonomically altered skull.
Character 37: changed from (0) to (1).
Character 79: changed from (1) to (0) based on Lacerda et al. (2018: page 8).
Character 299: changed from (4) to (1) because this character was modified here.
Character 591: changed from (0/1) to (0) based on Lacerda et al. (2018: page 13).

Pamelaria dolichotrachela
Character 75: changed from (2/3) to (3) because there are 18 tooth position in the dentary (ISIR 316/1).
Character 343: changed from (0) to (1) based on ISIR 316.

Panchet proterosuchid
Character 343: changed from (0) to (1).

Parasuchus angustifrons
Character 37: changed from (1) to (?).
Character 149: changed from (1) to (0).
Characters 140 and 227: changed from (0) to (1).

Parasuchus hislopi
Characters 10, 37 and 149: changed from (1) to (0).
Character 182: changed from (0) to (1).
Character 260: changed from (0) to (2).
Character 385: changed from (0) to (-).

Parringtonia gracilis (modified from the new information from Nesbitt et al., 2018b)
Characters 3, 4, 6, 8, 10, 11, 14, 15, 18, 22, 23, 24, 25, 26, 29, 32, 33, 35, 40, 46, 47, 59, 61, 64, 77, 78, 79, 80, 82, 83, 84, 87, 93, 94, 95, 98, 99, 107, 109, 110, 117, 118, 120, 121, 124, 125, 126, 127, 131, 132, 134, 139, 143, 151, 152, 154, 155, 159, 162, 167, 169, 170, 175, 178, 179, 180, 182, 188, 208, 218, 222, 227, 230, 232, 233, 237, 238, 240, 241, 243, 246, 247, 250, 251, 256, 257, 265, 268, 270, 271, 278, 279, 280, 300, 302, 303, 307, 308, 325, 328, 329, 336, 370, 371, 373, 381, 383, 397, 405, 418, 434, 449, 456, 457, 462, 465, 473, 475, 480, 481, 485, 487, 495, 498, 500, 501, 502, 503, 505, 506, 508, 514, 517, 520, 521, 522, 524, 526, 530, 531, 537, 538, 539, 540, 543, 550, 561, 565, 568, 572, 573, 575, 576, 582, 586, 593, 606, 607, 608, 609, 611, 622, 627, 629, 633, 634, 635, 639, 641, 642, 643, 644, 646, 647, 654, 655, 656, 663, 664, 669, 670, 671, 672, 673, 674, 694: changed from (?) to (0).
Characters 5, 21, 36, 39, 42, 88, 92, 157, 164, 171, 177, 202, 220, 283, 304, 327, 504, 557, 600: changed from (?) to (2).
Characters 7, 12, 16, 20, 27, 28, 30, 37, 50, 55, 58, 60, 63, 65, 71, 81, 85, 96, 97, 101, 113, 114, 115, 122, 135, 141, 142, 149, 150, 166, 168, 173, 176, 209, 210, 211, 212,

213, 214, 215, 221, 223, 225, 226, 228, 229, 231, 235, 236, 239, 245, 248, 252, 254, 255, 258, 262, 267, 284, 289, 294, 295, 296, 297, 332, 346, 366, 402, 408, 427, 433, 460, 470, 477, 493, 496, 497, 499, 511, 518, 523, 527, 533, 534, 536, 544, 545, 547, 548, 552, 553, 554, 555, 558, 559, 594, 599, 623, 624, 625, 636, 640, 645, 652: changed from (?) to (1).
Characters 19, 577: changed from (?) to (1/2).
Characters 48, 51, 56, 158, 161, 163, 165, 172, 219, 298, 345, 374, 668: changed from (?) to (-).
Character 66: changed from (1/2) to (2).
Character 153: changed from (?) to (2/3).
Character 217: changed from (?) to (4).
Characters 321, 588: changed from (2/3) to (3).
Character 435: changed from (?) to (0/1).

Prestosuchus chiniquensis (modified with new information from Roberto-Da-Silva et al., 2018 and Mastrantonio et al., 2019)
Character 25: changed from (0) to (1) because the posterior margin of the premaxillary body is concave in lateral view and when articulated with the maxilla both elements form an opening along its suture ventral to the external naris (Roberto-Da-Silva et al., 2016, 2018; Mastrantonio et al., 2019).
Character 54: changed from (2) to (3).
Characters 120, 121, 206, 412, 413, 585, 610, 638, 686: changed from (?) to (0).
Character 185, 186, 204, 309, 372, 404: changed from (?) to (1).
Character 187: changed from (?) to (3).
Character 210, 343, 652, 664: changed from (0) to (1).
Character 349: changed from (1/2) to (2).

Proterochampsa barrionuevoi
Characters 63 and 523: changed from (0) to (1).
Character 524: changed from (1) to (0).

Proterochampsa nodosa
Character 63: changed from (0) to (1).

Protorosaurus speneri
Character 430: changed from (2) to (0) based on NHMW 1943I4.
Character 431: changed from (0) to (-).
Character 432: changed from (1) to (?).

Pseudochampsa ischigualastensis
Character 523: changed from (0) to (1).
Character 524: changed from (1) to (0).

Qianosuchus mixtus

Character 480: changed from (0) to (1).

Rhadinosuchus gracilis
Character 75: changed from (?) to (3) because of the presence of an estimated of 23 tooth positions in the dentary.

Rhynchosaurus articeps
Character 266: changed from (?) to (-).

Riojasuchus tenuisceps
Character 53: changed from (?) to (-).
Character 220: changed from (?) to (0).
Character 321: changed from (3) to (1) following Baczko et al. (2020).

Scleromochlus taylori
Character 492: changed from (0) to (1) because the femoral head is distinctly offset from the shaft in NHMUK PV R3557.
Characters 502 and 503: changed from (0) to (?) following Kammerer et al. (2020).

Shringasaurus indicus
Characters 601−606: changed from (?) to (0) based on the scorings of Sengupta et al. (2017) for the same characters.
Characters 607, 609, 612, 613, 628, 629, 633, 635, 644, 647, 654, 657, 658, 659, 660, 661, 662, 663, 664, 666, 669, 670, 671, 672, 673, 674, 675: changed from (?) to (0).
Characters 614–621, 624, 668: changed from (?) to (-).
Characters 634, 643, 653, 655, 656, 667: changed from (?) to (1).

Silesaurus opolensis
Character 1: changed from (0) to (2) based on ZPAL Ab/III/361/26.
Character 7: changed from (1) to (0) because the dorsal raising of the orbital margin of the frontal is very low.
Character 37: changed from (1) to (?) because only the base of the postnarial process is preserved in ZPAL Ab III/361/34.
Character 38: changed from (0) to (1) because the dorsal margin of the base of the postnarial process is developed as a well-defined flange placed medially to the narial fossa, as also occurs in *Lewisuchus admixtus* and *Asilisaurus kongwe* (Nesbitt et al., in 2020).
Character 499: changed from (0) to (1) (see Nesbitt, 2011).
Character 521: changed from (1) to (2) because of the addition of a third state sampling a different morphology of the posterolateral process of the distal end of tibia.
Character 544 and 545: changed from (0) to (1). Contrasting with previous claims, the posterolateral corner of the calcaneum of *Silesaurus opolensis* has a low, but prominent and rounded calcaneal tuber (ZPAL Ab/III/361) that closely resembles those of *Asilisaurus kongwe* and *Lewisuchus admixtus*.

Character 546: changed from (-) to (2).
Character 547 and 552: changed from (-) to (1).
Character 548−551: changed from (-) to (0).

Smilosuchus spp.
Character 10: changed from (1) to (2).
Character 75: changed from (3/4) to (3&4).
Characters 140, 167 and 641: changed from (0) to (1).
Character 260: changed from (0) to (2).
Character 359: changed from (1) to (0) based on Stefanic and Nesbitt (2019) and UCMP 26699.
Character 385: changed from (0) to (-).

Spinosuchus caseanus
Character 105: changed from (?) to (-).
Character 343: changed from (1) to (?).
Characters 601, 603, 604 and 606: changed from (?) to (0) based on the scorings of Sengupta et al. (2017) for the same characters.
Characters 609, 656, 667: changed from (?) to (1) based on Spielmann et al. (2008).
Characters 612, 613, 626, 629, 633, 634, 637, 648, 657, 658, 671, 672, 673, 674, 675: changed from (?) to (0) based on Spielmann et al. (2008).
Characters 614−621, 624, 627, 636, 649, 650, 653, 668, 669: changed from (?) to (-) based on Spielmann et al. (2008).
Characters 654, 661, 662, 663, 666: changed from (?) to (0) based on Spielmann et al. (2009).
Characters 659, 660: changed from (?) to (1) based on Spielmann et al. (2009).

Spondylosoma absconditum
Character 421: changed from (1) to (0).

Stagonolepis robertsoni
Character 41: changed from (0) to (?).
Character 48: changed from (?) to (-).
Character 75: changed from (1) to (2).
Character 90: changed from (?) to (-).
Character 440: changed from (1) to (-).

Stagonosuchus nyassicus
Character 343: changed from (0) to (1).

Stenaulorhynchus stockleyi
Character 266: changed from (?) to (-).

Tanystropheus longobardicus

Character 75: changed from (2) to (3).

Teleocrater rhadinus
Character 386: changed from (1) to (2) based on the description of Nesbitt et al. (2018a: 157).

Teraterpeton hrynewichorum (modified with new information from Pritchard and Sues, 2019)
Character 105: changed from (2) to (-).
Character 328, 338, 370, 372, 373, 375, 378, 456, 459, 461, 462, 463, 465, 466, 467, 468, 472, 477, 479, 480, 481, 485, 487, 488, 492, 500, 501, 504, 505, 506, 507, 511, 522, 523, 546, 562, 568, 571, 572, 573, 576, 578, 580, 599, 601, 606, 607, 608, 609, 612, 613, 622, 625, 626, 627, 628, 629, 630, 631, 633, 634, 635, 637, 639, 641, 652, 656, 657, 660, 661, 664, 670, 674, 689: changed from (?) to (0).
Character 330, 369, 458, 464, 469, 471, 475, 482, 510, 528, 544, 545, 557, 566, 579, 623, 667: changed from (?) to (1).
Character 332: changed from (1/2) to (2).
Character 343: changed from (1) to (0).
Character 374, 470, 478, 614–621, 624, 636, 653, 668, 669: changed from (?) to (-).
Character 377: changed from (?) to (3).
Character 460, 476, 516, 569, 574, 577: changed from (?) to (2).
Character 567: changed from (?) to (0/1).

Teyujagua paradoxa
Character 343: changed from (?) to (1).

Trilophosaurus buettneri
Character 105: changed from (?) to (-).
Character 305: changed from (0) to (2).

Tropidosuchus romeri
Character 21, 120, 121, 160, 221, 242, 245, 264, 266, 270, 284, 290, 360, 417, 418, 422, 498, 514, 596, 597, 640, 682: changed from (?) to (0).
Character 27, 37, 76, 211, 254, 424, 499: changed from (?) to (1).
Characters 29, 523: changed from (0) to (1).
Character 81: changed from (0) to (-).
Character 171, 490: changed from (?) to (2).
Character 172, 219: changed from (?) to (-).
Character 304: changed from (1/2) to (1).
Character 427: changed from (1) to (2).
Character 524, 539: changed from (1) to (0).
Character 532: changed from (2) to (?).

Turfanosuchus dabanensis

Character 146: changed from (0) to (1).
Character 250: changed from (1) to (2).

Vancleavea campi
Character 301: changed from (0) to (1).

Venaticosuchus rusconii
Character 53: changed from (?) to (-).
Character 63: changed from (1) to (0).
Character 238: changed from (1) to (?).

Yarasuchus deccanensis
Character 386: changed from (1) to (2) based on the description of Nesbitt et al. (2018a: 157).

Youngosuchus sinensis
Character 363: changed from (0) to (?).

Ratios calculated for the scoring and/or discretization of characters (ratio-based characters are scored with the largest available, as a proxy of maturity, specimens)

Character 2
Carniadactylus rosenfeldi (Dalla Vecchia, 2014: fig. 4.1.137b): ca. 0.70
Eudimorphodon ranzii (Wild, 1979: fig. 2): ca. 0.55−0.60
Preondactylus buffarinii (Dalla Vecchia, 1998: fig. 1): 0.56−0.58
Rhamphorhynchus muensteri (Wellnhofer, 1975b): 0.57−0.73

Character 20
Aetosauroides scagliai (Brust et al., 2018: fig. 2): ca. 0.67
Austriadactylus cristatus (SMNS 56342): 0.64
Buriolestes schultzi (CAPPA/UFSM 0035): 0.50
Carniadactylus rosenfeldi (Dalla Vecchia, 2018: fig. 2): 0.55
Eudimorphodon ranzii (Wild, 1979: fig. 1): ca. 0.58
Lesothosaurus diagnosticus (Sereno, 1991b: fig. 11a): 0.45
Megapnosaurus rhodesiensis (Bristowe, 2004: fig. 7c): ca. 0.6
Parringtonia gracilis (Nesbitt et al., 2018b: fig. 2g): 0.49
Raeticodactylus filisurensis (Stecher, 2008: fig. 6c): 0.59
Rhamphorhynchus muensteri (Wellnhofer, 1975b: fig. 27): 0.63

Character 21
Aetosauroides scagliai (Brust et al., 2018: fig. 2): ca. 0.45
Austriadactylus cristatus (SMNS 56342): ca. 0.42
Cacibupteryx caribensis (cast of IGO-V 208): <0.41
Carniadactylus rosenfeldi (Dalla Vecchia, 2018: fig. 2): 0.23−0.36

Eudimorphodon ranzii (Wild, 1979: fig. 1): <0.33
Lesothosaurus diagnosticus (Sereno, 1991b: fig. 11a): 0.46
Parringtonia gracilis (Nesbitt et al., 2018b: fig. 2g): 0.59
Raeticodactylus filisurensis (Stecher, 2008: fig. 6c): <0.44
Tropidosuchus romeri (PVL 4604): 0.27
Rhamphorhynchus muensteri (Wellnhofer, 1975b: fig. 27): 0.31 (estimating the premxilla-maxilla suture in large individuals based on the position of the first maxillary tooth, the most procumbent of the upper tooth row based on small-sized specimens).

Character 28
Aetosauroides scagliai (Brust et al., 2018: fig. 2): 5.06
Asilisaurus kongwe: 2.44
Austriadactylus cristatus (SMNS 56342): ca. 3.3
Eudimorphodon ranzii (Wild, 1979: fig. 1): 4.20
Lesothosaurus diagnosticus (Sereno, 1991b: fig. 11a): 5.18
Megapnosaurus rhodesiensis (NHMB 11470): 2.35
Parringtonia gracilis (Nesbitt et al., 2018b: fig. 2g): 1.29
Preondactylus buffarinii (Wild, 1984: fig. 3): 4.3
Raeticodactylus filisurensis (Stecher, 2008: fig. 6c): ca. 1.8
Rhamphorhynchus muensteri (Wellnhofer, 1975b: fig. 27): 1.92

Character 50
Aetosauroides scagliai (Brust et al., 2018: fig. 3): ca. 0.40
Austriadactylus cristatus (SMNS 56342): ca. 0.55
Carniadactylus rosenfeldi (Dalla Vecchia, 2018: fig. 2): 0.50
Eudimorphodon ranzii (Wild, 1979: fig. 1): 0.46
Lesothosaurus diagnosticus (Sereno, 1991b: fig. 11a): 0.53
Megapnosaurus rhodesiensis (NHMB 11470): 0.32
Parringtonia gracilis (Nesbitt et al., 2018b: fig. 2g): 0.48
Preondactylus buffarinii (Wild, 1984: fig. 3): 0.47
Raeticodactylus filisurensis (Dalla Vecchia, 2014: fig. 4.1.159b): ca. 0.47
Rhamphorhynchus muensteri (Wellnhofer, 1975b: fig. 27): 0.67
Seazzadactylus venieri (Dalla Vecchia, 2019: fig. 4): 0.42

Character 55
Aetosauroides scagliai (Brust et al., 2018: fig. 3): 0.23
Lesothosaurus diagnosticus (Sereno, 1991b: fig. 11a): 3.55
Megapnosaurus rhodesiensis (NHMB 11470): <0.39
Parringtonia gracilis (Nesbitt et al., 2018b: fig. 2g): 0.66
Raeticodactylus filisurensis (Dalla Vecchia, 2014: fig. 4.1.159b): 0.11

Character 75
Aetosauroides scagliai (PVL 2059): 11 (dentary tooth positions)
Aetosaurus ferratus (Schoch, 2007: 18): 9

Caelestiventus hanseni (Britt et al., 2018): 12
Carniadactylus rosenfeldi (Wild, 1979): estimated in 14
Doswellia kaltenbachi (Weems, 1980): 33 (dentary tooth positions)
Eudimorphodon ranzii (Wild, 1979: fig. 1): 25
Ixalerpeton polesinensis (ULBRA-PVT059): 26 (dentary tooth positions)
Lagerpeton chanarensis (PVL 4625): 26 (dentary tooth positions)
Lesothosaurus diagnosticus (Porro et al., 2015): at least 15
Megapnosaurus rhodesiensis (Raath, 1977): 21–22
Pamelaria dolichotrachela (ISIR 316/1): 18 (dentary tooth positions)
Preondactylus buffarinii (Wild, 1984): 19
Raeticodactylus filisurensis (Stecher, 2008): 13
Rhadinosuchus gracilis (Ezcurra et al., 2015): 23 (dentary tooth positions)
Rhamphorhynchus muensteri (Wellnhofer, 1975a): 6–7
Seazzadactylus venieri (Dalla Vecchia, 2019): 14
Stagonolepis robertsoni (Walker, 1961: 132): 12
Tanystropheus longobardicus (Nosotti, 2007: 21): 15

Character 76
Aetosauroides scagliai (Brust et al., 2018: fig. 4): 1.91
Buriolestes schultzi (CAPPA/UFSM 0035): 1.10
Lesothosaurus diagnosticus (Sereno, 1991b: fig. 11b): 1.25
Tropidosuchus romeri (PVL 4604): 1.12

Character 100
Austriadraco dallavecchiai (SNSB-BSPG 1994 I 51): ca. 1.65
Eudimorphodon ranzii (Wild, 1979: fig. 1): 0.67
Megapnosaurus rhodesiensis (Bristowe, 2004: fig. 16): 1.88
Seazzadactylus venieri (Dalla Vecchia, 2019: fig. 6): 1.13

Character 177
Lesothosaurus diagnosticus (NHMUK PV RU B23): 115°
Megapnosaurus rhodesiensis (NHMB 11470): 137º
Parringtonia gracilis (Nesbitt et al., 2018b: fig. 2g): ca. 110°

Character 263
Aetosauroides scagliai (Brust et al., 2018: fig. 3): 0.62
Austriadraco dallavecchiai (SNSB-BSPG 1994 I 51): <0.14
Eoraptor lunensis (PVSJ 512): 0.16
Lesothosaurus diagnosticus (Sereno, 1991b: fig. 13f): 0.15
Megapnosaurus rhodesiensis (Raath, 1977: plate 8a): 0.21

Character 266
Allkaruen koi (Codorniú et al, 2016: fig. S2): <0.08
Austriadactylus cristatus (Dalla Vecchia, 2014: fig. 4.1.22b): <0.07

Austriadraco dallavecchiai (SNSB-BSPG 1994 I 51): <0.07
Buriolestes schultzi (CAPPA/UFSM 0035): 0.12
Caelestiventus hanseni (Britt et al., 2018: fig. 3b): <0.10
Carniadactylus rosenfeldi (Dalla Vecchia, 2014: fig. 4.1.139a, b): 0.10
Eoraptor lunensis (PVSJ 512): 0.10
Eudimorphodon ranzii (Wild, 1979: fig. 4): 0.07
Ixalerpeton polesinensis (ULBRA-PVT059): 0.09
Lagerpeton chanarensis (PVL 4625): 0.14
Lesothosaurus diagnosticus (Sereno, 1991b: fig. 13f): 0.13
Megapnosaurus rhodesiensis (Raath, 1977: plate 8a): 0.10
Preondactylus buffarinii (Wild, 1984: fig. 3): ≤0.07
Raeticodactylus filisurensis (Stecher, 2008: fig. 6c): 0.18
Seazzadactylus venieri (Dalla Vecchia, 2019: fig. 6): 0.07
Tropidosuchus romeri (PVL 4604): 0.05

Character 331
Asilisaurus kongwe (NMT RB851, RB159): 2.0
Coelophysis bauri (Rinehart et al., 2009: 138): 3.90−3.93
Lesothosaurus diagnosticus (NMQR 3076: Cv4): 1.63
Lewisuchus admixtus (PULR V-111): 2.46
Megapnosaurus rhodesiensis (Raath, 1977: plate 11a): 3.6−4.0
Rhamphorhynchus muensteri (Wellnhofer, 1991: page 84): ca. 3.5

Character 351
Lesothosaurus diagnosticus (Baron et al., 2016: fig. 4a): 1.46
Lewisuchus admixtus (PULR V-111): 1.60–1.82
Megapnosaurus rhodesiensis (Raath, 1977: table 6, QG 396): 1.69−1.96
Megapnosaurus rhodesiensis (Raath, 1977: table 6, QG 171): 1.89−1.93
Raeticodactylus filisurensis (BNM 14524): ca. 3.2

Character 352
Asilisaurus kongwe (NMT RB119, RB120): 1.5–1.7
Coelophysis bauri (CM 81768): 1.85
Lagerpeton chanarensis (PVL 4625): 1.81
Megapnosaurus rhodesiensis (Raath, 1977: table 6, NHMB 11470): 2.07
Peteinosaurus zambelli (Dalla Vecchia, 2014: fig. 4.1.67): 1.23−1.29
Preondactylus buffarinii (Wild, 1984: fig. 3): 1.68
Seazzadactylus venieri (Dalla Vecchia, 2019: fig. 16): 0.99

Character 377
Lagerpeton chanarensis (PVL 4625): 1.56
Lesothosaurus diagnosticus (Butler, 2005: fig. 9a, b): 0.95
Megapnosaurus rhodesiensis (Raath, 1969: fig 1c): ca. 1.0

Character 379
Lagerpeton chanarensis (PVL 4625): 1.56
Lesothosaurus diagnosticus (Butler, 2005: fig. 9b): 2.61
Peteinosaurus zambelli (Dalla Vecchia, 2014: fig. 4.1.70): 1.1

Character 387
Asilisaurus kongwe (NMT RB159): 6.44
Austriadactylus cristatus (Dalla Vecchia, 2009b: fig. 1): >8.1
Austriadraco dallavecchiai (SNSB-BSPG 1994 I 51): >9.4
Buriolestes schultzi (ULBRA-PVT280): slightly >7.25
Lagerpeton chanarensis (PVL 4625): ca. 9.18
Lesothosaurus diagnosticus (Butler, 2005: fig. 10a): 7.93
Megapnosaurus rhodesiensis (NHMB 11470): 8.15
Saturnalia tupiniquim (MCP 3844-PV): 7.41

Character 414
Asilisaurus kongwe (NMT RB159): slightly >0.47
Carniadactylus rosenfeldi (Dalla Vecchia, 2009a: table 1, manual digit IV vs. pedal digit III): 2.62
Lesothosaurus diagnosticus (NHMUK PV RU B17): ca. 0.35
Megapnosaurus rhodesiensis (Raath, 1977: table 4): 0.35
Peteinosaurus zambelli (Dalla Vecchia, 2014): 2.22−2.23
Preondactylus buffarinii (Wild, 1984: fig. 3): ca. 2.20−2.30 (none of the longest pedal digits is complete distally, thus this is an approximate).

Character 416
Asilisaurus kongwe (NMT RB159): 0.29
Lesothosaurus diagnosticus (Baron et al., 2016: table 2, SAM-PK-K1107): 0.22
Megapnosaurus rhodesiensis (NHMB 11470): 0.26
Raeticodactylus filisurensis (Dalla Vecchia, 2014: fig. 4.1.163a): ca. 0.21

Character 424
Asilisaurus kongwe (NMT RB159): 0.39
Austriadactylus cristatus (Dalla Vecchia, 2009b: fig. 1): ca. 0.28
Austriadraco dallavecchiai (SNSB-BSPG 1994 I 51): 0.31
Buriolestes schultzi (ULBRA-PVT280): 0.47
Carniadactylus rosenfeldi (Dalla Vecchia, 2014: fig. 4.1.142): 0.41
Eudimorphodon ranzii (Wild, 1979: fig. 2): 0.39
Lesothosaurus diagnosticus (NHMUK PV RU B17): ca. 0.46
Megapnosaurus rhodesiensis (NHMB 11470): 0.38
Peteinosaurus zambelli (Wild, 1979: fig. 35): 0.25
Preondactylus buffarinii (Wild, 1984: fig. 3): 0.39
Raeticodactylus filisurensis (Dalla Vecchia, 2014: fig. 4.1.163a): 0.33
Rhamphorhynchus muensteri (Wellnhofer, 1975a: fig. 11f): 0.46

Tropidosuchus romeri (PVL 4604): 0.31

Character 435
Asilisaurus kongwe (NMT RB159): 0.92
Austriadactylus cristatus (Dalla Vecchia, 2009b: fig. 1) 1.28
Carniadactylus rosenfeldi (Dalla Vecchia, 2009a: table 1): 1.24−1.26
Dimorphodon macronyx (NHMUK PV R1034): 1.33
Eudimorphodon ranzii (Wild, 1979: fig. 2): 1.35−1.41
Lesothosaurus diagnosticus (Baron et al., 2016: table 2, SAM-PK-K1106): 0.76
Megapnosaurus rhodesiensis (NHMB 11470): 0.61
Peteinosaurus zambelli (Wild, 1979: pl. 14): 1.18
Preondactylus buffarinii (Wild, 1984): 1.28
Raeticodactylus filisurensis (Stecher, 2008): ca. 1.28 (based on ulna)
Rhamphorhynchus muensteri (Wellnhofer, 1975b: table of measurements): 1.45−1.72
Seazzadactylus venieri (Dalla Vecchia, 2019: table S1): ca. 1.20–1.25 (based on ulna)

Character 446
Asilisaurus kongwe (NMT RB159): ca. 0.30
Carniadactylus rosenfeldi (Dalla Vecchia, 2009a: table 1): 0.95
Lesothosaurus diagnosticus (Thulborn, 1972: 48): 0.19
Megapnosaurus rhodesiensis (Raath, 1977: table 4): 0.20
Peteinosaurus zambelli (Dalla Vecchia, 2014: tables 4.1.1, 4.1.3): 0.91
Preondactylus buffarinii (Wild, 1984: fig. 3; Dalla Vecchia, 2014: fig. 4.1.8): 0.89
Raeticodactylus filisurensis (BNM 14524): 1.28
Rhamphorhynchus muensteri (Wellnhofer, 1975b: table of measurements): 0.69−1.03

Character 448
Austriadactylus cristatus (Dalla Vecchia, 2009b: fig. 4): ca. 0.09
Buriolestes schultzi (ULBRA-PVT280): 0.40
Carniadactylus rosenfeldi (Dalla Vecchia, 2009a: fig. 4.1.116): ca. 0.13
Dimorphodon macronyx (NHMUK PV R1034): ca. 0.12
Dromomeron romeri (GR 238): 0.22
Eudimorphodon ranzii (Wild, 1979: plate 2): ca. 0.09
Lesothosaurus diagnosticus (Baron et al., 2016: fig. 9b): 0.36
Megapnosaurus rhodesiensis (NHMB 11470): 0.41
Peteinosaurus zambelli (Dalla Vecchia, 2014: fig. 4.1.65): ca. 0.13
Preondactylus buffarinii (Dalla Vecchia, 1998: fig. 1): ca. 0.11
Raeticodactylus filisurensis (BNM 14524): 0.07
Rhamphorhynchus muensteri (Wellnhofer, 1975a: fig. 14): ca. 0.06
Seazzadactylus venieri (Dalla Vecchia, 2019: fig. 21): ca. 0.12

Character 458
Asilisaurus kongwe (NMT RB159): 0.17
Lesothosaurus diagnosticus (SAM-PK-K1105): 0.17

Lewisuchus admixtus (PULR V-111): 0.13
Megapnosaurus rhodesiensis (Raath, 1977: fig. 30c): 0.13
Rhamphorhynchus muensteri (Wellnhofer, 1975a: fig. 10g and femoral length of 37 mm, specimen 49 of Wellnhofer): 0.09
Teraterpeton hrynewichorum (Pritchard and Sues, 2009: fig. 4a and supplemental table 2): 0.26

Character 463
Coelophysis bauri (CM 81768): 1.84
Coelophysis bauri (USNM 529376): 1.73
Lesothosaurus diagnosticus (SAM-PK-K1105): 1.12
Lewisuchus admixtus (PULR V-111): 0.93
Lewisuchus admixtus (PULR V-113): 0.92
Megapnosaurus rhodesiensis (Raath, 1977: plate 19a, b): 1.62−1.65
Rhamphorhynchus muensteri (Wellnhofer, 1975a: fig. 10g): 1.17
Teraterpeton hrynewichorum (Pritchard and Sues, 2019: fig. 4): 0.45

Character 472
Acerosodontosaurus piveteaui (MNHN 1908-32-57): 0.36
Aetosauroides scagliai (PVL 2073): 0.60
Amotosaurus rotfeldensis (SMNS 54810): 0.29
Asilisaurus kongwe (Nesbitt et al., 2020: table 1): 0.84
Austriadraco dallavecchiai (SNSB-BSPG 1994 I 51): 0.32
Azendohsaurus madagaskarensis (Nesbitt et al., 2015: fig. 58, table 7): 0.57
Chanaresuchus bonapartei (PVL 4575): 0.35
'*Chasmatosaurus*' *yuani* (Young, 1978: table 1): 0.48
Coelophysis bauri (Colbert, 1989: table): 0.85−1.15
Cuyosuchus huenei (MCNAM 2669): <0.73
Decuriasuchus quartacolonia (França et al., 2011: fig. 1): 0.70−0.71
Diandongosuchus fuyuanensis (Sotcker et al., 2017: fig. 2): 0.49
Dimorphodon macronyx (NHMUK PV R41212-13): 0.28
Dynamosuchus collisensis (Müller et al., 2020: fig. 2): >0.68
Eodromeus murphi (PVSJ 560): 0.81
Eoraptor lunensis (PVSJ 512): 0.80
Erythrosuchus africanus (NHMUK PV R3592): 0.57
Euparkeria capensis (SAM-PK-5867): 0.50
Garjainia prima (Hune, 1960: plate 15): ca. 0.50
Gracilisuchus stipanicicorum (Lecuona and Desojo, 2012: tables 1, 2): 0.66
Herrerasaurus ischigualastensis (PVL 2566): 0.91
Heterodontosaurus tucki (Santa Luca, 1980): ca. 0.93
Hyperodapedon gordoni (Benton, 1983: table 1): 0.38−0.42
Hyperodapedon huxleyi (Chatterjee, 1974: table 2): 0.42
Isalorhynchus genovefae (Whatley, 2005: figs. 1.27, 1.29): 0.37
Ixalerpeton polesinensis (ULBRA-PVT059): 0.42
Lagerpeton chanarensis (PVL 4619): 0.32
Lagosuchus talampayensis (PVL 3870): 0.53
Langobardisaurus pandolfii (Renesto and Dalla Vecchia, 2000: fig.1): 0.29
Lesothosaurus diagnosticus (Butler, 2005: table 2): 1.15

Lewisuchus admixtus (PVL 4629): 0.72
Macrocnemus bassanii (PIMUZ T2472): 0.28
Macrocnemus fuyuanensis (Jiang et al., 2011: fig. 6): 0.41
Mandasuchus tanyauchen (Butler et al., 2018: tables 3, 4): 0.61
Megapnosaurus rhodesiensis (Raath, 1977): 0.98
Mesosuchus browni (SAM-PK-7416): 0.41
Noteosuchus colletti (AM 3591): 0.35
Nundasuchus songeaensis (Nesbitt et al., 2014: table 1): 0.45
Ornithosuchus woodwardi (Walker, 1964: figs. 11, 12): 0.78
Pamelaria dolichotrachela (ISIR 316): 0.44
Parasuchus hislopi (Chatterjee, 1978: table 2): 0.44
Pectodens zhenyuensis (Li et al., 2017: fig. 1): 0.29
Peteinosaurus zambelli (MCSNB 3359 pubis, MCSNB 3359 femur): 0.26
Prestosuchus chiniquensis (Desojo et al., 2020: table 1): >0.66
Prolacerta broomi (BP/1/2676): 0.35
Protorosaurus speneri (NHMW 1943I4): 0.37
Pseudochampsa ischigualastensis (PVSJ 567): ca. 0.41
Qianosuchus mixtus (Li et al., 2006: fig. 1b): 0.57
Rhamphorhynchus muensteri (Wellnhofer, 1975a: fig. 10g and femoral length of 37 mm, specimen 49 of Wellnhofer): 0.24
Rhynchosaurus articeps (Benton, 1990: table 1): 0.27
Riojasuchus tenuisceps (Bazcko et al., 2020): 0.95
Saturnalia tupiniquim (MCP 3845-PV): 0.82
Scleromochlus taylori (Benton, 1999: table 1): 0.27
Silesaurus opolensis (ZPAL Ab/III/361): 0.81
Smilosuchus spp. (USNM 18313): ca. 0.47
Tanystropheus longobardicus (PIMUZ T2817): 0.32
Tanytrachelos ahynis (Olsen, 1979: fig. 2): 0.26
Teraterpeton hrynewichorum (Pritchard and Sues, 2019: figs. 4a, 5a): 0.32
Ticinosuchus ferox (Krebs, 1965): 0.65
Trilophosaurus buettneri (Spielmann et al., 2008: figs. 78, 83): 0.35
Tropidosuchus romeri (PVL 4604): 0.35
Turfanosuchus dabanensis (IVPP 3237): 0.65
Yarasuchus deccanensis (ISIR 334): 0.55
Youngina capensis (Gow, 1975: fig. 9): 0.34

Discretization: (1) 0.26−0.29; (2) 0.32−0.45; (3) 0.48−0.57; (4) 0.60−1.15.

Character 478
Asilisaurus kongwe (NMT RB159): 0.27
Lagerpeton chanarensis (PVL 4625): 1.66

Character 482
Lesothosaurus diagnosticus (SAM-PK-K1105): 4.25
Lewisuchus admixtus (PULR V-111): 2.83
Megapnosaurus rhodesiensis (Raath, 1977: plate 19b): 3.81
Rhamphorhynchus muensteri (Wellnhofer, 1975a: fig. 10g): 2.50
Teraterpeton hrynewichorum (Pritchard and Sues, 2019: fig. 4a): 2.03

Character 489
Asilisaurus kongwe (NMT RB159): 1.59
Austriadraco dallavecchiai (SNSB-BSPG 1994 I 51): 0.95
Carniadactylus rosenfeldi (Dalla Vecchia, 2009a: table 1): 0.88
Coelophysis bauri (Rinehart et al., 2009: p. 168): 2.06
Coelophysis bauri (Rinehart et al., 2009: p. 170): 1.80
Coelophysis bauri (Rinehart et al., 2009: p. 185): 2.05
Coelophysis bauri (Rinehart et al., 2009: p. 224): 1.73
Eudimorphodon ranzii (Wild, 1979: table 1): 0.87
Lesothosaurus diagnosticus (Baron et al., 2016: tables 2, 3: SAM-PK-K1107): 2.29
Megapnosaurus rhodesiensis (Raath, 1977: table 4): 2.08
Peteinosaurus zambelli (Dalla Vecchia, 2014: table 4.1.1): 0.95
Preondactylus buffarinii (Dalla Vecchia, 1998: table 1): 1.01
Raeticodactylus filisurensis (BNM 14524): 0.69
Rhamphorhynchus muensteri (Wellnhofer, 1975b: table of measurements, specimens with skull length >89 mm): 0.68−0.98

Character 490
Asilisaurus kongwe (NMT RB159): 1.87
Lesothosaurus diagnosticus (Baron et al., 2016: tables 2, 3: NMQR 3076): 1.74
Megapnosaurus rhodesiensis (Raath, 1969: tables 5, 9): 1.78
Tropidosuchus romeri (PVL 4604): 1.25

Character 510
Asilisaurus kongwe (NMT RB159): 0.20
Austriadraco dallavecchiai (SNSB-BSPG 1994 I 51): 0.13
Dromomeron gregorii (TMM 31100-1306): 0.22
Dromomeron romeri (GR 218): 0.19
Ixalerpeton polesinensis (ULBRA-PVT059): 0.19
Lesothosaurus diagnosticus (Baron et al., 2016: table 3: NMQR 3076): 0.25
Lesothosaurus diagnosticus (Baron et al., 2016: table 3: SAM-PK-K1107): 0.22
Lewisuchus admixtus (PULR V-111): 0.14
Megapnosaurus rhodesiensis (Raath, 1977: table 9, NHMB 11470): 0.13
Megapnosaurus rhodesiensis (Raath, 1977: table 9, QG 755): 0.18
Megapnosaurus rhodesiensis (Raath, 1977: table 9, QG 76): 0.12
Megapnosaurus rhodesiensis (Raath, 1977: table 9, QG 738): 0.15
Megapnosaurus rhodesiensis (Raath, 1977: table 9, QG 691 left): 0.11
Raeticodactylus filisurensis (Dalla Vecchia, 2014: fig. 4.1.163c): 0.14
Rhamphorhynchus muensteri (Wellnhofer, 1975a: fig. 16c): 0.13
Teraterpeton hrynewichorum (Pritchard and Sues, 2019: fig. 5a): 0.18

Character 516
Asilisaurus kongwe (NMT RB159): 0.86
Austriadraco dallavecchiai (SNSB-BSPG 1994 I 51): 1.51

Carniadactylus rosenfeldi (Dalla Vecchia, 2009a: table 1): 1.46
Lesothosaurus diagnosticus (Baron et al., 2016: table 3: NMQR 3076): 1.17
Megapnosaurus rhodesiensis (NHMB 11470): 1.02
Peteinosaurus zambelli (MCSNB 3359): 1.30
Preondactylus buffarinii (Dalla Vecchia, 1998: table 1): 1.35
Raeticodactylus filisurensis (BNM 14524): 1.46
Rhamphorhynchus muensteri (Wellnhofer, 1975b: table of measurements, specimens with skull length >89 mm): 1.24−1.69
Teraterpeton hrynewichorum (Pritchard and Sues, 2019: supplemental table 2): ca. 0.78

Character 556
Lesothosaurus diagnosticus (Butler, 2005: fig. 17b): 0.47
Megapnosaurus rhodesiensis (QG cast): 0.33
Rhamphorhynchus muensteri (Wellnhofer, 1975a: fig. 17b): 0.95

Character 567
Asilisaurus kongwe (NMT RB159): 0.48
Austriadraco dallavecchiai (SNSB-BSPG 1994 I 51): 0.35−0.37
Carniadactylus rosenfeldi (Dalla Vecchia, 2009a: table 1): 0.41
Lesothosaurus diagnosticus (Baron et al., 2016: tables 3, 4: NMQR 3076): 0.40
Megapnosaurus rhodesiensis (NHMB 11470): 0.59
Peteinosaurus zambelli (Dalla Vecchia, 2014: tables 4.1.1, 3): 0.39
Preondactylus buffarinii (Dalla Vecchia, 2014: table 4.1.1): 0.36
Raeticodactylus filisurensis (BNM 14524): 0.38
Rhamphorhynchus muensteri (Wellnhofer, 1975b: table of measurements, specimens with skull length >89 mm): 0.49−0.66
Teraterpeton hrynewichorum (Pritchard and Sues, 2019: supplemental table 2): <0.29

Character 569
Asilisaurus kongwe (NMT RB159): 0.47
Carniadactylus rosenfeldi (Dalla Vecchia, 2009a: table 1): 0.98
Lesothosaurus diagnosticus (Baron et al., 2016: table 4: NMQR 3076): 0.58
Megapnosaurus rhodesiensis (NHMB 11470): 0.27
Peteinosaurus zambelli (MCSNB 3359): 0.94
Preondactylus buffarinii (Dalla Vecchia, 2014: fig. 4.1.8): ca. 1.00 or slightly higher
Raeticodactylus filisurensis (Stecher, 2008): ca. 1.00
Rhamphorhynchus muensteri (Wellnhofer, 1975a: fig. 17d, e): 0.91−0.95
Teraterpeton hrynewichorum (Pritchard and Sues, 2019: supplemental table 2): 0.49

Character 571
Asilisaurus kongwe (NMT RB159): 0.93
Carniadactylus rosenfeldi (Dalla Vecchia, 2009a: table 1): 1.13
Decuriasuchus quartacolonia (França et al., 2011: fig. 3g): ca. 1.00
Lesothosaurus diagnosticus (Baron et al., 2016: table 4: NMQR 3076): 0.99

Megapnosaurus rhodesiensis (NHMB 11470): 0.99
Peteinosaurus zambelli (Dalla Vecchia, 2014: table 4.1.3): 1.10
Raeticodactylus filisurensis (Stecher, 2008): ca. 1.00
Rhamphorhynchus muensteri (Wellnhofer, 1975a: fig. 17d, e): 1.12−1.15
Teraterpeton hrynewichorum (Pritchard and Sues, 2019: supplemental table 2): 0.69

Character 574
Asilisaurus kongwe (NMT RB159): 0.92
Carniadactylus rosenfeldi (Dalla Vecchia, 2009a: table 1): 0.93
Lesothosaurus diagnosticus (Baron et al., 2016: table 4: NMQR 3076): 0.98
Megapnosaurus rhodesiensis (NHMB 11470): 0.92
Peteinosaurus zambelli (Dalla Vecchia, 2014: table 4.1.3): 0.92
Rhamphorhynchus muensteri (Wellnhofer, 1975a: fig. 17d, e): 0.83−0.84
Teraterpeton hrynewichorum (Pritchard and Sues, 2019: supplemental table 2): 1.15

Character 581
Asilisaurus kongwe (NMT RB159): 1.15
Carniadactylus rosenfeldi (Dalla Vecchia, 2009a: table 1): 1.13
Dimorphodon macronyx (NHMUK PV OR 41212): 0.97
Megapnosaurus rhodesiensis (Raath, 1969: table 11): 1.37
Peteinosaurus zambelli (Dalla Vecchia, 2014: table 4.1.3): 0.90−0.92
Rhamphorhynchus muensteri (Wellnhofer, 1975a: fig. 17d, e): 1.02−1.07

Character 583
Asilisaurus kongwe (NMT RB159): 0.33
Carniadactylus rosenfeldi (Dalla Vecchia, 2009a: table 1): 2.26
Dimorphodon macronyx (Sangster, 2003: appendix 1): 2.62
Peteinosaurus zambelli (Dalla Vecchia, 2014: table 4.1.3): 3.38−3.58
Rhamphorhynchus muensteri (Wellnhofer, 1975a: fig. 17d, e): 1.77

Character 725
Buriolestes schultzi: ca. 25%
Dromomeron gregorii: ca. 42−44% (moderately deformed)
Ixalerpeton polesinensis: 44.2%
Saturnalia tupiniquim: 27.8%

Character 731
Allkaruen koi: 1.89
Arizonasaurus babbitti 1.30
Asilisaurus kongwe: 1.13
Buriolestes schultzi: 1.29
Dromomeron gregorii: 1.75
Euparkeria capensis: 1.09
Gracilisuchus stipanicicorum: 1.30

Herrerasaurus ischigualastensis: 1.35
Heterodontosaurus tucki: 1.14
Ixalerpeton polesinensis: 1.60
Lewisuchus admixtus: 1.25
Megapnosaurus rhodesiensis: 1.46
Mesosuchus browni: 1.22
Parasuchus hislopi: 1.46
Parringtonia gracilis: 1.00
Prolacerta broomi: 1.35
Proterosuchus fergusi: 1.35
Rhamphorhynchus muensteri: 1.52
Saturnalia tupiniquim: 1.57
Teleocrater rhadinus: 1.47
Discretization: (1) 1.00; (2) 1.09–1.14; (3) 1.22–1.35; (4) 1.46–1.60; (5) 1.75–1.89 (5%= 0.05).

Character 737
Allkaruen koi: 1.02
Arizonasaurus babbitti: 0.85
Asilisaurus kongwe: 0.64
Buriolestes schultzi: 0.61
Dromomeron gregorii: 1.00
Euparkeria capensis: 0.58
Gracilisuchus stipanicicorum: 0.60
Herrerasaurus ischigualastensis: 0.85
Heterodontosaurus tucki: 0.84
Ixalerpeton polesinensis: 1.00
Lewisuchus admixtus: 0.67
Mesosuchus browni: 0.53
Megapnosaurus rhodesiensis: 0.84
Parasuchus hislopi: 0.64
Parringtonia gracilis: 0.58
Prolacerta broomi: 0.59
Proterosuchus fergusi: 0.54
Rhamphorhynchus muensteri: 0.92
Saturnalia tupiniquim: 0.82
Teleocrater rhadinus: 0.78
Discretization: (1) 0.53−0.67; (2) 0.78–0.85; (3) 0.92–1.02 (5%= 0.03).

Character 738
Allkaruen koi: 1.87
Arizonasaurus babbitti: 1.33
Asilisaurus kongwe: 1.33
Buriolestes schultzi: 1.54

Dromomeron gregorii: 1.85
Euparkeria capensis: 1.13
Gracilisuchus stipanicicorum: 1.53
Herrerasaurus ischigualastensis: 1.39
Heterodontosaurus tucki: 1.34
Ixalerpeton polesinensis: 1.64
Lewisuchus admixtus: 1.35
Mesosuchus browni: 1.29
Megapnosaurus rhodesiensis: 1.32
Parasuchus hislopi: 1.60
Parringtonia gracilis: 1.31
Prolacerta broomi: 1.24
Proterosuchus fergusi: 1.20
Rhamphorhynchus muensteri: 2.37
Saturnalia tupiniquim: 1.28
Teleocrater rhadinus: 1.27
Discretization: (1) 1.13−1.39; (2) 1.53−1.64; (3) 1.85−1.87; (4) 2.37 (5%= 0.06).

Character 739
Allkaruen koi: 1.21
Arizonasaurus babbitti: 1.04
Asilisaurus kongwe: 1.09
Buriolestes schultzi: 2.74
Dromomeron gregorii: 1.20
Euparkeria capensis: 1.08
Gracilisuchus stipanicicorum: 1.02
Herrerasaurus ischigualastensis: 1.03
Heterodontosaurus tucki: 1.09
Ixalerpeton polesinensis: 1.20
Lesothosaurus diagnosticus: 1.13
Lewisuchus admixtus: 1.20
Megapnosaurus rhodesiensis: 1.16
Mesosuchus browni: 1.15
Parasuchus hislopi: 1.07
Parringtonia gracilis: 1.07
Prolacerta broomi: 1.15
Proterosuchus fergusi: 1.00
Rhamphorhynchus muensteri: 1.28
Saturnalia tupiniquim: 1.26
Teleocrater rhadinus: 1.11
Discretization: (1) 1.00−1.16; (2) 1.20−1.28 (5%= 0.02, excluding outlier).

Character 743
Allkaruen koi: 1.34

Arizonasaurus babbitti: 1.10
Asilisaurus kongwe: 1.20
Buriolestes schultzi: 1.15
Chanaresuchus bonapartei: 1.12
Dromomeron gregorii: 1.32
Euparkeria capensis: 1.11
Gracilisuchus stipanicicorum: 1.35
Herrerasaurus ischigualastensis: 1.09
Heterodontosaurus tucki: 1.16
Ixalerpeton polesinensis: 1.36
Lesothosaurus diagnosticus: 1.17
Lewisuchus admixtus: 1.31
Megapnosaurus rhodesiensis: 1.36
Mesosuchus browni: 1.32
Parasuchus hislopi: 1.02
Parringtonia gracilis: 1.05
Prolacerta broomi: 1.37
Proterosuchus fergusi: 1.09
Rhamphorhynchus muensteri: 1.46
Saturnalia tupiniquim: 1.15
Teleocrater rhadinus: 1.20
Wannia scurriensis: 1.15
Discretization: (1) 1.02−1.05; (2) 1.09−1.21; (3) 1.31−1.37; (4) 1.46 (5%= 0.03).

Character 777
Carniadactylus rosenfeldi (Dalla Vecchia, 2019: table S1): 0.38
Dimorphodon macronyx (NHMUK PV R1034): 0.24
Eudimorphodon ranzii (Dalla Vecchia, 2019: table S1): 0.41
Peteinosaurus zambellii (Dalla Vecchia, 2019: table S1): 0.25
Preondactylus buffarinii (Dalla Vecchia, 2019: table S1): 0.23
Rhamphorhynchus muensteri (Gross, 1937: fig. 2; Wellnhofer, 1975b: fig. 21; Bennett, 2016: fig. 1; Jura- Museum Eichstatt SOS 4784; Senckenberg Museum specimen): 0.33−0.38
Seazzadactylus venieri (Dalla Vecchia, 2019: table S1): 0.28

Character 782
Aetosaurus ferratus (Schoch, 2007: fig. 10c): 0.17
Austriadactylus cristatus (Dalla Vecchia, 2019: table S1): 0.40
Boreopricea funereal (PIN 3708/1): ca. 0.46
Carniadactylus rosenfeldi (Dalla Vecchia, 2019: table S1): 0.38−0.46
"*Chasmatosaurus*" *yuani* (Young, 1978: table 1): 0.30
Coelophysis bauri (Colbert, 1989: table 10, AMNH 7223): 0.30
Coelophysis bauri (Colbert, 1989: table 10, AMNH 7224): 0.26
Diandongosuchus fuyuanensis (Stocker et al., 2017: fig. 2): 0.25

Dimorphodon macronyx (Sangster, 2003: appendix 1, three specimens): 0.42−0.44
Dromomeron romeri (GR 238): 0.36
Eoraptor lunensis (Sereno et al., 2013: tables 7, 8): 0.25
Erpetosuchus granti (Benton and Walker, 2002: fig. 6): 0.19
Eudimorphodon ranzii (Wild, 1979: p. 2): 0.52−0.53
Euparkeria capensis (SAM-PK-13666): 0.27
Herrerasaurus ischigualastensis (Sereno and Novas, 1994, PVSJ 373): 0.35
Heterodontosaurus tucki (SAM-PK-K1332): 0.26
Isalorhynchus genovefae (Whatley, 2005: fig. 1.24b, 1.26b): 0.25
Langobardisaurus pandolfi (Renesto et al., 2002: table 1, MCSNB 4860 and MFSN 1921): 0.14−0.22
Lesothosaurus diagnosticus (Thulborn, 1972: 48): 0.21
Litorosuchus somnii (Li et al., 2016: table 1): 0.30
Megapnosaurus rhodesiensis (cast QG1): 0.26
Ornithosuchus woodwardi (Walker, 1964: table 1, fig. 10): ca. 0.28
Parasuchus hislopi (Chatterjee, 1978: fig. 11): 0.24
Peteinosaurus zambellii (Dalla Vecchia, 2019: table S1): 0.38
Preondactylus buffarinii (Dalla Vecchia, 2019: table S1): 0.44
Prolacerta broomi (Gow, 1975: fig. 23c): 0.22
Raeticodactylus filisurensis (BNM 14524): 0.49
Rhamphorhynchus muensteri (Wellnhofer, 1975a, b; specimens with skull length >89 mm): 0.41−0.56
Rhynchosaurus articeps (SHYMS 6): 0.33
Scleromochlus taylori (Benton, 1999: table 1, NHMUK PV R3556): ca. 0.13
Seazzadactylus venieri (Dalla Vecchia, 2019: table S1): 0.41
Stagonolepis robertsoni (Walker, 1961: table 1 and fig. 14): ca. 0.17
Stenaulorhynchus stockleyi (Huene, 1938: 102, 103): 0.23
Tanytrachelos ahynis (Olsen, 1979: fig. 2a): 0.19
Tawa hallae (Nesbitt et al., 2009b: fig. 2e, f): 0.38
Ticinosuchus ferox (Krebs, 1965: 62, 73): 0.21
Trilophosaurus buettneri (Spielmann et al., 2008: figs. 66b, 74b): 0.22
Vancleavea campi (Nesbitt et al., 2009c: fig. 13): 0.41

10. Abbreviations and acknowledgements of silhouettes in Figure 3

Abbreviations in Figure 3 are as follows: Aalen, Aalenian; Ch, Changhsingian; He, Hettangian; I, Induan; Olene, Olenekian; Wuchiapin, Wuchiapingian. Silhouette of *Tarjadia ruthae* (Pseudosuchia) modified from Ezcurra et al. (2017), silhouette of *Teleocrater rhadinus* (Aphanosauria) modified from Nesbitt et al. (2017), silhouette of *Asilisaurus kongwe* (Silesauridae) modified from Nesbitt et al. (2020), silhouettes of

Sanjuansaurus gordilloi (Dinosauria) modified from Alcober and Martínez, 2010; taken from http://phylopic.org/), silhouette of the lagerpetid is from this paper, and silhouette of *Preondactylus buffarinii* taken from http://phylopic.org/ (drawn by Mark Witton).

11. References

1. Alcober, O. A. & Martinez, R. N. A new herrerasaurid (Dinosauria, Saurischia) from the Upper Triassic Ischigualasto formation of northwestern Argentina. *ZooKeys* **63**, 55 (2010).
2. Andres, B. & Padian, K. in *Phylonyms: A Companion to the PhyloCode* (eds de Queiroz, K., Cantino, P. D. & Gauthier, J. A.) 149 (CRC Press, 2020).
3. Andres, B., Clark, J. M. & Xing, X. A new rhamphorhynchid pterosaur from the Upper Jurassic of Xinjiang, China, and the phylogenetic relationships of basal pterosaurs. *J. Vert. Paleontol.* **30**, 163−187 (2010).
4. Andres, B., Clark, J. & Xu, X. The earliest pterodactyloid and the origin of the group. *Current Biology* **24**, 1011−1016 (2014).
5. Arcucci, A. B. Nuevos materiales y reinterpretacion de *Lagerpeton chanarensis* Romer (Thecodontia, Lagerpetonidae nov.) del Triasico Medio de la Rioja, Argentina. *Ameghiniana* **23**, 233−242 (1986).
6. Baczko, M. B. von & Desojo, J. B. Cranial anatomy and palaeoneurology of the archosaur *Riojasuchus tenuisceps* from the Los Colorados Formation, La Rioja, Argentina. *PloS One* **11**, e0148575 (2016).
7. Baczko, M. B. von, Desojo, J. B. & Ponce, D. Postcranial anatomy and osteoderm histology of *Riojasuchus tenuisceps* and a phylogenetic update on Ornithosuchidae (Archosauria, Pseudosuchia). *J. Vert. Paleontol.* **39**, e1693396 (2019).

8. Bakker, R. T. & Galton, P. M. Dinosaur monophyly and a new class of vertebrates. *Nature* **248**, 168−172 (1974).

9. Baron, M. G., Norman, D. B. & Barrett, P. M. Postcranial anatomy of *Lesothosaurus diagnosticus* (Dinosauria: Ornithischia) from the Lower Jurassic of southern Africa: implications for basal ornithischian taxonomy and systematics. *Zoo. J. Linn. Soc.* **179**, 125−168 (2017).

10. Baron, M. G., Norman, D. B. & Barrett, P. M. A new hypothesis of dinosaur relationships and early dinosaur evolution. *Nature* **543,** 501–506 (2017).

11. Bennett, S. C. The phylogenetic position of the Pterosauria within the Archosauromorpha. *Zoo. J. Linn. Soc.* **118**, 261−308 (1996).

12. Benton, M. J. The Triassic reptile *Hyperodapedon* from Elgin: functional morphology and relationships. *Philos. T. R. Soc. B. Bio. Sci.* **302**, 605−718 (1983).

13. Benton, M. J. Classification and phylogeny of the diapsid reptiles. *Phil. Trans. R. Soc. Lond.* **302**, 605–720 (1984).

14. Benton, M. J. Classification and phylogeny of the diapsid reptiles. *Zoo. J. Linn. Soc.* **84**, 97−164 (1985).

15. Benton, M. J. The species of *Rhynchosaurus*, a rhynchosaur (Reptilia, Diapsida) from the Middle Triassic of England. *Philos. T. R. Soc. B. Bio. Sci.* **328**, 213−306 (1990).

16. Benton, M. J. *Scleromochlus taylori* and the origin of dinosaurs and pterosaurs. *Philos. T. R. Soc. B. Bio. Sci*. **354**, 1423−1446 (1999).

17. Benton, M. J. in *The Dinosauria 2nd Edtion* (eds Weishampel, D. B., Dobson, P. & Osmolska, H.) 7–24 (Univ. Cal. Press, 2004).

18. Benton, M. J. Archosaur remains from the otter sandstone formation (Middle Triassic, late Anisian) of Devon, southern UK. *Proc. Geo. Assoc.* **122**, 25−33 (2011).

19. Benton, M. J. & Allen, J. L. *Boreopricea* from the Lower Triassic of Russia, and the relationships of the prolacertiform reptiles. *Palaeontology* **40**, 931−954 (1997).

20. Benton, M. J. & Walker, A. D. *Erpetosuchus*, a crocodile-like basal archosaur from the Late Triassic of Elgin, Scotland. *Zoo. J. Linn. Soc.* **136**, 25-47 (2002).

21. Benton, M. J., & Walker, A. D. *Saltopus*, a dinosauriform from the Upper Triassic of Scotland. *Earth Environ. Sci. Trans. R. Soc. Edinb.* **101**, 285−299 (2010).

22. Bertin, T. J., Thivichon-Prince, B., LeBlanc, A. R., Caldwell, M. W. & Viriot, L. Current perspectives on tooth implantation, attachment, and replacement in Amniota. *Front. Physiol.* **9**, 1630 (2018).

23. Beyl, A., Nesbitt, S. J. Stocker, M. R. An Otischalkian dinosauromorph assemblage from the Los Esteros Member (Santa Rosa Formation) of New Mexico and its implications for biochronology and lagerpetid body size. J. Vert. Paleontol. e1765788 (2020).

24. Bonaparte J. F. & Powell, J. E. A continental asamblage of tetrapods from the Upper Cretaceous beds of el Brete, northwest Argentina (Sauropoda-Coelurosauria-Carnosauria-Ave). *Mem. Soc. Géo. Fr.* **139**, 19−28 (1980).

25. Bradley, A. B. et al. Sternal elements of early dinosaurs fill a critical gap in the evolution of the sternum in Avemetatarsalia (Reptilia: Archosauria). *J. Vert. Paleontol.* **39**, e1700992 (2020).

26. Bristowe, A. *The reconstruction of the skull of a juvenile ceratosaurian theropod dinosaur from the Forest Sandstone Formation (Karoo Sequence) of Zimbabwe,*

and its significance in identifying the taxon concerned (PhD Dissertation, Univ. Witwatersrand, 2004).

27. Bristowe, A. & Raath, M. A. A juvenile coelophysoid skull from the Early Jurassic of Zimbabwe, and the synonymy of *Coelophysis* and *Syntarsus*. *Palaeo. Afr.* **40**, 31−41 (2004).

28. Bristowe, A., Parrott, A., Hack, J., Pencharz, M. & Raath, M. A non-destructive investigation of the skull of the small theropod dinosaur, *Coelophysis rhodesiensis*, using CT scans and rapid prototyping. *Palaeo. Afr.* **40**, 159−163 (2004).

29. Britt, B. B. et al. *Caelestiventus hanseni* gen. et sp. nov. extends the desert-dwelling pterosaur record back 65 million years. *Nat. Ecol. Evol.* **2**, 1386−1392 (2018).

30. Bronzati, M., Rauhut, O. W., Bittencourt, J. S. & Langer, M. C. Endocast of the Late Triassic (Carnian) dinosaur *Saturnalia tupiniquim*: implications for the evolution of brain tissue in Sauropodomorpha. *Sci. Rep.* **7**, 1−7 (2017).

31. Bronzati, M., Müller, R. T. & Langer, M. C. Skull remains of the dinosaur *Saturnalia tupiniquim* (Late Triassic, Brazil): with comments on the early evolution of sauropodomorph feeding behaviour. *PloS One* **14**, e0221387 (2019).

32. Brust, A. C. B., Desojo, J. B., Schultz, C. L., Paes-Neto, V. D. & Da-Rosa, Á. A. S. Osteology of the first skull of *Aetosauroides scagliai* Casamiquela 1960 (Archosauria: Aetosauria) from the Upper Triassic of southern Brazil (*Hyperodapedon* Assemblage Zone) and its phylogenetic importance. *PloS One* **13**, e0201450 (2018).

33. Burch, S. H. Complete forelimb myology of the basal theropod dinosaur *Tawa hallae* based on a novel robust muscle reconstruction method. *J. Anat.* **225**, 271−297 (2014).

34. Butler, R. J. The 'fabrosaurid' ornithischian dinosaurs of the Upper Elliot Formation (Lower Jurassic) of South Africa and Lesotho. *Zoo. J. Linn. Soc.* **145**, 175−218 (2005).

35. Butler, R. J., Upchurch, P. & Norman D. B. The phylogeny of ornithischian dinosaurs. *J. Syst. Palaeontol.* **6**, 1−40 (2008).

36. Butler, R. J., et al. The sail-backed reptile *Ctenosauriscus* from the latest Early Triassic of Germany and the timing and biogeography of the early archosaur radiation. *PloS One* **6**, e25693 (2011).

37. Butler, R. J., Nesbitt, S. J., Charig, A. J., Gower, D. J. & Barrett, P. M. *Mandasuchus tanyauchen*, gen. et sp. nov., a pseudosuchian archosaur from the Manda Beds (?Middle Triassic) of Tanzania. *J. Vert. Paleontol.* **37**, 96−121 (2017).

38. Butler, R. J., Ezcurra, M. D., Liu, J., Sookias, R. B. & Sullivan, C. The anatomy and phylogenetic position of the erythrosuchid archosauriform *Guchengosuchus shiguaiensis* from the earliest Middle Triassic of China. *PeerJ* **7**, e6435 (2019).

39. Cabreira, S. F. et al. A unique Late Triassic dinosauromorph assemblage reveals dinosaur ancestral anatomy and diet. *Curr. Biol.* **26**, 3090−3095 (2016).

40. Carrano, M. T., Sampson, S. D. & Forster, C. A. The osteology of *Masiakasaurus knopfleri*, a small abelisauroid (Dinosauria: Theropoda) from the Late Cretaceous of Madagascar. *J. Vert. Paleontol.* **22**, 510−534 (2002).

41. Chatterjee, S. A rhynchosaur from the Upper Triassic Maleri formation of India. *Philos. T. R. Soc. B. Biol. Sci.* **267**, 209−261 (1974).

42. Chatterjee, S. A primitive parasuchid (phytosaur) reptile from the Upper Triassic Maleri Formation of India. *Palaeontol.* **21**, 83–127 (1978).

43. Clarke, J. A., Mindell, D. P., de Queiroz, K, Hanson, M., Norell, M. A. & Gauthier, J. A. in *Phylonyms: A Companion to the PhyloCode* (eds de Queiroz, K., Cantino, P. D. & Gauthier, J. A.) 113 (CRC Press, 2020).

44. Codorniú, L., Carabajal, A. P., Pol, D., Unwin, D. & Rauhut, O. W. A Jurassic pterosaur from Patagonia and the origin of the pterodactyloid neurocranium. *PeerJ* **4**, e2311 (2016).

45. Colbert, E. H. The Triassic dinosaur *Coelophysis*. *Mus. North. Ariz. Bull.* **57**, 1–160 (1989).

46. Cope, E. D. Synopsis of the extinct Batrachia, Reptilia and Aves of North America. *Trans. Am. Philos. Soc.* **14**, 1–252 (1869).

47. Dalla Vecchia, F. M. New observations on the osteology and taxonomic status of *Preondactylus bruffarinii* Wild, 1984 (Reptilia, Pterosauria). *Boll. Soc. Paleontol. Ital.* **36**, 355−366 (1998).

48. Dalla Vecchia, F. M. in *Evolution and Palaeobiology of Pterosaurs* (eds Buffetaut, E. & Mazin, J.-M.) 23−44 (Geol. Soc. Lond. 2003).

49. Dalla Vecchia, F. M. Anatomy and systematics of the pterosaur *Carniadactylus* gen. n. *rosenfeldi* (Dalla Vecchia, 1995). *Riv. Ital. Paleontol. S.* **115**, 159– 198 (2009a).

50. Dalla Vecchia, F. M. *Austriadactylus* (Diapsida, Pterosauria) from the Norian (Upper Triassic) of northeastern Italy. *Riv. Ital. Paleontol. S.* **115**, 291–304 (2009b).

51. Dalla Vecchia, F. M. in *Anatomy, phylogeny and palaeobiology of early archosaurs and their kin* (eds Nesbitt, S. J., Desojo, J. B. & Irmis, R. B.) 119−155 (Geol. Soc. Lond. 2013).

52. Dalla Vecchia F. M. *Gli pterosauri triassici* (Pubb. Mus. Fri. St. Nat. **54**, 2014).

53. Dalla Vecchia F. M. Comments on Triassic pterosaurs with a commentary on the "ontogenetic stages" of Kellner (2015) and the validity of *Bergamodactylus wildi*. *Riv. Ital. Paleontol. S.* **124**, 317−341 (2018).

54. Dalla Vecchia, F. M. *Seazzadactylus venieri* gen. et sp. nov., a new pterosaur (Diapsida: Pterosauria) from the Upper Triassic (Norian) of northeastern Italy. *PeerJ* **7**, e7363 (2019).

55. Dalla Vecchia, F. M., Wild, R., Hopf, H. & Reitner, J. A crested rhamphorhynchoid pterosaur from the Late Triassic of Austria. *J. Vert. Paleontol.* **22**, 196-199 (2002).

56. Daudin, F. M. *Histoire naturelle, generale et particuliere des reptiles. Vol. 1.* (F. Dufart, 1802).

57. de Queiroz, K., Cantino, P. D. & Gauthier, J. A. (eds) *Phylonyms: A Companion to the PhyloCode* (CRC Press, 2020).

58. Desojo, J. B., Baczko, M. B. von & Rauhut, O. W. M. Anatomy, taxonomy and phylogenetic relationships of *Prestosuchus chiniquensis* (Archosauria: Pseudosuchia) from the original collection of von Huene, Middle-Late Triassic of southern Brazil. *Palaeontol. Elect.* **23**, a04 (2020).

59. Dzik, J. A beaked herbivorous archosaur with dinosaur affinities from the early Late Triassic of Poland. *J. Vert. Paleontol.* **23**, 556−574 (2003).

60. Evans, S. E. The skull of *Cteniogenys*, a choristodere (Reptilia: Archosauromorpha) from the Middle Jurassic of Oxfordshire. *Zoo. J. Linn. Soc.* **99**, 205−237 (1990).

61. Ezcurra, M. D. A review of the systematic position of the dinosauriform archosaur *Eucoelophysis baldwini* Sullivan & Lucas, 1999 from the Upper Triassic of New Mexico, USA. *Geodiversitas* **28**, 649−684 (2006).

62. Ezcurra, M. D. The phylogenetic relationships of basal archosauromorphs, with an emphasis on the systematics of proterosuchian archosauriforms. *PeerJ* **4**, e1778 (2016).

63. Ezcurra, M. D. & Butler, R. J. The rise of the ruling reptiles and ecosystem recovery from the Permo-Triassic mass extinction. *Proc. R. Soc. B Biol. Sci* **285**, 20180361 (2018).

64. Ezcurra, M. D., Lecuona, A. & Martinelli, A. G. A new basal archosauriform diapsid from the Lower Triassic of Argentina. *J. Vert. Paleontol.* **30**, 1433−1450 (2010).

65. Ezcurra, M. D., Scheyer, T. M. & Butler, R. J. The origin and early evolution of Sauria: reassessing the Permian saurian fossil record and the timing of the crocodile-lizard divergence. PLoS One 9, e89165 (2014).

66. Ezcurra, M. D., Desojo, J. B. & Rauhut, O. W. Redescription and phylogenetic relationships of the proterochampsid *Rhadinosuchus gracilis* (Diapsida: Archosauriformes) from the early Late Triassic of southern Brazil. *Ameghiniana* **52**, 391−417 (2015).

67. Ezcurra, M. D. et al. Deep faunistic turnovers preceded the rise of dinosaurs in southwestern Pangaea. *Nat. Ecol. Evol.* **1**, 1477–1483 (2017).

68. Ezcurra, M. D., Gower, D. J., Sennikov, A. G. & Butler, R. J. The osteology of the holotype of the early erythrosuchid *Garjainia prima* (Diapsida: Archosauromorpha) from the upper Lower Triassic of European Russia. *Zoo. J. Linn. Soc.* **185**, 717−783 (2019).

69. Flynn, J. J., Nesbitt, S. J., Michael Parrish, J., Ranivoharimanana, L. & Wyss, A. R. A new species of *Azendohsaurus* (Diapsida: Archosauromorpha) from the Triassic Isalo Group of southwestern Madagascar: cranium and mandible. *Palaeontol.* **53**, 669−688 (2010).

70. França, M. A. G., Ferigolo, J. & Langer, M. C. Associated skeletons of a new middle Triassic “Rauisuchia” from Brazil. *Naturwissenschaften* **98**, 389 (2011).

71. França, M. A. G., Langer, M. C. & Ferigolo, J. in *Anatomy, phylogeny and palaeobiology of early archosaurs and their kin* (eds Nesbitt, S. J., Desojo, J. B. & Irmis, R. B.) 469−501 (Geol. Soc. Lond., 2013).

72. Fraser, N. C. A new rhynchocephalian from the British Upper Trias. *Paleontol.* **25**, 709−725 (1982).

73. Galton, P. M. Prosauropod dinosaur (Reptilia, Saurischia) of North America. *Postilla* **169**, 1−98 (1976).

74. Galton, P. M. & Upchurch, P. in *The Dinosauria 2nd Edition* (eds Weishampel, D. B., Dobson, P. & Osmolska, H.) 232–258 (Univ. Cal. Press, 2004).

75. Garcia, M. S., Müller, R. T., Da-Rosa, Á. A. & Dias-da-Silva, S. The oldest known co-occurrence of dinosaurs and their closest relatives: a new lagerpetid from a Carnian (Upper Triassic) bed of Brazil with implications for dinosauromorph biostratigraphy, early diversification and biogeography. *J. S. Am. Earth Sci.* **91**, 302−319 (2019).

76. Gasparini, Z., Fernández, M. & Fuente, M. D. L. A new pterosaur from the Jurassic of Cuba. *Palaeontol.* **47**, 919−927 (2004).

77. Gauthier, J. A. Saurischian monophyly and the origin of birds. *Mem. Cal. Acadm. Sci.* **8**, 1–55 (1986).

78. Gauthier, J. A. & de Queiroz, K. in *New Perspectives on the Origin and Early Evolution of Birds: Proceedings of the International Symposium in Honor of John H. Ostrom* (eds Gauthier, J. A & Gall, L. F.) 7−41 (Peabody Mus. Nat. Hist., 2001).

79. Gauthier, J. & Padian, K. 2020 in *Phylonyms: A Companion to the PhyloCode* (eds de Queiroz, K., Cantino, P. D. & Gauthier, J. A.) 173 (CRC Press, 2020).

80. Gelman, A. & Rubin, D. B. Inference from iterative simulation using multiple sequences. *Stat. Sci.* **7**, 457−472 (1992).

81. Goloboff, P. A. et al. Improvements to resampling measures of group support. *Cladistics* **19**, 324−332 (2003).

82. Gow, C. E. The morphology and relationships of *Youngina capensis* Broom and *Prolacerta broomi* Parrington. *Palaeo. Afr.* **18**, 89–131 (1975).

83. Gower, D. J. Cranial osteology of a new rauisuchian archosaur from the Middle Triassic of southern Germany. *Stutt. Beitr. Naturkd. B.* **280**, 1–49 (1999).

84. Gower, D. J. Osteology of the early archosaurian reptile *Erythrosuchus africanus*, Broom. *Ann. S. Afr. Mus.* **110**, 1–84 (2003).

85. Griffin, C. T. et al. Integrating gross morphology and bone histology to assess skeletal maturity in early dinosauromorphs: new insights from *Dromomeron* (Archosauria: Dinosauromorpha). *PeerJ* **7**, e6331 (2019).

86. Heath, T. A., Huelsenbeck, J. P. & Stadler, T. The fossilized birth–death process for coherent calibration of divergence-time estimates. *Proc. Natl. Acad. Sci. USA* **111**, E2957–E2966 (2014).

87. Horn, B. L. D. et al. A new third-order sequence stratigraphic framework applied to the Triassic of the Paraná Basin, Rio Grande do Sul, Brazil, based on structural, stratigraphic and paleontological data. *J. S. Am. Earth Sci.* **55**, 123−132 (2014).

88. Huene, F. von. Die Dinosaurier der europäischen Triasformation, mit Berücksichtigung der ausser–europäischen Vorkomnisse (part). *Geol. Paläontol. Abh.* **6**, 345–419 (1908).

89. Huene F. von. Die fossilen Reptilien des südamerikan-ischen Gondwanalandes. *Neues Jb. Miner. Geo. Paläontol.* **1938**, 142–151 (1938).

90. Huene F. von. Ein grosser Pseudosuchier aus der Orenburger Trias. *Palaeontogr. Abt. A* **114**: 105–111 (1960).

91. Irmis, R. B. et al. A Late Triassic dinosauromorph assemblage from New Mexico and the rise of dinosaurs. *Science* **317**, 358−361 (2007).

92. Jalil, N. E. A new prolacertiform diapsid from the Triassic of North Africa and the interrelationships of the Prolacertiformes. *J. Vert. Paleontol.* **17**, 506−525 (1997).

93. Jiang, D. Y. et al. New information on the protorosaurian reptile *Macrocnemus fuyuanensis* Li et al., 2007, from the Middle/Upper Triassic of Yunnan, China. *J. Vert. Paleontol.* **31**, 1230−1237 (2011).

94. Kammerer, C. F., Nesbitt, S. J. & Shubin, N. H. The first silesaurid dinosauriform from the Late Triassic of Morocco. *Acta Palaeontol. Pol.* **57**, 277−284 (2011).

95. Kammerer, C. F., Nesbitt, S. J., Flynn, J. J., Ranivoharimanana, L. & Wyss, A. R. A tiny ornithodiran archosaur from the Triassic of Madagascar and the role of

miniaturization in dinosaur and pterosaur ancestry. *Proc. Nat. Ac. Sci.*, 10.1073/pnas.1916631117 (2020).

96. Krebs, B. Die triasfauna der Tessiner Kalkalpen. XIX. *Ticinosuchus ferox*, nov. gen. nov. sp. Ein neuer Pseudosuchier aus der Trias des Monte San Georgio. *Schweiz. Palaeontol.* **81**, 1−140 (1965).

97. Kuhn-Schnyder, E. & Rieber, H. *Handbook of Paleozoology*. The John Hopkins Univ. Press (1986).

98. Lacerda, M. B., Franca, M. A. G. & Schultz, C. L. A new erpetosuchid (Pseudosuchia, Archosauria) from the Middle–late Triassic of Southern Brazil. *Zoo. J. Linn. Soc.* **184**, 804−824 (2018).

99. Langer, M. C. The pelvic and hind limb anatomy of the stem-sauropodomorph *Saturnalia tupiniquim* (Late Triassic, Brazil). *PaleoBios* **23**, 1–30 (2003).

100. Langer M. C. in *The Dinosauria 2nd Edition* (eds Weishampel, D. B., Dobson, P. & Osmolska, H.) 25–46 (Univ. Cal. Press, 2004).

101. Langer, M. C. & Benton, M. J. Early dinosaurs: a phylogenetic study. *J. Syst. Palaeontol.* **4**, 309−358 (2006).

102. Langer, M. C., Abdala, F., Richter, M. & Benton, M. J. A sauropodomorph dinosaur from the Upper Triassic (Carnian) of southern Brazil. *C. R. Acad. Sci. IIA* **329**, 511−517 (1999).

103. Langer, M. C., Franca, M. A. & Gabriel, S. The pectoral girdle and forelimb anatomy of the stem-sauropodomorph *Saturnalia tupiniquim* (Upper Triassic, Brazil). *Spec. Papers Palaentol.* **77**, 113–137 (2007).

104. Langer, M. C., Ramezani, J. & Da Rosa, Á. A. S. U-Pb age constraints on dinosaur rise from south Brazil. *Gond. Res.* **57**, 133−140 (2018).

105. Laurenti, J. N. *Specimen Medicum, Exhibens Synops in Reptilium Emendatus, etc.* (Vienna, 1768).
106. Lecuona, A. & Desojo, J. B. Hind limb osteology of *Gracilisuchus stipanicicorum* (Archosauria: Pseudosuchia). *Earth Environ. Sci. Trans. R. Soc. Edinb.* **102**, 105−128 (2012).
107. Lepage, T., Bryant, D., Philippe, H., & Lartillot, N. A general comparison of relaxed molecular clock models. *Mol. Biol. Evol.* **24**, 2669−2680 (2007).
108. Lewis, P. O. A likelihood approach to estimating phylogeny from discrete morphological character data. *Syst. Biol.* **50**, 913−925 (2001).
109. Li, C., Wu, X. C., Cheng, Y. N., Sato, T. & Wang, L. An unusual archosaurian from the marine Triassic of China. *Naturwissenschaften* **93**, 200−206 (2006).
110. Li, C., Wu, X. C., Zhao, L. J., Nesbitt, S. J., Stocker, M. R. & Wang, L. T. A new armored archosauriform (Diapsida: Archosauromorpha) from the marine Middle Triassic of China, with implications for the diverse life styles of archosauriforms prior to the diversification of Archosauria. *Sci. Nat.* **103**, 95 (2016).
111. Li, C., Fraser, N. C., Rieppel, O., Zhao, L. J. & Wang, L. T. A new diapsid from the Middle Triassic of southern China. *J. Paleontol.* **91**, 1306−1312 (2017).
112. Linnaeus C. Systema naturæ per regna tria naturæ, secundum classses, ordines, genera, species, cum characteribus, differentiis, synonymis, locis. *Holmiae, Laurentii Salvii* **1-4**, 1−824 (1758).
113. Lü , J., Unwin, D. M., Bo, Z., Chunling, G. & Caizhi, S. A new rhamphorhynchid (Pterosauria: Rhamphorhynchidae) from the Middle/Upper Jurassic of Qinglong, Hebei Province, China. *Zootaxa* **3158**, 1–19 (2012).
114. Junchang, L. Ü., Hanyong, P. U., Li, X. U., Yanhua, W. U. & Xuefang, W. E. I. Largest toothed pterosaur skull from the Early Cretaceous Yixian Formation of

western Liaoning, China, with comments on the Family Boreopteridae. *Acta Geol. Sin.-Engl.* **86**, 287−293 (2012).

115. Makovicky, P. J. & Sues, H. D. Anatomy and phylogenetic relationships of the theropod dinosaur *Microvenator celer* from the Lower Cretaceous of Montana. *Am. Mus. Nov.* **3240**, 1−27 (1998).

116. Marsh, O. C. Notice of gigantic horned Dinosauria from the Cretaceous. *Am. J. Sci. ser. 3* **38**, 173–176 (1889).

117. Marsh, A. D. A new record of *Dromomeron romeri* Irmis et al., 2007 (Lagerpetidae) from the Chinle Formation of Arizona, USA. *PaleoBios* **35**, 1−8 (2018).

118. Martínez, R. N. et al. Vertebrate succession in the Ischigualasto Formation. *J. Vert. Paleontol.* **32**, 10−30 (2013).

119. Martínez, R. N., Apaldetti, C., Correa, G. A. & Abelín, D. A Norian lagerpetid dinosauromorph from the Quebrada del Barro Formation, northwestern Argentina. *Ameghiniana* **53**, 1−13 (2016).

120. Martz, J. W. & Small, B. J. Non-dinosaurian dinosauromorphs from the Chinle Formation (Upper Triassic) of the Eagle Basin, northern Colorado: *Dromomeron romeri* (Lagerpetidae) and a new taxon, *Kwanasaurus williamparkeri* (Silesauridae). *PeerJ* **7**, e7551 (2019).

121. Mastrantonio, B. M., Baczko, M. B. von, Desojo, J. B. & Schultz, C. L. The skull anatomy and cranial endocast of the pseudosuchid archosaur *Prestosuchus chiniquensis* from the Triassic of Brazil. *Acta Palaeontol. Pol.* **64**, 171−198 (2019).

122. Müller, R. T., Langer, M. & Dias-da Silva, S. Ingroup relationships of Lagerpetidae (Avemetatarsalia: Dinosauromorpha): a further phylogenetic

investigation on the understanding of dinosaur relatives. *Zootaxa* **4392**, 149−158 (2018).

123. Müller, R. T., Baczko, M. B. von, Desojo, J. B. & Nesbitt, S. J. The first ornithosuchid from Brazil and its macroevolutionary and phylogenetic implications for Late Triassic faunas in Gondwana. *Acta Palaeontol. Pol.* **65**, 1−10 (2020).

124. Nesbitt, S. J. Osteology of the Middle Triassic pseudosuchian archosaur *Arizonasaurus babbitti*. *Hist. Biol.* **17**, 19−47 (2005).

125. Nesbitt, S. J. The early evolution of archosaurs: relationships and the origin of major clades. *Am. Mus. Nat. Hist. Bull.* **352**, 1−292 (2011).

126. Nesbitt, S. J., Irmis, R. B., Parker, W. G., Smith, N. D., Turner, A. H. & Rowe, T. Hindlimb osteology and distribution of basal dinosauromorphs from the Late Triassic of North America. *J. Vert. Paleontol.* **29**, 498−516 (2009a).

127. Nesbitt, S. J., Smith, N. D., Irmis, R. B., Turner, A. H., Downs, A. & Norell, M. A. A complete skeleton of a Late Triassic saurischian and the early evolution of dinosaurs. *Science* **326**, 1530−1533 (2009b).

128. Nesbitt, S. J., Stocker, M. R., Small, B. J. & Downs, A. The osteology and relationships of *Vancleavea campi* (Reptilia: Archosauriformes). *Zoo. J. Linn. Soc.* **157**, 814−864 (2009c).

129. Nesbitt, S. J., Liu, J. & Li, C. A sail-backed suchian from the Heshanggou Formation (Early Triassic: Olenekian) of China. *Earth Environ. Sci. Trans. R. Soc. Edinb.* **110**, 271–284 (2011).

130. Nesbitt, S. J., Butler, R. J. & Gower, D. J. A new archosauriform (Reptilia: Diapsida) from the Manda beds (Middle Triassic) of southwestern Tanzania. *PLoS One* **8**, e72753 (2013).

131. Nesbitt, S. J., Sidor, C. A., Angielczyk, K. D., Smith, R. M. & Tsuji, L. A. A new archosaur from the Manda beds (Anisian, Middle Triassic) of southern Tanzania and its implications for character state optimizations at Archosauria and Pseudosuchia. *J. Vert. Paleontol.* **34**, 1357−1382 (2014).

132. Nesbitt, S. J. et al. Postcranial osteology of *Azendohsaurus madagaskarensis* (?Middle to Upper Triassic, Isalo Group, Madagascar) and its systematic position among stem archosaur reptiles. *Am. Mus. Nat. Hist. Bull.* **398**, 1−126 (2015).

133. Nesbitt, S. J. et al. The earliest bird-line archosaurs and the assembly of the dinosaur body plan. *Nature* **544**, 484−487 (2017).

134. Nesbitt, S. J., Butler, R. J., Ezcurra, M. D., Charig, A. J. & Barrett, P. M. The anatomy of *Teleocrater rhadinus*, an early avemetatarsalian from the lower portion of the Lifua Member of the Manda Beds (Middle Triassic). *J. Vert. Paleontol.* **37**, 142−177 (2018a).

135. Nesbitt, S. J. et al. The braincase and endocast of *Parringtonia gracilis*, a Middle Triassic suchian (Archosaur: Pseudosuchia). *J. Vert. Paleontol.* **37**, 122−141. (2018b).

136. Nesbitt, S. J., Langer, M. C. & Ezcurra, M. D. The anatomy of *Asilisaurus kongwe*, a dinosauriform from the Lifua Member of the Manda Beds (~ Middle Triassic) of Africa. *Anat. Rec.* **303**, 813−873 (2020).

137. Nosotti, S. *Tanystropheus longobardicus* (Reptilia, Protorosauria): re-interpretations of the anatomy based on new specimens from the Middle Triassic of Besano (Lombardy, northern Italy). *Soc. It. Sci. Nat. Mus. Civ. St. Nat.* **35**, 1−88 (2007).

138. Novas, F. E. in *Los dinosaurios y su entorno biótico II* (eds Sanz, L. J. & Buscalioni, A. D.) 125−163 (Instituto Juan de Valdés, 1992).

139. Novas, F. E. Dinosaur monophyly. *J. Vert. Paleontol.* **16**, 723−741 (1996).
140. Olsen P. E. A new aquatic eusuchian from the Newark Basin (Late Triassic-Early Jurasic) of North Carolina and Virginia. *Postilla* **176**, 1−14 (1979).
141. Padian, K. Osteology and functional morphology of *Dimorphodon macronyx* (Buckland) (Pterosauria: Rhamphorhynchoidea) based on new material in the Yale Peabody Museum. Postilla **189**, 1–44 (1983).
142. Pol, D. & Escapa, I. H. Unstable taxa in cladistic analysis: identification and the assessment of relevant characters. *Cladistics* **25**, 515−527 (2009).
143. Porro, L. B., Witmer, L. M., & Barrett, P. M. Digital preparation and osteology of the skull of *Lesothosaurus diagnosticus* (Ornithischia: Dinosauria). *PeerJ* **3**, e1494 (2015).
144. Pritchard A. C., Turner A. H., Nesbitt S. J., Irmis R. B. & Smith N. D. Late Triassic tanystropheids (Reptilia, Archosauromorpha) from northern New Mexico (Petrified Forest Member, Chinle Formation) and the biogeography, functional morphology, and evolution of Tanystropheidae. *J. Vert. Paleontol.* **3**, e911186 (2015).
145. R, Core Team. *R: A Language and Environment for Statistical Computing (Version 3.5. 2)* (R Found. Stat. Comp., 2019).
146. Raath, M. A. A new coelurosaurian dinosaur from the Forest Sandstone of Rhodesia. *Nat. Mus. Rhod.* **4**, 1−25 (1969).
147. Raath, M. A. *The anatomy of the Triassic theropod.* Syntarsus rhodesiensis (PhD Dissertation, Rhodes University, 1977).
148. Rambaut, A., Drummond, A. J., Xie, D., Baele, G. & Suchard, M. A. Posterior summarization in Bayesian phylogenetics using Tracer 1.7. *Syst. Biol.* **67**, 901−904 (2018).

149. Rauhut O. W. M. The interrelationships and evolution of basal theropod dinosaurs. *Sp. Pap. Palaeontol.* **69**, 1−213 (2003).

150. Renesto S. & Dalla Vecchia, F. M. The unusual dentition and feeding habits of the Prolacertiform reptile *Langobardisaurus* (Late Triassic, Northern Italy). *J. Vert. Paleontol.* **20**, 622−627 (2000).

151. Renesto, S., Dalla Vecchia, F. M. & Peters, D. Morphological evidence for bipedalism in the Late Triassic prolacertiform reptile *Langobardisaurus*. *Senck. leth.* **82**, 94 (2002).

152. Rieppel, O., Li, C. & Fraser, N. C. The skeletal anatomy of the Triassic protorosaur *Dinocephalosaurus orientalis* Li, from the Middle Triassic of Guizhou Province, southern China. *J. Vert. Paleontol.* **28**, 95−110 (2008).

153. Rinehart, L. F., Lucas, S. G., Heckert, A. B., Spielmann, J. A. & Celeskey, M. D. The Paleobiology of *Coelophysis bauri* (Cope) from the Upper Triassic (Apachean) Whitaker quarry, New Mexico, with detailed analysis of a single quarry block. *N M Mus. Nat. Hist. Sci. Bull.* **45**, 1−260 (2009).

154. Roberto-da-Silva, L., Franca, M. A., Cabreira, S. F., Mueller, R. T. & Dias-da-Silva, S. On the presence of the subnarial foramen in *Prestosuchus chiniquensis* (Pseudosuchia: Loricata) with remarks on its phylogenetic distribution. *An. Acad. Bras. Ciênc.* **88**, 1309−1323 (2016).

155. Roberto-Da-Silva, L., Müller, R. T., França, M. A. G. D., Cabreira, S. F. & Dias-Da-Silva, S. An impressive skeleton of the giant top predator *Prestosuchus chiniquensis* (Pseudosuchia: Loricata) from the Triassic of Southern Brazil, with phylogenetic remarks. *Hist. Biol.*, latest articles (2018).

156. Romer, A. S. The Chañares (Argentina) Triassic reptile fauna. X. Two new but incompletely known long–limbed pseudosuchians. *Breviora* **378**, 1–10 (1971a).

157. Romer, A. S. The Chañares (Argentina) Triassic reptile fauna. XI. Two long-snouted thecodonts, *Chanaresuchus* and *Gualosuchus*. *Breviora* **379**, 1-22 (1971b).

158. Romer, A. S. The Chanares (Argentina) Triassic reptile fauna. XV. Further remains of the thecodonts *Lagerpeton* and *Lagosuchus. Breviora* **394**, 1–7 (1972a).

159. Romer, A. S. The Chañares (Argentina) Triassic reptile fauna. XIV. *Lewisuchus admixtus*, gen. et sp. nov., a further thecodont from the Chañares beds. *Breviora* **390**, 1–13 (1972b).

160. Ronquist, F., van der Mark, P. & Huelsenbeck, J. P. in *The Phylogenetic Handbook: a Practical Approach to Phylogenetic Analysis and Hypothesis Testing* (eds Lemey, P., Salemi, M. & Vandamme, A.-M.) 210−266 (Camb. Univ. Press, 2009).

161. Rowe, T. A new species of the theropod dinosaur *Syntarsus* from the Early Jurassic Kayenta Formation of Arizona. *J. Vert. Paleontol.* **9**, 125−136 (1989).

162. Russell-Sigogneau D. & Russel D. E. Etude osteologique du Reptile *Simeodosaurus* (Choristodera). *Ann. Paleontol. (Vertebres)* **64**, 1−84 (1978).

163. Sangster, S. *The Anatomy, Functional Morphology and Systematics of* Dimorphodon macronyx *(Diapsida: Pterosauria)* (PhD Disserttion, Univ. Cambridge, 2003).

164. Sampson, S. D. & Witmer, L. M. Craniofacial anatomy of *Majungasaurus crenatissimus* (Theropoda: Abelisauridae) from the late Cretaceous of Madagascar. *J. Vert. Paleontol.* **27**, 32−104 (2007).

165. Santa Luca, A. P. The postcranial skeleton of *Heterodontosaurus tucki* (Reptilia, Ornithischia) from the Stormberg of South Africa. *Ann. S. Afr. Mus.* **79**, 159−211 (1980).

166. Sarigül, V. New basal dinosauromorph records from the Dockum Group of Texas, USA. *Palaeontol. Electr.* **19**, 1−16 (2016).

167. Schoch, R. R. Osteology of the small archosaur *Aetosaurus* from the Upper Triassic of Germany. *Neues Jahrb. Geol. Paläotol. Abh.* **246**, 1−35 (2007).

168. Sengupta, S., Ezcurra, M. D. & Bandyopadhyay, S. A new horned and long-necked herbivorous stem-archosaur from the Middle Triassic of India. *Sci. Rep.* **7**, 1−9 (2017).

169. Sereno, P. C. Phylogeny of the bird-hipped dinosaurs (Order Ornithischia). *Nat. Geog. Res.* **2**, 234−256 (1986).

170. Sereno, P. C. Basal archosaurs: phylogenetic relationships and functional implications. *Soc. Vert. Paleont. Mem.* **2**, 1−53 (1991a).

171. Sereno, P. C. *Lesothosaurus*, "fabrosaurids," and the early evolution of Ornithischia. *J. Vert. Paleontol.* **11**, 168−197 (1991b).

172. Sereno, P. C. The evolution of dinosaurs. *Science* **284**, 2137−2147 (1999).

173. Sereno, P. C & Arcucci. A. B. Dinosaur precursors from the Middle Triassic of Argentina: *Marasuchus lilloensis* gen. nov. *J. Vert. Paleontol.* **14**, 53–73 (1994a).

174. Sereno, P. C & Arcucci. A. B. Dinosaur precursors from the Middle Triassic of Argentina: *Lagerpeton chanarensis*. *J. Vert. Paleontol.* **13**, 385–399 (1994b).

175. Sereno, P. C. & Novas, F. E. The skull and neck of the basal theropod *Herrerasaurus ischigualastensis*. *J. Vert. Paleontol.* **13**, 451−476 (1994).

176. Sereno, P. C., Forster, C. A., Rogers, R. R. & Monetta, A. M. Primitive dinosaur skeleton from Argentina and the early evolution of Dinosauria. *Nature* **361**, 64−66 (1993).

177. Sereno, P. C., McAllister, S. & Brusatte, S. L. TaxonSearch: a relational database for suprageneric taxa and phylogenetic definitions. *PhyloInformatics* **8**, 1−25 (2005).

178. Sereno P. C., Martínez R. N. & Alcober O. A. Osteology of *Eoraptor lunensis* (Dinosauria, Sauropodomorpha). *J. Vert. Paleontol.* **32**, 83–179 (2013).

179. Smith, N. D., Makovicky, P. J., Hammer, W. R. & Currie, P. J. Osteology of *Cryolophosaurus ellioti* (Dinosauria: Theropoda) from the Early Jurassic of Antarctica and implications for early theropod evolution. *Zool. J. Linn. Soc.* **151**, 377−421 (2007).

180. Sobral, G. & Müller, J. The braincase of *Mesosuchus browni* (Reptilia, Archosauromorpha) with information on the inner ear and description of a pneumatic sinus. *PeerJ* **7**, e6798 (2019).

181. Sömmerring, S. V. Über einen Ornithocephalus. *Denk. Königl Akadem. Wissensch.* **3**, 89−120 (1812).

182. Spielmann, J. A., Lucas, S. G., Rinehart, L. F. & Heckert, A. B. The Late Triassic archosauromorph *Trilophosaurus*. *N. M. Mus. Nat. Hist. Sci. Bull.* **43**, 1–177 (2008).

183. Spielmann, J. A., Lucas, S. G., Heckert, A. B., Rinehart, L. F. & Richards III, H. R. Redescription of *Spinosuchus caseanus* (Archosauromorpha: Trilophosauridae) from the Upper Triassic of North America. *Palaeodiversity* **2**, 283−313 (2009).

184. Stadler, T. Sampling-through-time in birth–death trees. *J. Theor. Biol.* **267**, 396−340 (2010).

185. Stecher, R. A new Triassic pterosaur from Switzerland (Central Austroalpine, Grisons), *Raeticodactylus filisurensis* gen. et sp. nov. *Sw. J. Geosc.* **101**, 185−201 (2008).

186. Stefanic, C. M. & Nesbitt, S. J. The evolution and role of the hyposphene-hypantrum articulation in Archosauria: phylogeny, size and/or mechanics? *R. Soc. O. Sci*. **6**, 190258 (2019).

187. Stocker, M. R. *Contextualizing vertebrate faunal dynamics: new perspectives from the Triassic and Eocene of western North America* (PhD Dissertation, University of Texas, 2013).

188. Stocker, M. R., Zhao, L. J., Nesbitt, S. J., Wu, X. C. & Li, C. A short-snouted, Middle Triassic phytosaur and its implications for the morphological evolution and biogeography of Phytosauria. *Sci. Rep.* **7**, 1−9 (2017).

189. Tatarinov, L. P. Triassic prolacertilians of the USSR. *Paleontol. Zh.* **4**, 88–100 (1978).

190. Thulborn, R.A., The post-cranial skeleton of the Triassic ornithischian dinosaur *Fabrosaurus australis*. *Palaeontol.* **15**, 29–60 (1972).

191. Tykoski, R. S. *Anatomy, ontogeny, and phylogeny of coelophysoid theropods* (PhD Dissertation, Univ. Texas, 2005).

192. Tykoski, R. S. & Rowe, T. in *The Dinosauria 2nd Edition* (eds Weishampel, D. B., Dobson, P. & Osmolska, H.) 47−70 (Univ. Cal. Press, 2004).

193. Unwin, D. M. in *Evolution and Palaeobiology of Pterosaurs* (eds Buffetaut, E. & Mazin, J.-M.) 139–190 (Geol. Soc. London Sp. Publ., 2003).

194. Unwin, D. M. *The Pterosaurs from deep time* (Pi Press, 2006).

195. Pipress, New York.Upchurch, P., Barrett P. M. & Galton P. M. A phylogenetic analysis of basal sauropodomorph relationships: implications for the origin of sauropod dinosaurs. *Sp. Pap. Palaeontol.* **77**, 57−90 (2007).

196. Wagner, J. A. Über einige im lithographischen Schiefer neu aufgefundene Schildkröten und Saurier. *Gel. Anz. Bayer. Akad. Wiss.* **49**, 553 (1859).

197. Walker, A. D. Triassic reptiles from the Elgin area: *Stagonolepis*, *Dasygnathus* and their allies. *P. T. R. Soc. L., S. B, Biol. Sci.* **244**, 103−204 (1961).

198. Walker, A. D. Triassic reptiles from the Elgin area: *Ornithosuchus* and the origin of carnosaurs. *P. T. R. Soc. L., S. B, Biol. Sci.* **248**, 53−134 (1964).

199. Wang, X., Kellner, A. W., Jiang, S. & Meng, X. An unusual long-tailed pterosaur with elongated neck from western Liaoning of China. *An. Acad. Bras. Ciênc.* **81**, 793−812 (2009).

200. Wang R. F. et al. A new specimen of *Shansisuchus shansisuchus* Young, 1964 (Diapsida: Archosauriformes) from the Triassic of Shanxi, China. *Acta Geol. Sin-Engl.* **87**, 1185–1197 (2013).

201. Whatley R. L. *Phylogenetic relationships of* Isalorhynchus genovefae*, the rhynchosaur (Reptilia, Archosauromorpha) from Madagascar* (PhD Dissertation, University of California, 2005).

202. Weems, R. E. An unusual newly discovered archosaur from the Upper Triassic of Virginia, USA. *Trans. Am. Philos. Soc.* **70**, 1−53 (1980).

203. Wellnhofer, P. Die Rhamphorhynchoidea (Pterosauria) der Oberjura-Plattenkalke Süddeutschlands. Teil I: Allgemeine Skelettmorphologie. *Palaeontogr. Abt. A* **148**, 1−33 (1975a).

204. Wellnhofer, P. Die Rhamphorhynchoidea (Pterosauria) der Oberjura-Plattenkalke Sueddeutschlands. Teil II: Systematische Beschreibung. *Palaeontogr. Abt. A* **148**, 132−186 (1975b).

205. Wellnhofer, P. A Late Triassic pterosaur from the Northern Calcareous Alps (Tyrol, Austria). *Geol. Soc. Spec. Publ.* **217**, 5−22 (2003).

206. Wild, R. Die Flugsaurier (Reptilia, Pterosauria) aus der Oberen Trias von Cene bei Bergamo, Italien. *Boll. Soc. Paleont. It.* **17**, 176−256 (1979).

207. Wild, R. A new pterosaur (Reptilia, Pterosauria) from the Upper Triassic (Norian) of Friuli, Italy. *Gortania* **5**, 45–62 (1984).

208. Yates, A. M. A definite prosauropod dinosaur from the lower Elliot Formation (Norian: Upper Triassic) of South Africa. *Paleont. Afr.* **39**, 63−68 (2003).

209. Yates, A. M. *Anchisaurus polyzelus* (Hitchcock): the smallest known sauropod dinosaur and the evolution of gigantism among sauropodomorph dinosaurs. *Postilla* **230**, 1−58 (2004).

210. Young, C. C. The pseudosuchians in China. *Palaeont Sin, New Ser C* **19**, 1–205 (1964).

211. Young, C. C. A complete skeleton of *Chasmatosaurus yuani* from Xinjinang. *Mem. Inst. Vert. Paleontol. Paleoanthrop., Academ. Sin., S. B* **13**, 26−46 (1978).

212. Zambelli, R. *Eudimorphodon ranzii* gen. nov., sp. nov., uno Pterosauro Triassico. *Rendic. Sci. Inst. L. Sci. Lett.* **107**, 27−32 (1973).

213. Zhang, C. Molecular clock dating using MrBayes. *arXiv preprint arXiv*, 1603.05707 (2016).


a
b
c
d
e
f
g
h
i

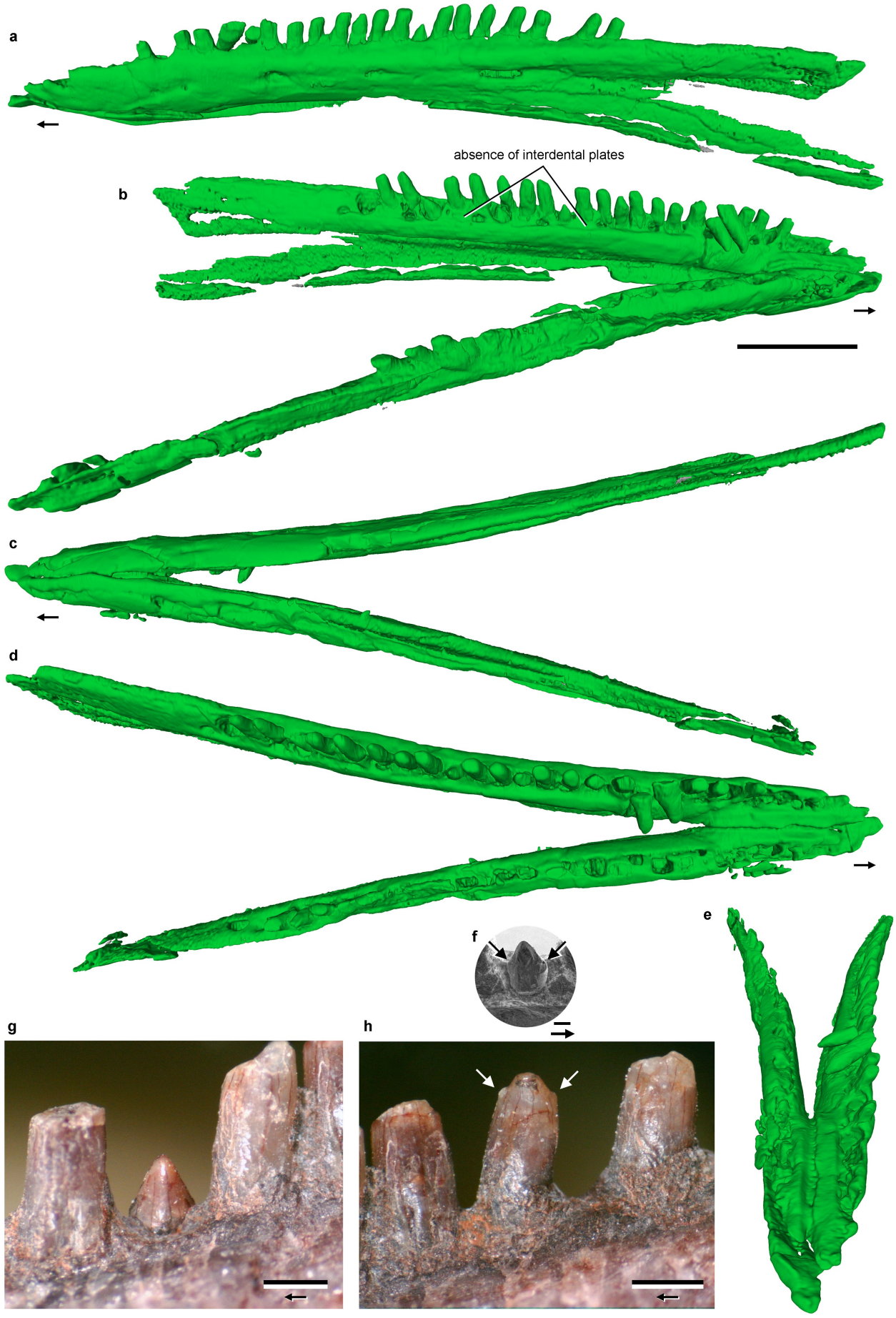
a
absence of interdental plates
b
c
d
e
f
g
h

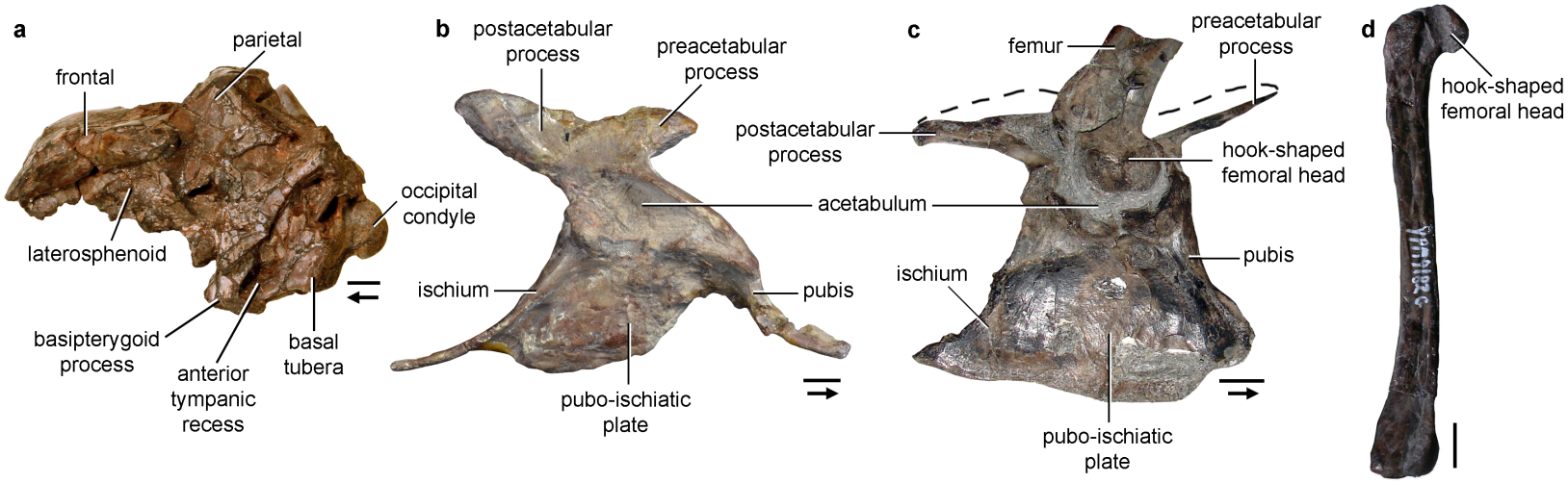
a
parietal
frontal
occipital condyle
laterosphenoid
basipterygoid process
anterior tympanic recess
basal tubera
b
postacetabular process
preacetabular process
ischium
pubis
pubo-ischiatic plate
c
femur
preacetabular process
postacetabular process
hook-shaped femoral head
acetabulum
pubis
ischium
pubo-ischiatic plate
d
hook-shaped femoral head

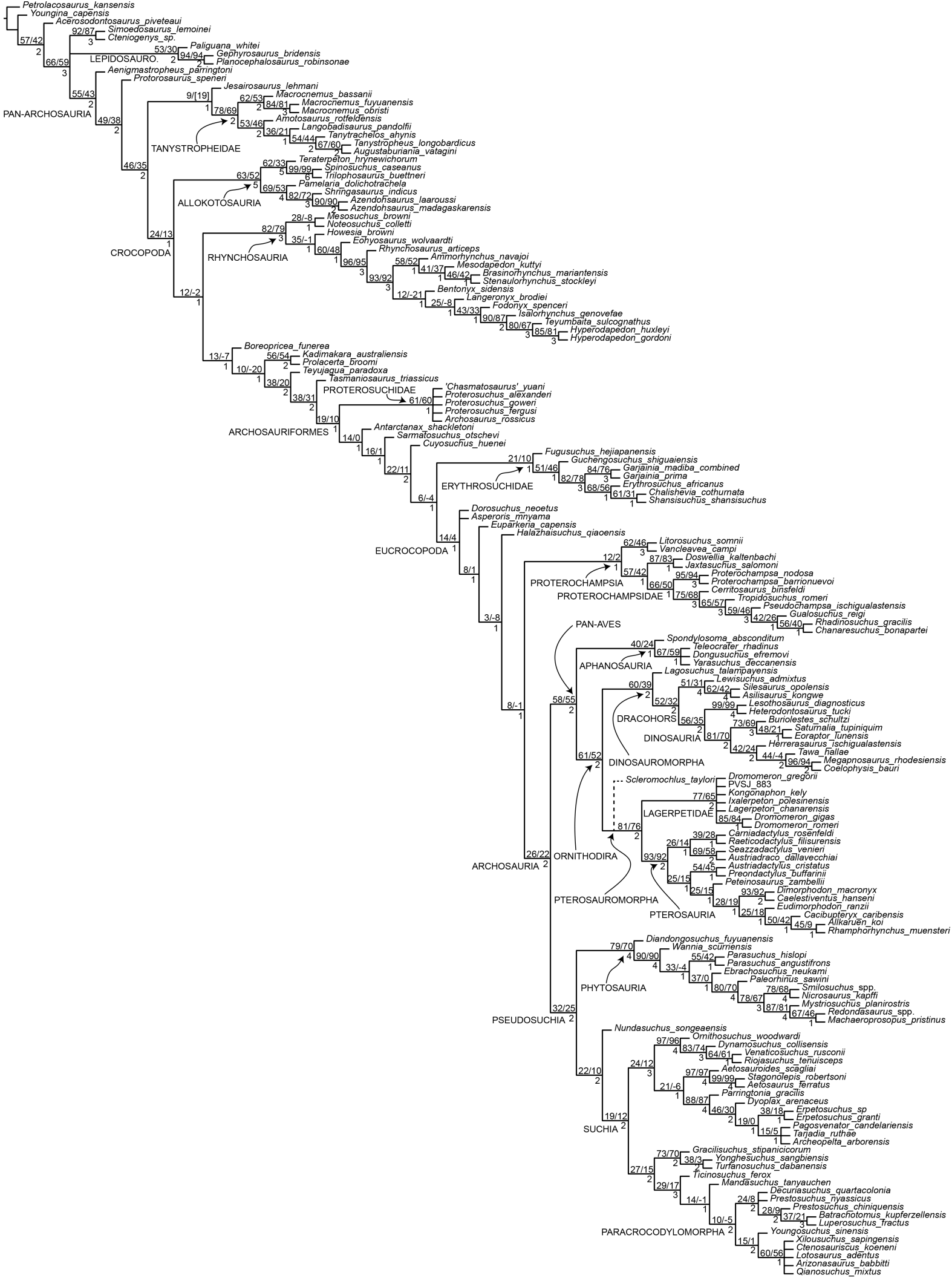
Petrolacosaurus_kansensis
Youngina_capensis
Acerosodontosaurus_piveteaui
Simoedosaurus_lemoinei
Cteniogenys_sp.
Paliguana_whitei
Gephyrosaurus_bridensis
Planocephalosaurus_robinsonae
LEPIDOSAURO.
Aenigmastropheus_parringtoni
Protorosaurus_speneri
PAN-ARCHOSAURIA
Jesairosaurus_lehmani
Macrocnemus_bassanii
Macrocnemus_fuyuanensis
Macrocnemus_obristi
Amotosaurus_rotfeldensis
Langobadisaurus_pandolfii
Tanytrachelos_ahynis
Tanystropheus_longobardicus
Augustaburiania_vatagini
TANYSTROPHEIDAE
Teraterpeton_hrynewichorum
Spinosuchus_caseanus
Trilophosaurus_buettneri
Pamelaria_dolichotrachela
Shringasaurus_indicus
Azendohsaurus_laaroussi
Azendohsaurus_madagaskarensis
ALLOKOTOSAURIA
CROCOPODA
Mesosuchus_browni
Noteosuchus_colletti
Howesia_browni
Eohyosaurus_wolvaardti
Rhynchosaurus_articeps
RHYNCHOSAURIA
Ammorhynchus_navajoi
Mesodapedon_kuttyi
Brasinorhynchus_mariantensis
Stenaulorhynchus_stockleyi
Bentonyx_sidensis
Langeronyx_brodiei
Fodonyx_spenceri
Isalorhynchus_genovefae
Teyumbaita_sulcognathus
Hyperodapedon_huxleyi
Hyperodapedon_gordoni
Boreopricea_funerea
Kadimakara_australiensis
Prolacerta_broomi
Teyujagua_paradoxa
Tasmaniosaurus_triassicus
PROTEROSUCHIDAE
'Chasmatosaurus'_yuani
Proterosuchus_alexanderi
Proterosuchus_goweri
Proterosuchus_fergusi
Archosaurus_rossicus
ARCHOSAURIFORMES
Antarctanax_shackleton
Sarmatosuchus_otschevi
Cuyosuchus_huenei
Fugusuchus_hejiapanensis
Guchengosuchus_shiguaiensis
Garjainia_madiba_combined
Garjainia_prima
Erythrosuchus_africanus
Chalishevia_cothurnata
Shansisuchus_shansisuchus
ERYTHROSUCHIDAE
Dorosuchus_neoetus
Asperoris_mnyama
Euparkeria_capensis
Halazhaisuchus_qiaoensis
EUCROCOPODA
Litorosuchus_somnii
Vancleavea_campi
Doswellia_kaltenbachi
Jaxtasuchus_salomoni
Proterochampsa_nodosa
Proterochampsa_barrionuevoi
Cerritosaurus_binsfeldi
Tropidosuchus_romeri
Pseudochampsa_ischigualastensis
Gualosuchus_reigi
Rhadinosuchus_gracilis
Chanaresuchus_bonapartei
PROTEROCHAMPSIA
PROTEROCHAMPSIDAE
PAN-AVES
Spondylosoma_absconditum
Teleocrater_rhadinus
Dongusuchus_efremovi
Yarasuchus_deccanensis
APHANOSAURIA
Lagosuchus_talampayensis
Lewisuchus_admixtus
Silesaurus_opolensis
Asilisaurus_kongwe
Lesothosaurus_diagnosticus
Heterodontosaurus_tucki
Buriolestes_schultzi
Saturnalia_tupiniquim
Eoraptor_lunensis
Herrerasaurus_ischigualastensis
Tawa_hallae
Megapnosaurus_rhodesiensis
Coelophysis_bauri
DRACOHORS
DINOSAURIA
DINOSAURomORPHA
Scleromochlus_taylori
Dromomeron_gregorii
PVSJ_883
Kongonaphon_kely
Ixalerpeton_polesinensis
Lagerpeton_chanarensis
Dromomeron_gigas
Dromomeron_romeri
LAGERPETIDAE
Carniadactylus_rosenfeldi
Raeticodactylus_filisurensis
Seazzadactylus_venieri
Austriadraco_dallavecchiai
Austriadactylus_cristatus
Preondactylus_buffarinii
Peteinosaurus_zambellii
Dimorphodon_macronyx
Caelestiventus_hanseni
Eudimorphodon_ranzii
Cacibupteryx_caribensis
Alkaruen_koi
Rhamphorhynchus_muensteri
ORNITHODIRA
PTEROSAUROMORPHA
PTEROSAURIA
ARCHOSAURIA
Diandongosuchus_fuyuanensis
Wannia_scurriensis
Parasuchus_hislopi
Parasuchus_angustifrons
Ebrachosuchus_neukami
Paleorhinus_sawini
Smilosuchus_spp.
Nicrosaurus_kapffi
Mystriosuchus_planirostris
Redondasaurus_spp.
Machaeroprosopus_pristinus
PHYTOSAURIA
PSEUDOSUCHIA
Nundasuchus_songeaensis
Ornithosuchus_woodwardi
Dynamosuchus_collisensis
Venaticosuchus_rusconii
Riojasuchus_tenuisceps
Aetosauroides_scagliai
Stagonolepis_robertsoni
Aetosaurus_ferratus
Parringtonia_gracilis
Dyoplax_arenaceus
Erpetosuchus_sp
Erpetosuchus_granti
Pagosvenator_candelariensis
Tarjadia_ruthae
Archeopelta_arborensis
SUCHIA
Gracilisuchus_stipanicicorum
Yonghesuchus_sangbiensis
Turfanosuchus_dabanensis
Ticinosuchus_ferox
Mandasuchus_tanyauchen
Decuriasuchus_quartacolonia
Prestosuchus_nyassicus
Prestosuchus_chiniquensis
Batrachotomus_kupferzellensis
Luperosuchus_fractus
PARACROCODYLOMORPHA
Youngosuchus_sinensis
Xilousuchus_sapingensis
Ctenosauriscus_koeneni
Lotosaurus_adentus
Arizonasaurus_babbitti
Qianosuchus_mixtus

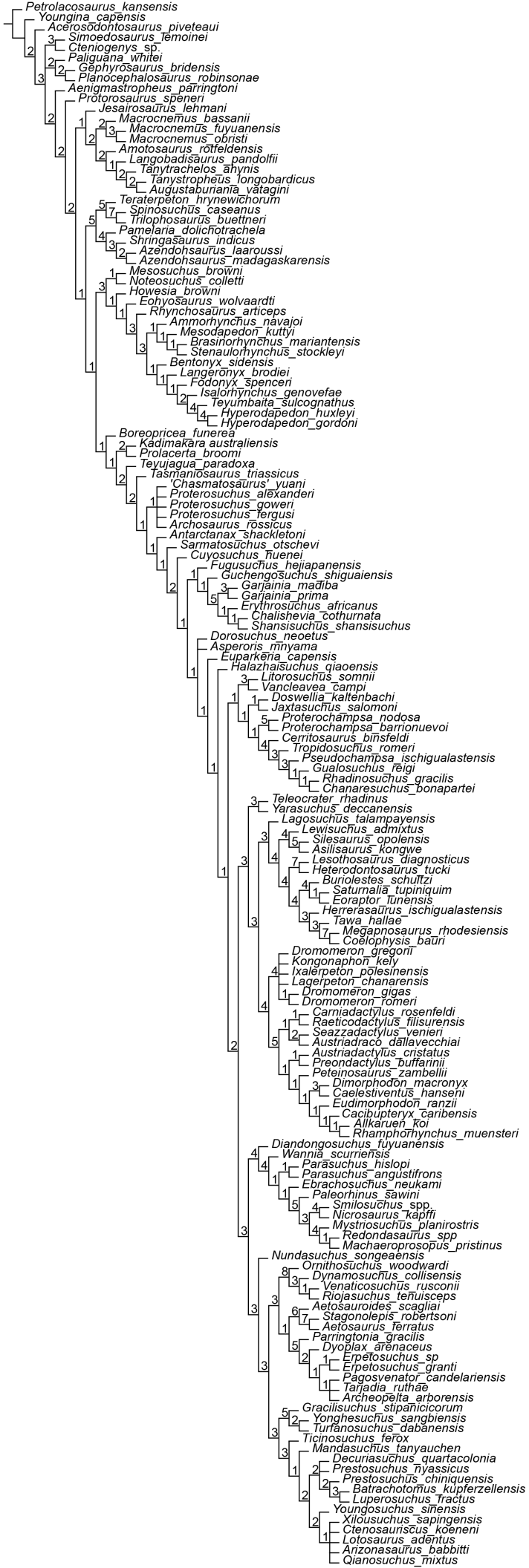
Petrolacosaurus_kansensis
Youngina_capensis
Acerosodontosaurus_piveteaui
Simoedosaurus_lemoinei
Cteniogenys_sp.
Paliguana_whitei
Gephyrosaurus_bridensis
Planocephalosaurus_robinsonae
Aenigmastropheus_parringtoni
Protorosaurus_speneri
Jesairosaurus_lehmani
Macrocnemus_bassanii
Macrocnemus_fuyuanensis
Macrocnemus_obristi
Amotosaurus_rotfeldensis
Langobadisaurus_pandolfii
Tanytrachelos_ahynis
Tanystropheus_longobardicus
Augustaburiania_vatagini
Teraterpeton_hrynewichorum
Spinosuchus_caseanus
Trilophosaurus_buettneri
Pamelaria_dolichotrachela
Shringasaurus_indicus
Azendohsaurus_laaroussi
Azendohsaurus_madagaskarensis
Mesosuchus_browni
Noteosuchus_colletti
Howesia_browni
Eohyosaurus_wolvaardti
Rhynchosaurus_articeps
Ammorhynchus_navajoi
Mesodapedon_kuttyi
Brasinorhynchus_mariantensis
Stenaulorhynchus_stockleyi
Bentonyx_sidensis
Langeronyx_brodiei
Fodonyx_spenceri
Isalorhynchus_genovefae
Teyumbaita_sulcognathus
Hyperodapedon_huxleyi
Hyperodapedon_gordoni
Boreopricea_funerea
Kadimakara_australiensis
Prolacerta_broomi
Teyujagua_paradoxa
Tasmaniosaurus_triassicus
'Chasmatosaurus'_yuani
Proterosuchus_alexanderi
Proterosuchus_goweri
Proterosuchus_fergusi
Archosaurus_rossicus
Antarctanax_shackletoni
Sarmatosuchus_otschevi
Cuyosuchus_huenei
Fugusuchus_hejiapanensis
Guchengosuchus_shiguaiensis
Garjainia_madiba
Garjainia_prima
Erythrosuchus_africanus
Chalishevia_cothurnata
Shansisuchus_shansisuchus
Dorosuchus_neoetus
Asperoris_minyama
Euparkeria_capensis
Halazhaisuchus_qiaoensis
Litorosuchus_somnii
Vancleavea_campi
Doswellia_kaltenbachi
Jaxtasuchus_salomoni
Proterochampsa_nodosa
Proterochampsa_barrionuevoi
Cerritosaurus_binsfeldi
Tropidosuchus_romeri
Pseudochampsa_ischigualastensis
Gualosuchus_reigi
Rhadinosuchus_gracilis
Chanaresuchus_bonapartei
Teleocrater_rhadinus
Yarasuchus_deccanensis
Lagosuchus_talampayensis
Lewisuchus_admixtus
Silesaurus_opolensis
Asilisaurus_kongwe
Lesothosaurus_diagnosticus
Heterodontosaurus_tucki
Buriolestes_schultzi
Saturnalia_tupiniquim
Eoraptor_lunensis
Herrerasaurus_ischigualastensis
Tawa_hallae
Megapnosaurus_rhodesiensis
Coelophysis_bauri
Dromomeron_gregorii
Kongonaphon_kely
Ixalerpeton_polesinensis
Lagerpeton_chanarensis
Dromomeron_gigas
Dromomeron_romeri
Carniadactylus_rosenfeldi
Raeticodactylus_filisurensis
Seazzadactylus_venieri
Austriadraco_dallavecchiai
Austriadactylus_cristatus
Preondactylus_buffarinii
Peteinosaurus_zambellii
Dimorphodon_macronyx
Caelestiventus_hanseni
Eudimorphodon_ranzii
Cacibupteryx_caribensis
Allkaruen_koi
Rhamphorhynchus_muensteri
Diandongosuchus_fuyuanensis
Wannia_scurriensis
Parasuchus_hislopi
Parasuchus_angustifrons
Ebrachosuchus_neukami
Paleorhinus_sawini
Smilosuchus_spp.
Nicrosaurus_kapffi
Mystriosuchus_planirostris
Redondasaurus_spp
Machaeroprosopus_pristinus
Nundasuchus_songeaensis
Ornithosuchus_woodwardi
Dynamosuchus_collisensis
Venaticosuchus_rusconii
Riojasuchus_tenuisceps
Aetosauroides_scagliai
Stagonolepis_robertsoni
Aetosaurus_ferratus
Parringtonia_gracilis
Dyoplax_arenaceus
Erpetosuchus_sp
Erpetosuchus_granti
Pagosvenator_candelariensis
Tarjadia_ruthae
Archeopelta_arborensis
Gracilisuchus_stipanicicorum
Yonghesuchus_sangbiensis
Turfanosuchus_dabanensis
Ticinosuchus_ferox
Mandasuchus_tanyauchen
Decuriasuchus_quartacolonia
Prestosuchus_nyassicus
Prestosuchus_chiniquensis
Batrachotomus_kupferzellensis
Luperosuchus_fractus
Youngosuchus_sinensis
Xilousuchus_sapingensis
Ctenosauriscus_koeneni
Lotosaurus_adentus
Arizonasaurus_babbitti
Qianosuchus_mixtus

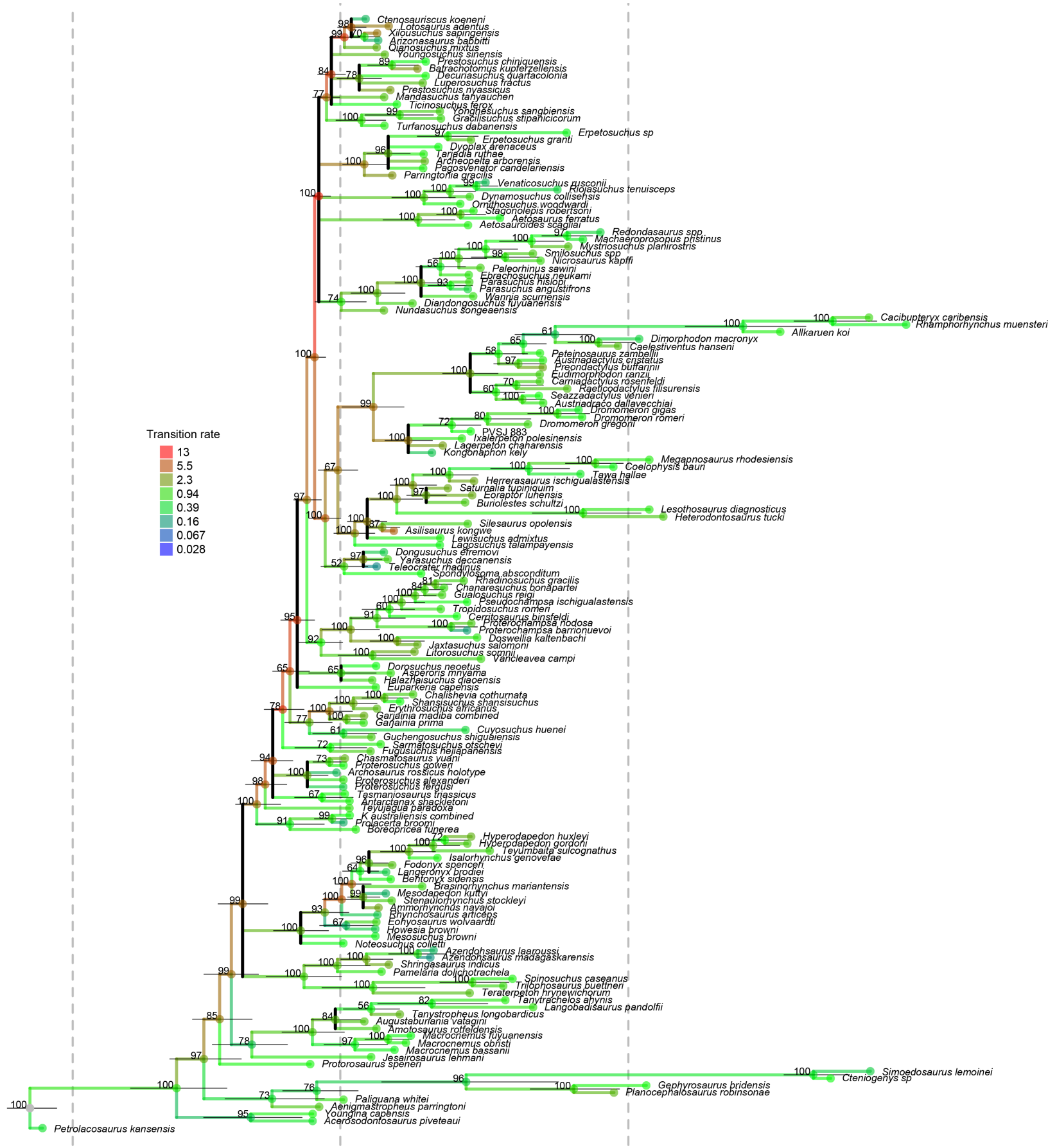
Transition rate
13
5.5
2.3
0.94
0.39
0.16
0.067
0.028
Ctenosauriscus koeneni
Lotosaurus adentus
Xilousuchus sapingensis
Arizonasaurus babbitti
Qianosuchus mixtus
Youngosuchus sinensis
Prestosuchus chiniquensis
Batrachotomus kupferzellensis
Decuriasuchus quartacolonia
Luperosuchus fractus
Prestosuchus nyassicus
Mandasuchus tanyauchen
Ticinosuchus ferox
Yonghesuchus sangbiensis
Gracilisuchus stipanicicorum
Turfanosuchus dabanensis
Erpetosuchus sp
Erpetosuchus granti
Dyoplax arenaceus
Tarjadia ruthae
Archeopelta arborensis
Pagosvenator candelariensis
Parringtonia gracilis
Venaticosuchus rusconii
Riojasuchus tenuisceps
Dynamosuchus collisensis
Ornithosuchus woodwardi
Stagonolepis robertsoni
Aetosaurus ferratus
Aetosauroides scagliai
Redondasaurus spp
Machaeroprosopus pristinus
Mystriosuchus planirostris
Smilosuchus spp
Nicrosaurus kapffi
Paleorhinus sawini
Ebrachosuchus neukami
Parasuchus hislopi
Parasuchus angustifrons
Wannia scurriensis
Diandongosuchus fuyuanensis
Nundasuchus songeaensis
Cacibupteryx caribensis
Rhamphorhynchus muensteri
Allkaruen koi
Dimorphodon macronyx
Caelestiventus hanseni
Peteinosaurus zambelli
Austriadactylus cristatus
Preondactylus buffarinii
Eudimorphodon ranzii
Carniadactylus rosenfeldi
Raeticodactylus filisurensis
Seazzadactylus venieri
Austriadraco dallavecchiai
Dromomeron gigas
Dromomeron romeri
Dromomeron gregorii
PVSJ 883
Ixalerpeton polesinensis
Lagerpeton chanarensis
Kongonaphon kely
Megapnosaurus rhodesiensis
Coelophysis bauri
Tawa hallae
Herrerasaurus ischigualastensis
Saturnalia tupiniquim
Eoraptor lunensis
Buriolestes schultzi
Lesothosaurus diagnosticus
Heterodontosaurus tucki
Silesaurus opolensis
Asilisaurus kongwe
Lewisuchus admixtus
Lagosuchus talampayensis
Dongusuchus efremovi
Yarasuchus deccanensis
Teleocrater rhadinus
Spondylosoma absconditum
Rhadinosuchus gracilis
Chanaresuchus bonapartei
Gualosuchus reigi
Pseudochampsa ischigualastensis
Tropidosuchus romeri
Ceratosaurus binsfeldi
Proterochampsa nodosa
Proterochampsa barrionuevoi
Doswellia kaltenbachi
Jaxtasuchus salomoni
Litorosuchus somnii
Vancleavea campi
Dorosuchus neoetus
Asperoris mnyama
Halazhaisuchus qiaoensis
Euparkeria capensis
Chalishevia cothurnata
Shansisuchus shansisuchus
Erythrosuchus africanus
Garjainia madiba combined
Garjainia prima
Cuyosuchus huenei
Guchengosuchus shiguaiensis
Sarmatosuchus otschevi
Fugusuchus hejiapanensis
Chasmatosaurus yuani
Proterosuchus goweri
Archosaurus rossicus holotype
Proterosuchus alexanderi
Proterosuchus fergusi
Tasmaniosaurus triassicus
Antarctanax shackletoni
Teyujagua paradoxa
K australiensis combined
Prolacerta broomi
Boreopricea funerea
Hyperodapedon huxleyi
Hyperodapedon gordoni
Teyumbaita sulcognathus
Isalorhynchus genovefae
Fodonyx spenceri
Langeronyx brodiei
Bentonyx sidensis
Brasinorhynchus mariantensis
Mesodapedon kutyi
Stenaulorhynchus stockleyi
Ammorhynchus navajoi
Rhynchosaurus articeps
Eofyosaurus wolvaardti
Howesia browni
Mesosuchus browni
Noteosuchus colletti
Azendohsaurus laaroussi
Azendohsaurus madagaskarensis
Shringasaurus indicus
Pamelaria dolichotrachela
Spinosuchus caseanus
Trilophosaurus buettneri
Teraterpeton hrynewichorum
Tanytrachelos ahynis
Langobadisaurus pandolfii
Tanystropheus longobardicus
Augustaburiania vatagini
Amotosaurus rotfeldensis
Macrocnemus fuyuanensis
Macrocnemus obristi
Macrocnemus bassanii
Jesairosaurus lehmani
Protorosaurus speneri
Simoedosaurus lemoinei
Cteniogenys sp
Gephyrosaurus bridensis
Planocephalosaurus robinsonae
Paliguana whitei
Aenigmastropheus parringtoni
Youngina capensis
Acerosodontosaurus piveteaui
Petrolacosaurus kansensis

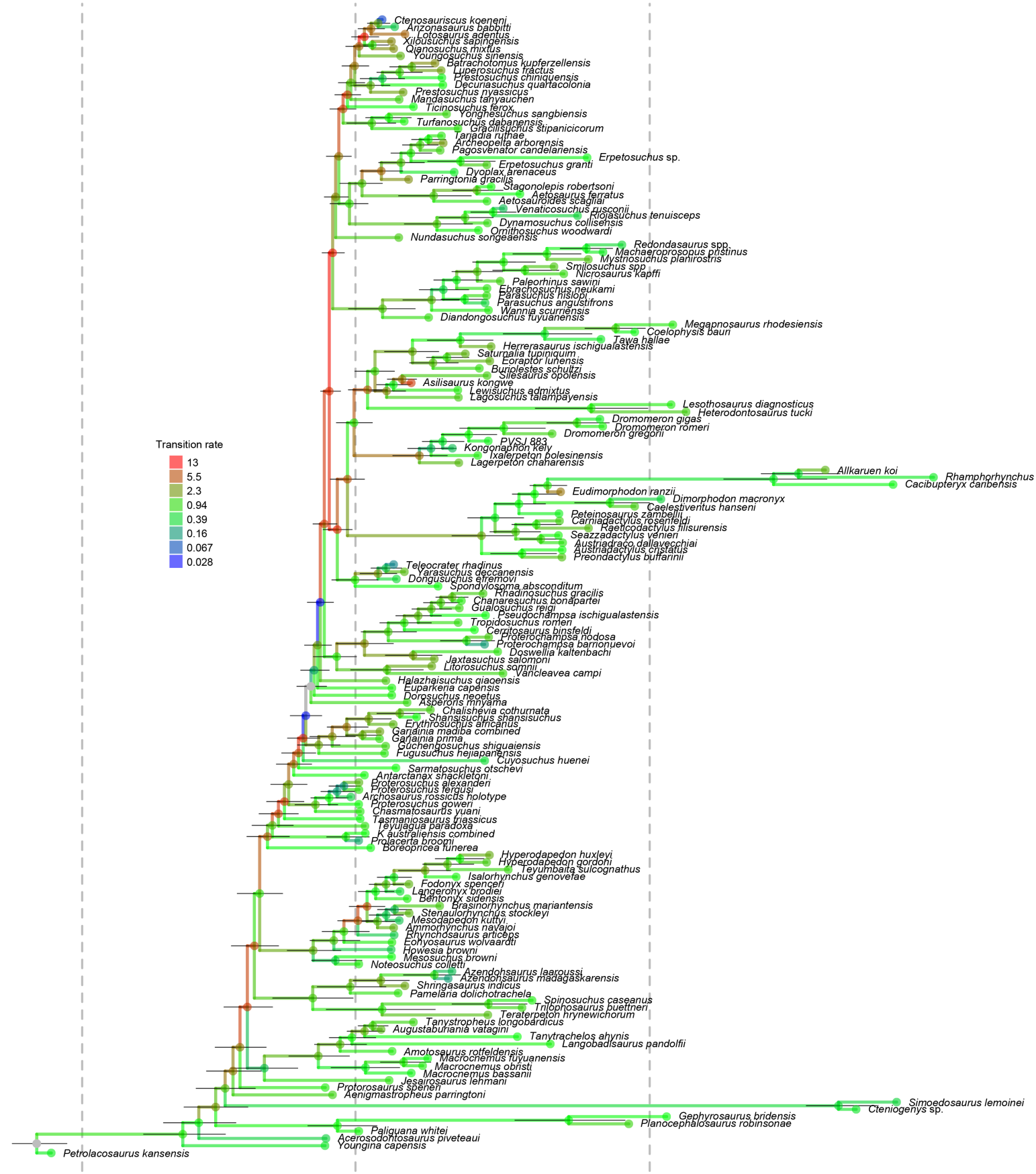
Transition rate
13
5.5
2.3
0.94
0.39
0.16
0.067
0.028
Ctenosauriscus koeneni
Arizonasaurus babbitti
Lotosaurus adentus
Xilousuchus sapingensis
Qianosuchus mixtus
Youngosuchus sinensis
Batrachotomus kupferzellensis
Luperosuchus fractus
Prestosuchus chiniquensis
Decuriasuchus quartacolonia
Prestosuchus nyassicus
Mandasuchus tanyauchen
Ticinosuchus ferox
Yonghesuchus sangbiensis
Turfanosuchus dabanensis
Gracilisuchus stipanicicorum
Tarjadia ruthae
Archeopelta arborensis
Pagosvenator candelariensis
Erpetosuchus sp.
Erpetosuchus granti
Dyoplax arenaceus
Parringtonia gracilis
Stagonolepis robertsoni
Aetosaurus ferratus
Aetosauroides scagliai
Venaticosuchus rusconii
Riojasuchus tenuisceps
Dynamosuchus collisensis
Ornithosuchus woodwardi
Nundasuchus songeaensis
Redondasaurus spp.
Machaeroprosopus pristinus
Mystriosuchus planirostris
Smilosuchus spp.
Nicrosaurus kapffi
Paleorhinus sawini
Ebrachosuchus neukami
Parasuchus hislopi
Parasuchus angustifrons
Wannia scurrensis
Diandongosuchus fuyuanensis
Megapnosaurus rhodesiensis
Coelophysis bauri
Tawa hallae
Herrerasaurus ischigualastensis
Saturnalia tupiniquim
Eoraptor lunensis
Buriolestes schultzi
Silesaurus opolensis
Asilisaurus kongwe
Lewisuchus admixtus
Lagosuchus talampayensis
Lesothosaurus diagnosticus
Heterodontosaurus tucki
Dromomeron gigas
Dromomeron romeri
Dromomeron gregorii
PVSJ 883
Kongonaphon kely
Ixalerpeton polesinensis
Lagerpeton chanarensis
Allkaruen koi
Rhamphorhynchus muensteri
Cacibupteryx caribensis
Eudimorphodon ranzii
Dimorphodon macronyx
Caelestiventus hanseni
Peteinosaurus zambelli
Carniadactylus rosenfeldi
Raeticodactylus filisurensis
Seazzadactylus venieri
Austriadraco dallavecchiai
Austriadactylus cristatus
Preondactylus buffarinii
Teleocrater rhadinus
Arasuchus deccanensis
Dongusuchus efremovi
Spondylosoma absconditum
Rhadinosuchus gracilis
Chanaresuchus bonapartei
Gualosuchus reigi
Pseudochampsa ischigualastensis
Tropidosuchus romeri
Cerritosaurus binsfeldi
Proterochampsa nodosa
Proterochampsa barrionuevoi
Doswellia kaltenbachi
Jaxtasuchus salomoni
Litorosuchus somnii
Vancleavea campi
Halazhaisuchus qiaoensis
Euparkeria capensis
Dorosuchus neoetus
Asperoris minyama
Chalishevia cothurnata
Shansisuchus shansisuchus
Erythrosuchus africanus
Garjainia madiba combined
Garjainia prima
Guchengosuchus shiguaiensis
Fugusuchus hejiapanensis
Cuyosuchus huenei
Sarmatosuchus otschevi
Antarctanax shackletoni
Proterosuchus alexanderi
Proterosuchus fergusi
Archosaurus rossicus holotype
Proterosuchus goweri
Chasmatosaurus yuani
Tasmaniosaurus triassicus
Teyujagua paradoxa
K australiensis combined
Prolacerta broomi
Boreopricea funerea
Hyperodapedon huxleyi
Hyperodapedon gordoni
Teyumbaita sulcognathus
Isalorhynchus genovefae
Fodonyx spenceri
Langeronyx brodiei
Bentonyx sidensis
Brasinorhynchus mariantensis
Stenaulorhynchus stockleyi
Mesodapedon kuttyi
Ammorhynchus navajoi
Rhynchosaurus articeps
Eohyosaurus wolvaardti
Howesia browni
Mesosuchus browni
Noteosuchus colletti
Azendohsaurus laaroussi
Azendohsaurus madagaskarensis
Shringasaurus indicus
Pamelaria dolichotrachela
Spinosuchus caseanus
Trilophosaurus buettneri
Teraterpeton hrynewichorum
Tanystropheus longobardicus
Augustaburiania vatagini
Tanytrachelos ahynis
Langobadisaurus pandolfii
Amotosaurus rotfeldensis
Macrocnemus fuyuanensis
Macrocnemus obristi
Macrocnemus bassanii
Jesairosaurus lehmani
Protorosaurus speneri
Aenigmastropheus parringtoni
Simoedosaurus lemoinei
Cteniogenys sp.
Gephyrosaurus bridensis
Planocephalosaurus robinsonae
Paliguana whitei
Acerosodontosaurus piveteaui
Youngina capensis
Petrolacosaurus kansensis

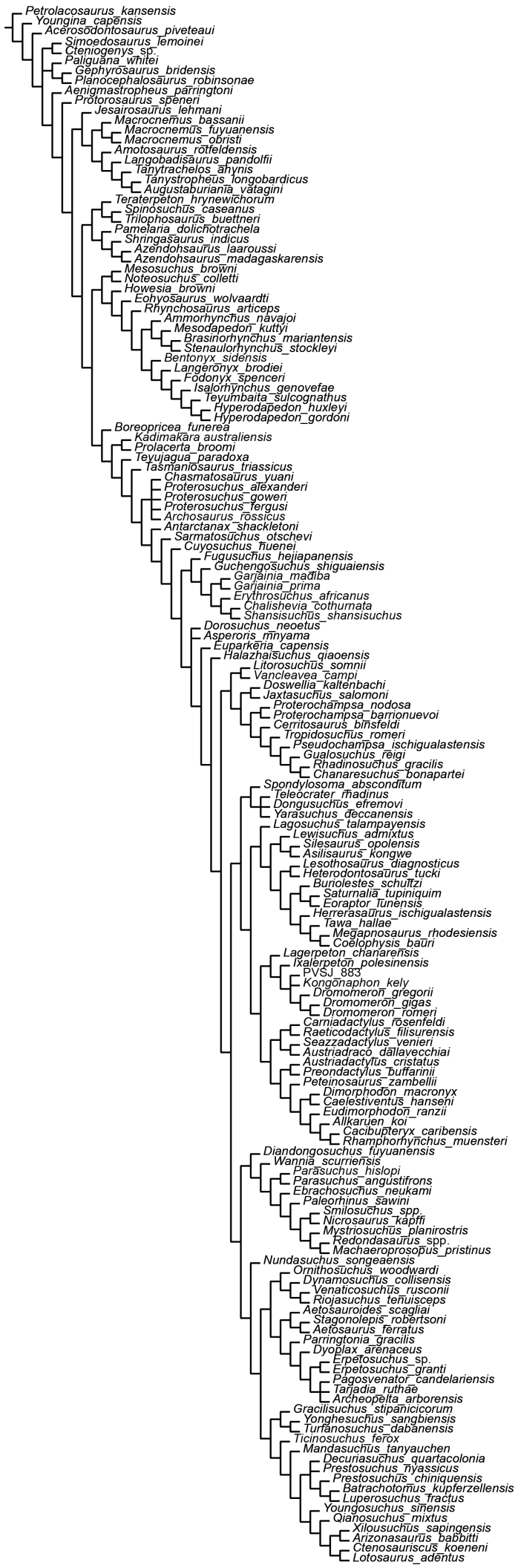
Petrolacosaurus_kansensis
Youngina_capensis
Acerosodontosaurus_piveteaui
Simoedosaurus_lemoinei
Cteniogenys_sp.
Paliguana_whitei
Gephyrosaurus_bridensis
Planocephalosaurus_robinsonae
Aenigmastropheus_parringtoni
Protorosaurus_speneri
Jesairosaurus_lehmani
Macrocnemus_bassanii
Macrocnemus_fuyuanensis
Macrocnemus_obristi
Amotosaurus_rotfeldensis
Langobadisaurus_pandolfii
Tanytrachelos_ahynis
Tanystropheus_longobardicus
Augustaburiania_vatagini
Teraterpeton_hrynewichorum
Spinosuchus_caseanus
Trilophosaurus_buettneri
Pamelaria_dolichotrachela
Shringasaurus_indicus
Azendohsaurus_laaroussi
Azendohsaurus_madagaskarensis
Mesosuchus_browni
Noteosuchus_colletti
Howesia_browni
Eohyosaurus_wolvaardti
Rhynchosaurus_articeps
Ammorhynchus_navajoi
Mesodapedon_kuttyi
Brasinorhynchus_mariantensis
Stenaulorhynchus_stockleyi
Bentonyx_sidensis
Langeronyx_brodiei
Fodonyx_spenceri
Isalorhynchus_genovefae
Teyumbaita_sulcognathus
Hyperodapedon_huxleyi
Hyperodapedon_gordoni
Boreopricea_funerea
Kadimakara_australiensis
Prolacerta_broomi
Teyujagua_paradoxa
Tasmaniosaurus_triassicus
Chasmatosaurus_yuani
Proterosuchus_alexanderi
Proterosuchus_goweri
Proterosuchus_fergusi
Archosaurus_rossicus
Antarctanax_shackletoni
Sarmatosuchus_otschevi
Cuyosuchus_huenei
Fugusuchus_hejiapanensis
Guchengosuchus_shiguaiensis
Garjainia_madiba
Garjainia_prima
Erythrosuchus_africanus
Chalishevia_cothurnata
Shansisuchus_shansisuchus
Dorosuchus_neoetus
Asperoris_minyama
Euparkeria_capensis
Halazhaisuchus_qiaoensis
Litorosuchus_somnii
Vancleavea_campi
Doswellia_kaltenbachi
Jaxtasuchus_salomoni
Proterochampsa_nodosa
Proterochampsa_barrionuevoi
Cerritosaurus_binsfeldi
Tropidosuchus_romeri
Pseudochampsa_ischigualastensis
Gualosuchus_reigi
Rhadinosuchus_gracilis
Chanaresuchus_bonapartei
Spondylosoma_absconditum
Teleocrater_rhadinus
Dongusuchus_efremovi
Yarasuchus_deccanensis
Lagosuchus_talampayensis
Lewisuchus_admixtus
Silesaurus_opolensis
Asilisaurus_kongwe
Lesothosaurus_diagnosticus
Heterodontosaurus_tucki
Buriolestes_schultzi
Saturnalia_tupiniquim
Eoraptor_lunensis
Herrerasaurus_ischigualastensis
Tawa_hallae
Megapnosaurus_rhodesiensis
Coelophysis_bauri
Lagerpeton_chanarensis
Ixalerpeton_polesinensis
PVSJ_883
Kongonaphon_kely
Dromomeron_gregorii
Dromomeron_gigas
Dromomeron_romeri
Carniadactylus_rosenfeldi
Raeticodactylus_filisurensis
Seazzadactylus_venieri
Austriadraco_dallavecchiai
Austriadactylus_cristatus
Preondactylus_buffarinii
Peteinosaurus_zambellii
Dimorphodon_macronyx
Caelestiventus_hanseni
Eudimorphodon_ranzii
Alkaruen_koi
Cacibupteryx_caribensis
Rhamphorhynchus_muensteri
Diandongosuchus_fuyuanensis
Wannia_scurriensis
Parasuchus_hislopi
Parasuchus_angustifrons
Ebrachosuchus_neukami
Paleorhinus_sawini
Smilosuchus_spp.
Nicrosaurus_kapffi
Mystriosuchus_planirostris
Redondasaurus_spp.
Machaeroprosopus_pristinus
Nundasuchus_songeaensis
Ornithosuchus_woodwardi
Dynamosuchus_collisensis
Venaticosuchus_rusconii
Riojasuchus_tenuisceps
Aetosauroides_scagliai
Stagonolepis_robertsoni
Aetosaurus_ferratus
Parringtonia_gracilis
Dyoplax_arenaceus
Erpetosuchus_sp.
Erpetosuchus_granti
Pagosvenator_candelariensis
Tarjadia_ruthae
Archeopelta_arborensis
Gracilisuchus_stipanicicorum
Yonghesuchus_sangbiensis
Turfanosuchus_dabanensis
Ticinosuchus_ferox
Mandasuchus_tanyauchen
Decuriasuchus_quartacolonia
Prestosuchus_hyassicus
Prestosuchus_chiniquensis
Batrachotomus_kupferzellensis
Luperosuchus_fractus
Youngosuchus_sinensis
Qianosuchus_mixtus
Xilousuchus_sapingensis
Arizonasaurus_babbitti
Ctenosauriscus_koeneni
Lotosaurus_adentus

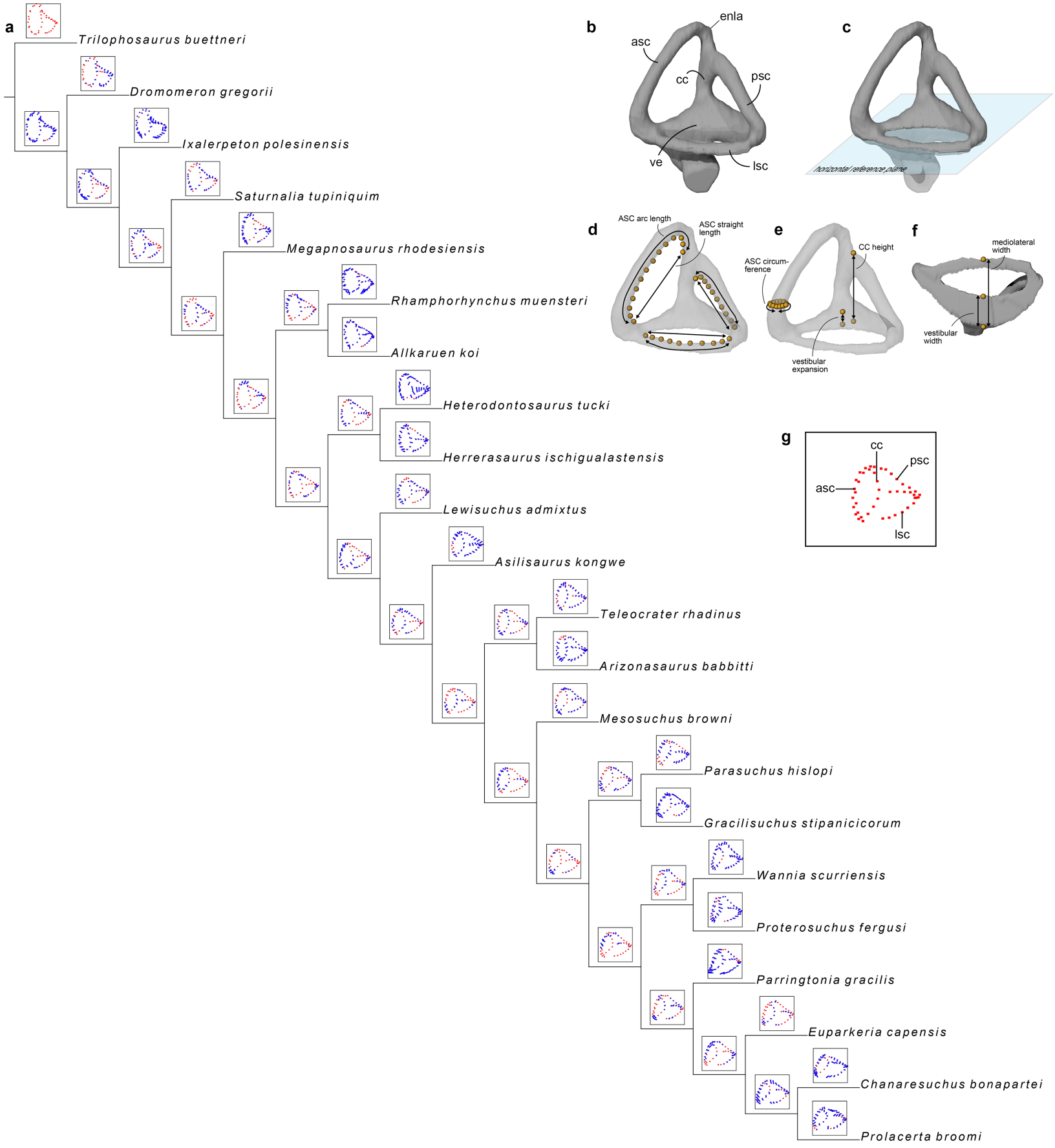
a
Trilophosaurus buettneri
Dromomeron gregorii
Ixalerpeton polesinensis
Saturnalia tupiniquim
Megapnosaurus rhodesiensis
Rhamphorhynchus muensteri
Allkaruen koi
Heterodontosaurus tucki
Herrerasaurus ischigualastensis
Lewisuchus admixtus
Asilisaurus kongwe
Teleocrater rhadinus
Arizonasaurus babbitti
Mesosuchus browni
Parasuchus hislopi
Gracilisuchus stipanicicorum
Wannia scurriensis
Proterosuchus fergusi
Parringtonia gracilis
Euparkeria capensis
Chanaresuchus bonapartei
Prolacerta broomi
b
enla
asc
cc
psc
ve
lsc
c
horizontal reference plane
d
ASC arc length
ASC straight length
e
ASC circum-ference
CC height
vestibular expansion
f
mediolateral width
vestibular width
g
cc
psc
asc
lsc

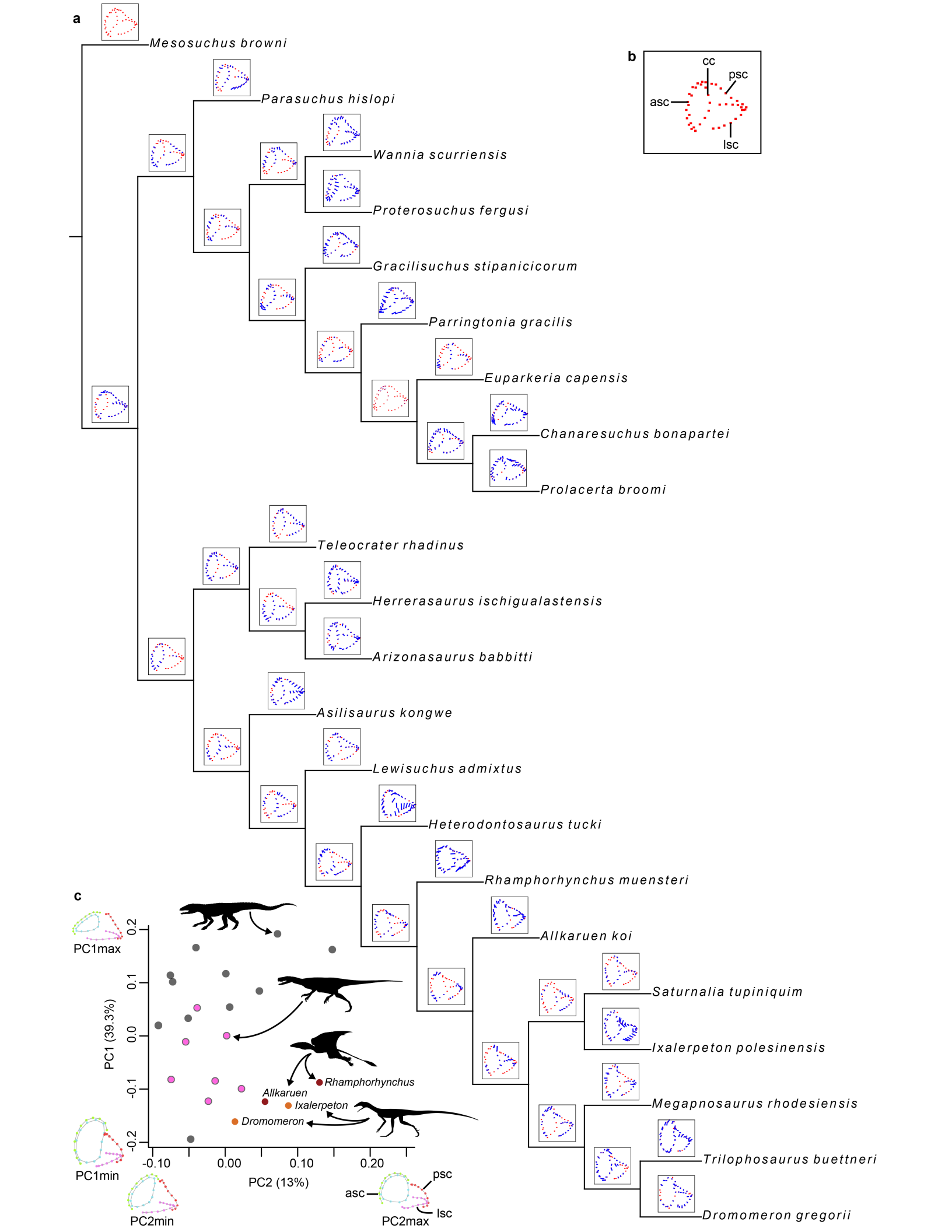
a
Mesosuchus browni
Parasuchus hislopi
Wannia scurriensis
Proterosuchus fergusi
Gracilisuchus stipanicicorum
Parringtonia gracilis
Euparkeria capensis
Chanaresuchus bonapartei
Prolacerta broomi
Teleocrater rhadinus
Herrerasaurus ischigualastensis
Arizonasaurus babbitti
Asilisaurus kongwe
Lewisuchus admixtus
Heterodontosaurus tucki
Rhamphorhynchus muensteri
Allkaruen koi
Saturnalia tupiniquim
Ixalerpeton polesinensis
Megapnosaurus rhodesiensis
Trilophosaurus buettneri
Dromomeron gregorii
b
cc
psc
asc
lsc
c
PC1max
PC1min
PC2min
PC2max
PC1 (39.3%)
PC2 (13%)
0.2
0.1
0.0
-0.1
-0.2
-0.10
0.00
0.10
0.20
Rhamphorhynchus
Allkaruen
Ixalerpeton
Dromomeron
psc
asc
lsc